Protein Epitope Mimetics in the Fight Against Malaria and Drug Resistant Bacterial Infections

---

Dissertation

zur

Erlangung der naturwissenschaftlichen Doktorwürde
(Dr. sc. nat.)

vorgelegt der

Mathematisch-naturwissenschaftlichen Fakultät

der

Universität Zürich

von

Sonya James

aus Grossbritannien

Promotionskomitee

Prof. Dr. John A. Robinson

Prof. Dr. Heinz Heimgartner

Prof. Dr. Gerd Pluschke

Zürich 2006

Table of contents

1 Potential candidates for a multi-antigen malaria vaccine

1.1 Introduction

1.1.1 Malaria

1.1.1.1 Disease burden

Malaria is a debilitating disease occurring most frequently in tropical and sub-tropical areas. The disease is not only a physical burden on those experiencing its symptoms, but is also an economical and developmental burden on endemic areas. Recent studies estimate that there are around 3.2 billion people currently at risk from malaria, with transmission reported to occur in 107 countries and territories[1]. There are believed to be between 350 and 500 million clinical cases of the disease annually. The greatest proportion of these cases occurs in Africa, where there are still over 1 million deaths per year due to malaria. Young children and pregnant women are often the worst affected by malaria, indeed, most of the deaths from malaria in Africa are of children under 5 years of age. If untreated in children, the disease can develop very rapidly (often within 24 hours) from the initial symptoms of fever, vomiting and flu-like symptoms, to convulsions, coma and death. Chronic anaemia caused by malaria may have adverse effects on the growth and intellectual development of children. Pregnant women in areas of unstable malaria transmission are two- to three times more likely to experience severe disease in the case of malaria infection than non-pregnant adults in the same area. This can lead to death either directly from severe malaria or indirectly from malaria-related severe anaemia. Infection of the mother can also lead to adverse effects including spontaneous abortion, neonatal death and low birth weight. In areas of stable malaria transmission, mothers have usually developed enough immunity to avoid clinical symptoms, and the main impact of malaria infection is associated with anaemia in the mother and the presence of parasites in the placenta, which impairs foetal nutrition and is one of the main causes of low birth weights and infant deaths.

It is difficult to estimate the economic burden of malaria, which is recognised as both a disease of poverty and a cause of poverty. The direct costs of malaria are spread between individuals and public bodies. Personal expenditures include the purchase of anti-malarial drugs, insecticide-treated nets, doctors' fees and transport to health centres. Public spending can be on maintaining healthcare facilities and infrastructure, on large-scale vector control programs, on education and on research. Malaria is estimated to account for up to 40% of public health spending in some countries. The indirect costs of malaria include the loss of productivity due to illness or death. The disease also has an adverse effect on children's development and therefore possibly their future earning potential. Children's development is affected both by absence from school due to illness, and also by permanent neurological and other damage associated with the disease. Other indirect effects of malaria include the under-development of tourism in malaria-endemic areas, and the reluctance of farmers to grow labour-intensive cash crops, due to the effect of malaria on labour during the harvest season.

1.1.1.2 Transmission and distribution

Malaria is caused in humans by the four *Plasmodium* species *P. falciparum, P. vivax, P. ovale and P. malariae*. Other *Plasmodium* species of interest are those that can be grown in laboratory mice and rats (such as *P. yoelii*, *P. vinckei*, *P. berghei* and *P. chabaudi*, all originally found in thicket rats in Africa), and those that infect rhesus monkeys, namely *P. knowlesi* (*P. falciparum*-like) and *P. cynomolgi* (*P. vivax*-like). *P. falciparum* causes the most cases of malaria in humans, followed by *P. vivax*. The most serious cases, and hence also the most deaths due to malaria, are caused by *P. falciparum*. The parasite is transmitted to humans by female anopheles mosquitoes. There are currently at least 40 anopheline species known to transmit human malaria, and the species vary in their transmission potential. The maps in **Figure 1** illustrate the most recent estimates of the incidence of clinical malaria episodes caused by any species, and those caused by *P. falciparum.*

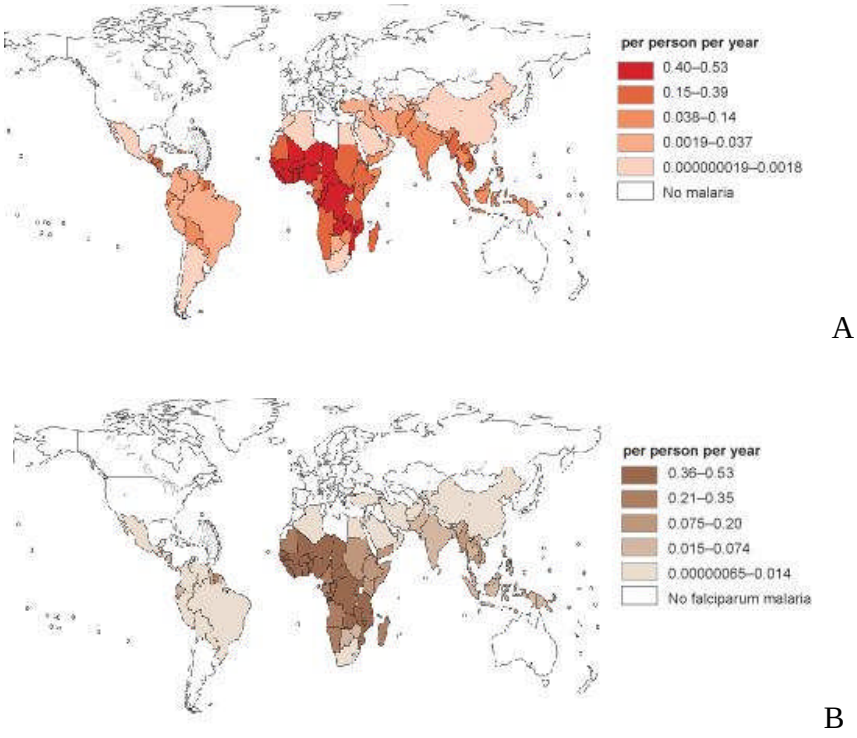

Figure 1: (A) Incidence of clinical malaria episodes per person per year (all species). (B) Incidence of *P. falciparum* malaria per person per year. (World Malaria Report 2005) [1]

1.1.1.3 Life cycle

The parasite has a complex life cycle which requires both the human and the mosquito host for its successful completion. The life cycle is illustrated in **Figure 2**. When an infected mosquito feeds on human blood, the parasite enters the body in the form of sporozoites (A) which travel very quickly to the liver. The sporozoites are then believed to migrate through several hepatocytes [2] before invading a hepatocyte by the formation of a parasitophorous vacuole (B). The migration through the cytosol of liver cells is necessary to activate the sporozoites for invasion [3]. Within the parasitophorous vacuole, the sporozoites are able to differentiate and undergo asexual multiplication to produce thousands of merozoites - the next infective stage of the parasite life cycle. The length of the stage depends on the species but takes, for example, approximately 14 days in the case of *P. falciparum*. The merozoites then burst out of the hepatocyte (C) and begin to invade erythrocytes. Inside red blood cells, the merozoites differentiate into trophozoites, which use the erythrocyte's haemoglobin to replicate their nucleus, and form 12-16 new merozoites. During this stage, the parasite also directs the formation of

'knobs' on the surface of the red blood cell that makes the infected cell 'sticky' and helps to fix it to a blood vessel wall, so that it cannot be easily transported to the spleen and destroyed. The build-up of these 'sticky' erythrocytes in a blood vessel can block circulation and can lead to coma or death in cerebral malaria. When a certain concentration of merozoites has been formed, the erythrocyte is ruptured, releasing merozoites which are able to reinvade new erythrocytes and recommence the cycle of multiplication. This cycle takes approximately two days in infections of *P. falciparum*, *P. vivax* and *P. ovale*, and three days for *P. malariae*. This is the stage of the disease at which the symptoms of malaria – cycles of fever and chills begin to occur. Approximately ten days after the first invasion of erythrocytes, some of the merozoites are able to mature into male and female gametocytes (E). If taken up by a feeding mosquito, the male microgametes fertilize the female macrogamete to produce a zygote (F). After further maturation (G) (the whole process taking 10-15 days), sporozoites are once again available in the mosquito's salivary glands for invasion of a human host (H).

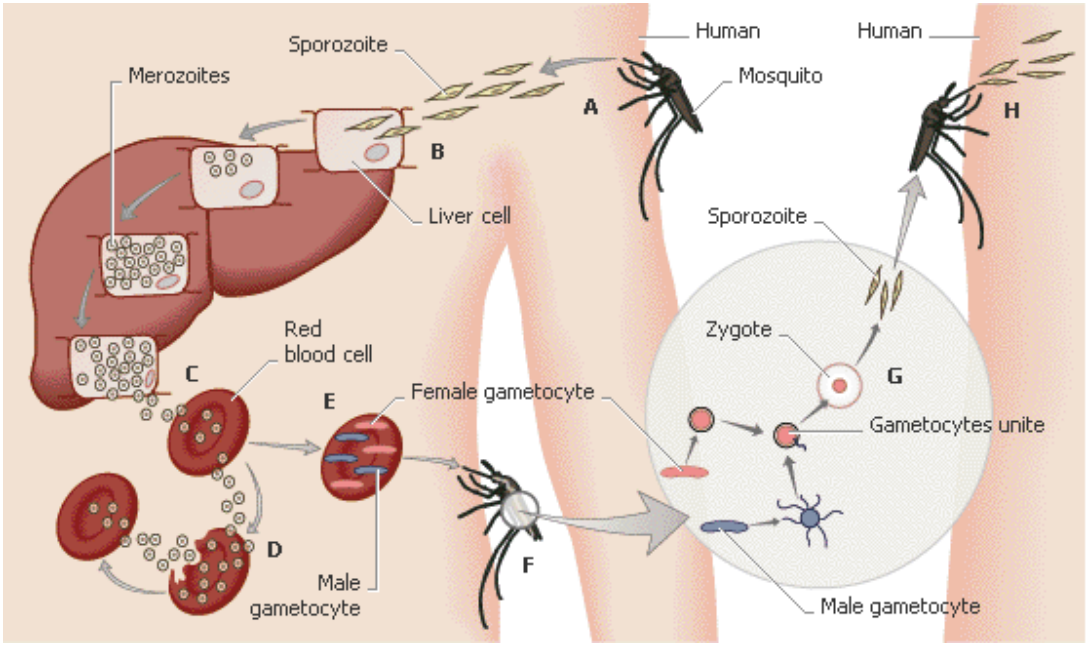

Figure 2: Malaria Life Cycle [4].

1.1.1.4 Current Control Policies

As with most diseases, malaria control policies must focus both on prevention and treatment. In the case of malaria, transmission can be prevented by preventing infected mosquitoes from biting, or the parasite could be prevented from causing the disease once it reached the human. Treatment targets the parasite which is already present in the body. A very important aspect of current prevention policies is the use of insecticide-treated mosquito nets. This is a simple and effective general control method, as long as the nets are retreated with insecticide as frequently as necessary. Traditional nets need retreating roughly every year, whereas nets developed more recently can remain effective for up to 5 years. The insecticide treatment is necessary because mosquitoes are able to bite through untreated nets in order to feed on human blood. Untreated nets can also divert extra biting to people in the same room who are not protected with nets [5], whereas treated nets would be expected to improve protection for all inhabitants.

Mosquitoes can also be controlled by indoor insecticide spraying, which is particularly important for reducing rates of transmission in times of epidemic. Unfortunately, development of insecticides for such purposes has struggled to keep up with the emergence of insecticide-resistant insects.

Travellers to malaria-endemic areas are obviously also advised to avoid mosquito bites, but should also take antimalarial drugs (chemoprophylaxis) to prevent any possible infection from developing into disease. The drug to be taken depends on the region to be visited, due to the varying occurrence of drug resistance.

Malaria has been treated in the past using traditional drugs which fall into two broad classes according to their targets in the parasite. Antifolates, along with naphthoquinones, interrupt nucleic acid metabolism within the parasite [6, 7]. Quinolines interfere with the detoxification of haem within the parasite. The antifolates inhibit enzymes of the folate pathway, thus decreasing pyrimidine synthesis and therefore reducing DNA, serine and methionine formation. Quinolines are believed to prevent the polymerisation of haem which is used by the parasite as a detoxification mechanism. Therefore the parasite is believed be poisoned by the haem produced as a side product of its feeding on haemoglobin.

Unfortunately, there are now many strains of *P. falciparum* that have developed

resistance to the traditional drugs such as the quinolines chloroquine and mefloquine, and the antifolate combination sulfadoxine-pyrimethamine [7]. The map in **Figure 3** shows areas where *P. falciparum* resistance to drugs has been found. Current World Health Organization policy recommends the use of artemisinin-based combination therapies (ACTs) as the most highly efficacious treatment method currently available [8].

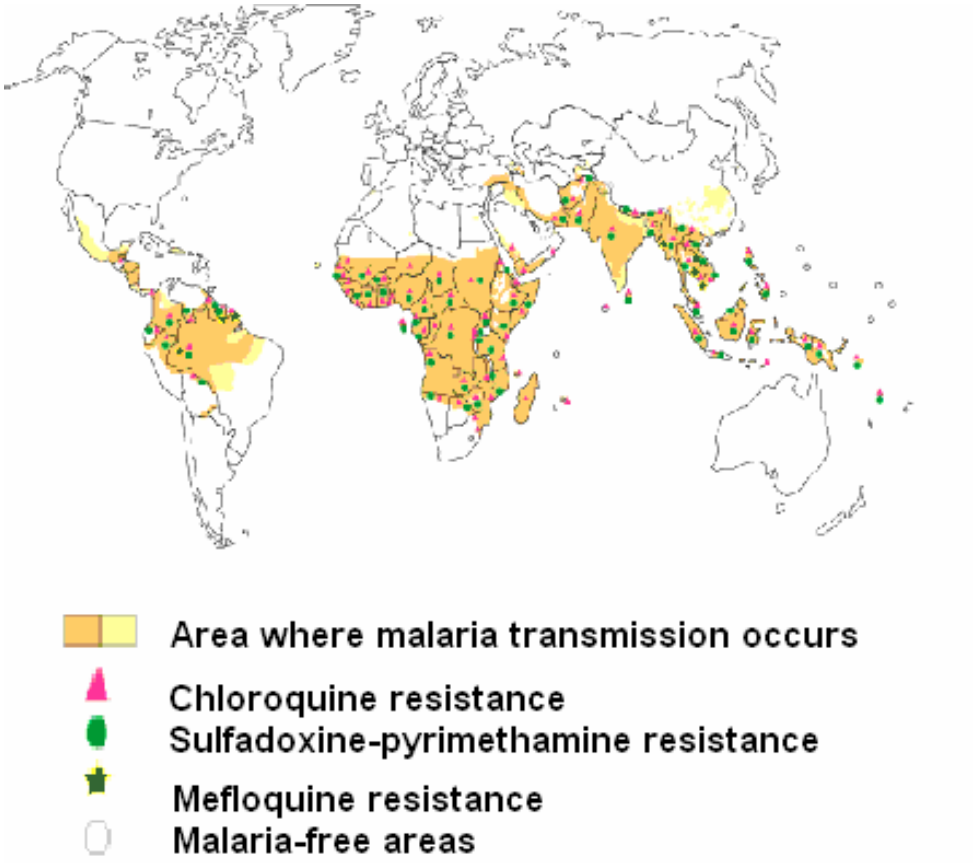

Figure 3: Worldwide occurrence of *P. falciparum* resistance to traditional antimalarials. (World Malaria Report 2005)[1]

Artemisinin is an interesting compound with an unusual endoperoxide bridge (**Figure 4**) [9]. It is extracted from the plant *Artemisia annua*, which is mainly cultivated in China and Vietnam, and has been used for many centuries in traditional Chinese medicine as a treatment for the symptoms of malaria. Artemisinin and its derivatives are believed to act by inhibiting the action of the ATPase PfATP6 [10], and the endoperoxide bridge has been shown to be essential both for the inhibitory and for the antimalarial action [10]. Although artemisinin is able to rapidly kill all asexual stages of *P. falciparum*

when acting alone [11], its use in combination with conventional drugs is recommended for several reasons. For example, it has been shown in studies in South-East Asia that combinations of artemisinin compounds with some synthetic drugs can produce high cure rates after only 3 days of treatment, compared to around 7 days of treatment when artemisinins are used alone [8]. There is also evidence that the development of resistance to the partner drug can be slowed down to a great extent by using it in combination with artemisinin [12]. In general, derivatives of artemisinin are used in therapy, due to their superior pharmacological properties. For the preparation of these deriviatives, artimisinin is extracted from *Artimisia annua*, and reactions are carried out on the extract, as the *de novo* synthesis of the compounds has proved extremely difficult. However, drug discovery projects are underway to discover synthetic peroxide antimalarial drugs, and a promising candidate has recently been identified [13].

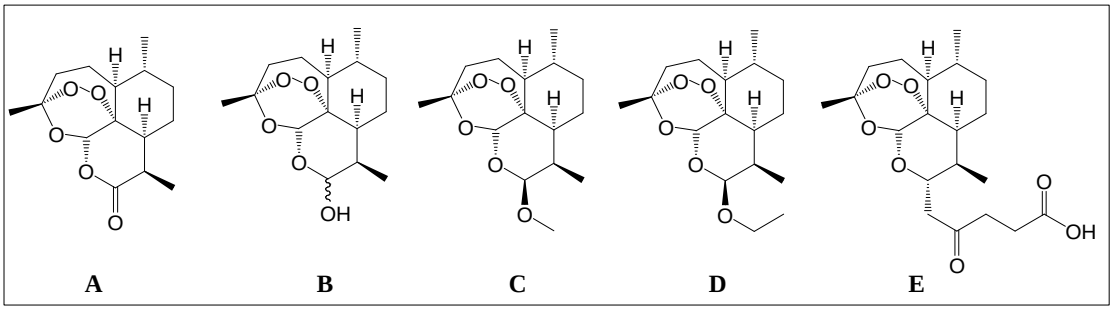

Figure 4*:* Artemisinins. **A:** artemisinin, **B:** dihydroartemisinin, **C**: artemether, **D**: arteether, **E**: artesunic acid (artesunate)

Although artemisinin-based combination therapies are still effective at the moment, and only isolated cases of resistance to artemisinin derivatives, in vitro, have been reported [14], we must expect that strains of the parasite will develop resistance to these compounds at some stage in the future. Also, anopheline species must be expected to continue to develop resistance to currently-used insecticides. Therefore there must be continued and relentless research into new possible preventive measures and treatments, and the development of a malaria vaccine must form an important part of this research.

1.1.1.5 Vaccine development

Despite the global impact of malaria, and the clear advantages of vaccines as a method of control of infectious diseases, no malaria vaccine is as yet approved or

available for use. This fact does not represent a lack of interest in or of research effort towards a vaccine, but is rather due to a complex combination of several other factors. A major obstacle is the complexity of the parasite's life cycle. The parasite presents different antigens to the immune system at different stages of its life cycle, and thousands of antigens are presented throughout the course of a *Plasmodium* infection. It is difficult to pinpoint which antigens could be key to an effective vaccine, and it is to be expected that a fully effective vaccine would target more than one stage of the life cycle, so that any parasite 'escaping' the immune response at one stage could be 'caught' at a later stage. Infections of several strains of the same species, or indeed of more than one species, can occur simultaneously, so an effective vaccine would also need to be as general as possible, rather than strain-specific.

In 1967, it was reported that mice immunized with radiation-attenuated *P. berghei* sporozoites were protected against subsequent challenge with fully infectious sporozoites [15]. Studies were then carried out in humans during the 1970s, and the same effect was found [16-19]. It was possible to protect volunteers from *P. falciparum* challenge by immunizing them with the bites of irradiated mosquitoes carrying *P. falciparum* sporozoites in their salivary glands. These investigations demonstrated that a malaria vaccine offering protective immunity was feasible. It has also been shown that non-immune individuals who receive immunoglobulins from volunteers with naturally acquired immunity are subsequently protected against infection. Additionally, as previously mentioned, people living in malaria endemic areas gradually obtain immunity to severe disease and even to mild disease, over several years when regularly exposed to infection [20] – also a good indication of the possibility of a working vaccine.

The role of a vaccine is to prepare the immune system to work quickly and effectively in the case of a true infection, by presenting antigens to it in a 'harmless' form so that the antigens can be promptly dealt with in subsequent 'real' attacks. Vaccines that are currently approved and used occur in a number of forms. Some consist of live, attenuated or intact, killed viruses or bacteria (for example the polio, typhoid and chickenpox viruses [21]), others involve purified antigens.

Based on the knowledge that attenuated sporozoites can induce clinical immunity, it would seem reasonable to develop a method for the use of sporozoites in a vaccine. However, there would be many practical problems to overcome in this approach. The

sporozoites must be delivered live either via mosquito bites (studies suggested that the best protection was obtained when volunteers were immunized with more that 1000 bites [22]), or intravenously. The delivery of vaccine by mosquito bite would not be practicable, and all vaccines that are currently used as public health measures are administered by intradermal, subcutaneous or intramuscular methods. There would also be difficulties in producing a vaccine in mosquitoes that would meet safety requirements.

An obvious place to look when seeking an effective vaccine is at the naturally-acquired immunity of people living in endemic areas. It is believed that acquired immunity to malaria is probably due to low to moderate responses to many antigens [23]. However, the development of a vaccine containing a cocktail of many antigens, aiming to mimic natural immunity, could be a very complex and costly venture. Research activity has therefore focussed on the development of a vaccine presenting a few antigens, which would therefore need to induce stronger and longer-lasting immune responses than are observed in naturally-acquired immunity. Some of the antigens that have been investigated as possible components of a subunit vaccine will now be discussed.

1.1.1.6 Subunit vaccines

As discussed earlier, an effective subunit vaccine would probably target more than one stage of the *Plasmodium* life cycle. However, the individual antigens to be used can be classed according to the stage of the life cycle that they would target.

Firstly, a vaccine candidate could target pre-erythrocytic stages. The immune response elicited by immunization with irradiated sporozoites involves both neutralizing antibodies that recognize the surface of sporozoites, and cell-mediated mechanisms that inhibit liver-stage (exoerythrocytic stage) development[24]. Antibody-mediated protection could be elicited by targeting sporozoite surface molecules. The most intensively studied sporozoite surface antigens are the circumsporozoite (CS) protein, and the thrombospondin-related anonymous protein (TRAP). The CS protein is a very abundant sporozoite surface antigen, and neutralizing antibodies against it are found for all malaria species [25]. CS plays an important role in the development of sporozoites in the mosquito [26] and in the early stages of hepatocyte invasion. CS proteins from different *Plasmodium* species have common structural features, which include a signal peptide, a central repeat domain and a C-terminal hydrophobic sequence [27]. The central region of

CS consists of tandem repeat regions, the sequence of which is species-specific (**Figure 5**). This tandem repeat region contains the immunodominant B-cell epitopes. In *P. falciparum*, the repeat motif comprises 37 tandem repeats of the tetrapeptide Asn-Ala-Asn-Pro (NANP), interspersed with four copies of Asn-Val-Asp-Pro (NVDP). The B epitope $(NANP)_3$ is found in all isolates of *P. falciparum* from all over the world [28], and monoclonal antibodies to the repeat regions inhibit sporozoite cell invasion.

Figure 5: Schematic representation of the sequence of circumsporozoite protein. The flanking regions R1 and R2 are highly conserved among different species.

A CS-based vaccine, RTS,S/AS02A, is currently the most advanced malaria vaccine candidate in clinical development, and has been shown to reduce risk of clinical malaria and to reduce episodes of severe malaria in African children [29]. Although this vaccine has as yet only been shown to confer partial protection, the results confirm that a malaria vaccine can become a credible control tool. It has been shown that TRAP is present on the plasma membrane of the parasite, and is required for cell invasion [30]. Unfortunately, it seems that most TRAP molecules are released when the parasite makes contact with hepatocytes, and a tight junction is established between the extracellular domain of TRAP and the cellular receptors. At this stage, therefore, antibodies to TRAP are ineffective in sporozoite neutralization [31].

Liver stage antigens are attractive targets because the liver stage of the parasite remains in the liver for at least one week, without symptoms of clinical malaria occurring. However, there could be some difficulty in delivery of a vaccine targeting liver stage antigens. It has been shown that intra-splenic injection of infected liver cells into mice can elicit sterile immunity without the presence of antibodies [32], and that administration of a virus expressing a cytotoxic T cell epitope of *P. yoelii* CS can induce protective immunity in mice [33]. Studies have shown that immunization of non-human primates with liver stage antigen 3 (LSA-3), which is a well-conserved blood stage as well as a liver stage antigen, could induce protection [34]. It is hoped that heterologous prime-boost methods could help to induce a good T-cell response to liver-stage antigens. This technique involves the delivery of the same antigen in two different vectors, for example, first ‘priming’ with a DNA vaccine, then ‘boosting’ with the same antigen in a

viral vector [35].

The next stage to be considered would be the blood stage**.** Vaccines aimed at the blood stage of the malaria life cycle, that is, at the merozoite, would not prevent infection, but if they could interfere with the entry of the merozoite into the red blood cells, they would prevent the clinical symptoms of the disease from occurring. Important targets are proteins believed to be involved in the recognition and initial contact between merozoites and red blood cells, as well as proteins that play important roles in the fusion of the merozoite and red blood cell membranes. Many merozoite surface antigens have been identified and studied, some of the most important being apical membrane protein 1 (AMA 1), merozoite surface protein 1 (MSP 1), merozoite surface protein 2 (MSP 2), merozoite surface protein 3 (MSP 3), glutamate rich protein (GLURP) and serine repeat antigen (SERA).

Finally, the sexual stages of the parasite's life cycle could be targeted. Vaccines aimed at the sexual stages of the malaria life cycle would not protect the individual who was immunized, but would help to reduce transmission of the disease. The aim would be to produce antibodies against the gametocytes, which would then be taken up by the mosquito in a blood meal, along with the gametocytes, and would block the fertilization step. This would prevent further development of the parasite – it would not be able to produce mature sporozoites, and therefore transmission would be blocked. A vaccine aimed at sexual stages of the parasite's life cycle, in combination with targets at other stages of the life cycle, could be an important tool in the battle against the spread of malaria. Another target under consideration is the mosquito itself (so-called anti-mosquito vaccines). Trials carried out with *Plasmodium vivax* Pvs25 [36] and *Plasmodium falciparum* Pfs25 [37] have shown promising results, and another antigen, P28, has been shown to be essential for the infection of mosquitoes, and is also considered a very important candidate.

1.1.2 Vaccine formulation

1.1.2.1 Adjuvants

As early as 1926, Glenny and co-workers discovered that diphtheria toxoid

precipitated with alum represented a better vaccine than the toxoid alone [38]. In general, most antigens, for example proteins or peptides, have only limited immunogenicity when they are used as pure substances, and much research has been carried out into methods for inducing a better immune response, since the first use of adjuvants in the form of aluminium salts. One of the most famous adjuvants, complete Freund's adjuvant (CFA) was developed in 1937, and is an oil-in-water emulsion containing killed mycobacteria. Vaccine components derived from pathogenic bacteria, such as derivatives of lipid A, or lipopeptides, induce an innate immune response which is crucial for the subsequent activation of the adaptive immune response. The set of structures that can induce such a response is termed pathogen-associated molecular pattern (PAMP), and includes microbial cell wall components, microbial structural proteins and microbial nucleic acids [39]. Many PAMPs have been investigated as possible adjuvants, and at least one vaccine using a PAMP, mono-phosphoryl lipid A (MPL), has been approved for use [40]. The signal instructing the adaptive immune system to take an attack seriously can either be a danger signal provided by the pathogen, such as the PAMPs described above or a microbial toxin, or it can be in the form of a substance released by the host itself. Therefore, there has been recent interest in the possibility of employing host-derived substances as adjuvants, in particular the so-called heat shock proteins (HSPs) that seem to possess very good immunological properties. The role of HSPs is to bind to hydrophobic stretches of denatured proteins, in a variety of stress situations, in order to prevent their aggregation. As well as this chaperone function, HSPs initiate either the refolding of their substrate, or the proteolytic degradation if the unfolding was irreversible. Due to their chaperone function, heat shock proteins can act as peptide carriers, and HSP-peptide complexes have been shown to have a very strong immunogenic potential [38]. Studies have shown that HSP-based immunization therapy using a personalized tumour vaccine is well tolerated and can produce favourable results, but the techniques have not yet been fully evaluated [41].

It has been shown that some of the reactivity induced by immunization with DNA plasmid vaccines is not due to the antigen sequence, thus, DNA plasmid vaccines can be said to be acting as an intrinsic adjuvant as well as encoding the antigen DNA [39].

1.1.2.2 Particulate vaccine delivery systems

The Freund's adjuvants mentioned earlier can be considered as particulate adjuvants, since they contain 'particles' of oil in water. There has been much research in recent years into microparticles as vaccine delivery systems. It has been shown that an adjuvant effect occurs when antigens are linked to synthetic particles. The use of polylactide-coglycolides (currently used as controlled-release drug-delivery systems) to encapsulate antigens [42], and also the adsorption of antigens on similar particles has been the subject of recent research. Another interesting approach is the use of recombinant proteins that self-assemble into particulates.

An obvious method for delivering pure antigens to the immune system, whilst retaining immunogenicity, is to include the antigen in a particle that looks like a pathogen. Liposomes and virus-like particles are important examples of this type of delivery system, which also includes cochleates and immune-stimulating complexes (**Figure 6**).

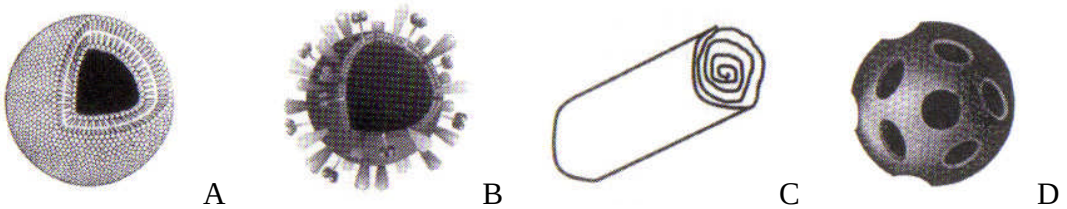

Figure 6: Schematic representations of (A) a lipsome; (B) a virosome; (C) a cochleate; (D) an immune-stimulating complex.

Classical liposomes do not elicit a very strong immune response, but their effectiveness as a delivery system can be enhanced by the inclusion in the lipid bilayer of amphiphilic adjuvants, such as the monophosphoryl lipid A mentioned earlier. Cochleates differ from most other liposome-related delivery systems in that they are not spherical. They consist of bilayer sheets containing phosphatidyl ethanolamine, phosphatidyl serine and cholesterol. They also contain calcium ions intercalated with the bilayers. Immune-stimulating complexes are made up of saponin, cholesterol and phospholipid, and the amphipathic antigen is usually included during the preparation, and the products have a cage-like structure.

1.1.2.3 Immunopotentiating reconstituted influenza virosomes (IRIVs)

Research in the Robinson group has focused on the use of immunopotentiating reconstituted influenza virosomes (IRIVs) for vaccine delivery. IRIVs are small unilamellar vesicles with a mean diameter of 150 nm (**Figure 7**).

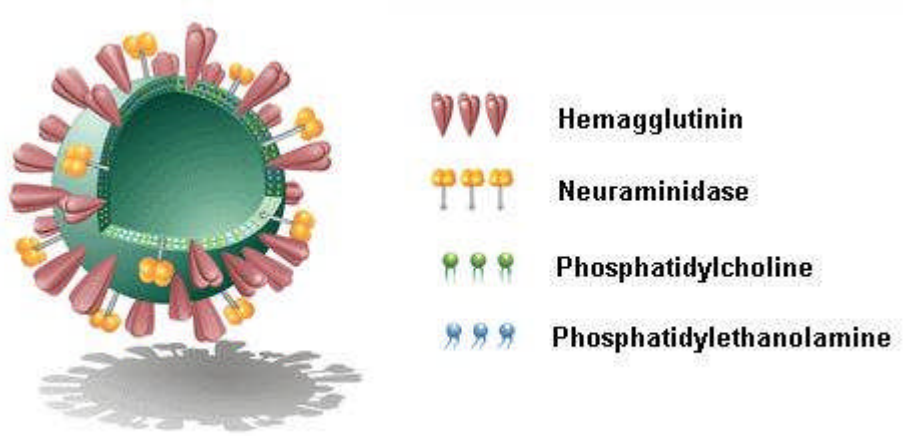

Figure 7: Schematic representation of an immunostimulating reconstituted influenza virosome.

The virosomes represent reconstituted empty influenza virus envelopes, devoid of the genetic material of the source virus, so they are unable to replicate but are fusion-active due to the presence of the influenza glycoproteins. More specifically, the IRIV vesicle is constituted of phosphatidylcholine and phosphatidylethanolamine, with functional viral envelope glycoproteins: hemagglutinin (HA) and neuraminidase (NA) intercalated in the phospholipid bilayer. The influenza viral envelope proteins are important both for the stability of the virosome and for its immunological properties [43]. Influenza viruses enter cells via receptor-mediated endocytosis, and virosomes have been shown to act in the same way [44]. The influenza HA is believed to play an important role in binding to receptors on antigen-presenting cells, to initiate a successful immune response, and also to mediate the fusion of virosomal and endosomal membranes, to initiate the infection of cells.

The composition of virosomes allows different models of antigen incorporation, depending on properties of the antigen and the required type of immune response.

Antibodies may be adsorbed on the surface, encapsulated in the virosomal cavity, or integrated into the lipid membrane (**Figure 8**).

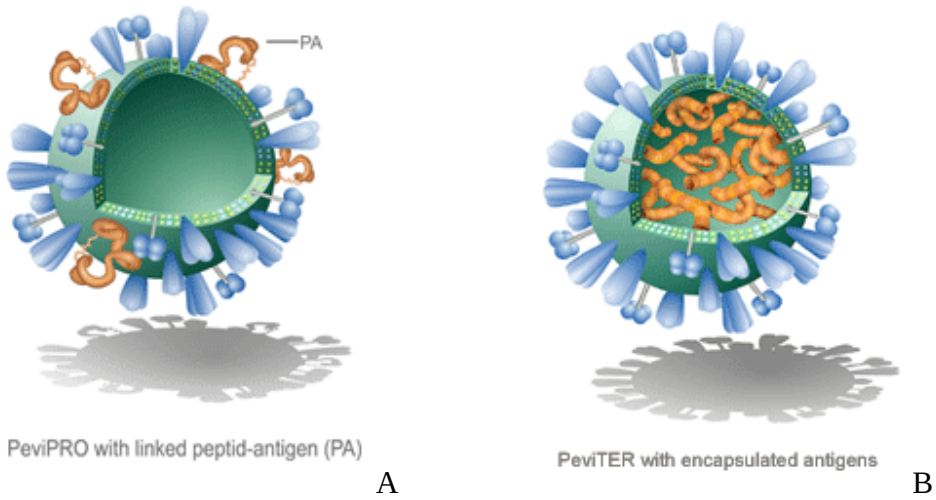

Figure 8: Schematic representation of virosome with antigens integrated into the lipid membrane (A), or encapsulated in the virosomal cavity (B). (see www.pevion.com)

Studies have shown that physical association between the virosomal carrier and the antigen leads to optimal adjuvant effect of the virosome [45]. Depending on the location of the antigens, virosomes can activate either a B-cell or a T-cell response. Antigens linked to the virosomal surface are degraded within the endosome and peptide fragments are presented to the immune system by MHC class II receptors, activating $CD4^+$ helper T cells, which in turn activate a B cell response. Antigens encapsulated within a virosome are delivered to the cytosol during fusion and are presented by MHC class I receptors, activating $CD8^+$ killer T cells. In a mouse model, the use of synthetic conformational malaria B-cell epitopes to induce highly specific antibodies has been demonstrated [46, 47]. In our studies, peptide mimetics of malaria antigens are bound to a phospholipid moiety so that the phospholipid tail can form part of the phospholipid bilayer of the virosome, and the peptide mimetic is displayed to the immune system on the surface of the virosome. This system has already been used for phase 1 clinical trials of circumsporozoite and AMA-1 mimetics designed and developed in our group as part of the malaria vaccine project. There are also already licensed vaccines against influenza (Inflexal V, Berna Biotech) and hepatitis A (Epaxal, Berna Biotech) that make use of the virosome technology.

1.1.3 Epidermal Growth Factor-like Domains

1.1.3.1 Definition

The epidermal growth factor-like module was first sequenced in 1972 [48] within epidermal growth factor itself and it has since become apparent that the module occurs in a wide range of proteins. The domain usually comprises 40-50 residues including 5 to 6 cysteine residues forming two or three disulfide bonds. A domain can be classified as an EGF-like domain if it is consistent with either the general definition (A) or with the rather more stringent consensus pattern proposed by Campbell and Bork [49] (B) which are both outlined in **Figure 9**:

(A) Cysteine and glycine residues in a pattern consistent with the consensus pattern:

$$Cx_nCx_nCx_nCxGx_2C$$

Where: x = any amino acid

n = any number

(B) More stringent consensus pattern proposed by Campbell and Bork:

$$Cx_{2-7}Cx_{1-4}(G/A)xCx_{1-13}ttaxCxCxxGax_{1-6}GxxC$$

Where: t = non-hydrophobic amino acid

a = aromatic amino acid

Figure 9: Consensus patterns defining EGF-like domains [49].

The disulfide bonding connectivities have been confirmed for murine EGF [50], and for many other EGF-like domains, as forming a canonical 1-3, 2-4, 5-6 pattern as illustrated in **Figure 10.**

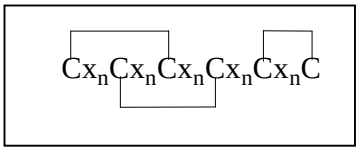

Figure 10: Disulfide bonding pattern of human and murine EGF, and many EGF-like domains.

1.1.3.2 Features

The EGF-like module is found in many proteins in nature, including those involved in cell adhesion, blood coagulation and neural development [49]. Many of them have a membrane-bound precursor, including EGF itself, the heparin-binding EGF-like domain, and *Plasmodium falciparum* merozoite surface protein 1. EGF–like modules are believed to generally be involved in the mediation of protein-protein interactions, and their structures usually show similar features, including stretches of β-sheet [49, 51].

1.1.3.3 Folding pathway

The folding pathway of human EGF [52-54] has been the subject of intensive investigation. Experiments carried out to trap the intermediates formed during the folding of human EGF show that the first two disulfide bonds (the Cys2-Cys4 and Cys5-Cys6 bonds) are formed rapidly, and a stable two-disulfide kinetic trap is obtained. The third disulfide bond (the Cys1-Cys3 bond) is then formed slowly, and can only be formed via substantial unfolding of the two-disulfide protein, despite its already representing a native-like structure. The protein passes through three-disulfide scrambled isomers before the native folded structure is finally attained. Although it is not certain that other EGF-like domains follow an analogous folding pathway, the folding of human EGF has been compared to the folding of other, non-EGF-like, multiply disulfide bonded proteins [55]. The accumulation of predominant intermediates was only seen in the case of EGF, but it was observed that the folding pathways of three other three disulfide-containing proteins also involved scrambled three-disulfide isomers. For three proteins (hirudin, potato carboxypeptidase inhibitor, and tick anticoagulant peptide), but not for EGF, the accumulation of scrambled isomers could be enhanced by including oxidized glutathione or cystine in the folding buffer. A further protein, bovine pancreatic trypsin inhibitor,

whose folding pathway has also been the subject of much investigation, was shown to fold correctly without passing through three-disulfide scrambled intermediates. An interesting point was that, although tick anticoagulant peptide and bovine pancreatic trypsin inhibitor belong to the same family of inhibitors and share structural homology in their disulfide bonding pattern and three-dimensional structure, they follow diverse folding pathways and their disulfide bonds seem to be stabilized in different ways. It would seem, therefore, that at least until many more studies have been performed, it will remain difficult to predict from the native structure of a multiply-disulfide bonded protein, what its folding pathway may be, and indeed which may be the best conditions for obtaining the correctly folded product. Optimal oxidative folding conditions for various proteins are thus usually arrived at by trial and error, based on a few general rules.

1.2 Design, synthesis and characterisation of a merozoite surface protein-1 mimetic

1.2.1 Merozoite surface proteins

To date, ten *Plasmodium falciparum* merozoite surface proteins (MSPs) have been identified, and they can be divided into two groups: proteins that are linked to the merozoite membrane via a glycosylphosphatidylinositol (GPI) anchor (MSP-1, 2, 4, 5, 8 and 10) and those that are soluble and, in some cases, non-covalently associated with the merozoite surface (MSP-3, MSP-6, MSP-7 and MSP-9) [56]. It is interesting to note that all of the GPI-anchored MSPs, except MSP-2, contain either one or two EGF-like domains at the C-terminal end. It therefore seems possible that these MSPs could be involved in important protein-protein interactions, as has been demonstrated for other EGF-like domains. However, the exact function of the EGF-like domains on the merozoite surface remains unknown. The location of these proteins on the surface of merozoites means that they are exposed to the immune system during the blood stages of malaria, and have therefore been extensively studied as possible targets for the development of a blood-stage malaria vaccine.

1.2.2 Merozoite surface protein 1

The first *Plasmodium* MSP to be discovered was MSP-1, which is therefore also the most intensively studied and the best characterised of the merozoite surface proteins. *Plasmodium falciparum* MSP-1 is expressed as a ~200 kDa protein with a GPI anchor, and is processed in two proteolytic steps before invasion of the human erythrocyte. In the first step, the protein is cleaved into four fragments of 83 kDa (N-terminal fragment), 30 and 38 kDa (central fragments) and 42 kDa (C-terminal fragment) (**Figure 11**). The C-terminal fragment, MSP-1_{42}, remains linked to the merozoite surface via the GPI anchor, and the other fragments remain associated with the merozoite surface as a non-covalent complex [57, 58]. In the second proteolytic step, which seems to occur just before or at the point of erythrocyte invasion a further 33 kDa fragment is shed from the GPI-anchored

protein, to leave a 19 kDa fragment attached to the membrane [59, 60].

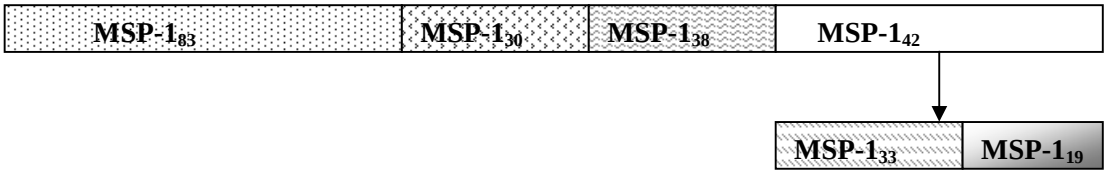

Figure 11: Schematic representation of the fragments formed during proteolytic processing of MSP-1.

The 19 kDa fragment, MSP-1_{19} is the only part of the protein that is carried into the invaded erythrocyte, and the final processing step is believed to be essential for the invasion of erythrocytes [61]. MSP-1_{19} is a well-structured protein consisting of two EGF-like domains [62]. The solution structure of *P. falciparum* MSP1_{19} has been calculated from NMR studies (**Figure 12),** and the crystal structure of *P. cynomolgi* MSP-1_{19} has also been determined [51, 63].

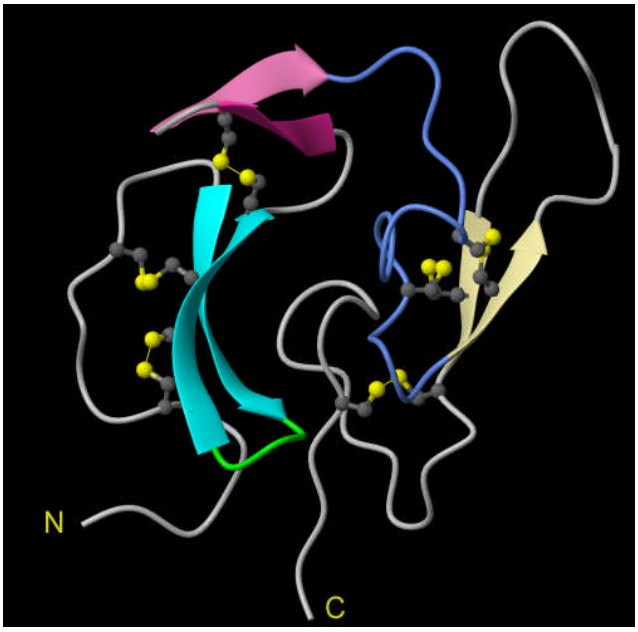

Figure 12: Solution NMR structure of MSP-1_{19}.

MSP-1 is believed to be one of the most abundant merozoite surface proteins and is evenly distributed on the surface of the merozoite [64, 65], which suggests that it may play an important role in the initial interaction of the merozoite with the red blood cell.

The protein appears to be essential for the invasion of the erythrocyte and for the survival of the parasite, as it has not been possible to knock out the gene [56]. Further evidence for its importance in invasion is that antibodies directed against MSP-1 have been shown to prevent erythrocyte invasion in vitro. It has also been demonstrated that immunisation with recombinant MSP-1_{19} or MSP-1_{42} provides protection against subsequent parasite challenge in mice and monkeys [66-70]. The presence of antibodies to MSP-1_{19} in exposed adults is associated with clinical immunity [71], and some human antibodies to MSP-1_{19} possess parasite growth-inhibitory activity [72]. The binding of protective antibodies to MSP-1 inhibits the second proteolytic processing step, and it has been suggested that the blocking of this step is the basis of their protective function [73].

Several monoclonal antibodies (mAbs) specific to MSP-1_{19} have been identified [64] and these can be sorted into three classes. Some mAbs, as described, inhibit MSP-1 processing and erythrocyte invasion. These are called inhibitory antibodies. Other antibodies interfere with the binding of inhibitory antibodies by competing with the inhibitory antibodies for binding on the merozoite surface. These allow the secondary processing step and erythrocyte invasion to take place [74] and are called blocking antibodies. The third class consists of the neutral antibodies that bind to MSP-1 but neither inhibit invasion nor block the inhibitory action of inhibitory antibodies.

Some MSP-1_{19} monoclonal antibodies have been studied in detail by several groups, using various methods including site-directed mutagenesis, TROSY NMR and PEPSCAN [75, 76]. These investigations show that some of the inhibitory antibodies studied bind only to the first (N-terminal) EGF-like domain of MSP-1_{19}, whereas others require both domains in order to bind, and are probably binding to a non-continuous conformational epitope involving both domains. It has also been shown that known blocking antibodies bind to the same regions as the inhibitory antibodies [77, 78]. However, in the mutagenesis studies, it was demonstrated that all of the antibodies studied (a selection of inhibitory, blocking, and neutral) showed a different response to the various mutations [76]. That is, no two antibodies showed the same pattern of binding to the range of mutant proteins tested. This suggests that even antibodies binding to the same region recognise slightly different epitopes. It is interesting to note that it was possible, based on information from the first round of mutations, to design a mutant protein to which only the inhibitory antibodies studied, and none of the blocking

antibodies, could bind [76]. This gives rise to the hope that it would eventually be possible to design a mimetic that would induce only (or at least predominantly) inhibitory antibodies.

1.2.3 Mimetic Design

As well as the established importance of this antigen in erythrocyte invasion, *Plasmodium falciparum* MSP-1_{19} was chosen as a good potential vaccine candidate because of its low polymorphism (only 5 dimorphic sites, as illustrated in **Figure 13**), and because antibodies to this region are found in most malaria-exposed individuals. Both of these points suggest that it could be an important component in a broad-range malaria vaccine.

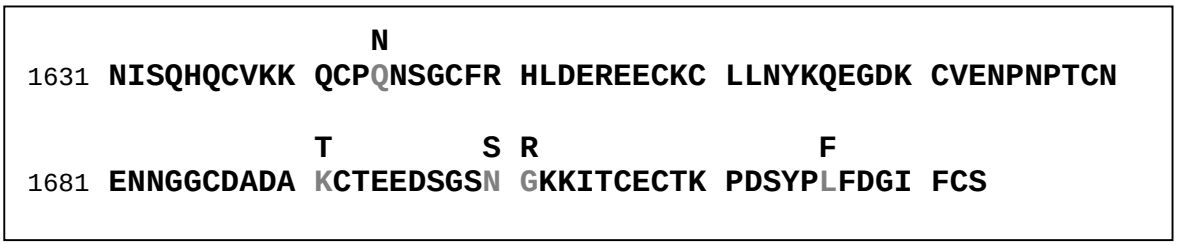

Figure 13: The sequence of the C-terminal region of MSP-1 for the Wellcome strain of *P. falciparum* is shown. Residues in grey are dimorphic sites, and the possible amino acids found in different strains are given above.

In initial work in the Robinson group, several co-workers were involved in the design and synthesis of mimetics of the three hairpin loops highlighted in the NMR structure of MSP-1_{19} in **Figure 14** [79, 80]. The sequence of these loops was transplanted onto a ^{D}Pro ^{L}Pro, template, in order to induce a hairpin-like structure, and the mimetics were produced bound to a phospholipid linker, to make them suitable for inclusion in virosomes for immunization studies. Unfortunately, these early mimetics failed to induce antibodies which could recognise the parasite, and so did not represent good vaccine candidates.

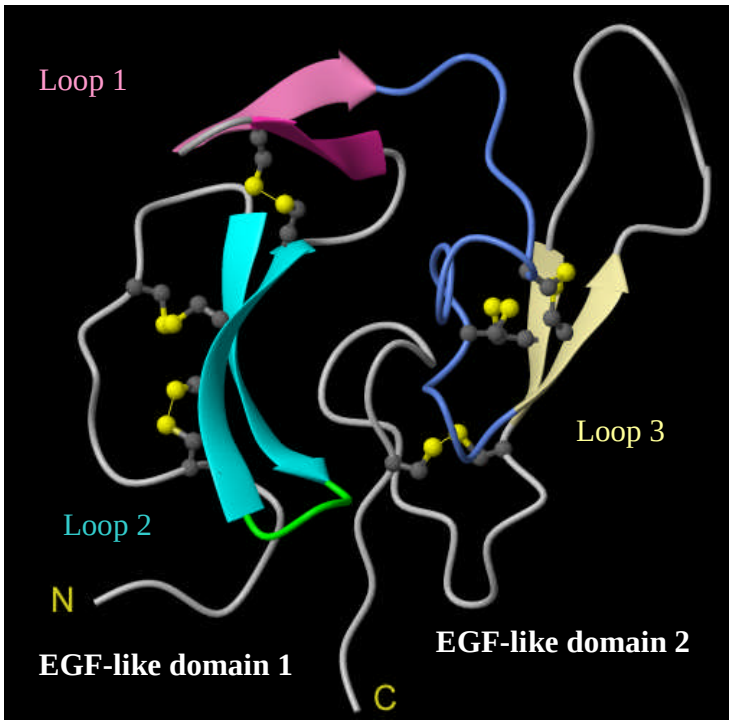

Figure 14: NMR structure of *P. falciparum* MSP-1_{19} highlighting the two EGF-like domains and the loops on which the first MSP-1 mimetics were based.

Studies have shown that the disulfide bonds in MSP-1_{19} are crucial to its immunological properties [78], therefore, the next logical step was to produce mimetics containing disulfide bonds. Efforts were concentrated on the first EGF-like domain, since several antibodies had been shown to bind exclusively to this domain. Also, only one of the five dimorphic sites appears in this domain. A first series of mimetics was designed and synthesised containing either no, one or two disulfide bonds, based on the first 30 residues of the sequence. Unfortunately, as before, these mimetics failed to induce antibodies that could recognise the parasite. Therefore, in a final effort to develop a good vaccine candidate based on MSP-1_{19}, it was decided to synthesise the whole of EGF-like domain 1 as a phospholipid-bound peptidomimetic.

NISQHQCVKKQCPQNSGCFRHLDEREECKCLLNYKQEGDKCVENPNPT-NH_2

Figure 15: Amino acid sequence of peptide **1**, a proposed MSP-1_{19} domain 1 mimetic.

It was decided to initially synthesise the peptide sequence of EGF-like domain 1

of MSP-1 (**Figure 15**) without any phospholipid anchor, in order to establish optimal oxidative folding conditions for the peptide. A method has already been presented in the literature [81] for the synthesis of MSP-1_{19} domain 1. This method involved an orthogonal protecting group strategy, where two cysteine residues were protected with Acm groups, and the other four with Trt groups. Under acidic cleavage conditions, the Trt side chain protection was removed and the peptide could be oxidized to give a two-disulfide intermediate. In a second step, the Acm groups were removed and the third disulfide bond was formed in the presence of iodine. The strategy is briefly outlined in **Scheme 1**.

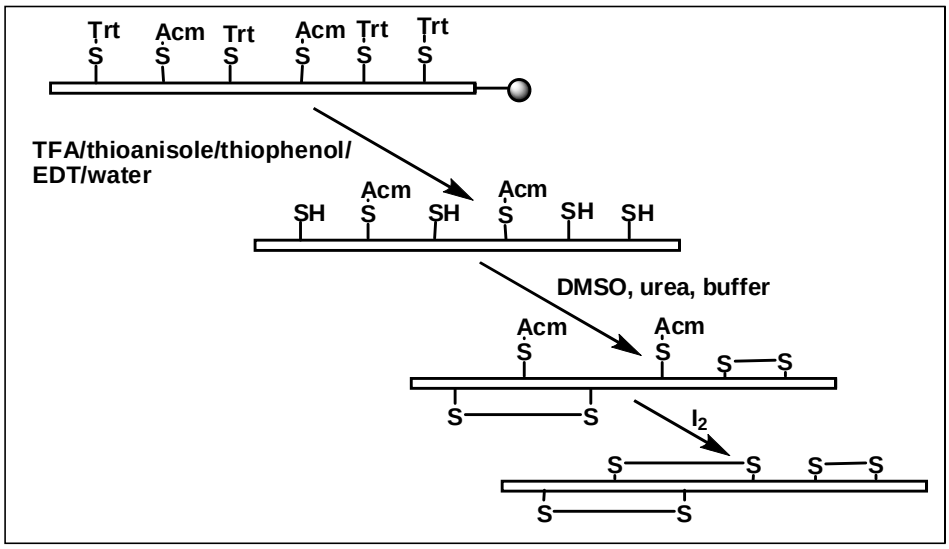

Scheme 1: Illustration of the two-step oxidation method developed by Spetzler et al. for the synthesis of the first EGF-like domain of MSP-1_{19} [81]

Encouraged, however, by the many descriptions of successful folding of multiply disulfide-bonded proteins and peptides in the literature [82-89] we decided to attempt a one-step oxidative folding of the synthetic peptide, in an effort to reduce time and yield losses due to intermediate purification steps – an important consideration should the mimetic eventually be developed as a commercial product. Therefore, the same protecting group was used for all cysteine residues in our synthesis.

1.2.4 Results

1.2.4.1 Peptide synthesis

The assembly of the 48-mer peptide, containing 6 Trt-protected cysteine residues, was carried out on the solid phase using an ABI-433A peptide synthesiser and the Fmoc strategy, illustrated in **Scheme 2**. The sequence was assembled on Rink Amide MBHA resin, which releases a C-terminal amidated product on acid-mediated peptide cleavage. The amino acids used were Fmoc-Asn(Trt)-OH, Fmoc-Ile-OH, Fmoc-Ser(^{t}Bu)-OH, Fmoc-Gln(Trt)-OH, Fmoc-His(Trt)-OH, Fmoc-Cys(Trt)-OH, Fmoc-Val-OH, Fmoc-Lys(Boc)-OH, Fmoc-Pro-OH, Fmoc-Gly-OH, Fmoc-Phe-OH, Fmoc-Arg(Pbf)-OH, Fmoc-Leu-OH, Fmoc-Asp(^{t}Bu)-OH, Fmoc-Tyr(^{t}Bu)-OH, Fmoc-Glu(^{t}Bu)-OH and Fmoc-Thr(^{t}Bu)-OH. The synthesis was carried out on a 0.25 mmol scale, and a capping step was introduced from the 20th coupling cycle onwards in order to block unreacted amine groups. This step is important in the synthesis of long peptides, as it reduces the number of side-products of similar molecular weights to the desired product and leads therefore, in most cases, to a significantly simplified purification process.

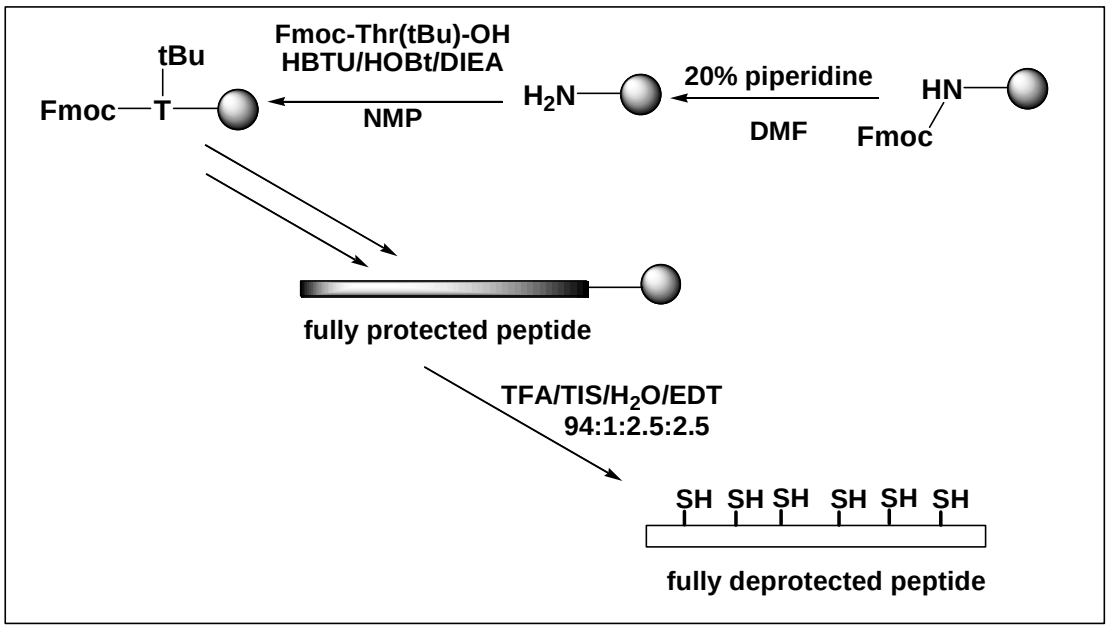

Scheme 2: Fmoc strategy for solid-phase peptide synthesis

After assembly, the full peptide sequence was cleaved from the resin and the side chains were fully deprotected in one step, using 2.5% EDT, 2.5% water and 1% TIS in trifluoroacetic acid. Analytical RP-HPLC showed that one main product was obtained from the synthesis. This product was purified by preparative RP-HPLC and analysed by RP-HPLC and ESI-MS, and found to have the expected molecular weight for the desired product. Calculated MW: 5592.3 g/mol, measured m/z (ESI-Tof-MS): 5591.72 (± 0.01%). The analytical chromatograms of the crude and the purified products are shown in **Figure 16**.

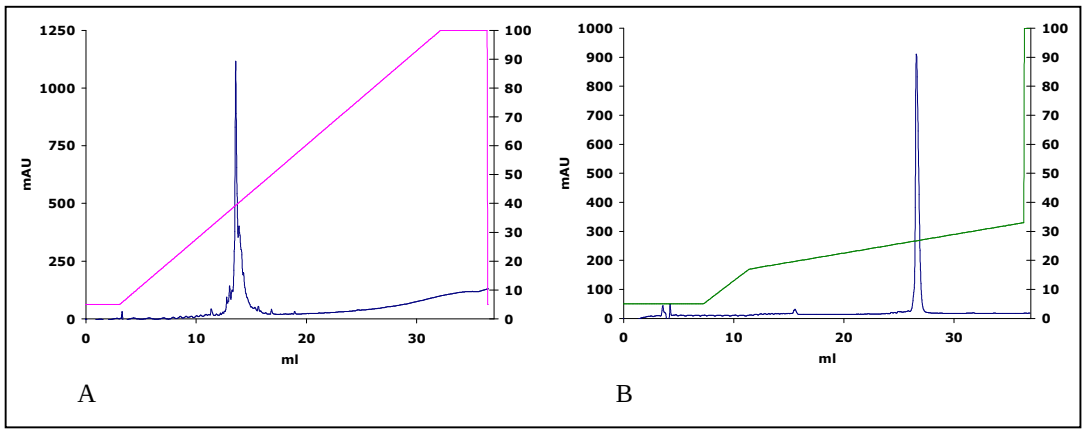

Figure 16: Chromatograms of crude linear peptide 1 (A) and purified peptide 1 (B). For HPLC conditions see appendix 4.

1.2.4.2 Oxidative folding

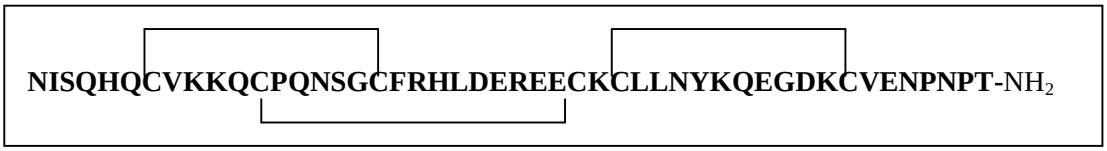

Figure 17: Amino acid sequence and disulfide bonding pattern of desired oxidation product, peptide **2**.

From a survey of recent literature methods [82-95] it was noted that successful oxidative folding of multiply disulfide bonded proteins is often carried out in a slightly basic buffer, at fairly low protein concentration, in the presence of a denaturant such as urea or DMF, and with reduced and oxidised glutathione, or with cysteine and cystine as a redox pair to help with the disulfide shuffling which seems to occur along many

refolding pathways. Therefore, in an initial trial, small portions of peptide were dissolved in 0.1 M Tris buffer at 0.1 mM peptide concentration and pH 8.4. 2mM reduced glutathione and 1mM oxidised glutathione were included in the buffer, and amounts of urea and DMF were varied in a systematic way as shown in **Table 1**. The peptide oxidation solutions were stirred for 24 hours in closed vessels but without the exclusion of oxygen. The solutions were then analysed by analytical RP-HPLC and the chromatograms compared to that of the starting material.

trial	Urea concentration (M)	DMF %	Peptide concentration mg/ml	Oxidised glutathione concentration mM	Reduced glutathione concentration mM	pH
1	0	0	0.5	1	2	8.4
2	1	0	0.5	1	2	8.4
3	2	0	0.5	1	2	8.4
4	3	0	0.5	1	2	8.4
5	0	5	0.5	1	2	8.4
6	1	5	0.5	1	2	8.4
7	2	5	0.5	1	2	8.4
8	3	5	0.5	1	2	8.4
9	0	15	0.5	1	2	8.4
10	1	15	0.5	1	2	8.4
11	2	15	0.5	1	2	8.4
12	3	15	0.5	1	2	8.4
13	0	25	0.5	1	2	8.4
14	1	25	0.5	1	2	8.4
15	2	25	0.5	1	2	8.4
16	3	25	0.5	1	2	8.4

Table 1: Conditions used for 16 trial oxidations of peptide **1**.

The chromatograms of the products obtained from a selection of these trials are illustrated in **Figure 18**.

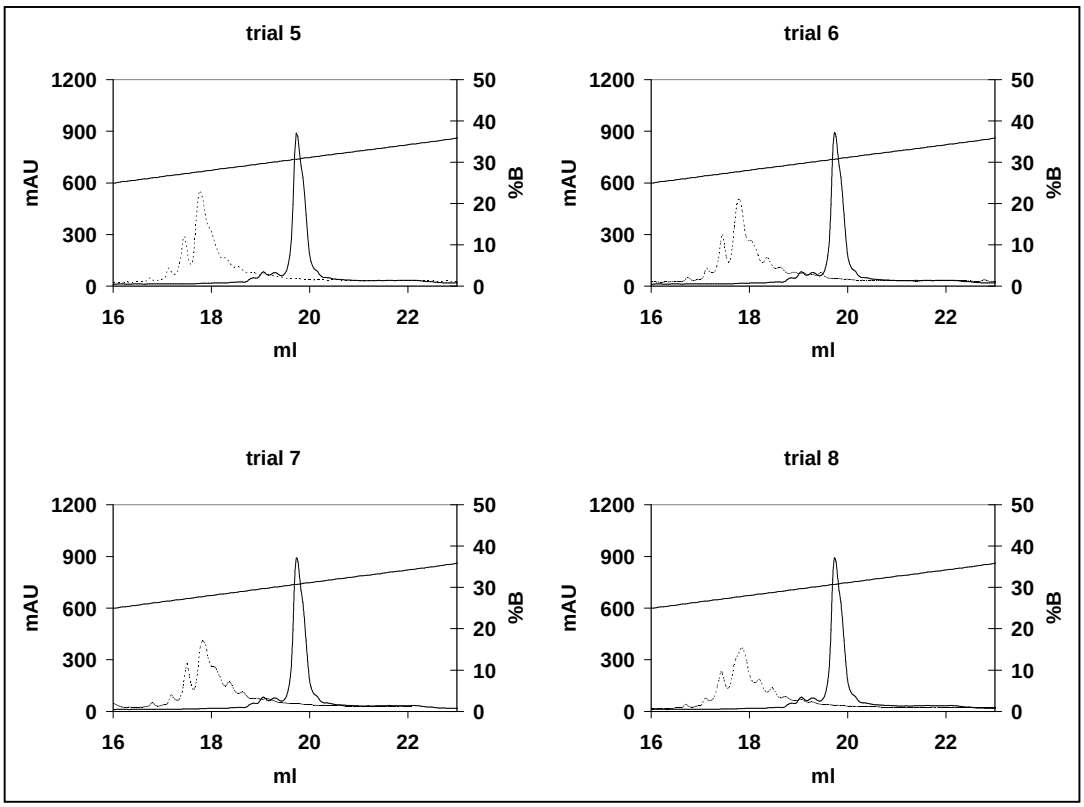

Figure 18: Comparison of the RP-HPLC chromatograms of reaction mixtures from the oxidation trials 5-8 described in **Table 1**. The chromatogram of the starting material is shown by the solid line and the chromatograms of the oxidised products by the dotted line. For HPLC conditions see appendix 4.

These trials seemed to lead to the formation of a product mixture containing one major peak and several side-products. It was difficult to notice any trend in the results obtained under systematically altered conditions, although the use of very high concentrations of urea seemed to lead to a higher proportion of side products where 0% or 5% DMF was used. It also seemed that higher concentrations of DMF led to fewer side products, although little difference was seen between the products obtained when 15% or 25% DMF was used. At this point, the products were not further characterised because it was decided to try a wider variety of different reaction conditions, with the aim of obtaining a better yield of the major product. In the next trials, several different oxidation conditions were used, based on methods found in the literature.

Trial	Peptide mg/ml	$NaHCO_3$ M	Guanidinium-HCl M	Cysteine mM	Cystine mM	pH	Reduced Glutathione (mM)	Oxidised Glutathione (mM)	Urea M	DMF %	EDTA mM
17	0.25	0.1	1	3	0.3	8.1	-	-	-	-	-
18	0.5	0.1	-	-	-	8.4	3	0.3	2	15	-
19	0.25	-	-	-	-	8.4	0.15	0.3	-	-	1
20	0.1	-	-	-	-	8.4	0.15	0.3	-	-	1
21	0.1	-	-	3	0.3	8.4	-	-	-	-	10
22	0.25	-	-	-	-	8.4	1	1	1.5	-	-
23	0.25	-	1	-	-	8.1	-	-	-	-	-
24	0.1	-	-	-	-	8.4	1.5	3	-	-	1

Table 2: Conditions used for the second round of oxidation condition trials. All reactions except for trials 17 and 18 were carried out in 0.1M Tris buffer. All reactions except trial 23 (air oxidation) were carried out in closed vessels but without the exclusion of oxygen.

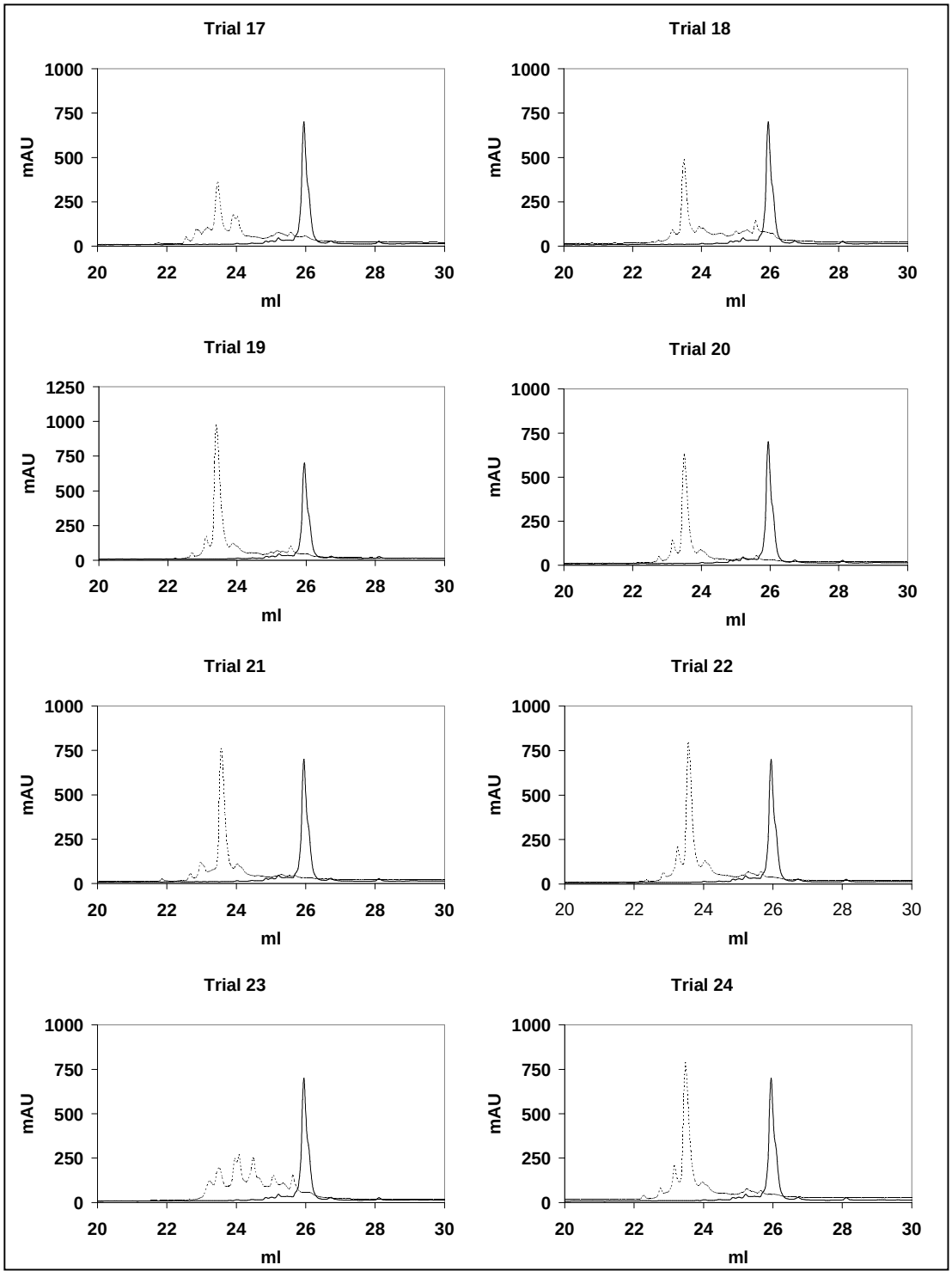

Figure 19: RP-HPLC chromatograms from the oxidation trials described in Table 2. The chromatogram of the starting material is shown by the solid line, oxidation products are shown by dotted lines. For HPLC conditions see appendix 4.

Table 2 shows the conditions that were used for the second round of oxidation trials. The peptide solutions were again stirred at room temperature for 24 hours before

analysis by analytical RP-HPLC to compare the products obtained with each other and with the starting material. The chromatograms of the oxidation products from these trials are shown in **Figure 19**.

The chromatograms show, for each trial except the air oxidation (trial 23), a major peak with shorter retention time than the starting material, along with several side peaks, the retention times and relative intensities of which vary with the different oxidation conditions. The major peak from each trial has the same retention time. It seems that in order to form this major peak, the presence of a redox couple such as cysteine/cystine or reduced and oxidised glutathione is necessary. This is not surprising as it is known that the folding pathways of several multi-disulfide bonded proteins go through fully oxidised disulfide scrambled intermediates before the correct fold is attained. In the air oxidation trial, in the absence of a redox couple, the peptide may well become 'trapped' in these intermediate folds, preventing the completion of the folding pathway.

The yields of the major product from several of the trials in the second round seemed to be quite similar. The conditions of trial 21 were chosen for further development because these oxidation conditions led to a major product with very few side products, and the separation of the side products from the main peak also seemed slightly better than under the other assay conditions. It was now decided to investigate the effect of increased peptide concentration on the outcome of the oxidation reaction. Trials were carried out using the same conditions as in trial 21, but with peptide concentrations of 0.5 mg/ml, 1 mg/ml, 2 mg/ml and 5 mg/ml. Increasing the peptide concentration did not seem to have any detrimental effect on the yield of the major product, as illustrated in **Figure 20**, which shows the chromatogram of the product of oxidation at a peptide concentration of 5 mg/ml.

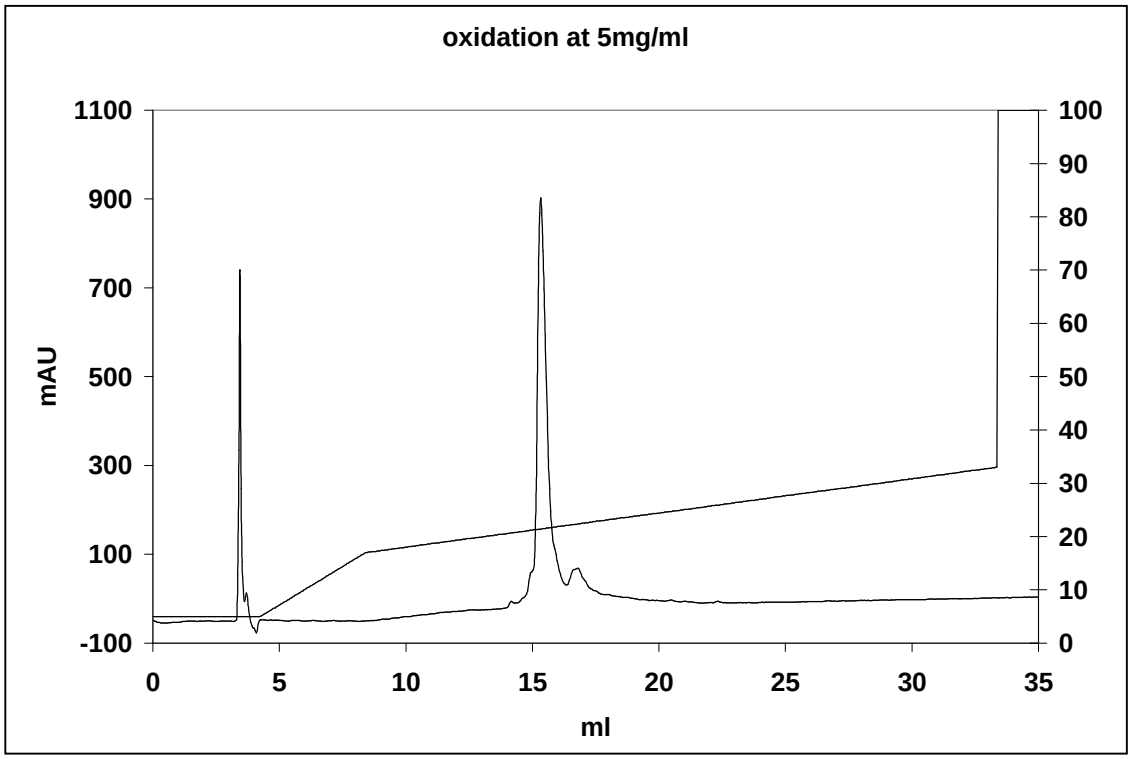

Figure 20: Chromatogram of the product of oxidation of peptide 1 at a peptide concentration of 5 mg/ml. For HPLC conditions see appendix 4.

This higher concentration was therefore used in a larger-scale oxidation reaction which provided sufficient oxidised product for purification by semi-preparative RP-HPLC to yield a product of high purity that could be analysed by ESI-MS and NMR. Calculated MW: 5586.31 g/mol, measured m/z (ESI-Tof-MS): 5586.3 ±0.1%. An expansion of the amide proton region of the ^{1}H NMR spectra of linear peptide **1** and folded peptide **2** is shown in **Figure 21**. The wide spread of signals in the spectrum of the oxidised product are a good indication that a well-structured product has been formed. In order to confirm that three disulfide bonds had been formed, the Ellman test was carried out on samples of both the linear and the oxidised peptide. The test showed that no free thiol groups were present in the oxidised product.

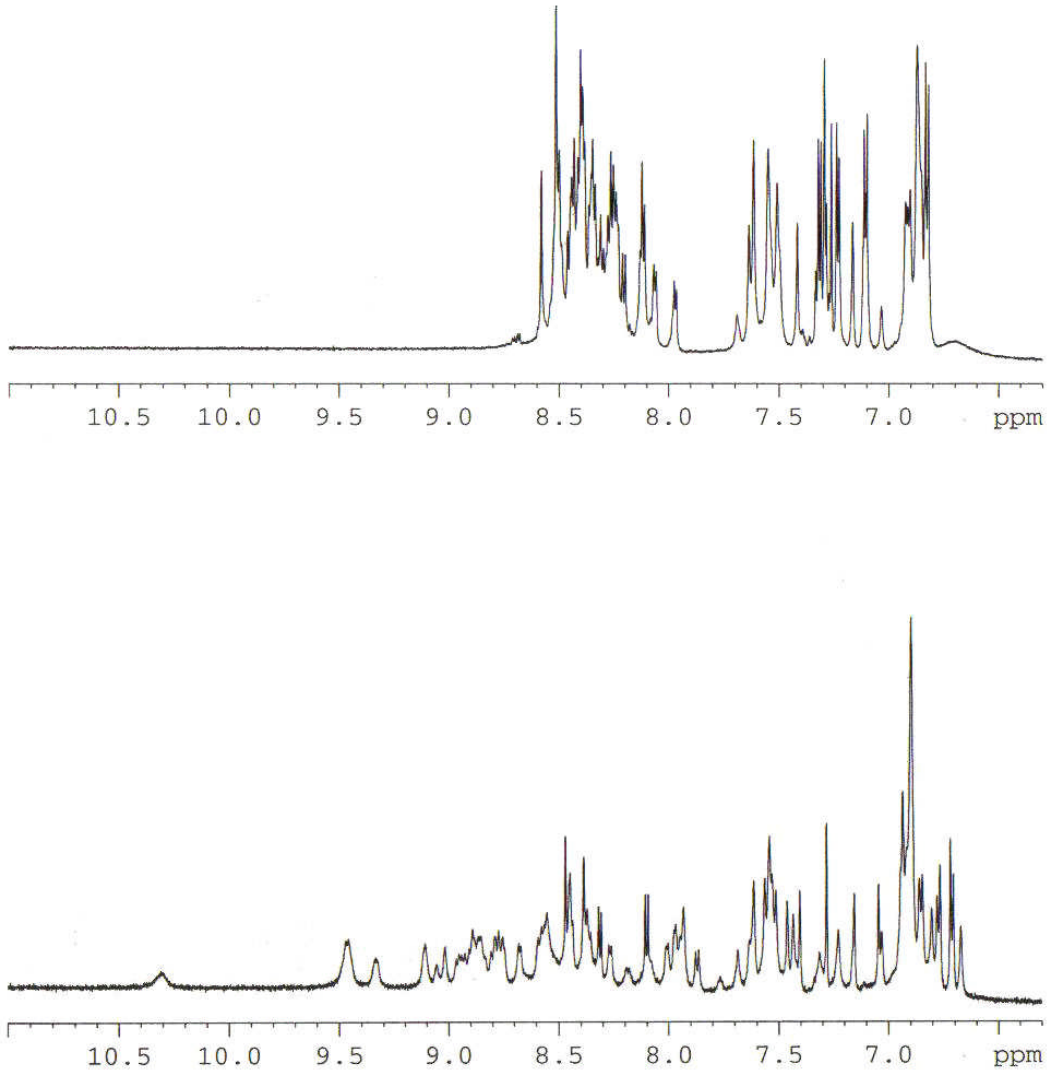

Figure 21: Expanded amide proton region of the NMR spectra of linear (**1**) (above) and the oxidatively folded (**2**) (below) MSP-1 mimetics.

1.2.4.3 Disulfide connectivity determination

In order to unambiguously determine the disulfide bond connectivities of the six Cys residues in the synthetic peptide, a combination of proteolytic digestion and mass spectrometry methods was used. The principle of this technique is to obtain, by partial proteolysis, peptidic fragments containing a single disulfide bond, which can be identified by their molecular weight. Therefore, both the enzyme and the proteolysis conditions

should be selected such that at least one potential cleavage site exists between each pair of neighbouring cysteine residues. It was not possible to identify any single specific enzyme that could fulfill these conditions. In particular, a cleavage in the region ^{12}CPQNSG^{18}C could only be expected to occur in the presence of a fairly unspecific enzyme such as thermolysin, whereas a cleavage in the region ^{28}CK^{30}C could best be achieved using trypsin.

Therefore, it was decided to carry out in parallel large scale trypsin and thermolysin digestions of the synthetic folded peptide, under pH conditions that would minimize the possibility of disulfide scrambling. The cleavage fragments were separated and isolated by RP-HPLC and the corresponding chromatograms are shown in **Figures 22** and **23**. All main fractions were analyzed by ESI-MS and the measured masses were compared to the theoretical masses of fragments which could be expected from the digestion of each isomer. Key fragments containing a single disulfide bridge were submitted to N-Edman sequencing to confirm the mass results. The fractions obtained and the fragments identified are presented in **Tables 3** and **4**. **Table 5** relates to the reduction of a selection of fragments with DTT in order to confirm the structure implied by the measured masses. The combination of the data obtained serves to confirm the expected connectivity 1-3, 2-4 and 5-6.

In the case of the trypsin digests, four main products were identified for each of the four main fractions 13, 19, 20 and 21. The two fragments identified in peaks 13 and 19 (MW = 2827.2 and MW= 4972.6) corresponded to peptides linked by two and three disulfide bridges, respectively. In fragment 13, consisting of peptides ^{1}NISQHQ^{7}**C**V^{9}K, ^{10}KQ^{12}**C**PQNSG^{18}**C**F^{20}R and ^{26}EREE^{28}**C**^{29}K, linked by two disulfide bridges involving ^{7}C (Cys-1), ^{12}C (Cys-2), ^{18}C (Cys-3) and ^{28}C (Cys-4), the exact connectivity of the four Cys residues could not be unequivocally attributed and could be either 1-2/3-4 or 1-3/2-4. Masses determined for fractions 19 and 20 were consistent with 2 fragments, one containing two discontinuous peptides ^{30}**C**LLNY^{35}K and ^{41}**C**VENPNP^{48}T linked *via* the disulfide bond between ^{30}C (Cys-5) and ^{41}C (Cys-6), and the other corresponding to the single stretch ^{30}**C**LLNYKQEGDK^{41}**C**VENPNP^{48}T, containing the same disulfide bond. The results of the trypsin digestion thus confirmed the connection of the cysteine residues 5 and 6, as already identified in the NMR structure. The exact pairing between Cys-1, Cys-2, Cys-3 and Cys-4, however, remained ambiguous at this stage.

Many fragments were generated by the thermolytic digestion, of which fifteen could be identified (**Table 4**). The fragments identified in the main fractions 3, 11 and 12 appeared to be of special interest for the attribution of the exact connectivities of the four remaining cysteine residues ^{7}C (Cys-1), ^{12}C (Cys-2), ^{18}C (Cys-3) and ^{28}C (Cys-4). Indeed, peak 3 contained two fragments (MW=1092.2 and MW=1005.1) whose masses are consistent with the peptide ^{1}NISQHQ^{7}C linked *via* one disulfide bond to either the tripeptide ^{16}SG^{18}C or the dipeptide ^{17}G^{18}C, thus confirming unequivocally the connection between ^{7}C (Cys-1) and ^{18}C (Cys-3). Furthermore, three structurally related fragments identified in fractions 11 and 12 were found to be constituted of three peptides linked by two disulfide bridges involving the four cysteine residues ^{12}C (Cys-2), and ^{28}C (Cys-4), ^{30}C (Cys-5) and ^{41}C (Cys-6). Since the connection between ^{30}C (Cys-5) and ^{41}C (Cys-6) had already been proved by the trypsin digestion experiment, the connection between the two remaining cysteine residues ^{12}C (Cys-2), and ^{28}C (Cys-4) was implied.

In summary, the combination of the results of the trypsin digestion and of the thermolysin digestion confirmed unambiguously, for this peptide, the disulfide bonding pattern 1-3, 2-4 and 5-6 found in many EGF domains.

Tryptic fragments.

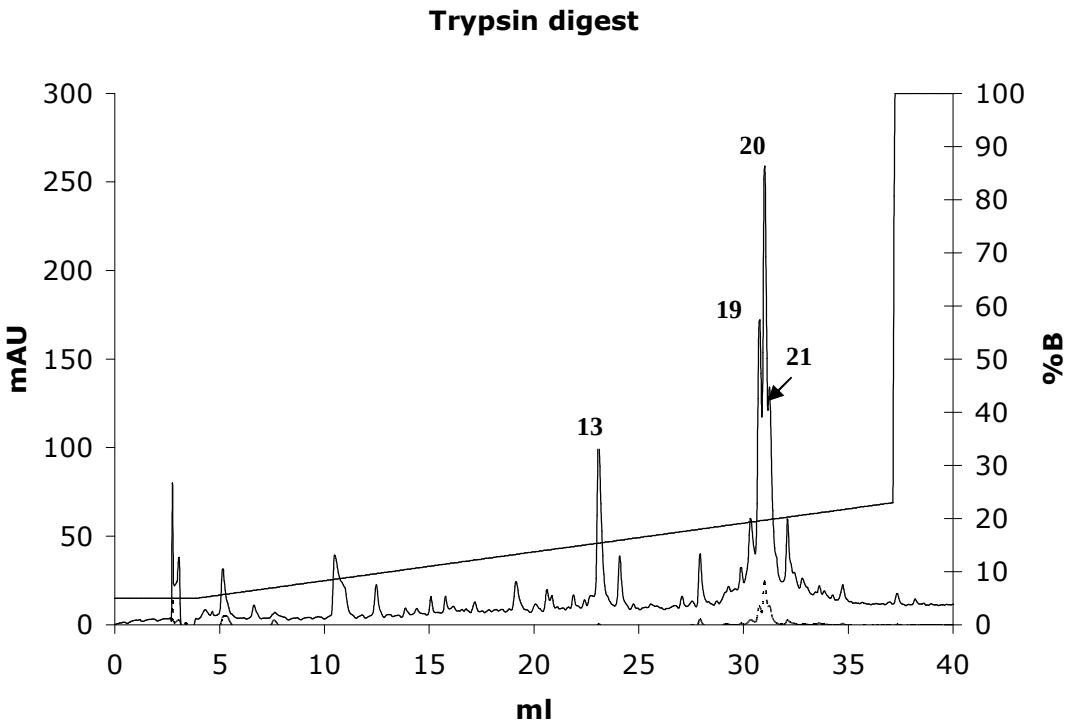

Figure 22: RP-HPLC of the trypsin digest of peptide **2.** For HPLC conditions see appendix 4.

HPLC Peak	Fragment	Mass calc.	m/z calc.	m/z exp.	Disulfides Present
13	NISQHQ**C**VK KQ**C**PQNSG**C**FR EE**C**K	2827.2	707.8(+4) 566.4(+5)	707.7(+4) 566.4(+5)	Cys^1-Cys^3 Cys^2-Cys^4
19	NISQHQ**C**VK KQ**C**PQNSG**C**FR EE**C**K**C**LLNYKQEGDK**C**VENPNPT	4972.6	1244.2(+4) 995.5(+5) 829.8(+6) 711.4(+7)	1244.4(+4), 995.6(+5), 830.4(+6), 711.5(+7)	Cys^1-Cys^3 Cys^2-Cys^4 Cys^5-Cys^6
20	**C**LLNYK **C**VENPNPT	1623.9	813.0(+2)	813.1 (+2)	Cys^5-Cys^6
21	**C**LLNYKQEGDK**C**VENPNPT	2163.4	1082.7(+2) 722.1(+3)	1082.9(+2), 722.3(+3)	Cys^5-Cys^6

Table 3: Fragments identified by LC-MS from the trypsin digest of peptide **2**.

Thermolytic fragments

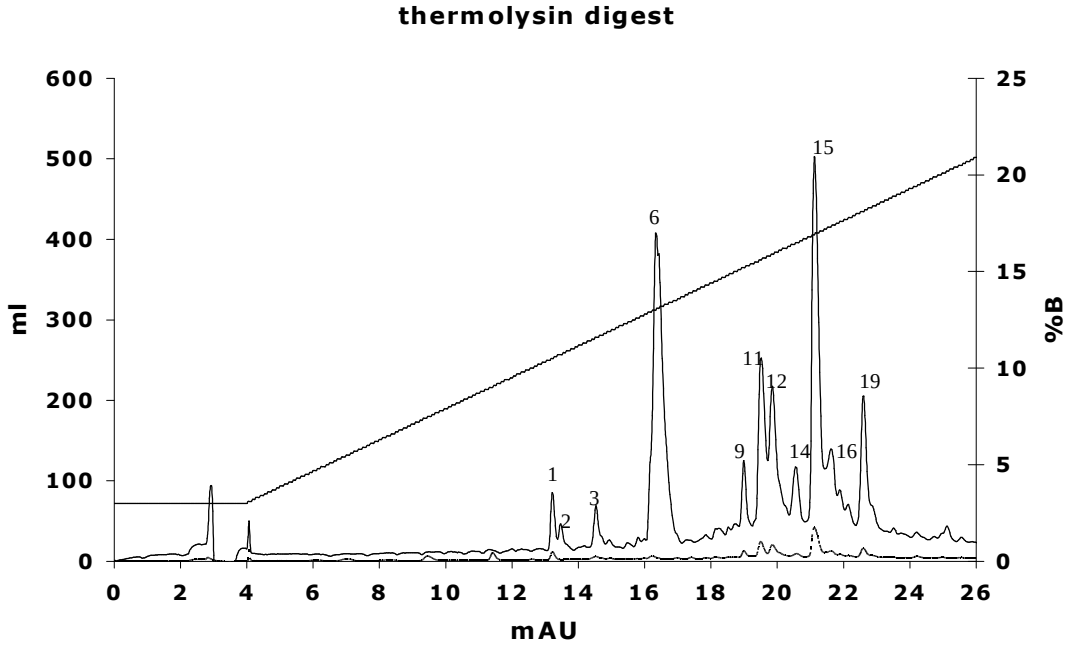

Figure 23: RP-HPLC of thermolysin digest of peptide **2.** For HPLC conditions see appendix 4.

HPLC Peak	Fragment	Mass calc.	M/z calc.	M/z exp.	Disulfides Present
1	YKQE	566.6	567.6(+1)	567.3(+1)	-
	C YKQEGDK**C**	1089.2	1090.2(+1) 545.6(+3)	1089.7(+1), 545.3(+2)	Cys^5-Cys^6
2	NISQH	597.6	598.6(+1)	598.4(+1)	-
3	**C**PQ E**C**K**C** DK**C**	1188.4	1189.4(+1) 595.2(+2)	1189.7(+1), 595.7(+2)	Cys^2-Cys^4 Cys^5-Cys^6
6	NISQHQ**C** G**C**	1005.1	1006.1(+1)	1005.4(+1)	Cys^1-Cys^3
	NISQHQ**C** SG**C**	1092.2	1093.2(+1)	1093.1(+1)	Cys^1-Cys^3
	VENPNPT	769.8	770.8(+1)	770.5(+1)	-
	FRH	458.5	459.5(+1)	459.2(+1)	-
9	Q**C**PQN HLDEREE**C**K**C** DK**C**	2210.5	1106.3(+2) 737.8(+3) 553.6(+4)	1107.7(+2) 738.6(+3) 554.4(+4)	Cys^2-Cys^4 Cys^5-Cys^6
11	VKKQ**C**PQN LDEREE**C**K**C** YKQEGDK**C**	3034.4	1012.5(+3) 759.6(+4) 607.9(+5)	1012.4(+3), 759.4(+4), 607.9(+5)	Cys^2-Cys^4 Cys^5-Cys^6
12	VKKQ**C**PQ LDEREE**C**K**C** YKQEGDK**C**	2920.3	974.4(+3) 731.1(+4) 585.1(+5)	974.3(+3), 730.9(+4), 585.0(+5)	Cys^2-Cys^4 Cys^5-Cys^6
14	NISQHQ**C** VKKQ**C**PQNSG**C** DEREE**C**K**C** YKQEGDK**C**	3995.5	1332.8(+3) 999.9(+4)	1332.6(+3) 1000.2(+4)	Cys^1-Cys^3 Cys^2-Cys^4 Cys^5-Cys^6
15	NISQHQ**C** VKKQ**C**PQNSG**C** LDEREE**C**K**C** YKQEGDK**C**	4108.6	1028.2(+4) 822.7(+5) 685.8(+6) 587.9(+7)	1028.8(+4) 823.5(+5) 686.3(+6) 588.6(+7)	Cys^1-Cys^3 Cys^2-Cys^4 Cys^5-Cys^6
16	LLN	358.4	359.4(+1)	359.8(+1)	-
19	NISQHQ**C** VKKQ**C**PQNSG**C** LDEREE**C**K**C** YKQEGDK**C**VENPNPT	4860.4	1621.1(+3) 1216.1(+4) 973.1(+5)	1621.2(+3) 1216.1(+4) 973.3(+5)	Cys^1-Cys^3 Cys^2-Cys^4 Cys^5-Cys^6

Table 4: Fragments identified by LC-MS from the thermolysin digest of peptide **2**.

Important tryptic fragments of the thermolytic fragment 11:

Fragment 11:

* The fraction collected was found to contain both fragments with and without this serine residue.

HPLC Peak	Fragment	Mass calc.	M/z calc.	M/z exp.	Disulfides present
1	KQ**C**PQNS EE**C**K	1309.5	655.8(+2)	656.0(+2)	Cys^2-Cys^4
2	YKQEGDK	866.9	867.9(+1) 434.5(+2)	867.8(+1) 434.2(+2)	-
3	**C** YKQEGDK**C**	1089.2	1090.2(+1) 545.6(+2)	1089.6(+1) 545.5(+2)	Cys^5-Cys^6

Table 5: Fragments identified by LC-MS from the trypsin digest of the thermolytic fragment 11.

Reduction samples:

	Fragment	Mass calc.	Reduced mass calc.	Reduced mass exp. (MALDI)
1	NISQHQ**C**VK KQ**C**PQNSG**C**FR EE**C**K	2827.2	1056.2 1267.5 507.6	1056.5 1267.5 n.f.
	or			
	NISQHQ**C**VKK Q**C**PQNSG**C**FR EE**C**K		1184.4 1139.3 507.6	n.f. n.f. n.f.
2	NISQHQ**C**VK KQ**C**PQNSG**C**FR EE**C**K**C**LLNYKQEGDK**C**VENPNPT	4972.6	1056.2 1267.5 2655.0	1056.6 1267.6 2653.1 (Cys^5-Cys^6 not reduced)
	or			
	NISQHQ**C**VKK Q**C**PQNSG**C**FR EE**C**K**C**LLNYKQEGDK**C**VENPNPT		1184.4 1139.3 2655.0	n.f. 1139.5 n.f.
3	**C**LLNYK **C**VENPNPT	1623.9	752.9 873.0	n.f. 873.5
4	VENPNPT	769.8	769.8	770.1
5	VKKQ**C**PQ LDEREE**C**K**C** YKQEGDK**C**	2920.3	830.0 1124.3 970.1	830.5 1124.5 970.5

Table 6: Masses found after the reduction of a selection of the fragments identified in the trypsin and thermolysin digestion experiments.

1.2.4.4 NMR structure

From further synthesis, purification and oxidation reactions, carried out as described above, it was possible to obtain enough pure folded peptide for 2D NMR measurements. A series of ^{1}H NMR spectra were first measured at temperatures ranging from 278K to 303K, in order to determine the optimal temperature for 2D measurements. 298K was chosen as the best temperature and measurements were carried out at 600MHz in H_2O/D_2O 9:1 at pH 5. NOESY spectra revealed a large number of well-resolved medium- and long-range NOEs. The peaks could be assigned based on DQF-COSY and TOCSY measurements, and distance restraints obtained from NOESY spectra with mixing times of 50, 150 and 300 ms could be employed by Dr Kerstin Moehle to

calculate a solution structure using CYANA [96]. The final ensemble of 20 structures reveal a structure highly similar to that of the corresponding domain in the two-domain protein MSP-1_{19}, as illustrated in **Figure 24**. The structures have been deposited in the Protein Data Bank under the accession number 2FLG.

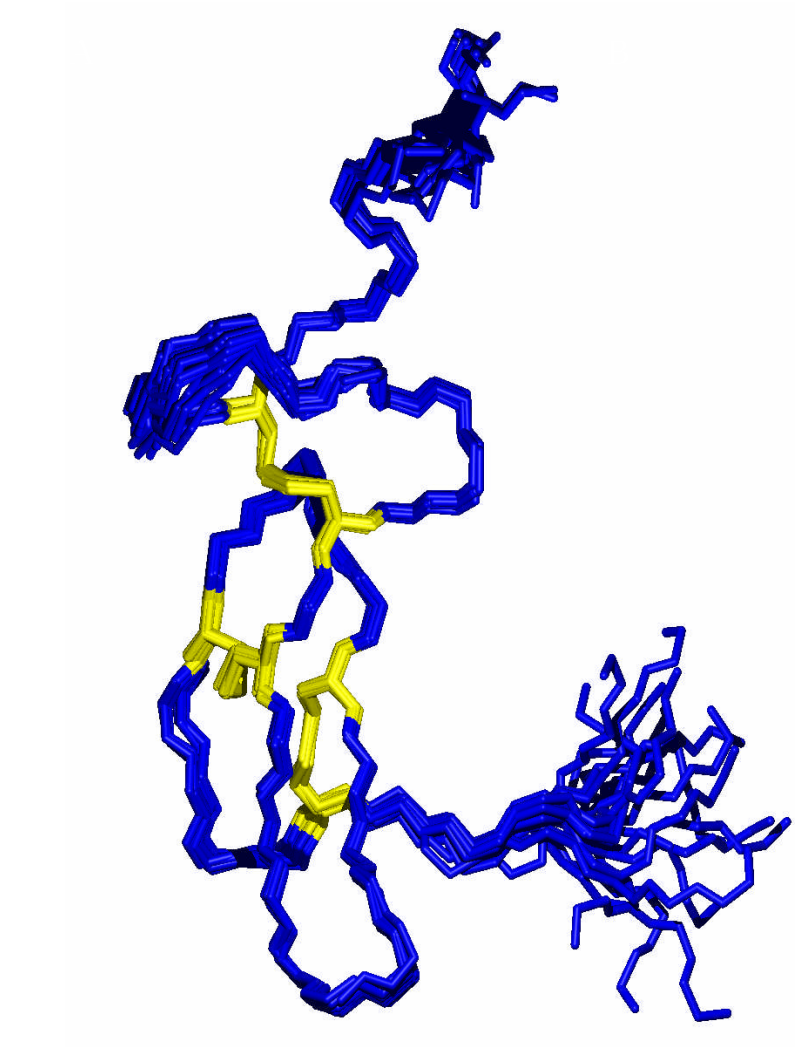

Figure 24: (A) Overlay of 20 best structures of peptide **2**

B

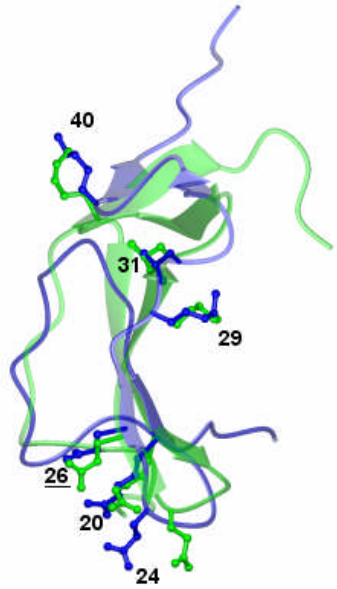

Figure 24 (B): Comparison of solution structure of peptide **2** (blue) with that of domain 1 in the structure of the whole MSP-1_{19} protein (green) (published in the protein data bank under the accession number 1CEJ).

The N-terminal residues up to Cys^{7} appear to be disordered, whereas the region between Cys^{7} and Pro^{13} is associated with both strong sequential H_N-H_N Val^{8}-Lys^{9}, Lys^{9}-Lys^{10}) and H_α-H_N (Lys^{10}-Gln^{11}, Gln^{11}-Cys^{12}, Cys^{12}-Pro^{13}) NOEs. A large ~2ppm downshifted H_N resonance of Val^{8}, which seems to be caused by close contact to the side chain of Glu^{26} was also observed in the structure of MSP-1_{19} protein [51]. A type I β-turn conformation is seen between Pro^{13} and Ser^{16}. A type 3:5 β-turn is found between residues Cys^{18} and Cys^{28}, as defined by strong sequential $d_{\alpha,N}$ NOEs and typical cross-strand H_α-H_α(Cys^{18}-Cys^{28}, Arg^{20}-Glu^{26}), H_N-H_α (Phe^{19}-Cys^{28}, His^{21}-Glu^{26}) and H_N-H_N (Phe^{19}-Glu^{27}, His^{21}-Arg^{25}) NOEs. A further type I β-turn conformation occurs between Leu^{31} and Tyr^{34}. In the final hairpin loop between Tyr^{34} and Glu^{43}, a distorted type II β-turn conformation is found with Gly^{38} and Asp^{39} at positions i+1 and i+2.

Table 7 outlines the ideal ϕ and ψ torsion angles for some common types of β-turns [97], and **Figure 25** illustrates how β-hairpins are classified.

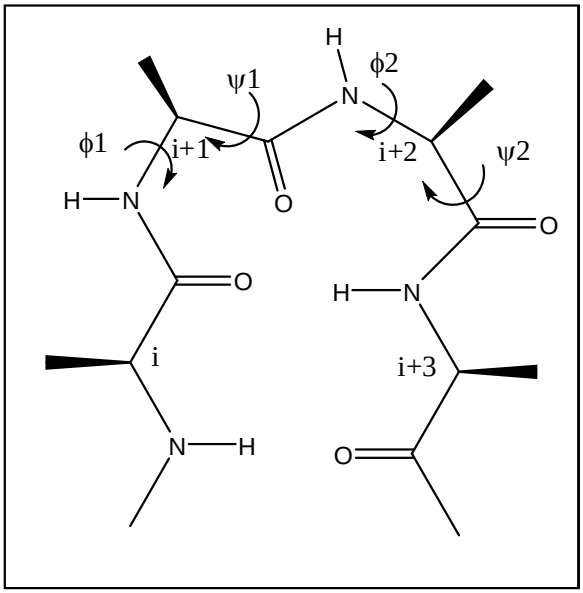

Figure 25: Definition of ϕ and ψ angles in a β-turn.

Type	ϕ1	ψ1	ϕ2	ψ2
I	-60	-30	-90	0
II	-60	120	80	0
III	-60	-30	-60	-30
I'	60	30	90	0
II'	60	-120	-80	0
III'	60	30	60	30

Table 7: Ideal torsion angles for some common β-turns.

The NMR results show that the single domain mimetic adopts a native-like structure, although an interesting feature of MSP-1_{19} is the interface between the two EGF-like domains, which involves several interacting non-polar amino acids (Phe^{19}, Leu^{31}, Leu^{32}, Leu^{86}, Phe^{87}, Ile^{90} and Phe^{91}) [51]. Nevertheless, the Phe^{19}, Leu^{31} and Leu^{32} side chains in peptide **2** adopt positions similar to those seen in the dual domain protein, with the exception that the Phe^{19} side chain is rotated by 120^{o}, and surface representations

suggested that this exposed face of the EGF-like domain was not exceptionally hydrophobic.

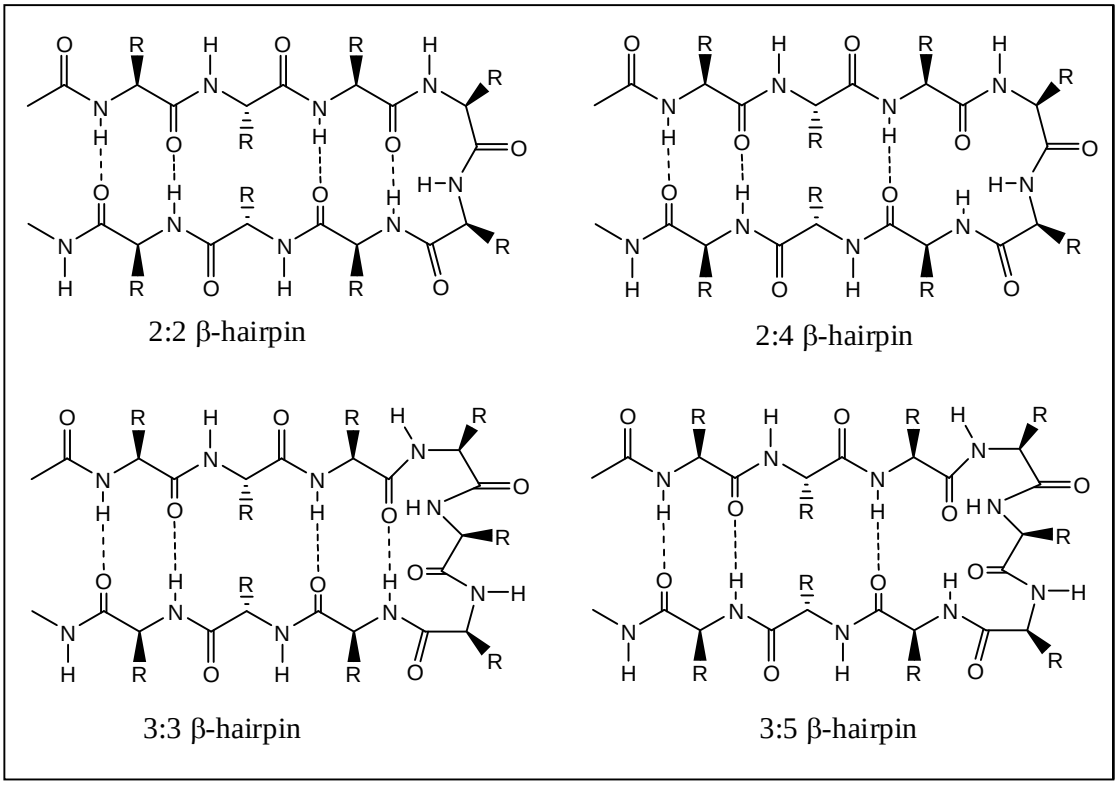

Figure 26: Classification of β-hairpins [98, 99]

1.2.4.5 Synthesis of lipopeptide mimetic for immunization studies

The usual strategy for the synthesis of phospholipid-coupled peptide mimetics in the Robinson group involves the coupling of a modified phosphatidyl ethanolamine group to the N-terminus of the peptide sequence whilst still attached to the solid support. The linear phospholipidyl-peptide is then cleaved from the resin and further purification and modification steps are carried out on the whole mimetic. This approach is outlined schematically in **Scheme 3**.

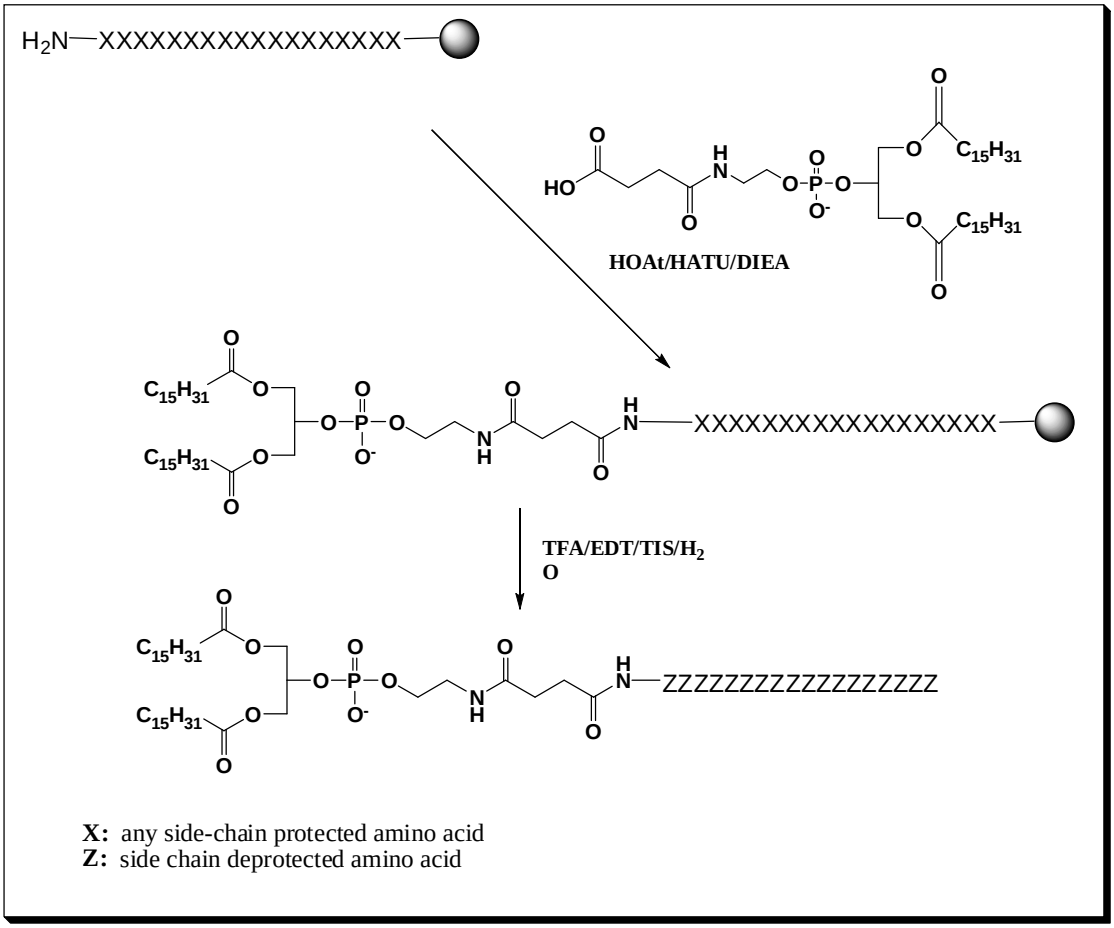

Scheme 3: Standard procedure for synthesis of PE-coupled peptide mimetics

The coupling of the phosphatidyl-ethanolamine moiety to the sequence of peptide **1** could be carried out satisfactorily and the product could be purified by RP-HPLC using a C4 column to yield a clean product which showed the expected mass of the desired product by LC-MS. The analytical HPLC chromatogram of this product is shown in **Figure 27**.

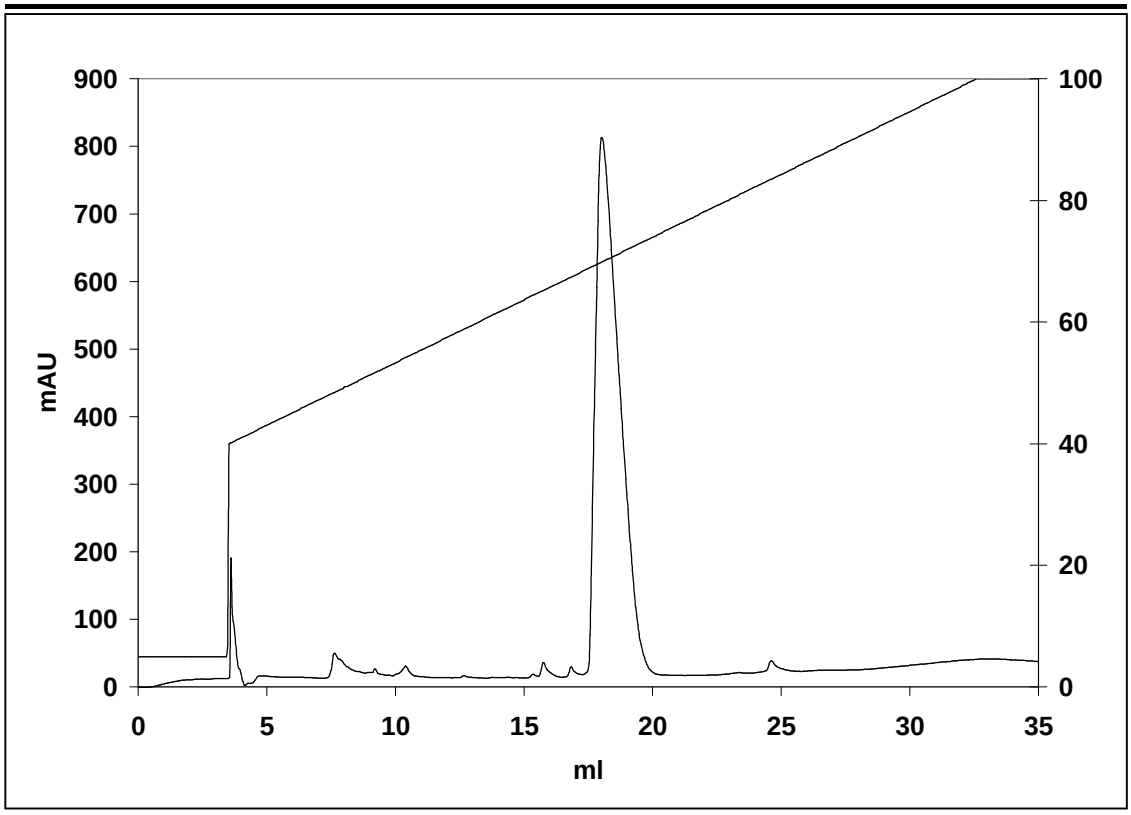

Figure 27: Chromatogram of purified lipopeptide **3.** For HPLC conditions see appendix 4.

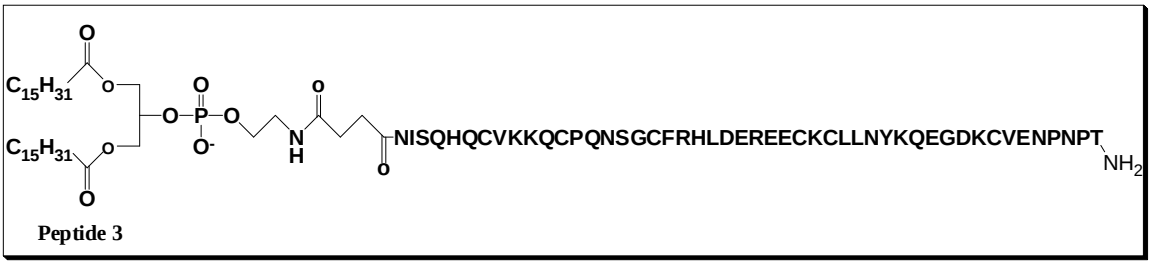

Figure 28: Structure of lipopeptide **3**

After purification, the oxidative folding of this linear mimetic was attempted. The mimetic could be dissolved in the same oxidation solution as used for peptide **1**, albeit at a lower concentration. However, after several hours stirring, a precipitate was formed that could not be solubilised although a number of solvents were tested. Trials were also carried out with the addition of DMSO to the oxidation solution, but no satisfactory results could be obtained. Therefore, it was decided to adopt a different strategy for the synthesis of the lipopeptide mimetic.

It has recently been demonstrated that under suitable pH conditions, it is possible to distinguish between the reactivity of amine groups and the NH_2 of a hydrazine group

within the same molecule [100]. This means that it should be possible to couple an activated phospholipid chemoselectively to a hydrazine group in a fully deprotected peptide containing lysine side chains. In order to produce a suitably modified peptide for this coupling method, fully Boc-protected hydrazinoglycine was synthesised as described in **Scheme 4** [101].

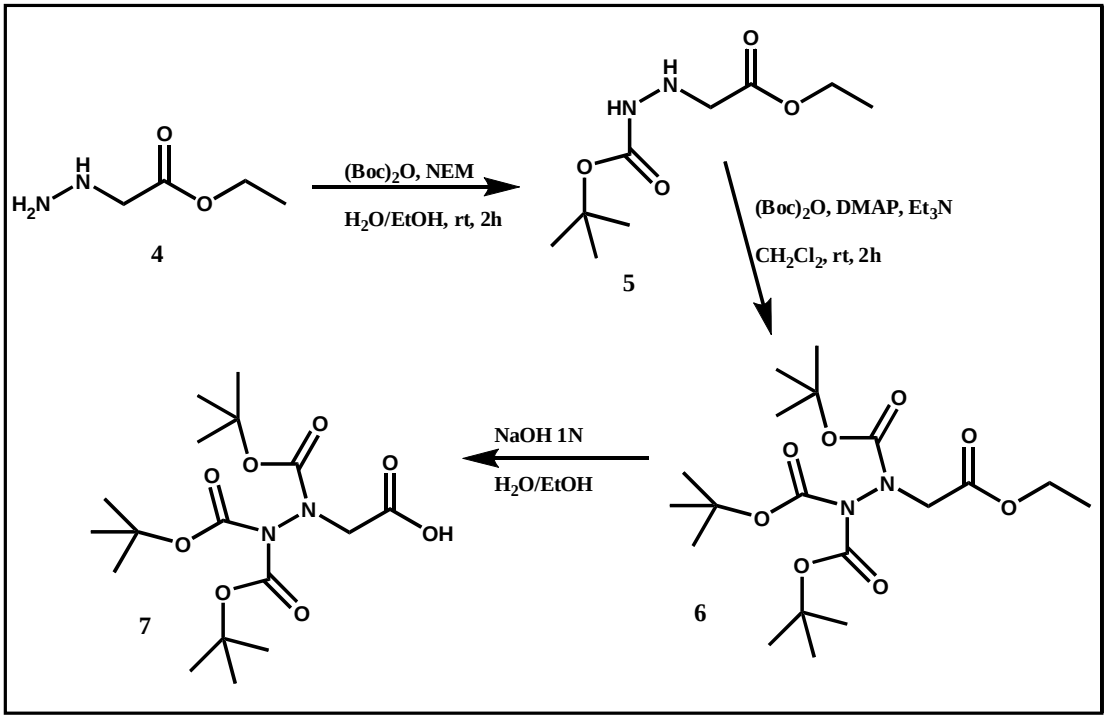

Scheme 4: Synthetic route to Boc-protected hydrazinoglycine.

Figure 29: Structure of peptide **8**

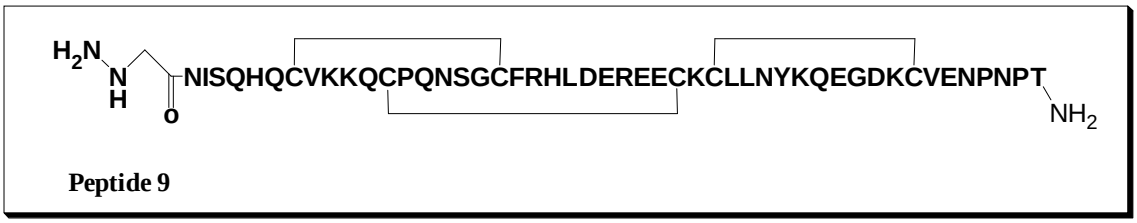

Figure 30: Structure of oxidised peptide **9**

This derivative could then be introduced into the peptide synthesis in the same way as a side-chain protected amino acid, at the N-terminal end of the peptide sequence. Cleavage from the resin and side-chain deprotection were then carried out in a single step as described previously. Calculated mass: 5665.41 mol/g, measured: 1416.7 $(M+4H)^{4+}$, 1133.8 $(M+5H)^{5+}$, 945.1 $(M+6H)^{6+}$, 810.2 $(M+7H)^{7+}$ (± 0.01%). The modified linear peptide **8** could then be oxidatively folded under the conditions described above, to yield folded peptide **9**. An example of the chromatogram of the modified peptide before and after oxidative folding is shown in **Figure 31**.

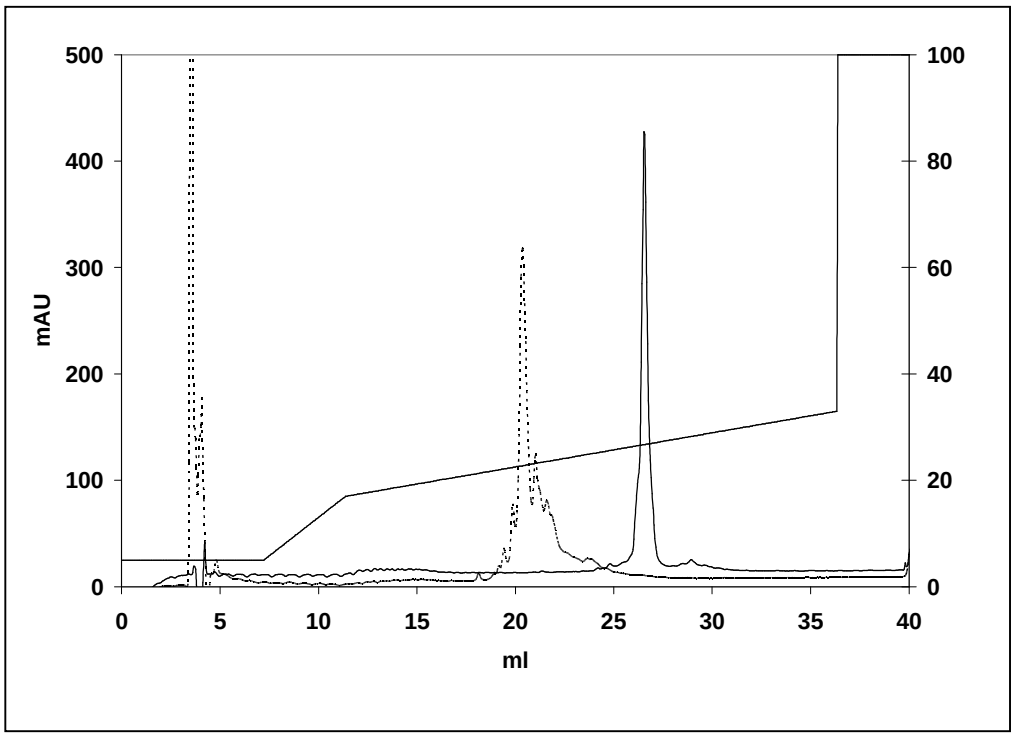

Figure 31: Oxidation of peptide **8** to give peptide **9**. Chromatogram of peptide **8** is shown by the solid line. Chromatogram of peptide **9** is shown by the dotted line. For HPLC conditions see appendix 4.

In later assays, it was discovered that it was possible to perform the oxidative folding reaction on the crude peptide taken directly from solid-phase assembly, thus

eliminating the intermediate purification steps and leading to higher overall yields of the final product. Chromatograms of the linear and oxidatively folded crude product are shown in **Figure 32**.

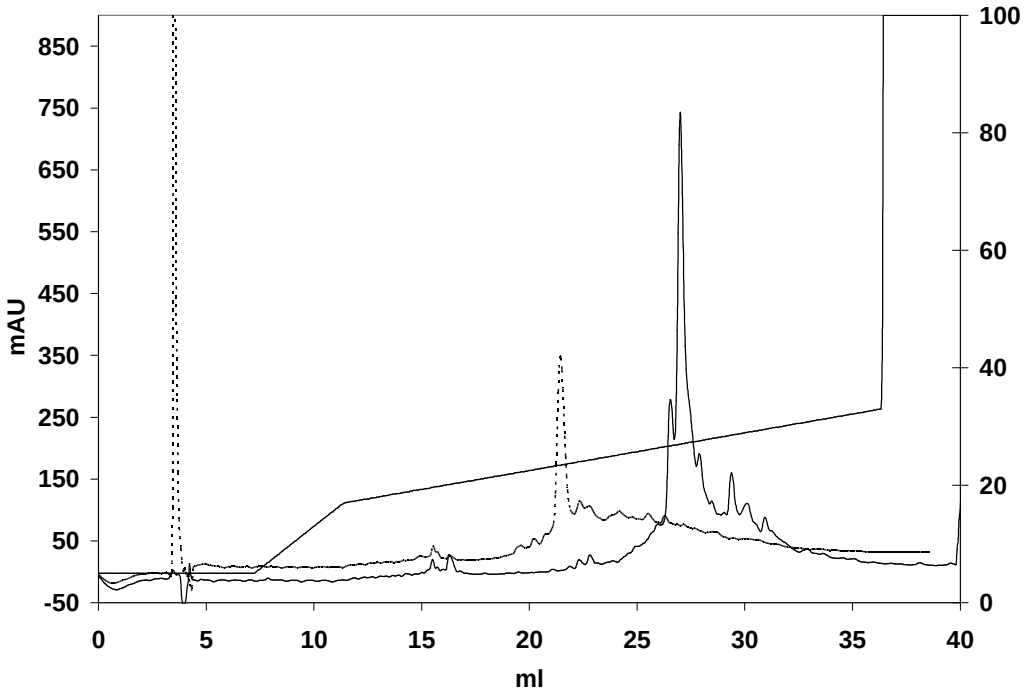

Figure 32: Oxidation of crude peptide **8**. The chromatogram of crude peptide **8** is shown by the solid line, the chromatogram of crude oxidised peptide **9** by the dotted line. For HPLC conditions see appendix 4.

The chromatogram of purified oxidised peptide **9** is shown in **Figure 33**. Calculated MW: 5659.36 g/mol, measured (ESI-Tof-MS): 5658.4 (± 0.1%).

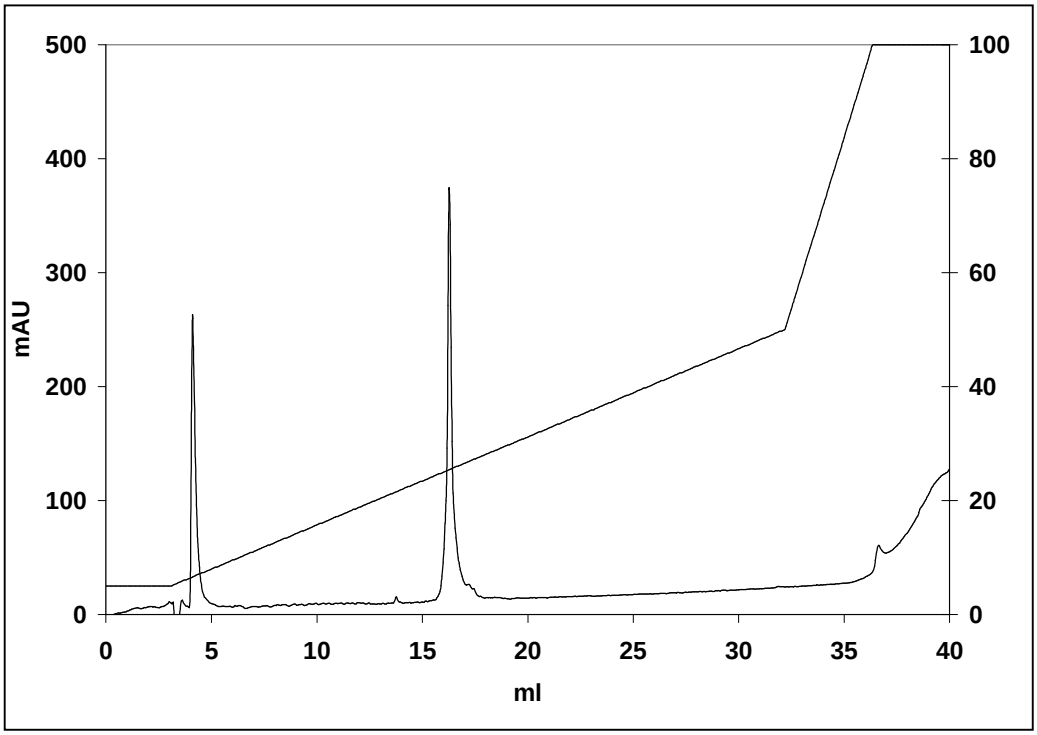

Figure 33: Chromatogram of purified peptide **9**. For HPLC conditions see appendix 4.

After purification of this peptide, phospholipidyl peptide **13** could be obtained via the reaction of peptide **9** with activated modified phosphatidyl ethanolamine. The phospholipid was activated in the form of an N-hydroxysuccinimide ester, which was freshly synthesised as described in **Scheme 5** [102] and used for the coupling reaction without further purification.

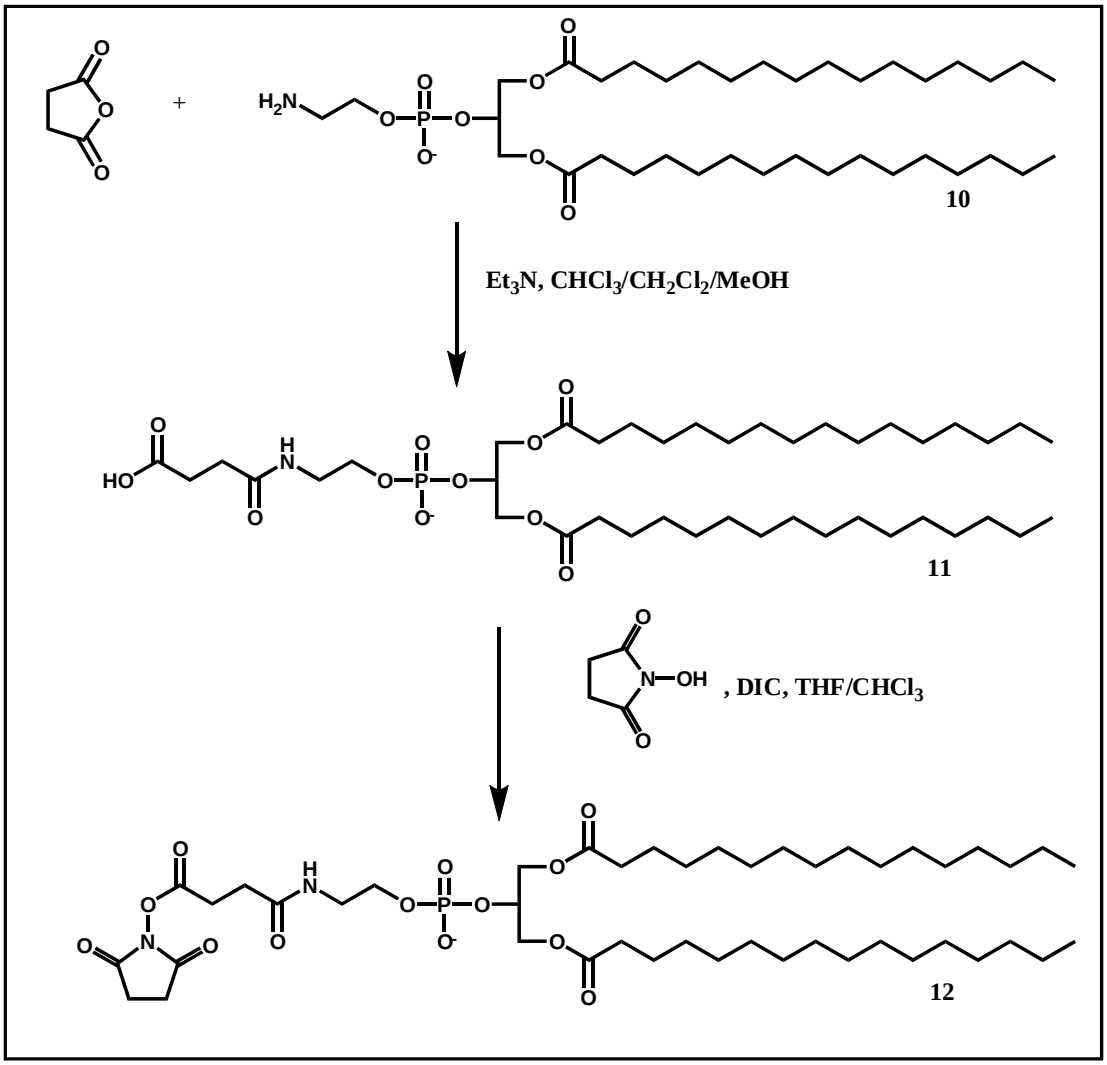

Scheme 5: Synthetic route to activated phosphatidylethanolamine **12**.

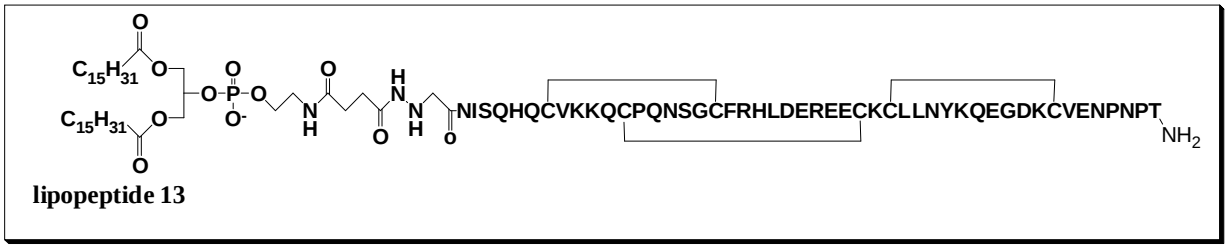

Figure 34: Structure of lipopeptide **13**

For the coupling reaction, peptide **9** was dissolved in water at high concentration (6.5mg/ml) and the pH of the solution was adjusted to between pH 5.1 and 5.3 using 10mM NaOH. 1.5 to 2 eq. of the activated phospholipid **12** were dissolved in an equal

volume of tert-butanol and the two solutions were stirred together. The progress of the reaction was monitored by LC-MS and the product was purified by RP-HPLC directly as soon as it was observed that no further lipopeptide product was being formed. An HPLC chromatogram of the reaction mixture is shown in **Figure 35**. The peak at short retention time is the unreacted peptide and the peak at a longer retention time is the newly formed lipopeptide **13.**

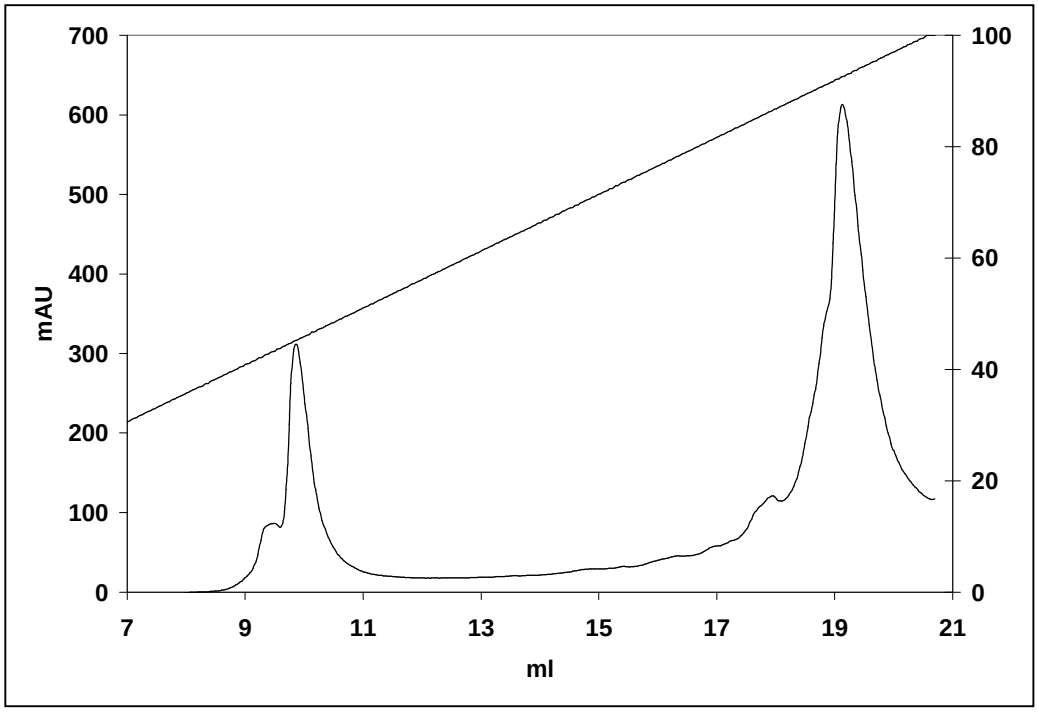

Figure 35: Chromatogram of the solution from the coupling of peptide **9** with activated phosphatidylethanolamine **12**. For HPLC conditions see appendix 4.

The lipopeptide **13** could be purified and ESI-TOF-MS could be measured. Calculated MW: 6432.4 g/mol, measured m/z (ESI-Tof-MS): 6432.5. The mass of the product corresponded to the expected mass for the desired product. This product could therefore be used for inclusion in virosomes for subsequent immunization studies.

1.2.4.6 Immunological activity of MSP-1_{19} domain 1 mimetic

For immunological studies, lipopeptide **13** was incorporated into virosomes by Dr R Zurbriggen and co-workers at Pevion Biotech, using methods established earlier for short linear peptides and peptidomimetics [47, 103, 104]. BALB/c mice were pre-immunized with whole virus influenza antigen, and were then immunized three weeks later with peptide **13**-loaded IRIVs, with subsequent immunizations at intervals of three weeks. Peptide **13**-loaded virosomes generated strong antibody responses in mice. In collaboration with Prof. G. Pluschke (Swiss Tropical Institute) it was shown that all mice immunized produced IgG that reacted with lipopeptide **13** in ELISA and that were cross-reactive with *P. falciparum* blood stage parasites in IFA. IFA staining patterns characteristic of the major parasite surface protein were obtained. In competition IFA, the binding of sera to the parasite surface could only be fully blocked by folded peptide mimetic **43**, and not by unfolded reduced peptide **42** or unfolded reduced and alkylated peptide **44** (see page 62) (**Figure 36**). Parasites were incubated with sera raised against lipopeptide **13** and with linear or with folded peptide mimetic. Folded peptide blocked the binding of sera to parasites (Figure 36(A)), suggesting that all antibodies recognised some part of the folded peptide, whereas linear peptide mimetics seemed to block little or no binding to the parasite surface (Figure 36(C) and (D)), suggesting that at least some antibodies were present that did not recognise linear peptide. Moreover, the control where no peptide was added to the solution (Figure 36 (B)) shows that antibodies raised against the mimetic were able to recognise and bind to parasites. These results suggest that antibodies raised against the mimetic recognise conformational epitopes, and therefore that correct oxidative folding could be vital to the development of an MSP-1-based malaria vaccine candidate.

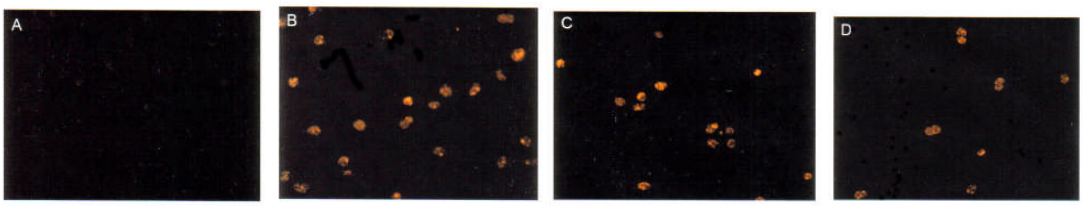

Figure 36: Inhibition IFA results. Parasites were incubated for 30 mins with a mixture of mouse serum (1:1000 diluted) and 50μg/ml peptide. A: folded oxidised peptide **43**, B: control without peptide, C: reduced alkylated peptide **44**, D:unfolded reduced peptide **42**.

For a detailed analysis of the humoral immune response, mimetic **13**-specific mouse B-cell hybridomas were generated in the group of Prof. G. Pluschke. From these hybridomas it was possible to produce 50 monoclonal antibodies. Characterisation of the mAbs is in progress.

1.2.4.7 Synthesis of alanine-scanning mimetics for epitope mapping studies

In order to investigate the epitopes recognised by the monoclonal antibodies induced by immunization with peptide mimetic **13**-loaded virosomes, it was decided to synthesize a library of alanine-scanning mimetics.

peptide	Sequence
14	NISQHQ**C**A**C**KKQ**C**PQNS**G**C**C**FRHLDEREE**C**K**C**LLNYKQE**G**DK**C**VENPNPT
15	NISQHQ**C**V**C**AKQ**C**PQNS**G**C**C**FRHLDEREE**C**K**C**LLNYKQE**G**DK**C**VENPNPT
16	NISQHQ**C**VK**C**AQ**C**PQNS**G**C**C**FRHLDEREE**C**K**C**LLNYKQE**G**DK**C**VENPNPT
17	NISQHQ**C**VKK**C**A**C**PQNS**G**C**C**FRHLDEREE**C**K**C**LLNYKQE**G**DK**C**VENPNPT
18	NISQHQ**C**VKKQ**C**A**C**QNS**G**C**C**FRHLDEREE**C**K**C**LLNYKQE**G**DK**C**VENPNPT
19	NISQHQ**C**VKKQ**C**P**C**ANS**G**C**C**FRHLDEREE**C**K**C**LLNYKQE**G**DK**C**VENPNPT
20	NISQHQ**C**VKKQ**C**PQ**C**AS**G**C**C**FRHLDEREE**C**K**C**LLNYKQE**G**DK**C**VENPNPT
21	NISQHQ**C**VKKQ**C**PQN**C**A**G**C**C**FRHLDEREE**C**K**C**LLNYKQE**G**DK**C**VENPNPT
22	NISQHQ**C**VKKQ**C**PQNS**G**C**C**A**C**RHLDEREE**C**K**C**LLNYKQE**G**DK**C**VENPNPT
23	NISQHQ**C**VKKQ**C**PQNS**G**C**C**F**C**AHLDEREE**C**K**C**LLNYKQE**G**DK**C**VENPNPT
24	NISQHQ**C**VKKQ**C**PQNS**G**C**C**FR**C**ALDEREE**C**K**C**LLNYKQE**G**DK**C**VENPNPT
25	NISQHQ**C**VKKQ**C**PQNS**G**C**C**FRH**C**ADEREE**C**K**C**LLNYKQE**G**DK**C**VENPNPT
26	NISQHQ**C**VKKQ**C**PQNS**G**C**C**FRHL**C**AEREE**C**K**C**LLNYKQE**G**DK**C**VENPNPT
27	NISQHQ**C**VKKQ**C**PQNS**G**C**C**FRHLD**C**AREE**C**K**C**LLNYKQE**G**DK**C**VENPNPT
28	NISQHQ**C**VKKQ**C**PQNS**G**C**C**FRHLDE**C**AEE**C**K**C**LLNYKQE**G**DK**C**VENPNPT
29	NISQHQ**C**VKKQ**C**PQNS**G**C**C**FRHLDER**C**AE**C**K**C**LLNYKQE**G**DK**C**VENPNPT
30	NISQHQ**C**VKKQ**C**PQNS**G**C**C**FRHLDERE**C**AC**K**C**L**LNYKQE**G**DK**C**VENPNPT
31	NISQHQ**C**VKKQ**C**PQNS**G**C**C**FRHLDEREE**C**A**C**LLNYKQE**G**DK**C**VENPNPT
32	NISQHQ**C**VKKQ**C**PQNS**G**C**C**FRHLDEREE**C**K**C**A**L**NYKQE**G**DK**C**VENPNPT
33	NISQHQ**C**VKKQ**C**PQNS**G**C**C**FRHLDEREE**C**K**C**L**A**NYKQE**G**DK**C**VENPNPT
34	NISQHQ**C**VKKQ**C**PQNS**G**C**C**FRHLDEREE**C**K**C**LL**A**YKQE**G**DK**C**VENPNPT
35	NISQHQ**C**VKKQ**C**PQNS**G**C**C**FRHLDEREE**C**K**C**LLN**A**KQE**G**DK**C**VENPNPT
36	NISQHQ**C**VKKQ**C**PQNS**G**C**C**FRHLDEREE**C**K**C**LLNY**A**QE**G**DK**C**VENPNPT
37	NISQHQ**C**VKKQ**C**PQNS**G**C**C**FRHLDEREE**C**K**C**LLNYK**A**E**G**DK**C**VENPNPT
38	NISQHQ**C**VKKQ**C**PQNS**G**C**C**FRHLDEREE**C**K**C**LLNYKQ**A**G**G**DK**C**VENPNPT
39	NISQHQ**C**VKKQ**C**PQNS**G**C**C**FRHLDEREE**C**K**C**LLNYKQE**G**A**G**K**C**VENPNPT
40	NISQHQ**C**VKKQ**C**PQNS**G**C**C**FRHLDEREE**C**K**C**LLNYKQE**G**D**A**C**C**VENPNPT

Table 8: Sequences of alanine-scanning peptide mimetics

These mimetics could then be used in binding assays with the antibodies, to discover which mutations caused differences in binding behaviour. Initially, it was

planned to synthesise a library where each residue, apart from cysteines and glycines and omitting the N-terminal and C-terminal extremities, would be systematically mutated to an alanine residue. The peptide sequences described in **Table 8** were to be assembled by parallel synthesis methods using a peptide synthesis robot.

The mimetics were to be synthesised in two batches, and the synthesis of the first batch of peptides – peptides **14** to **26** was started on a Multisyntech Syro II parallel peptide synthesiser. The synthesis was carried out on chlorotrityl chloride resin preloaded with Fmoc-Thr(^{t}Bu)-OH, on a 0.03mmol scale. Since the robot used had no automatic synthesis monitoring system, the syntheses were monitored by the regular sampling of resin from several reaction vessels. After 10, 20 and 29 amino acid coupling cycles, resin samples were taken and the peptide was cleaved from the resin and side-chain deprotected for RP-HPLC and LC-MS analysis. The synthesis was then allowed to continue until all coupling cycles were complete, and the final products were cleaved from the solid support and side-chain deprotected using TFA containing H_2O, EDT and TIS as scavengers. Examples of chromatograms of the products obtained after 10, 20, 29 and 47 coupling cycles are shown in **Figure 37**.

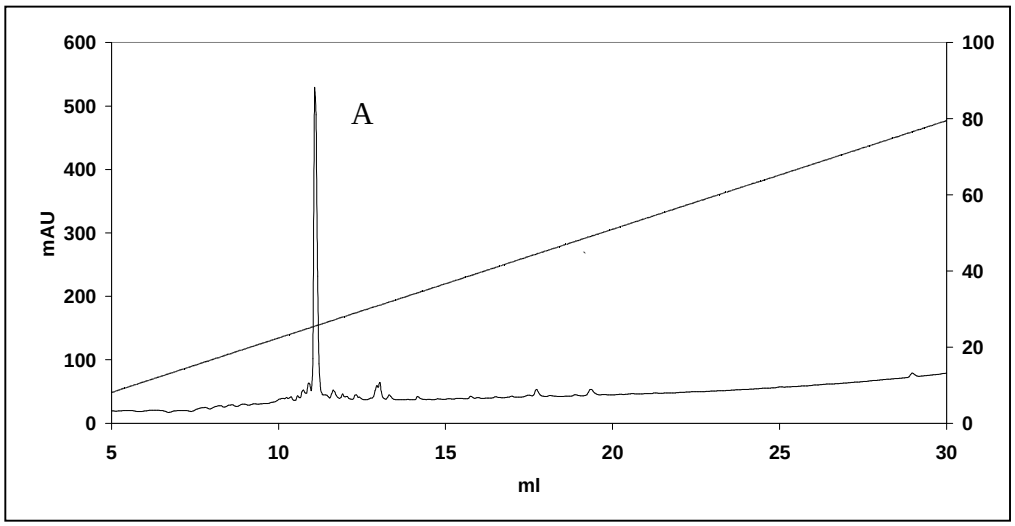

Figure 37: (A) Chromatogram of a peptide cleaved from the solid support after 10 coupling cycles.

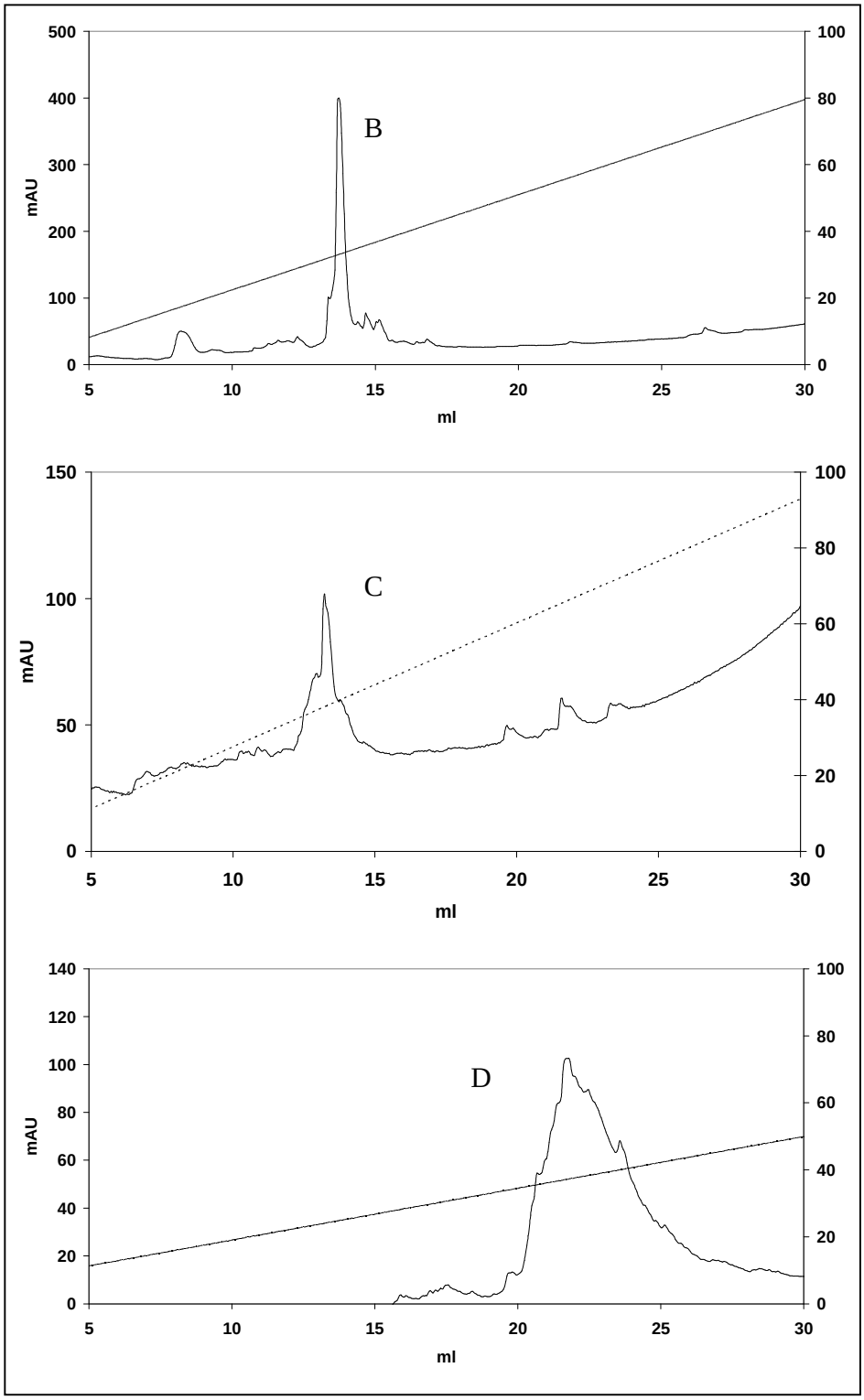

Figure 37 (continued): (B) Chromatogram of peptide cleaved after 20 cycles of coupling. (C) Chromatogram of peptide cleaved after 29 cycles of coupling. (D) Chromatogram of peptide cleaved after 48 cycles of coupling. For HPLC conditions see appendix 4.

Unfortunately, all of the products obtained from the robot after 47 coupling cycles gave disappointing chromatograms similar to the example in **Figure 37**. The crude peptide products were subjected to oxidising conditions, in the hope that the many peaks may be due to the presence of several partially oxidised structures, which would resolve themselves into one fully oxidised product under the correct conditions. Unfortunately, no improvement was observed in the chromatograms of the products after oxidation, although it seemed that oxidation occurred, since all peaks shifted slightly to lower retention times, as illustrated by the chromatograms in **Figure 38**.

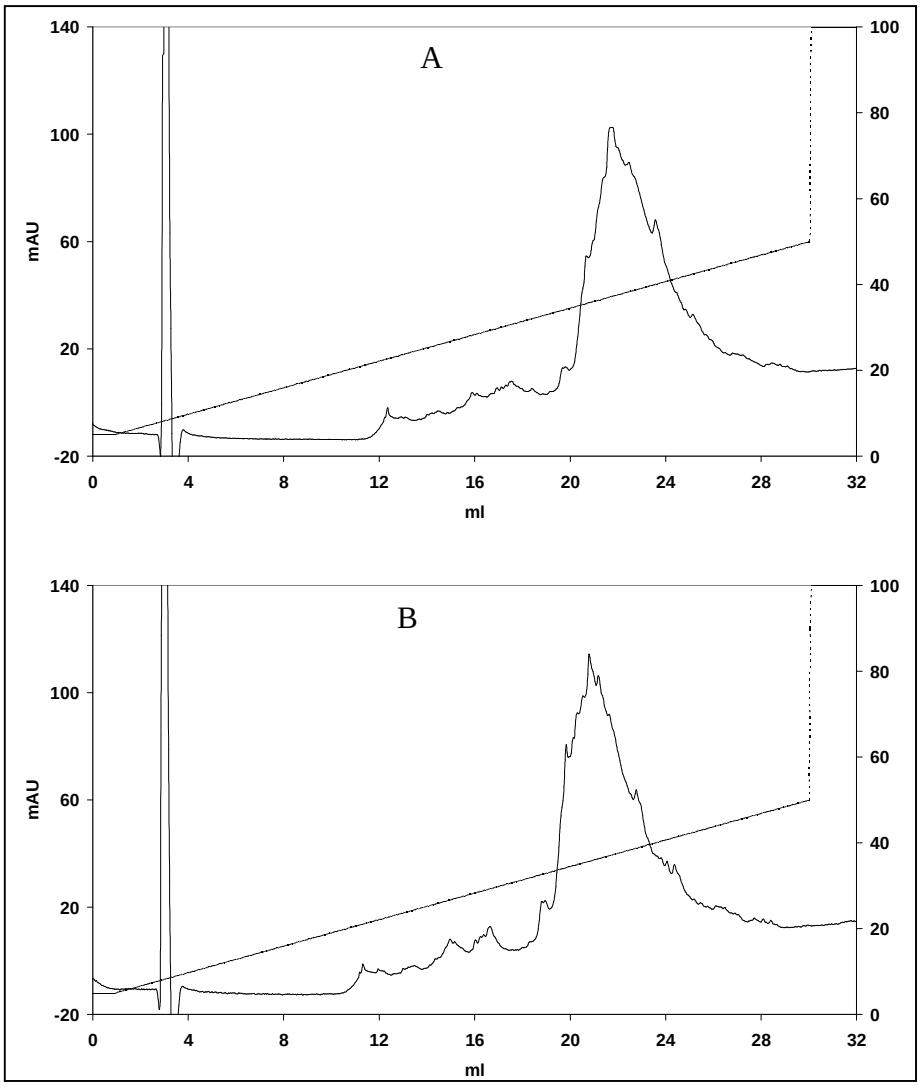

Figure 38: Chromatograms of a peptide product from the robot synthesis before (A) and after (B) treatment in oxidative conditions. For HPLC conditions see appendix 4.

It was concluded that the assembly of such a long peptide sequence was beyond the scope of a parallel synthesis robot where no monitoring of the success of coupling steps and no feedback loops were available. Therefore, it was decided to revert to usual batchwise peptide synthesis methods, and to begin with a smaller library of mimetics.

A new, smaller library was therefore designed, where only positively charged and aromatic residues were to be mutated to alanine. This would provide a group of eleven peptide mimetics, with the advantage that the mutations would be fairly well spread throughout the peptide sequence. **Table 9** gives the sequences of the mimetics in the small library.

peptide	sequence
40	NISQHQCVKKQCPQNSGCFRHLDEREECKCLLNYKQEGDACVENPNPT
36	NISQHQCVKKQCPQNSGCFRHLDEREECKCLLNYAQEGDKCVENPNPT
35	NISQHQCVKKQCPQNSGCFRHLDEREECKCLLNAKQEGDKCVENPNPT
31	NISQHQCVKKQCPQNSGCFRHLDEREECACLLNYKQEGDKCVENPNPT
28	NISQHQCVKKQCPQNSGCFRHLDEAEECKCLLNYKQEGDKCVENPNPT
24	NISQHQCVKKQCPQNSGCFRALDEREECKCLLNYKQEGDKCVENPNPT
23	NISQHQCVKKQCPQNSGCFAHLDEREECKCLLNYKQEGDKCVENPNPT
22	NISQHQCVKKQCPQNSGCARHLDEREECKCLLNYKQEGDKCVENPNPT
16	NISQHQCVKAQCPQNSGCFRHLDEREECKCLLNYKQEGDKCVENPNPT
15	NISQHQCVAKQCPQNSGCFRHLDEREECKCLLNYKQEGDKCVENPNPT
41	NISQAQCVKKQCPQNSGCFRHLDEREECKCLLNYKQEGDKCVENPNPT

Table 9: Sequences of peptides to be synthesised in the small library

These peptides were prepared via a divergent synthesis method, beginning with the synthesis of a large batch (1 mmol) of resin loaded with the sequence CVENPNPT, common to all of the peptide mimetics. The resin was then split into three batches corresponding to approximately 0.25 mmol, 0.375 mmol and 0.375 mmol. The first of the 0.375 mmol batches was further split into four equal parts which were used for the synthesis of peptides **31, 35, 36** and **40**. The second of the 0.375 mmol batches was used for the synthesis of the sequence EECKCLLNYKQEGDKCVENPNPT. The resin from this synthesis was then split into four equal parts and used for the preparation of peptides **22, 23, 24** and **28**. The remaining 0.25 mmol batch of resin was used for the assembly of the sequence QCPQNSGCFRHLDEREECKCLLNYKQEGDKCVENPNPT. Peptides **15, 16** and **41** were then prepared from this resin. The synthetic strategy is summarised in **Scheme 6**.

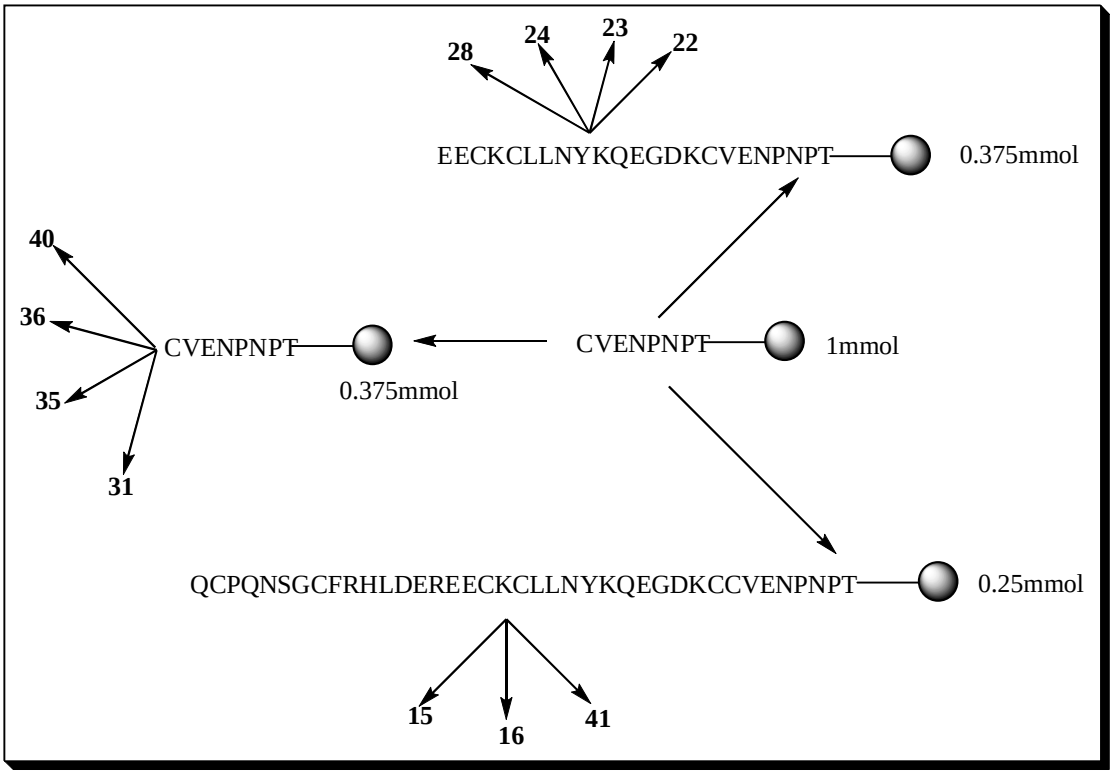

Scheme 6: Divergent synthetic strategy for the synthesis of a small library of mimetics based on peptide **2**.

The peptides could all be synthesised successfully by this method, each showing one major peak when the crude cleaved and deprotected product was analysed by RP-HPLC. The crude products were directly treated with oxidising conditions (5 mg/ml peptide in 0.1 M Tris buffer at pH 8.4 containing 3 mM cysteine, 0.3 mM cystine and 5 mM EDTA). Examples of the chromatograms of two crude linear products and the corresponding oxidised products are shown in **Figure 39**. As illustrated here, the oxidative folding of most of the peptides led to one major product in RP-HPLC which could easily be purified to provide a good yield of a single clean product. However, the oxidation of crude peptides **22** and **23** did not lead to a clear single product, as illustrated in **Figure 40**. The two peaks of equal intensity seen in the chromatogram of peptide **23** were collected and analysed separately. Peptide **22** was not further developed, since peptides **23** and **24** could be expected to give a good indication of whether this region is important for binding to the antibodies.

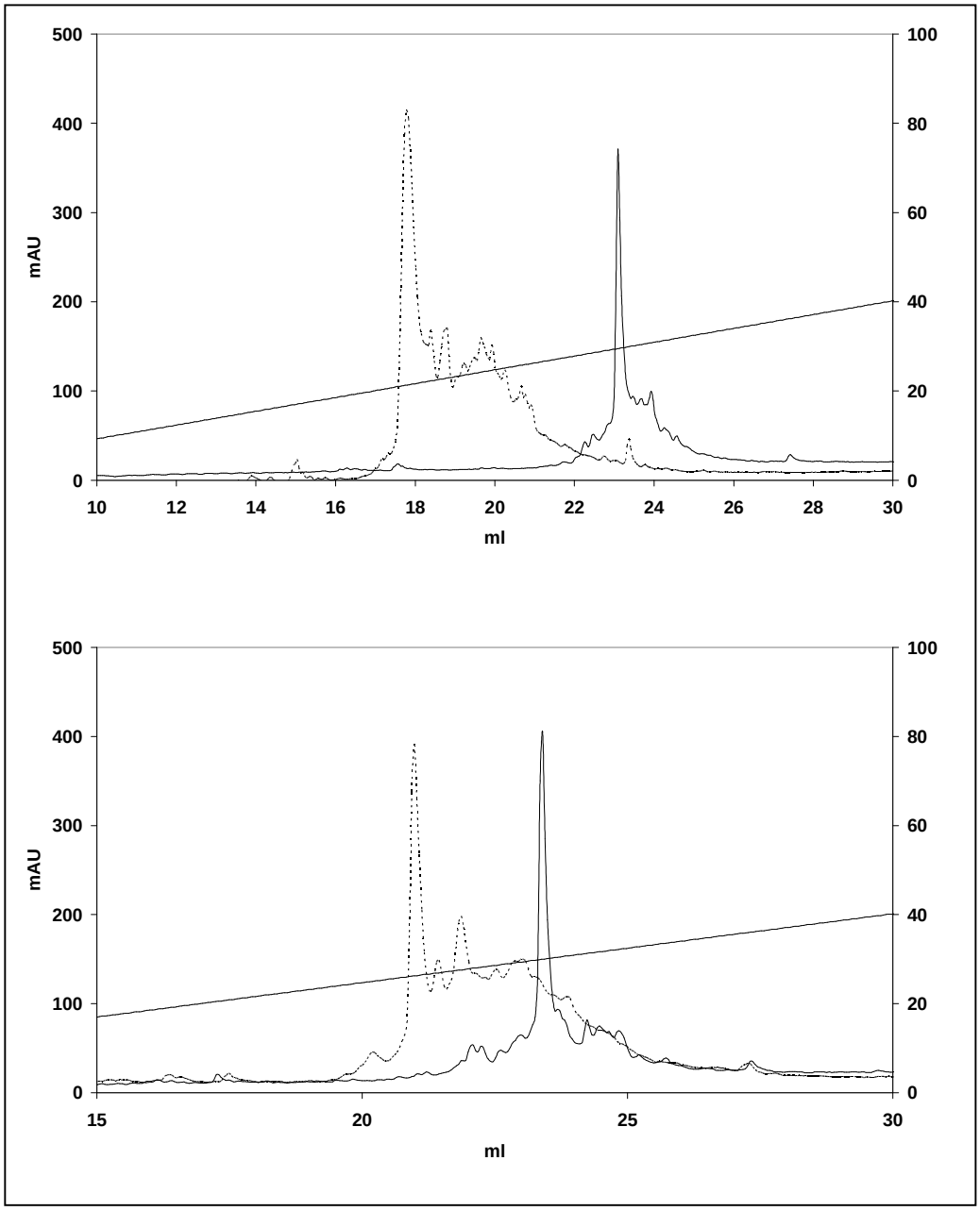

Figure 39: Oxidative folding of peptide **15** (above) and peptide **24** (below). The chromatograms of the unfolded peptides are shown by the solid lines, and the chromatograms of the oxidatively folded products by the dotted lines. For HPLC conditions see appendix 4.

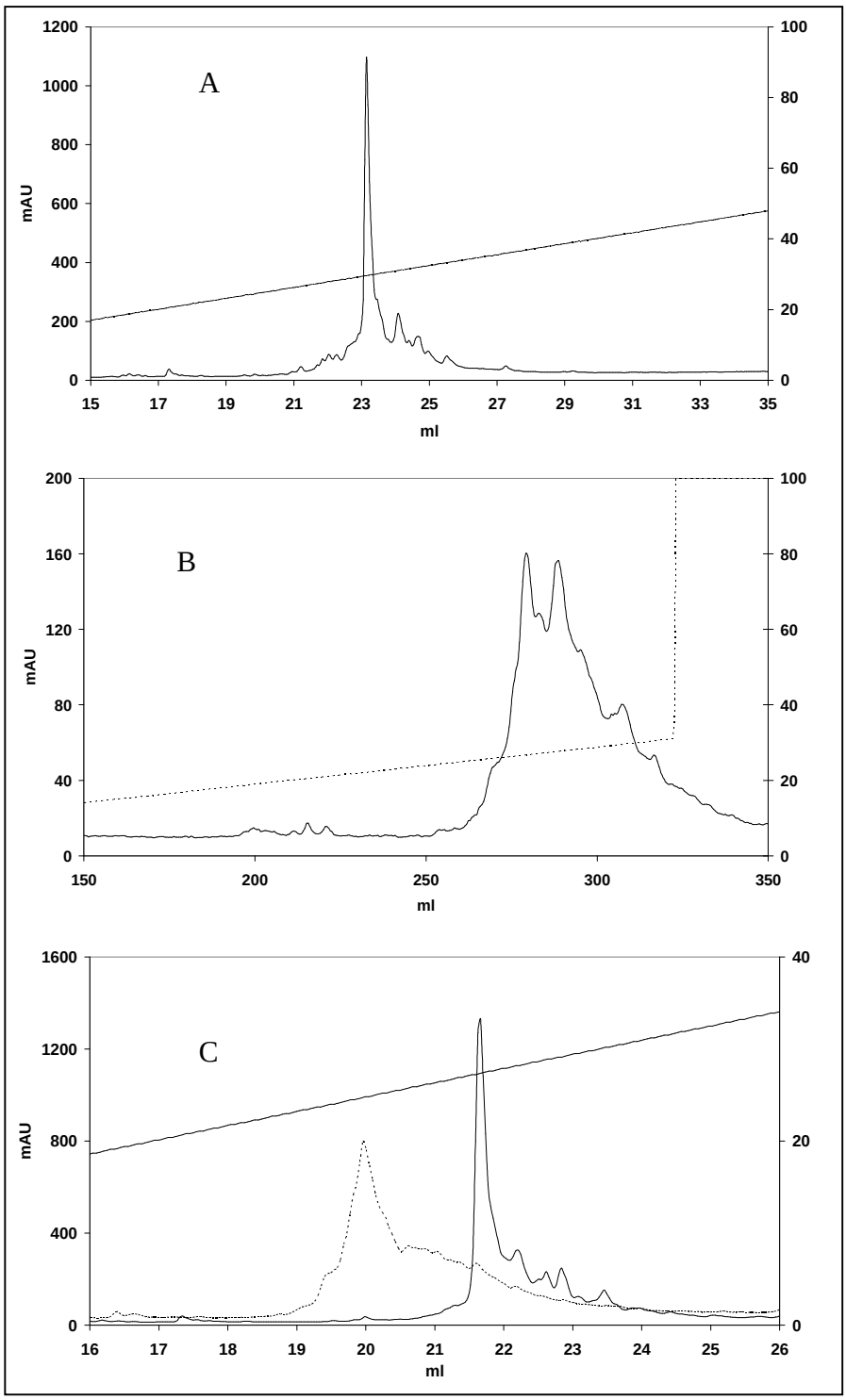

Figure 40: (A) Analytical HPLC chromatogram of unfolded peptide **23** (A), Chromatogram of oxidatively folded peptide **23** from HPLC purification (B) and analytical chromatograms of unfolded (solid line) and oxidatively folded (dotted line) peptide **22** (C).

All of the purified oxidised peptides were analysed by RP-HPLC, MALDI-MS, amino acid analysis, ^{1}H, TOCSY and NOESY NMR measurements, and circular dichroism. Circular dichroism spectra of peptide **42**, peptide **43** (C-terminal free acid analogues of peptides **1** and **2**) and peptide **44**, a modified analogue of peptide **42**, where the cysteine thiol groups were alkylated using iodoacetamide, were also measured for comparison (**Figure 41**). Expected and measured masses of the products are given in **Table 10**.

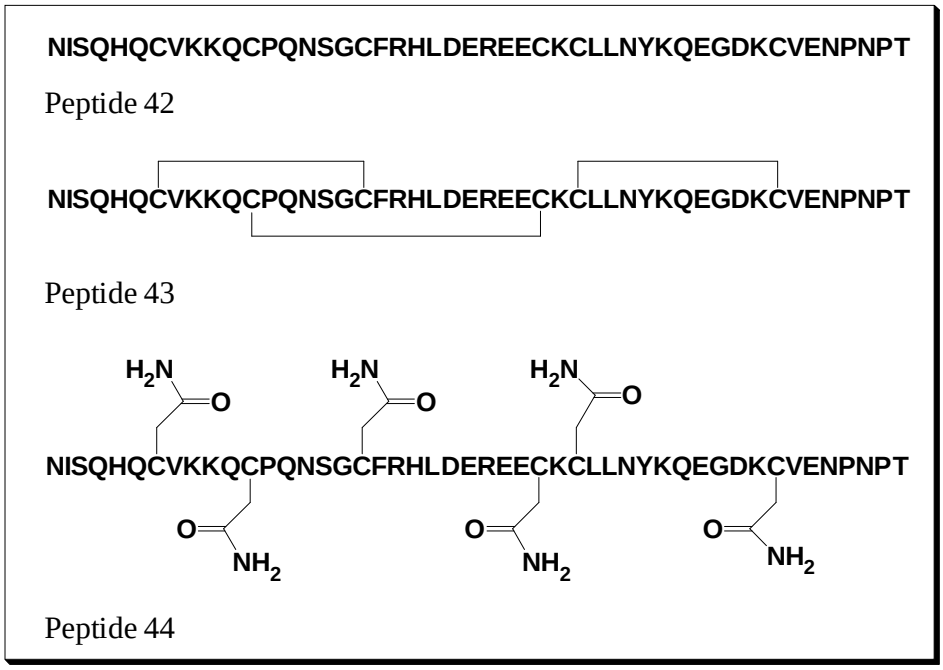

Figure 41: Structures of peptides **42, 43** and **44**

The NMR and circular dichroism spectra were measured in order to evaluate the 3-dimensional structural similarity between the mutant peptides and the original peptide structure **2**. It was considered important to be sure that the 3D structure was maintained in the new mimetics before they could be used for epitope-mapping studies with the monoclonal antibodies. Otherwise, changes in binding affinity could be due to structural factors rather than due to the amino acid mutations.

Linear peptide	Calculated mass linear peptide	Oxidised peptide	Calculated mass oxidised peptide	Measured mass oxidised peptide (MALDI-Tof)
15	5536.2	**45**	5530.2	5529.838
16	5536.2	**46**	5530.2	5531.001
22	5517.2	**47**	5511.2	n.d.
23	5508.2	**48**	5502.2	5502.351
24	5527.2	**49**	5521.2	5520.637
28	5508.2	**50**	5502.2	5502.052
31	5536.2	**51**	5530.2	5530.885
35	5501.2	**52**	5495.2	5496.490
36	5536.2	**53**	5530.2	5530.525
40	5536.2	**54**	5530.2	5530.607
41	5527.2	**55**	5521.2	5520.631
42	5593.3	**43**	5587.3	5585.9

Table 10: Masses of peptides based on peptide **2**. Typical error in the measurements was ±0.1%

1.2.4.8 NMR and circular dichroism

The ^{1}H NMR spectra of the alanine scanning mimetics showed similarity to each other and to the spectrum of the native peptide sequence. To identify in which residues the few differences that were observed were occurring, TOCSY and NOESY spectra were measured, to facilitate comparison with the assigned spectra of the native peptide.

The circular dichroism spectra are displayed in **Figure 42** below. As can be seen, all of the spectra of oxidised products, except that of **52** show a weak positive band at 232-234 nm, which is also observed in the spectrum of mouse EGF [105] and of other EGF-like domains [106]. All spectra are dominated by a negative band at 201-203 nm, which is also seen in other EGF-like domains. The spectra can be sorted into two main categories: in most spectra, as in the spectrum of the native folded sequence, the positive band has an intensity of around +1000 degcm^{2}dmol^{-1}, and the negative band around -18000 degcm^{2}dmol^{-1}. Two spectra, those of peptides **48** and **50** show a weaker negative band, whilst the positive band maintains a similar intensity. The spectra of the unfolded peptides show a marked difference to those of the folded peptides in the absence of any positive band. The lack of positive band in the spectrum of peptide **52** suggests that it may have a different 3-dimensional structure. The alkylated linear peptide shows a weaker positive band than its analogue containing free thiol groups. The peptide with free thiol groups is possibly more likely to adopt a conformation related to the native structure. Although some differences are seen in the CD spectra of the mimetics, all

except mimetic **52** show positive and negative bands at the same positions and were therefore presumed to be structurally related to the native peptide and useful for epitope-mapping studies.

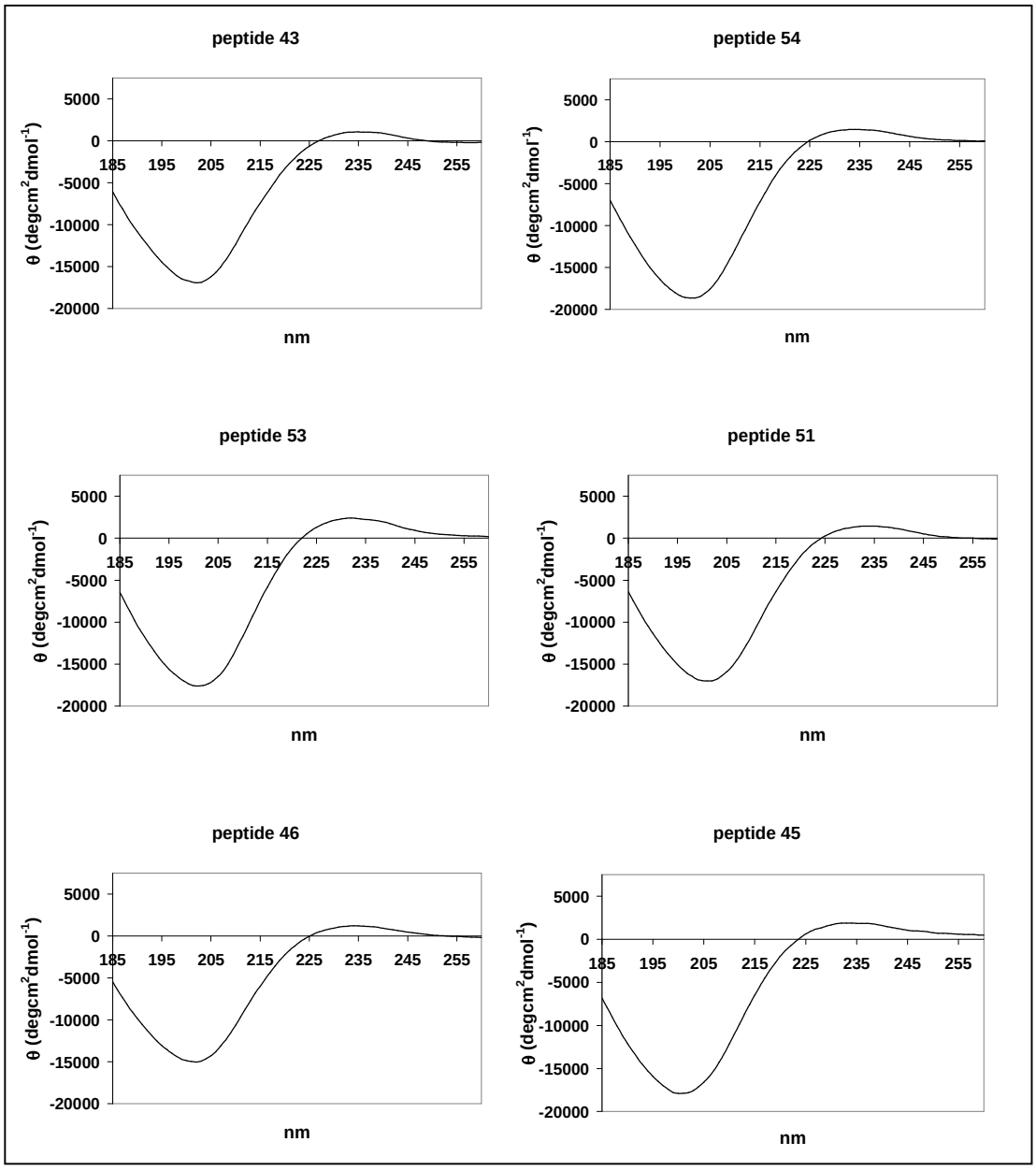

Figure 42: CD spectra of native peptide **43** and mutant peptides **54**, **53**, **51**, **46** and **45.** samples were measured in a 0.1 mm quartz thermostatable cuvette at 25°C, using a JASCO J-715 spectropolarimeter. A scan speed of 50 nm/min, a 1 second response time and a 1 nm spectral bandwidth were used. CD spectra are presented after subtraction of a blank containing only buffer and the optical activity is reported in units of mean residue ellipticity (deg cm^2 $dmol^{-1}$). Spectra are presented as an average of four scans and results are given for the range 185-260 nm.

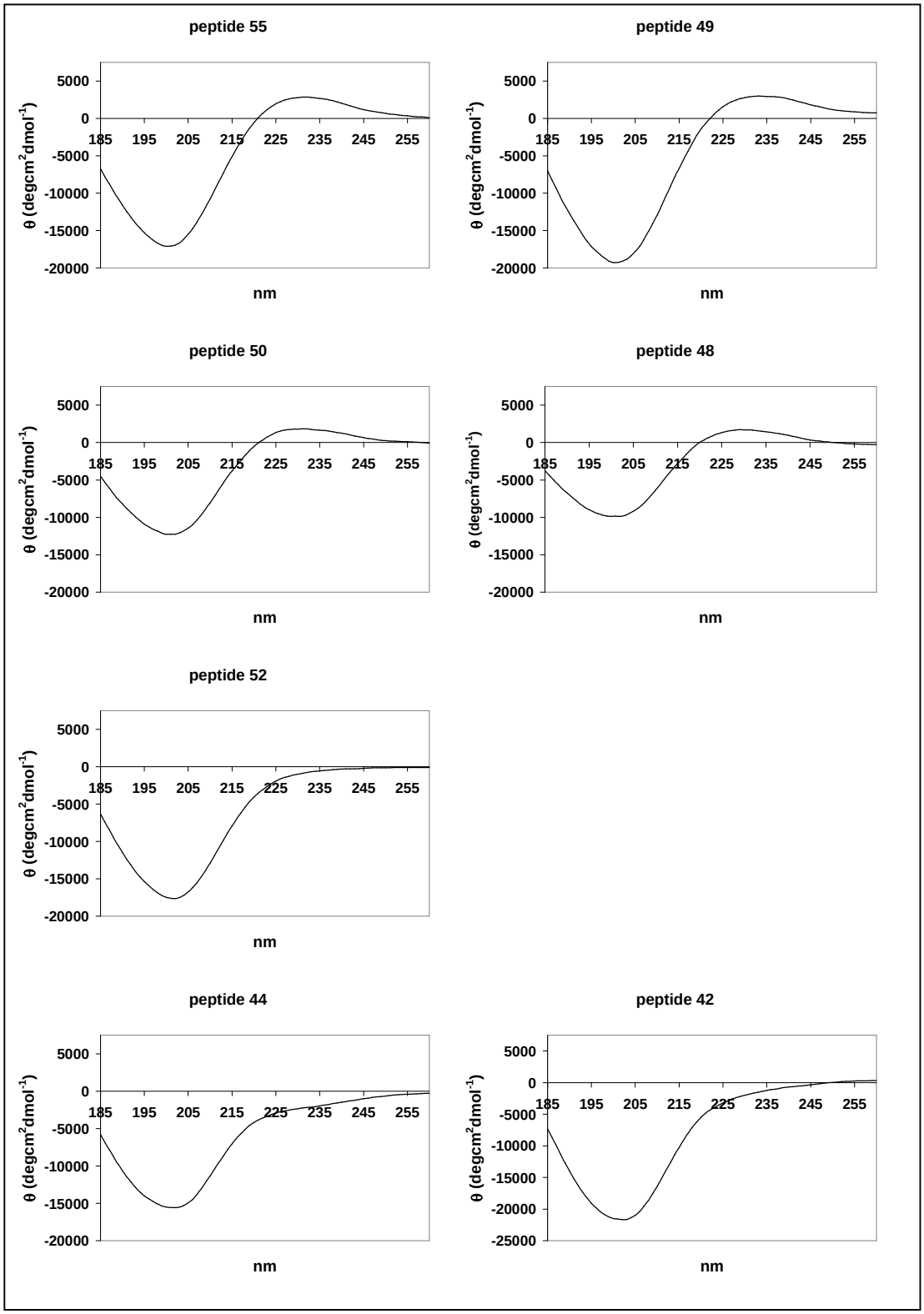

Figure 42 (continued): CD spectra of linear peptides **42** and **44**, and mutant folded peptides **48, 49, 50, 52** and **55**.

1.2.5 Discussion

Plasmodium falciparum merozoite surface protein 1 (MSP-1) is a major merozoite surface antigen [64, 65] and the MSP-1_{19} fragment that remains anchored to the merozoite surface during erythrocyte invasion, along with its precursor MSP-1_{42}, are leading malaria vaccine candidates now in clinical development [107]. MSP-1_{19} contains epitopes recognized by inhibitory antibodies [72]. Epitope mapping studies have identified epitopes in the first EGF-like domain as well as conformational epitopes involving both EGF-like domains [75, 76]. Immunization studies have shown that MSP-1_{19} induces, as well as inhibitory antibodies, blocking antibodies that block the invasion-inhibitory function of the inhibitory antibodies [74], and also neutral antibodies that bind to epitopes on the protein but have neither an inhibitory, nor a blocking function. The correct folding of both EGF-like domains seems to be essential for induction of parasite cross-reactive immune responses.

The aim of this project was to produce a synthetic, conformationally accurate mimetic of the first EGF domain of *P. falciparum* MSP-1_{19}, to be tested as a potential constituent of a multi-antigen malaria vaccine candidate. In initial studies, a 48-amino acid residue peptide mimetic corresponding to the first EGF-like domain of the *P. falciparum* MSP-1 could be synthesised.

Oxidation studies based on published methods for the oxidative folding of multiply-disulfide bonded proteins and peptides showed that all conditions involving a redox couple such as reduced and oxidised glutathione, or cyteine/cystine, led to one major fully oxidised product. Air oxidation led to a complex mixture of products. After optimisation, favourable conditions could be found for the oxidation of the linear peptide mimetic to one major fully oxidised product, which could be shown by NMR and proteolysis studies to possess the 1-3, 2-4, 5-6 disulfide bonding pattern expected for an EGF-like domain. The solution structure of the peptide could be solved from NMR measurements and was shown to compare favourably with the published structure of MSP-1_{19}, the membrane-anchored double EGF-like domain protein that remains on the merozoite surface during erythrocyte invasion.

Parallel to the structural investigation of the peptide mimetic, a lipopeptide was developed for inclusion in virosomes for immunization studies. Attempted oxidative

folding of a linear lipopeptide mimetic was unsuccessful due to solubility problems, but through modification of the peptide sequence with a highly nucleophilic hydrazine group, the oxidised peptide could be coupled to an activated phospholipid to provide a lipopeptide that could be included in virosomes and used in immunizations of mice to elicit an immune response. The sera obtained from the mice were found to be cross-reactive with both the mimetic, and with *Plasmodium falciparum* parasites. Binding of merozoites to antibodies could be competed by oxidised peptide, but not by reduced, linear peptide, demonstrating the importance of a conformationally correct mimetic. 50 monoclonal antibodies could be produced from the immunized mice. These results suggest that the synthetic peptide represents a good mimetic of the first EGF-like domain of MSP-1_{19}.

For epitope mapping studies on these antibodies, a series of mutant peptides, where a single residue of the original sequence was replaced by alanine, was produced by solid-phase peptide synthesis, followed by oxidation using previously established methods. Most of these mimetics were shown by circular dichroism and NMR studies to be structurally related to the original mimetic structure. In future work the binding of the monoclonal antibodies to these mimetics, along with the original natural sequence mimetic, and reduced, linear analogues should be investigated, in a first step towards the characterisation of the epitopes. Based on these investigations, and studies into the immunological properties of the individual antibodies, it may be possible to develop further mutants for binding studies, and the results could be exploited for the design of vaccine candidates capable of eliciting only protective, rather than protecting and blocking antibody responses. The chemical synthesis of a highly disulfide-bonded and structured peptide mimetic of an important malaria antigen could be an important step towards a synthetically feasible, immunologically competent vaccine candidate.

1.3 Design, synthesis and characterisation of a merozoite surface protein 4 mimetic

1.3.1 EGF-like domains in *Plasmodium falciparum*

As mentioned above, ten merozoite surface proteins (MSPs) have so far been identified in *Plasmodium falciparum*. Five of these proteins contain EGF-like domains, as does the sexual stage antigen Pfs25 [108]. Encouraged by the success of the oxidative folding method developed for the first EGF-like domain of MSP-1, and by the immunological results of immunizations with the synthetic EGF-like mimetic, we decided to investigate the synthesis, oxidative folding and immunological properties of other *P. falciparum* EGF-like domains. The synthesis of the first EGF-like domain of MSP-8 was attempted in the Robinson group, but investigation of this mimetic could unfortunately not be continued due to synthetic problems during the solid phase peptide assembly, that could not be overcome by the usual methods (unpublished results). MSP-8 contains two epidermal-growth factor-like domains [109], and it has been shown that parasites whose MSP-1 EGF-like domains are substituted with the equivalent regions of MSP-8 are still able to invade erythrocytes and grow efficiently [110], which suggests that the EGF-like domains of MSP-8 play a related role to those in MSP-1, or that they play a redundant role. Indeed, it has been recently shown that MSP-8 is non-essential for *P. falciparum* growth [111].

MSP-4 was identified in 1997 and shown to be a 40kDa protein containing a single EGF-like domain at the C-terminus [112]. Studies have shown that recombinantly produced MSP-4 is immunogenic in laboratory animals and that several regions of the protein are also natural antigens in *P. falciparum* infection of humans [113]. These investigations also showed that the EGF-like domain is very important for the conformation of the whole protein, since the disruption of the EGF-like domain led to greatly reduced antibody reactivity of some sera, even in regions of the protein outside the EGF-like domain. Later studies by the same group showed that oral immunization of mice with MSP-4 could induce antibodies reacting with all regions of the protein, including antibodies to at least one conformational epitope in the region containing the

EGF-like domain [114]. During this study, mice were also orally immunized with the *Plasmodium yoelii* homologue of MSP-4, PyMSP4/5. It was shown that this immunization induced partial protection against subsequent lethal challenge with *P. yoelii*. It has also been demonstrated that immunization with a combination of PyMSP4/5 and PyMSP-1_{19} induced improved protection against lethal challenge compared to immunization with either of these proteins alone [115, 116]. In some cases, a combination of antigens led to an increase in antibody response to MSP-1_{19}, but a combination of antigens always caused improved protection, whether an increased anti-MSP-1_{19} response was observed or not. It has also been shown that immunization with MSP4/5 from one species can induce protection against challenge by another species in mice [117]. Although several polymorphic sites have been identified in *Plasmodium falciparum* MSP-4, they do not seem to be frequent in the EGF-like region [118]. These results provide evidence that an MSP-4 mimetic could form a useful component of a multi-antigen subunit malaria vaccine.

1.3.2 Mimetic design

To date, no 3D structure of the MSP-4 protein is available. However, we decided to synthesise a mimetic of the EGF-like domain of MSP-4 using the methods developed for the synthesis of the MSP-1_{19} mimetic, in order to study the structure of the mimetic and to test it as a possible malaria vaccine component. The amino acid sequence selected for these studies is illustrated in **Figure 43**.

LEDEDLCKHNNGDCGDDKLCEYVGNRRVKCKCKEGYKLEGIECVELLSLAS-NH_2

Figure 43: Sequence of peptide **56**.

1.3.3 Results

1.3.3.1 Peptide synthesis

The first attempted synthesis was monitored, as mentioned in the previous chapter, by the measurement of the UV absorbance at 301 nm of the Fmoc-deprotection

solution. The amount of dibenzofulvene present in the solution flowing from the solid phase reaction vessel gives a qualitative indication of how much Fmoc was present on the resin before deprotection and thus of the efficiency of the preceding amino acid coupling step. These UV absorbance values are stored in the machine as a 'deprotection profile'.

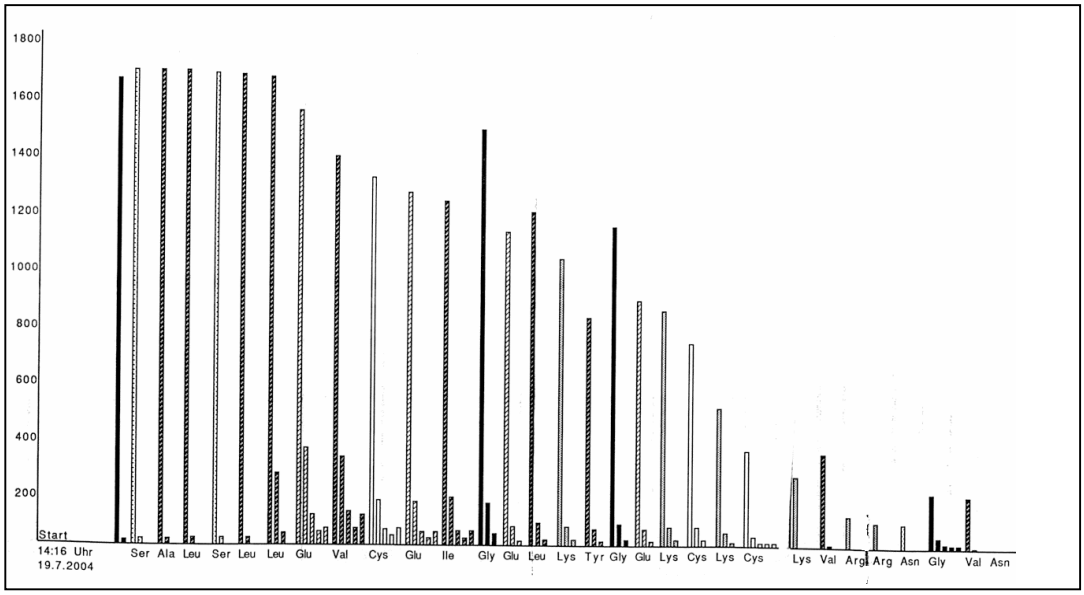

Figure 44: Fmoc deprotection profile from initial attempted synthesis of peptide **56**.

Unfortunately, as illustrated in **Figure 44**, there was a rapid drop in the absorbance of the deprotection solution after the 6th coupling reaction in the initial attempted synthesis of peptide **56**, indicating a decrease in coupling efficiencies. The coupling efficiencies continued to drop rapidly from this point onwards so that after 23 coupling reactions almost no coupling was occurring any more. This kind of profile is not unusual for the first attempt at synthesis of a new long peptide sequence. Indeed, the most frequently encountered synthetic problem in the solid phase assembly of peptides is the occurrence of a rapid decrease in amino acid coupling yields, which leads to poor yields of the desired peptide product and, where no capping of free amine sites is employed in between the coupling reactions, a mixture of undesired products of similar molecular weights and physical properties to the desired product, which lead to difficult purification steps. These drops in coupling yields can occur anywhere in the peptide sequence, and their occurrence is not predictable from knowledge of the sequence alone. Obviously, the longer the peptide sequence, the higher the probability of such a problem arising at some point during the peptide assembly, so that this phenomenon is quite

familiar to those involved in the preparation of longer peptide mimetics. There are some general features of peptide sequences which can indicate whether they are more or less likely to present synthetic problems, since the problem is in general believed to be caused by the formation of intra-chain or inter-chain hydrogen bonding between backbone residues, or hydrophobic interactions, which can reduce the permeability of the peptidyl-resin for reagents and solvents. The problem is more likely to occur, for example, where there are several consecutive identical residues, or a series of consecutive uncharged residues or consecutive charged residues. The chances of the problem occurring are reduced in sequences containing proline residues, which are known for their structure-disrupting properties. Many solutions have been proposed to overcome the problems of 'difficult sequences', including reduced resin loading [119], the use of polar matrices as the solid support [120, 121], solubilizing protecting groups [122] and amide protecting groups within the peptide chain [123]. In order to improve the yield of peptide **56**, two of these techniques were employed, namely diminished resin loading and the use of pseudoproline residues to introduce solubilizing protecting groups. Pseudo-prolines [122] (ΨPro) are serine-, threonine-, and cysteine-derived cyclic building blocks that act as reversible protecting groups for Ser Thr and Cys and disrupt β-sheet structures that can be a source of interchain aggregation in peptide synthesis. A generalized structure is shown in **Figure 45.**

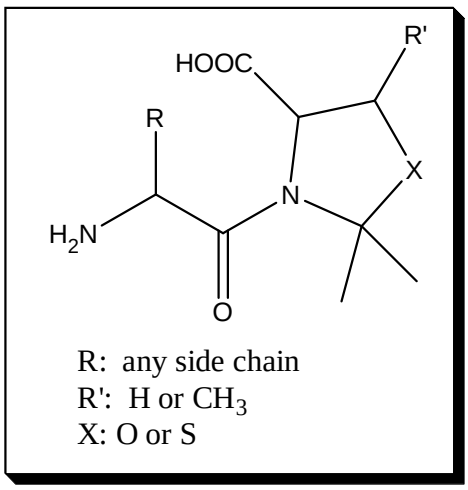

Figure 45: The general structure of a pseudo-proline building block.

These building blocks can therefore be incorporated into any sequences where Ser, Thr and Cys residues occur. Thus, where difficulties are encountered in an initial

trial synthesis of a certain sequence, a second trial can be carried out including a ΨPro, preferably such that the ΨPro is introduced in the peptide assembly a few synthetic steps before the drop in coupling was observed in the initial trial synthesis. In general, it is desirable to introduce the ΨPro rather closer to the beginning of the peptide assembly than to the end. Many of these ΨPro building blocks are now commercially available in a form suitable for use in automated solid phase peptide synthesis. In the assembly of peptide **56**, a ΨPro could be introduced at position 48, that is, in the fourth amino acid coupling cycle. The building block used was Fmoc-Leu-Ser($\Psi^{Me,Me}$pro)-OH, **57**, illustrated in **Figure 46**.

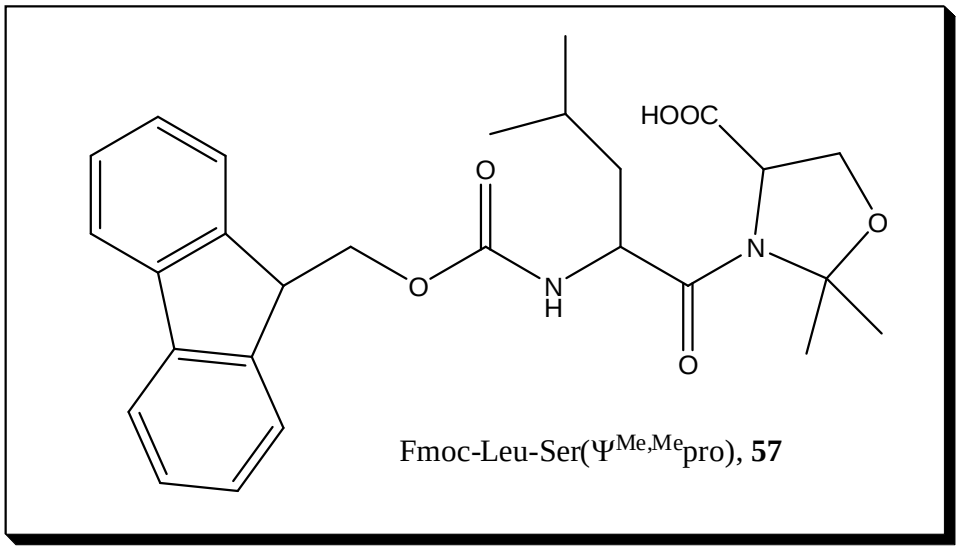

Fmoc-Leu-Ser($\Psi^{Me,Me}$pro), **57**

Figure 46. Structure of pseudoproline **57**.

The Rink amide MBHA resin, which is supplied in the Fmoc-protected form, is usually supplied with a loading of around 0.6-0.7 mmol/g. In order to reduce the loading of peptide on this resin, 1g of resin was filled into the reaction vessel of the peptide synthesiser and Fmoc-deprotected. 0.27 mmol Fmoc-Ser(^{t}Bu)-OH were used for the loading of the resin, with an extended coupling reaction time, with the aim of producing resin loaded with approximately 0.25 mmol/g Ser(^{t}Bu). Capping was then carried out using acetic anhydride in order to block the remaining free amine site on the resin, to prevent the loading of other amino acid residues on these sites at later stages of the peptide assembly. The peptide sequence was then assembled as usual, with the use of 4 equivalents (1 mmol) of each protected amino acid for the coupling steps. The

combination of reduced loading and the inclusion of a pseudoproline building block, along with some double coupling cycles (coupling is repeated with a fresh aliquot of the amino acid/activation agent/base) led to a much more successful peptide assembly, which could be carried all the way to the final 51 residue product. The Fmoc deprotection profile from the improved synthetic method is illustrated in **Figure 47**.

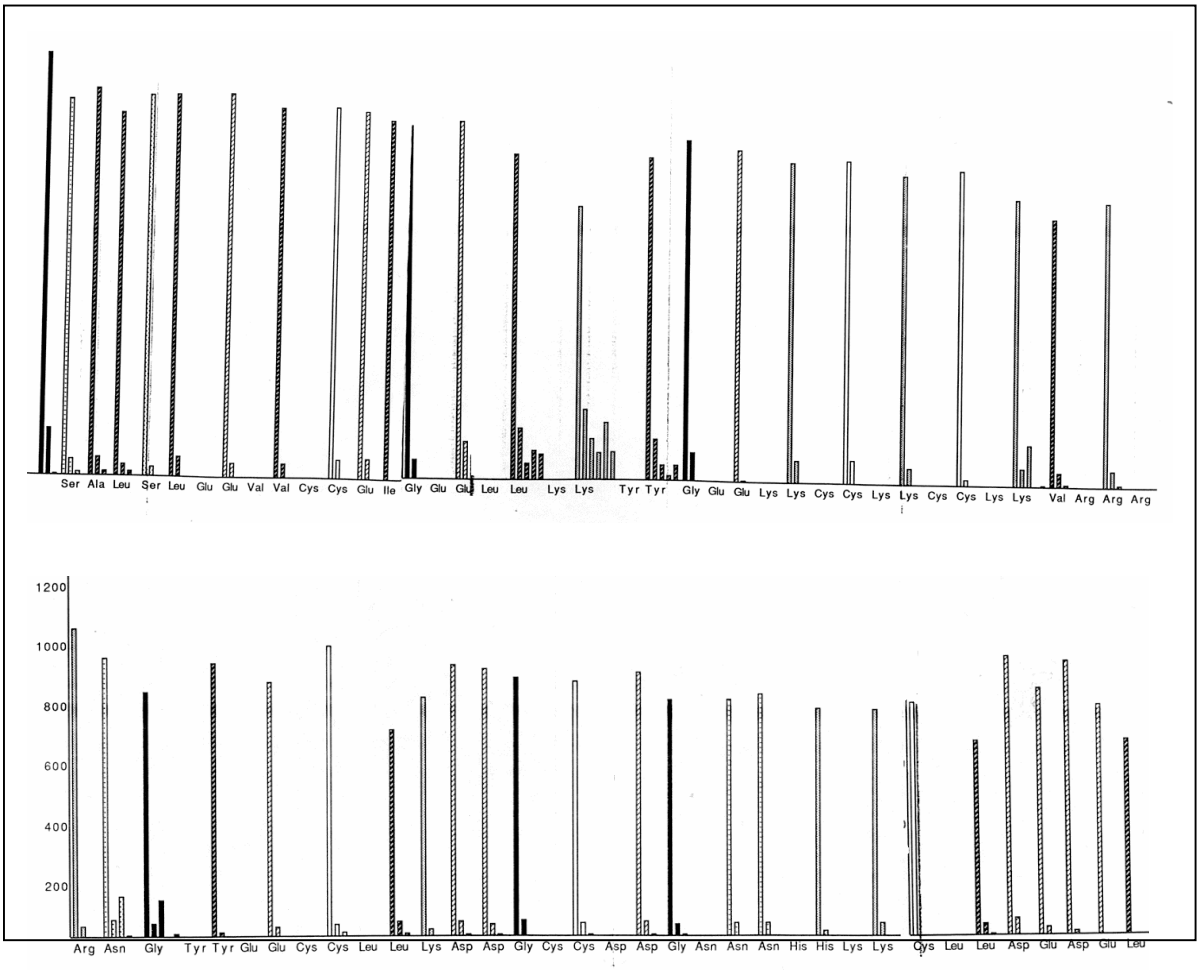

Figure 47: Fmoc deprotection profile from synthesis of peptide **56** after improvements in synthetic methods.

The peptide sequence could thus be completely assembled, and was subsequently cleaved from the resin and side-chain deprotected in one step using TFA containing 1% TIS, 2.5% EDT and 2.5% water as scavengers. This step also removed the protecting group from the pseudoproline building block to release it as a Leu-Ser dipeptide unit. The RP-HPLC profile of the crude deprotected peptide is shown in **Figure 48**. As illustrated by the chromatogram, the assembly of this peptide sequence did not result in

such a clean product as seen after the assembly of peptide **1**. However, it was possible to identify the peak corresponding to the desired peptide by mass spectrometry, and to separate it by RP-HPLC to obtain a purified product, the chromatogram of which is shown in **Figure 49**.

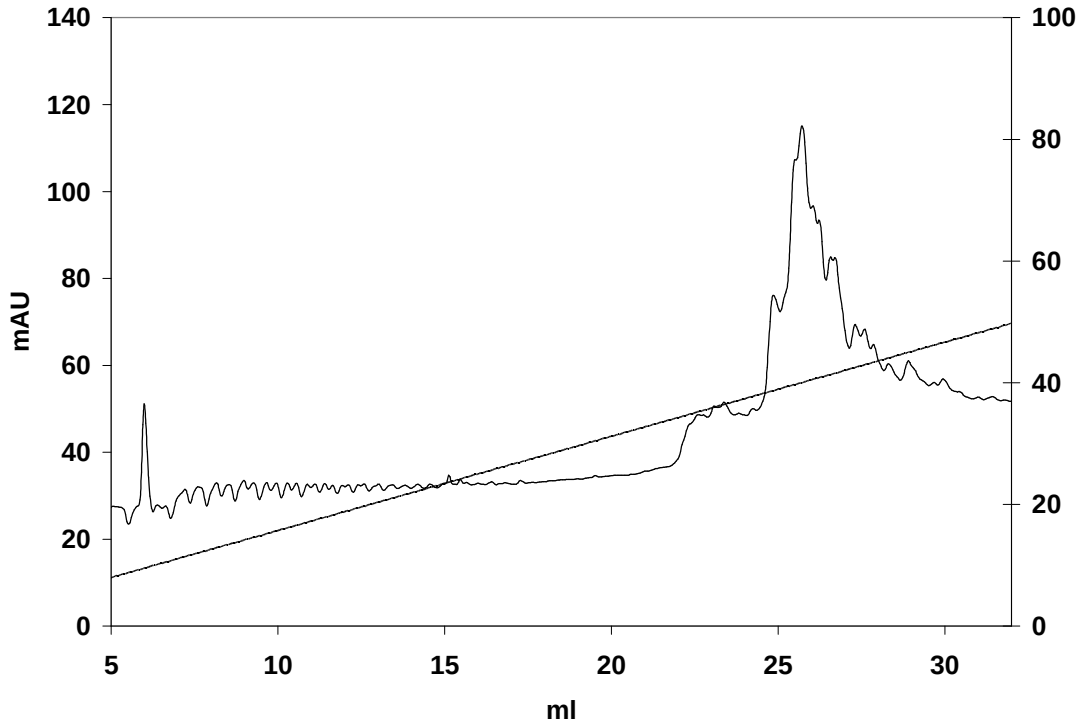

Figure 48: Chromatogram of crude peptide **56**. For HPLC conditions see Appendix 4.

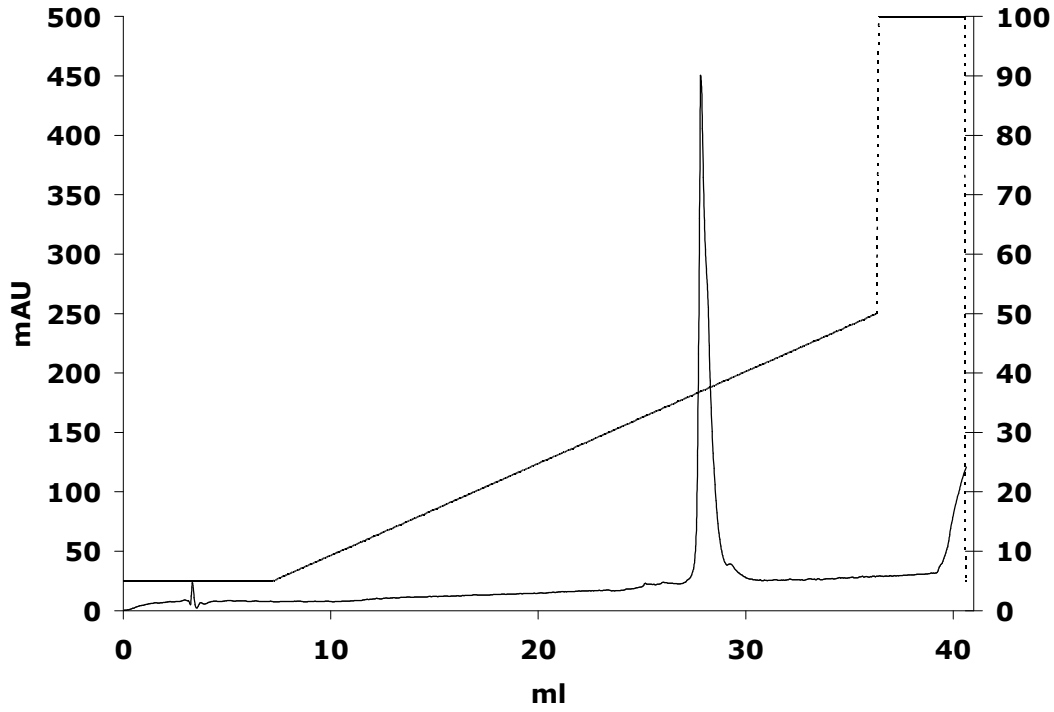

Figure 49: Chromatogram of purified linear peptide **56**. For HPLC conditions see Appendix 4.

Calculated MW: 5735.42 g/mol, measured ESI-Tof-MS: 5735.1±0.01% (m/z).

1.3.3.2 Oxidative folding

This product was treated under the same oxidation conditions as peptide 1, namely 5mg/ml peptide in 0.1 M Tris buffer at pH 8.4 containing 3 mM cysteine, 0.3 mM cystine and 10 mM EDTA. After 48 h stirring at room temperature, the chromatogram shown in **Figure 50** was recorded. The product that forms the main peak in this chromatogram could be separated, and the chromatogram of the purified product is shown in **Figure 51**. Calculated MW: 5729.53g/mol, measured ESI-Tof MS: 5729.2±0.01% (m/z). The peptide was shown by the Ellman test to contain no free thiol groups. The ^{1}H NMR spectrum of this oxidised product showed a wide spread of peaks in the amide proton region, as illustrated in **Figure 52**, suggesting that the product should have a well-defined structure.

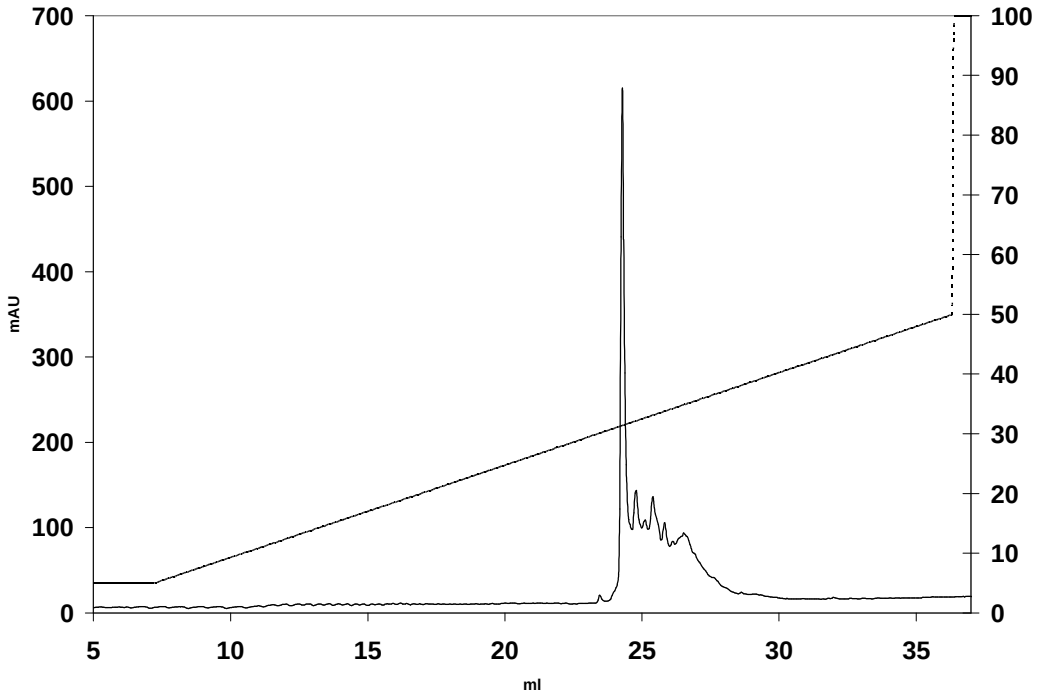

Figure 50: Chromatogram of crude oxidised peptide **58**. For HPLC conditions see Appendix 4.

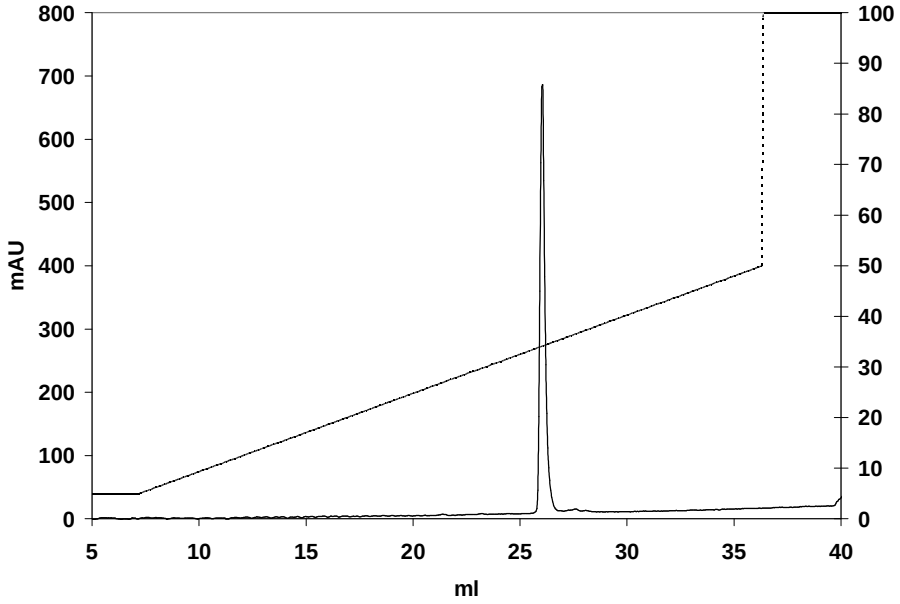

Figure 51: Chromatogram of purified peptide **58.** For HPLC conditions see Appendix 4.

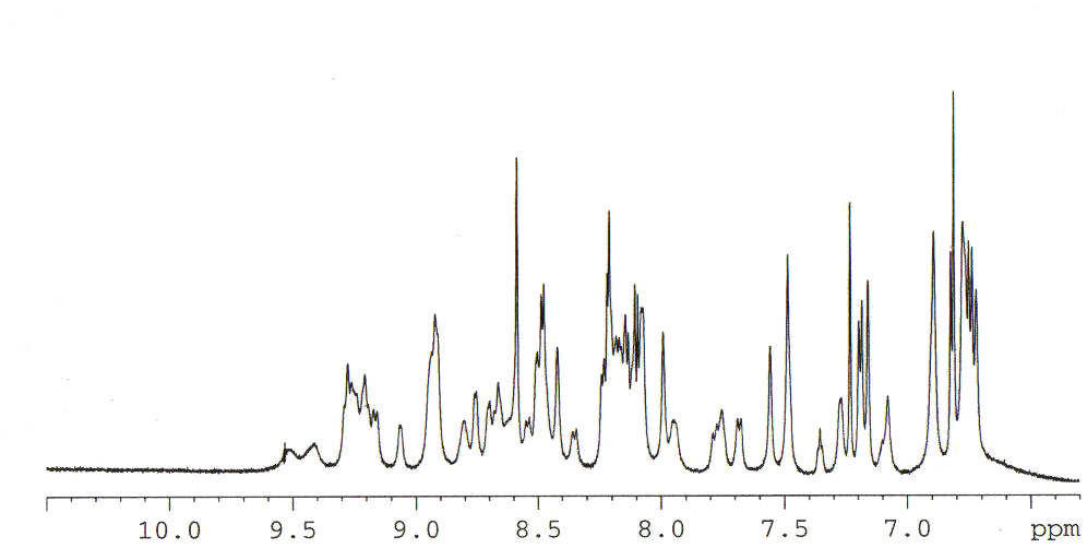

Figure 52: NH region of NMR spectrum of peptide **58**.

It is presumed that the product obtained was the desired peptide mimetic **58** illustrated in **Figure 53**, although due to the lack of a 3D structure, and since disulfide mapping of this product has not been completed, the exact pattern of the disulfide bonding has not yet been confirmed.

Figure 53: Presumed disulfide bonding in oxidised peptide **58**.

1.3.3.3 Synthesis of modified MSP-4 mimetic for immunizations

Based on the success of the oxidative folding of peptide **56** to form peptide **58**, it was decided to directly use the hydrazinoglycine-based coupling method in order to produce a phospholipid-bound peptide to be used for immunizations. The modified peptide **59** could be assembled using the same methods as described for peptide **56**, and could be oxidatively folded in the same way, to produce the putative oxidised mimetic

peptide **60**. These products were analysed by ESI-MS and RP-HPLC. The chromatograms of the purified linear peptide **59**, as well as the crude oxidation product and the purified peptide **60** are shown in **Figure 55**. Calculated MW of **59**: 5807.65 g/mol, measured ESI-Tof-MS (m/z): 5806.9±0.01%. Calculated MW of **60**: 5801.60 g/mol), measured ESI-Tof-MS (m/z): 5801.4±0.01%.

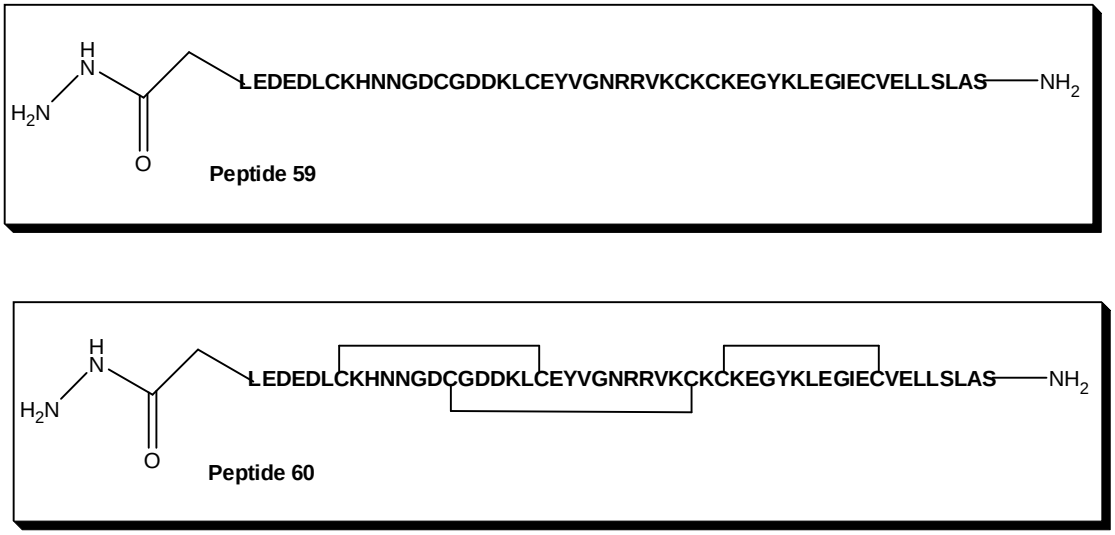

Figure 54: Structures of peptide mimetics **59** and **60**.

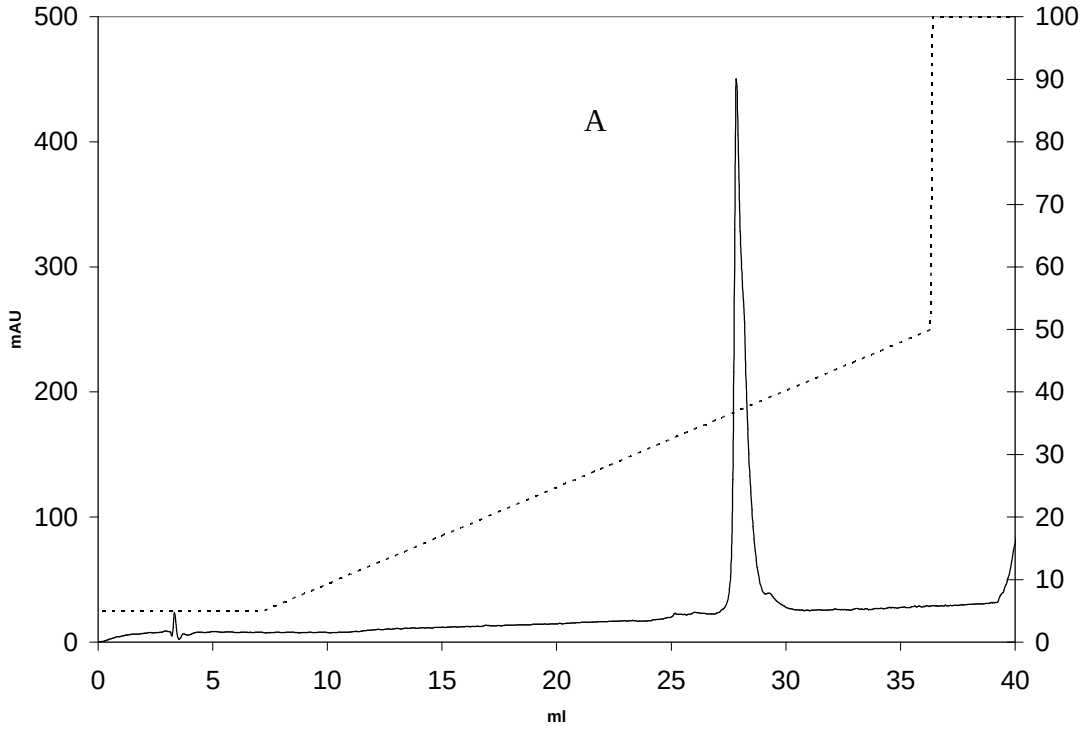

Figure 55: (A) Chromatogram of purified peptide mimetic **59**. For HPLC conditions see Appendix 4.

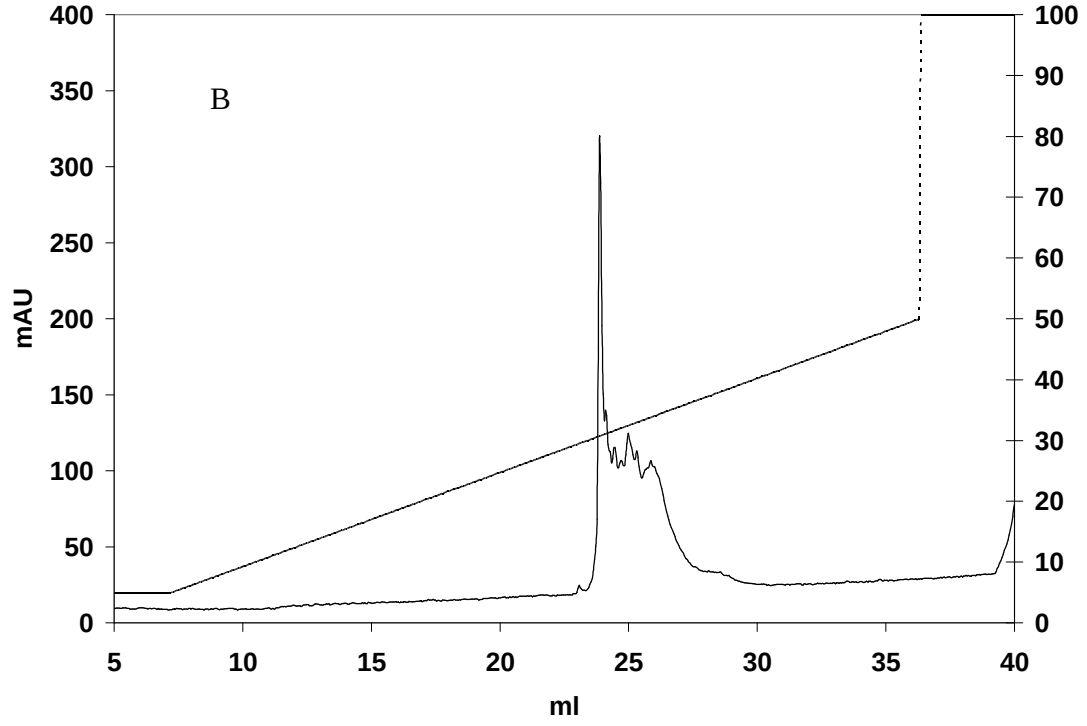

Figure 55 (B): Chromatogram of crude peptide **60.** For HPLC conditions see Appendix 4.

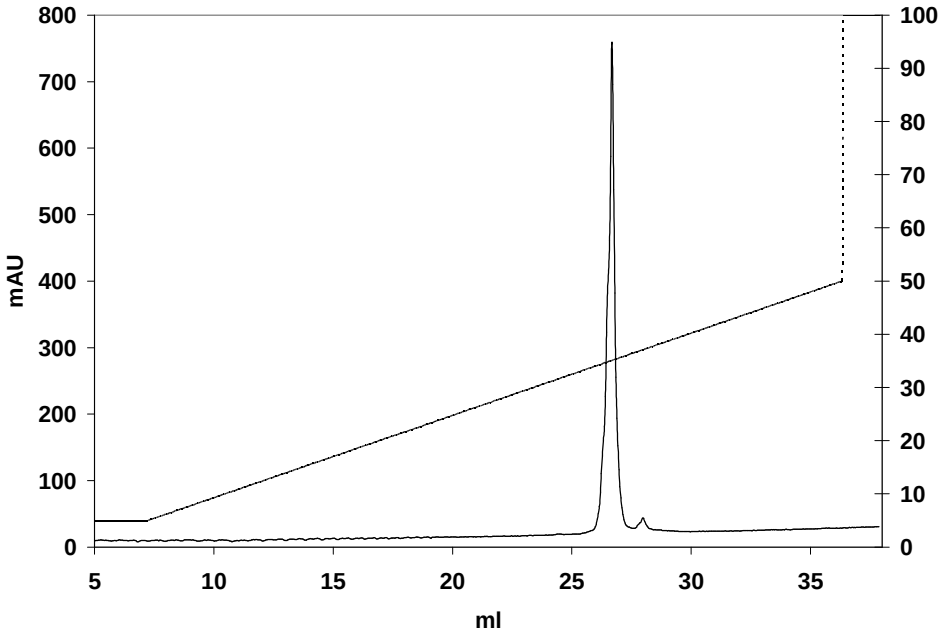

Figure 55 (C) Chromatogram of purified peptide **60**. For HPLC conditions see Appendix 4.

1.3.3.4 Lipopeptide synthesis

Peptide **60** was used in coupling reactions with activated phosphatidyl ethanolamine (**12**). The peptide was dissolved in water at a concentration of between 5 mg/ml and 7.5 mg/ml and the pH of the solution was adjusted to between 5.1 and 5.4. This solution was then mixed with between 1 and 2 equivalents of the NHS-activated ester of phosphatidyl ethanolamine (**12**), dissolved in *tert*-butanol. The mixture was stirred at room temperature and the progress of the reaction was monitored by LC-MS. After 1 h of reaction it was possible to observe a peak which displayed a mass spectrum corresponding to the desired product: 1316 (M+5H)/5, 1097 (M+6H)/6. The RP-HPLC chromatogram of the coupling reaction mixture is shown in **Figure 56**. After 4 h of reaction, it was observed that no more of the product peak was being formed. The product was therefore purified. Calculated MW for lipopeptide **61**: 6574.45, measured ESI-Tof-MS (m/z): 6575.1±0.01%.

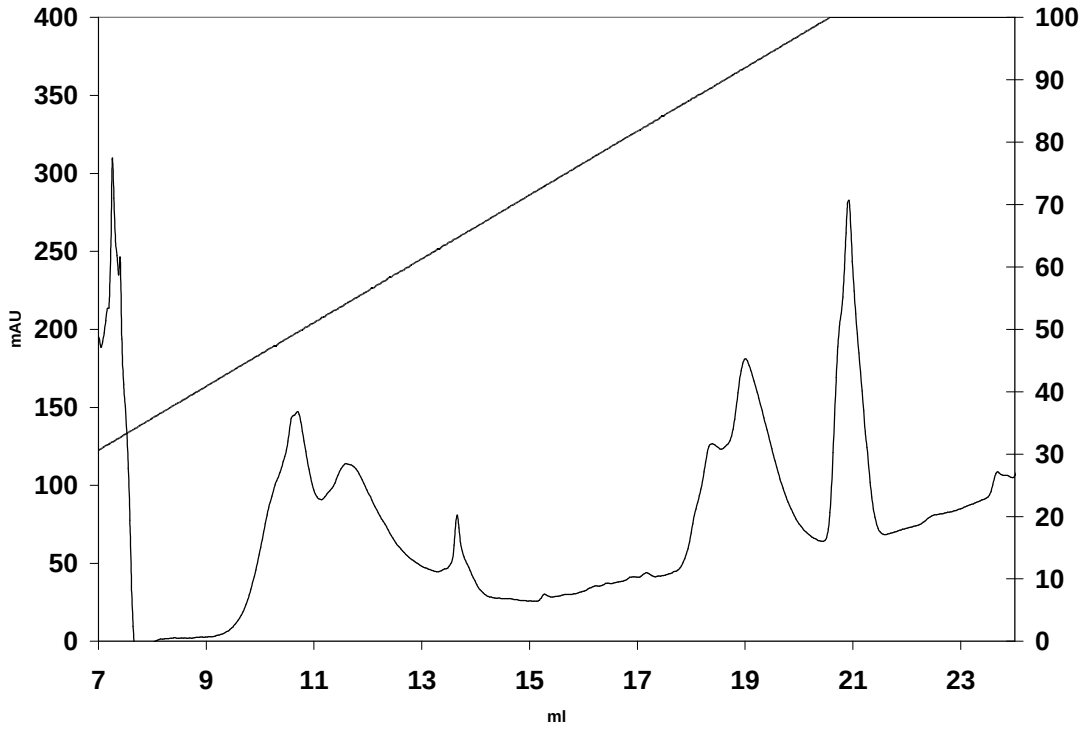

Figure 56: Crude reaction mixture after reaction of peptide **60** with activated phosphatidyl ethanolamine (**12**). The final peak is the lipopeptide **61**. For HPLC conditions see Appendix 4.

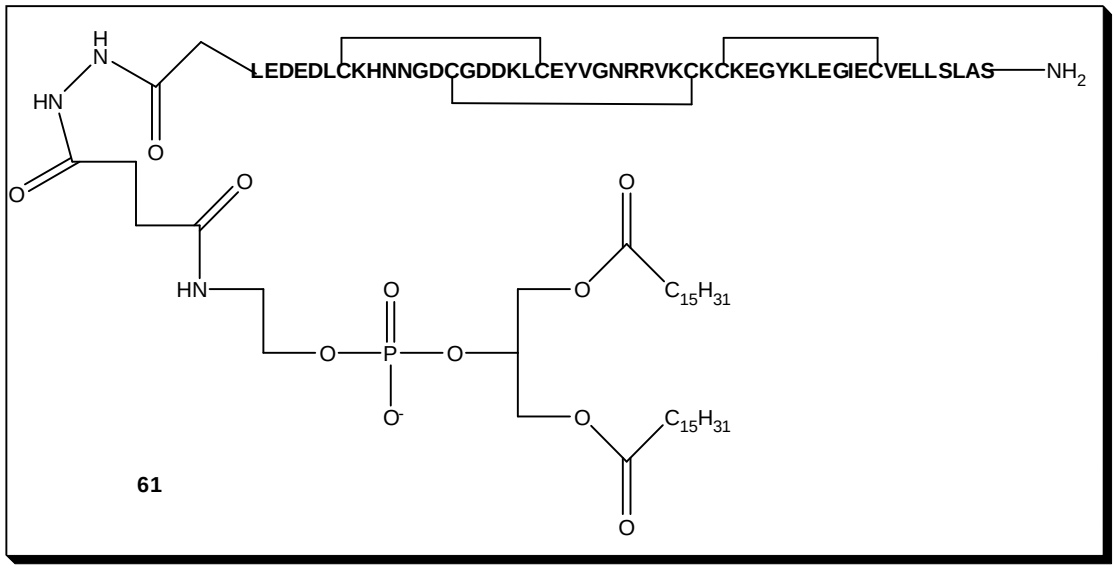

Figure 57: Structure of the lipopeptide **61**.

Unfortunately, the yields of product **61** were quite low (~10%), and variation of the reaction conditions, for example, by increasing or decreasing concentrations, or increasing the number of equivalents of the activated phospholipid, or the proportion of

tert-butanol in the reaction mixture, had very little effect on the outcome. This problem could be explained by the nature of the purified product, which had a waxy consistency and was not easily water-soluble, and could possibly be adhering to reaction vessels as it was formed, without being easily observed. Attempts to clean glass vessels with various solvents in order to recover adsorbed product met with little success. However, it was possible to obtain a sufficient quantity of the product for immunization studies. Unfortunately, probably due to the physical properties of the product, it was not found to induce any immune response after loading into virosomes under standard conditions. It is as yet unclear whether the waxy product had truly been incorporated into the virosomes. In any case, it seemed that this poorly soluble mimetic did not represent a good vaccine candidate.

1.3.3.5 Synthesis of modified MSP-4 mimetic with improved solubility

In the Robinson group, some success has been seen in the improvement of solubility of phospholipidyl-peptide mimetics by the inclusion of a series of lysine residues at the N-terminus of the peptide sequence adjacent to the linker used for phospholipid attachment. It was decided to test the effect of such a modification on the properties of mimetic **61**. Therefore the modified amino acid sequence of peptide **62**, illustrated below, was assembled on Rink amide resin.

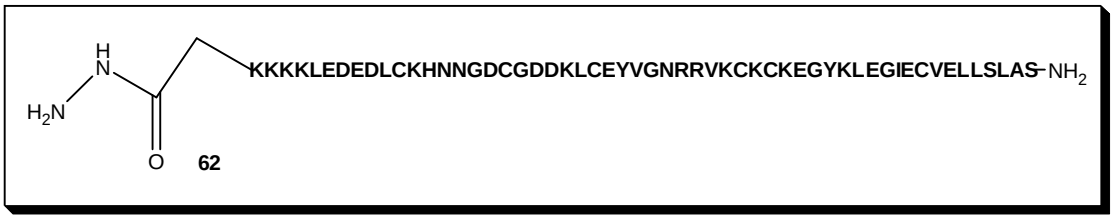

Figure 58: Structure of modified peptide mimetic **62**.

The crude product, cleaved from the resin and side-chain deprotected could be oxidatively folded without any previous purification, using the same conditions as described for the oxidation of peptide **56**, and leading to the product (**63**) illustrated by the chromatogram in **Figure 59 (A)**. The peak at lowest retention time was shown by LC-MS to correspond to the expected molecular weight of the desired product, and was

separated to obtain the purified product illustrated in the chromatogram in **Figure 59** (B). Calculated MW of mimetic **63**: 6314.30, measured MALDI-MS (m/z): 6314.021.

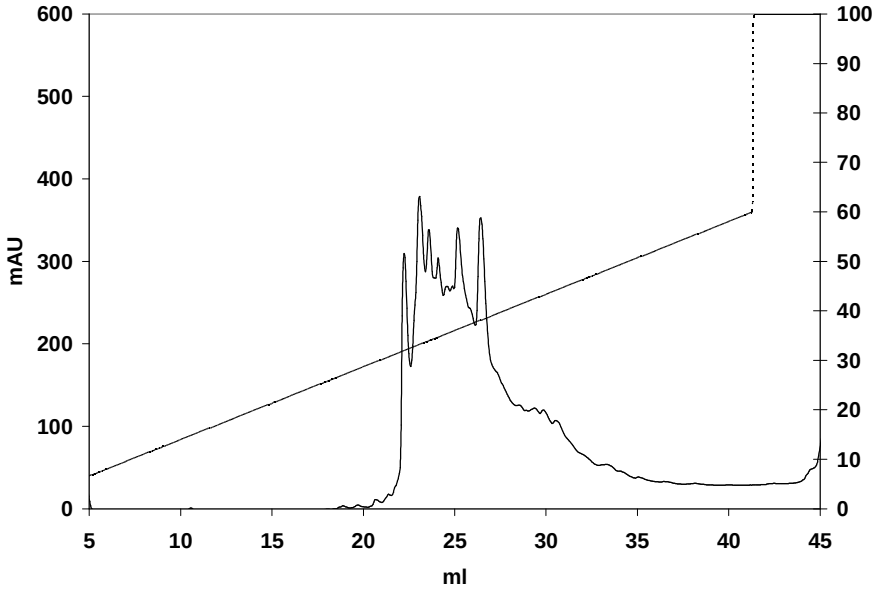

Figure 59 (A): Chromatogram of crude peptide mimetic **63.** For HPLC conditions see Appendix 4.

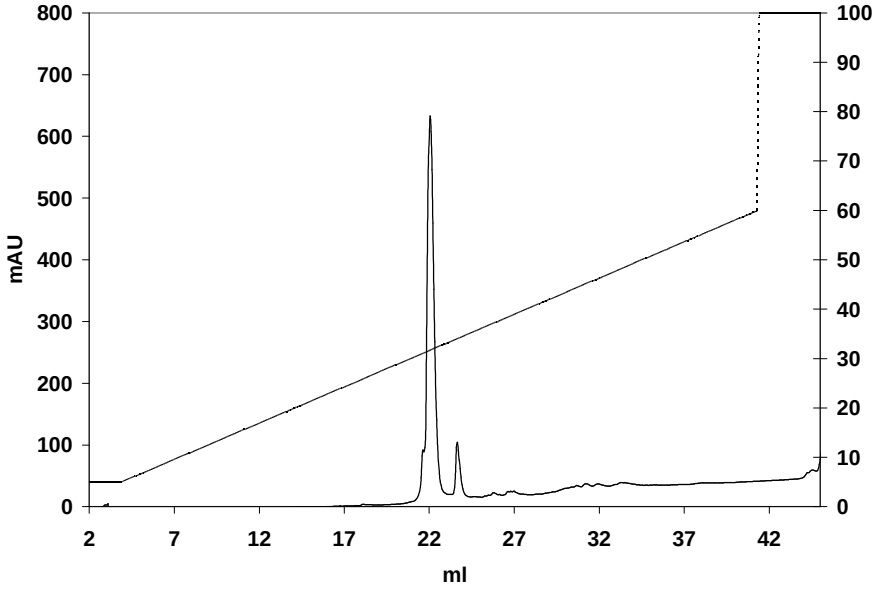

Figure 59 (B): Purified peptide mimetic **63**. For HPLC conditions see Appendix 4.

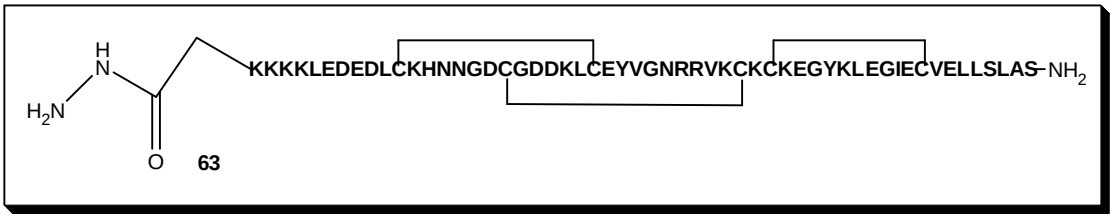

Figure 60: Presumed disulfide bonding in peptide mimetic **63**.

This oxidised peptide could be used in coupling reactions with activated phosphatidyl ethanolamine (**12**) as previously described. An example of a RP-HPLC chromatogram of the reaction mixture is given in **Figure 61**. The marked peak was shown by LC-MS analysis to correspond to the expected mass of the desired product. Calculated MW of lipopeptide **64**: 7087.33, measured m/z (ESI-MS): 1418.2 (M+5H/5), 1182.0 (M+6H/6), 1012.5 (M+7H)/7) (±0.01%). After HPLC purification, lipopeptide **64** was shown by MALDI-MS to have a molecular weight of 7088.022 (±0.1%).

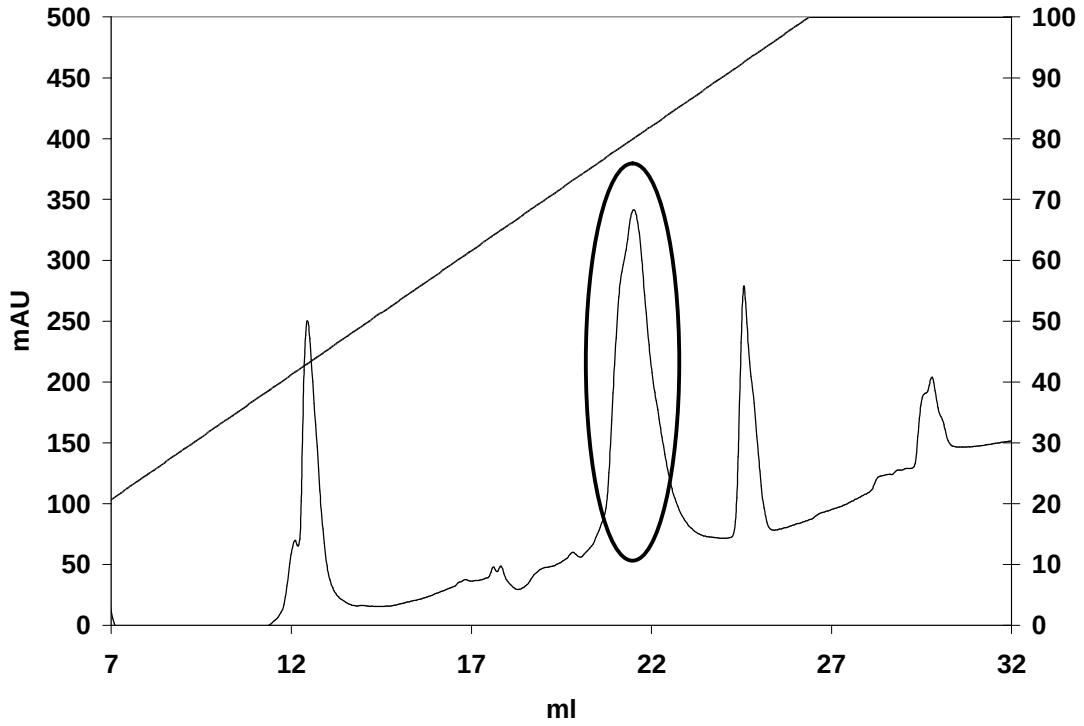

Figure 61: Crude mixture after reaction of peptide **63** with activated phospholipid (**12**). The marked peak corresponds to the lipopeptide **64**.

This product showed better physical properties than peptide mimetic **61**, being a white fluffy powder which was easily soluble in acetonitrile-water mixtures. Investigations into the immunological properties of this peptide when incorporated into virosomes have yet to be carried out.

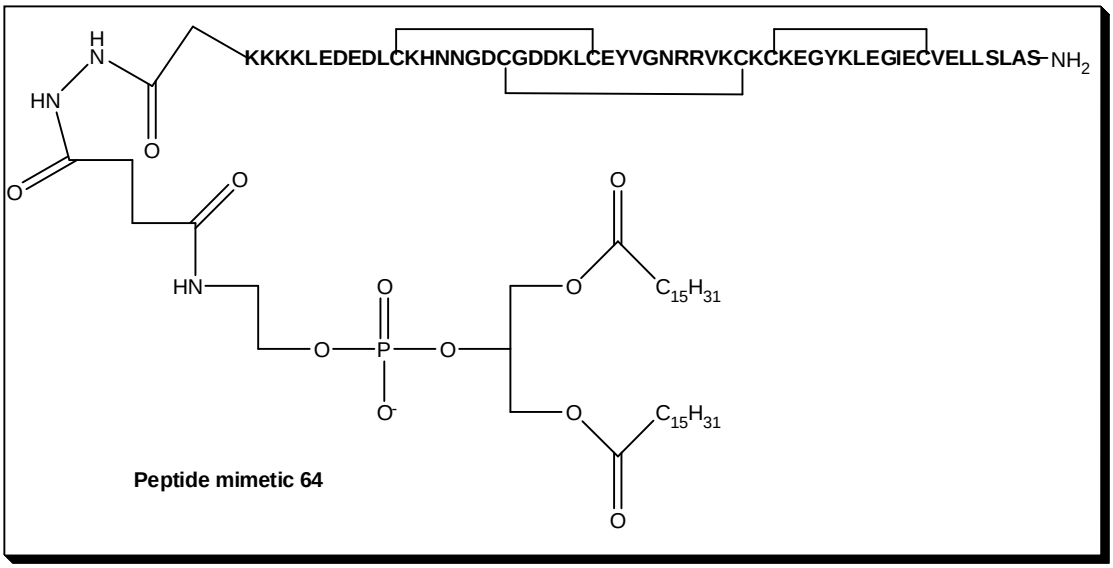

Figure 62: Structure of lipopeptide **64**.

1.3.4 Discussion

MSP-4 is an immunogenic protein containing a single EGF-like domain at its C-terminus, and regions of the protein are natural antigens in malaria infections. The correct conformation of the EGF-like domain is important for the folded structure and the immunogenicity of the whole protein [113]. The combination of MSP-4 and MSP-1_{19} has been shown to induce improved protection against *P. falciparum* and in some cases an increased antibody response to MSP-1_{19} [115, 116]. Therefore, this protein was chosen as an interesting target for development as a potential component of a multi-antigen synthetic malaria vaccine candidate.

Based on the successful methods developed for the synthesis of the MSP-1 peptides **2** and **13**, a peptide mimetic based on the EGF-like domain of MSP-4 of *P. falciparum* was synthesised. Initial peptide chain assembly difficulties could be overcome by the introduction of a pseudoproline unit. Pseudoprolines are used to disrupt β-sheet formation, [122] which can be a source of interchain aggregation, leading to poor

amino acid coupling yields in peptide assembly. The peptide chain could be oxidatively folded under conditions described in the previous chapter. The oxidative conditions led to the formation of one main product which was shown by Ellman test to contain no free thiol groups. NMR studies showed a wide spread of peaks in the amide proton region, suggestive of a well-structured product.

A modified analogue of the linear peptide chain containing an N-terminal hydrazinoglycine could be oxidatively folded in the same way, and the side chain deprotected folded product could be coupled in solution with an activated form of phosphatidylethanolamine to provide a poorly soluble phospholipidyl peptide. This product proved difficult to handle and gave negative results in immunological testing as a vaccine candidate.

However, the modification of the peptide sequence to include 4 further N-terminal lysine residues permitted the synthesis, in better yields, of an MSP-4 mimetic with more favourable physical properties. Inclusion of this mimetic in virosomes and immunisation of mice would make it possible to evaluate the suitability of this EGF-like domain mimetic for inclusion in a multi-stage, multi-antigen malaria vaccine. In these studies, it would also be very interesting to investigate the effect of combining MSP-1_{19} mimetics with the MSP-4 mimetic in the same immunization. An MSP-4 mimetic could prove a useful adjuvant if it were to enhance the response to other antigens such as MSP-1_{19}. Enzymatic digestion of the peptide mimetic should also be carried out in the future in order to confirm the disulfide bonding connectivities. Proteolytic studies on the native protein should also be undertaken, as there is currently no evidence available about the disulfide bonding in this EGF-like domain.

1.4 Glutamate-rich protein (GLURP)

1.4.1 Structure and location of GLURP

The 220 kDa glutamate rich protein (GLURP) was identified in 1991. It was investigated as an antigen that is released on the rupture of *P. falciparum* schizonts, but was subsequently found to be expressed at all stages of the parasite's life cycle within the human host, including on the surface of newly released merozoites [124]. Three regions of interest are identified in the protein: the repeat regions R1 and R2, and the N-terminal non-repeat region which is termed R0, illustrated in **Figure 63.**

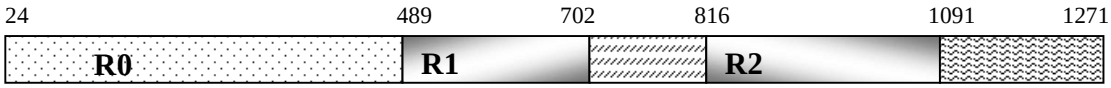

Figure 63: Schematic representation of the structure of the glutamate rich protein.

The R0 region is found to be relatively well-conserved between several laboratory lines and field isolates of *P. falciparum*, showing, for example, considerably less polymorphism than the circumsporozoite protein [125]. In an extensive study involving a phage-display library and a library of synthetic peptides in affinity studies with IgG from immune adults, six major B-cell epitopes were identified in the R0 region, of which four were frequently recognized by high-titre IgG antibodies from immune adults, suggesting them as good potential targets for vaccine development [126]. No three-dimensional structural information for GLURP is as yet available, but the epitopes P1, P3 and P4 (three of the four epitopes well-recognized by immune sera) share a common sequence motif and could therefore be structurally related.

1.4.2 Evidence for GLURP as a vaccine candidate

Several studies have shown that high levels of anti-GLURP antibodies are associated with low levels of parasitemia and with absence of disease in humans in malaria-endemic regions [127-131]. Furthermore, purified human anti-GLURP antibodies have been shown to induce antibody-dependent monocyte-mediated inhibition (ADCI) of parasite growth in vitro [132]. This study showed that none of the human antibodies

investigated that reacted with GLURP were able to inhibit invasion of erythrocytes by merozoites directly, but when they were allowed to co-operate with monocytes they showed a dose-dependent, monocyte-dependent parasite growth inhibitory activity. It has recently been shown that the combination of *P. falciparum* GLURP and MSP-3 in the form of a recombinant protein can induce partial protection against subsequent challenge with *P. falciparum*-infected red blood cells in Saimiri monkeys [133]. Antibodies against MSP-3 are also believed to protect via ADCI. The limited polymorphism mentioned above also suggests that GLURP mimetics could provide good candidates for a non-species-specific vaccine, and could also indicate that GLURP is important for parasite survival.

1.4.3 GLURP peptide mimetics

1.4.3.1 Mimetic design.

Based on the findings of Theisen et al. [126], it was decided to synthesise a small library of 16 peptide mimetics incorporating the epitopes P1, P3 and P4, as well as the peptide sequence P2, which overlaps with P1 and P3. The epitopes identified by Theisen et al. are illustrated in **Figure 64** and the peptide mimetics to be synthesised in this study are presented in **Figure 65**.

(a)

```
160          170          180          190          200
LENSSQDNLD KDTIST EPFP NQKHKDLQQD LNDEPL EPFP TQIHKDYKEK

210          220          230
NLINEEDS EP FPRQKHKKVD NHNEEKNVFH
```

(b)

```
     173          183          193          203
P1)  ISTEPFPNQK HKDLQ
P2)            QK HKDLQQDLND EPL
P3)                         EPLEPFPTQI HKDYK
     216          226
P4)  DSEPFPRQKH KKVD
```

Figure 64: (a) Fragment of the sequence of the R0 region of GLURP. The repeated motif is highlighted in bold. **(b)** Sequences of the epitopes P1, P3 and P4 and of the peptide sequence P2 identified by Theisen et al. [126].

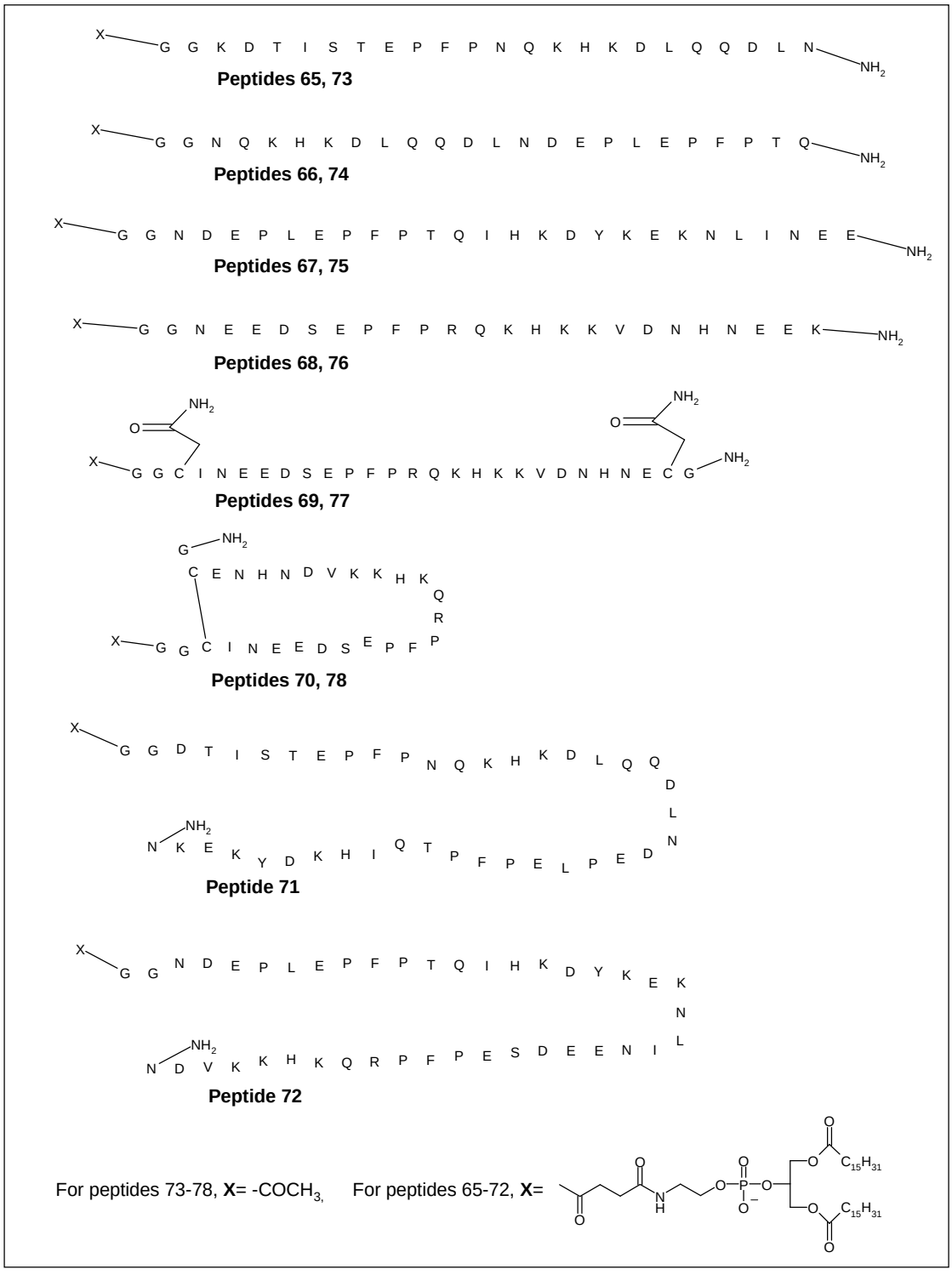

Figure 65: Structures of peptide mimetics designed to mimic epitopes on GLURP. Peptides **65-72** were designed for loading into virosomes and immunizations, peptides **73-78** for NMR studies.

As can be clearly seen in **Figure 65**, peptides **65** and **73** were designed to mimic epitope P1, peptides **66** and **74** to mimic peptide P2, peptides **67** and **75** to mimic epitope P3, peptides **68-70** and **76-78** to mimic epitope P4, peptide **71** to cover the entire sequence from P1 to P3 and peptide **72** to cover the sequence from P3 to P4. In each peptide mimetic, glycine residues were introduced at the N-terminal end as a linker to provide some space between the epitope sequence and the phospholipid moiety, in the cases of the phospholipidyl-peptides **65-72**. In mimetics **69, 70, 77** and **78**, cysteine residues were introduced. A disulfide bond was to be formed between the two cysteines in mimetics **70** and **78**, in order to study the effect of this constraint on NMR properties and on immunological responses. In mimetics **69** and **77**, the cysteine thiol groups were alkylated for comparison with mimetics **70** and **78**. In order to synthesise the N-terminal acetylated products **73-78**, peptidyl-resin was treated after final Fmoc-deprotection with acetic anhydride. The success of the acetylation reaction was monitored using the Kaiser test [134], which gave a positive result, indicating free amine, before the reaction, and a negative result after the reaction. To synthesise the lipopeptide mimetics **65-72**, Fmoc-deprotected peptidyl resin was treated with succinyl-PE **11**, HATU and HOAt in DMF with DIEA. This reaction was carried out overnight and completion was monitored by the Kaiser test.

1.4.3.2 Mimetics 65-68 and 73-76

For the synthesis of peptides **65** and **73**, the peptide sequence GGKDTISTEPFPNQKHKDLQQDLN was assembled on Rapp Polymere amide resin with an initial loading of 0.74 mmol/g.

For the synthesis of peptides **66** and **74**, the peptide sequence GGNQKHKDLQQDLNDEPLEPFPTQ was assembled on Rink amide resin with an initial loading of 0.64 mmol/g.

For the synthesis of peptides **67** and **75**, the peptide sequence GGNDEPLEPFPTQIHKDYKEKNLINEE was assembled on Rink amide resin with an initial loading of 0.64 mmol/g.

For the synthesis of peptides **68** and **76**, the peptide sequence GGNEEDSEPFPRQKHKKVDNHNEEK was assembled on Rink amide resin with an initial loading of 0.64 mmol/g.

For all peptides, single (20 mins) coupling cycles were used for each amino acid, with an acetic anhydride capping step before each Fmoc deprotection, in order to cap unreacted sites and thus simplify purification steps.

The resin was then split into two portions, one being treated with succinyl-PE as described above to provide mimetics **65-68**, and the other with acetic anhydride to provide mimetics **73-76**. Both peptidyl resins were then treated with TFA containing 2.5% EDT, 2.5% water and 1% TIS, to provide the fully side-chain deprotected products which could be purified by RP-HPLC. The purified products were analysed by RP-HPLC and ESI-MS. The chromatograms of the products are shown in **Figures 66-69**. The masses found were as follows:

65: Calculated MW: 3484.02 g/mol
Measured: 1742.5 (M+2H)/2, 1162.3 (M+3H)/3, 871.8 (M+4H)/4 (± 0.01%)

73: Calculated MW:2752.02 g/mol
Measured: 1376.8 (M+2H)/2, 918.0 (M+3H)/3, 688.7 (M+4H)/4 (± 0.01%)

66: Calculated MW: 3522.02 g/mol
Measured: 1761.7 (M+2H)/2, 1174.9 (M+3H)/3, 881.0 (M+4H)/4 (± 0.01%)

74: Calculated MW: 2790.02 g/mol
Measured: 1395.8 (M+2H)/2, 930.8 (M+3H)/3, 698.6 (M+4H)/4 (± 0.01%)

67: Calculated MW: 3928.50 g/mol
Measured: 1964.9 (M+2H)/2, 1310.5 (M+3H)/3, 982.8 (M+4H)/4 (± 0.01%)

75: Calculated MW: 3196.50 g/mol
Measured: 1066.2 (M+3H)/3, 800.0 (M+4H)/4 (± 0.01%)

68: Calculated MW: 3722.18 g/mol
Measured: 1241.7 (M+3H)/3, 931.4 (M+4H)/4, 745.2 (M+5H)/5 (± 0.01%)

76: Calculated MW: 2990.18 g/mol
Measured: 997.6 (M+3H)/3, 748.5 (M+4H)/4, 599.0 (M+5H)/5 (± 0.01%)

For HPLC conditions for all peptides see Appendix 4.

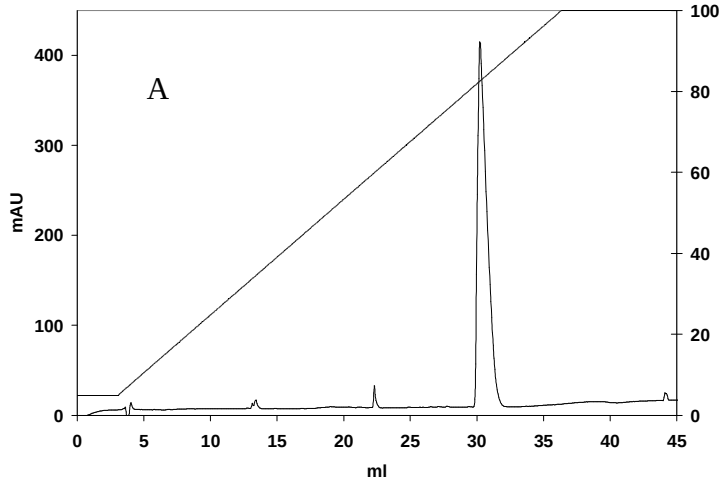

Figure 66: (A) Chromatogram of pure lipopeptide **65**.

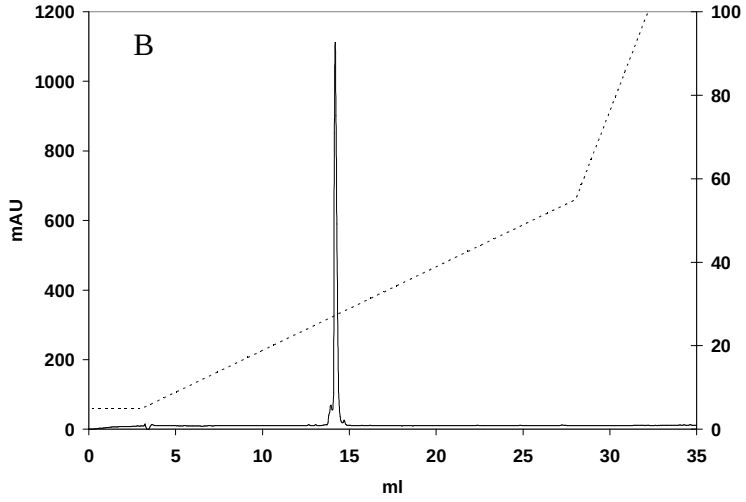

Figure 66: (B) Chromatogram of pure peptide **73.**

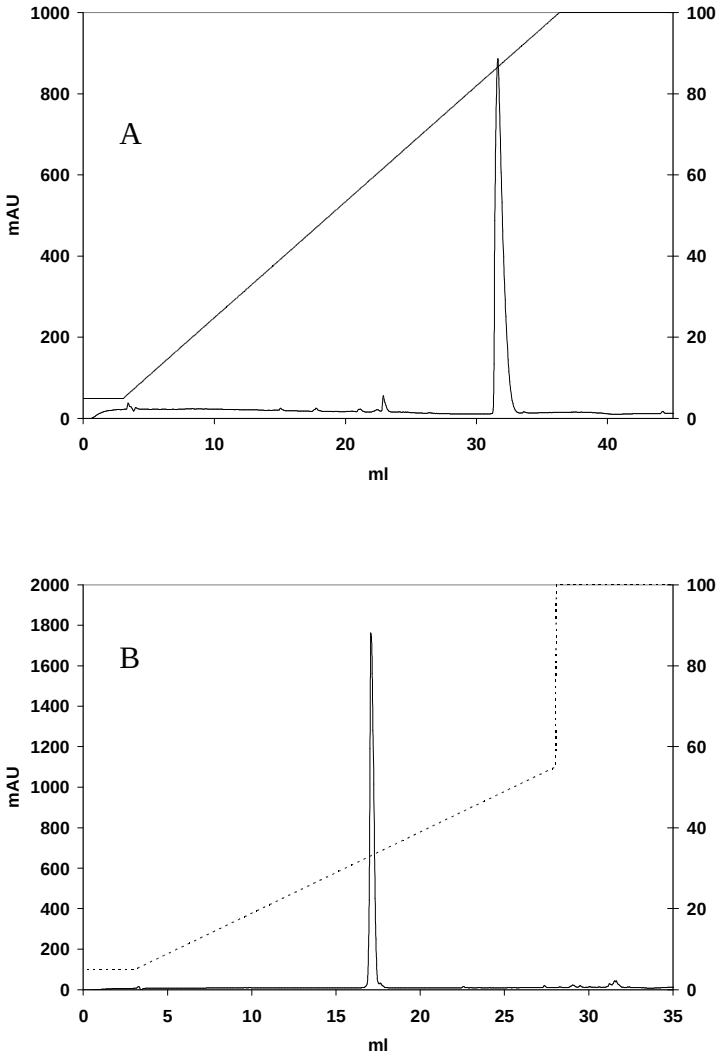

Figure 67: (A) Chromatogram of lipopeptide **66**. (B) Chromatogram of peptide **74**.

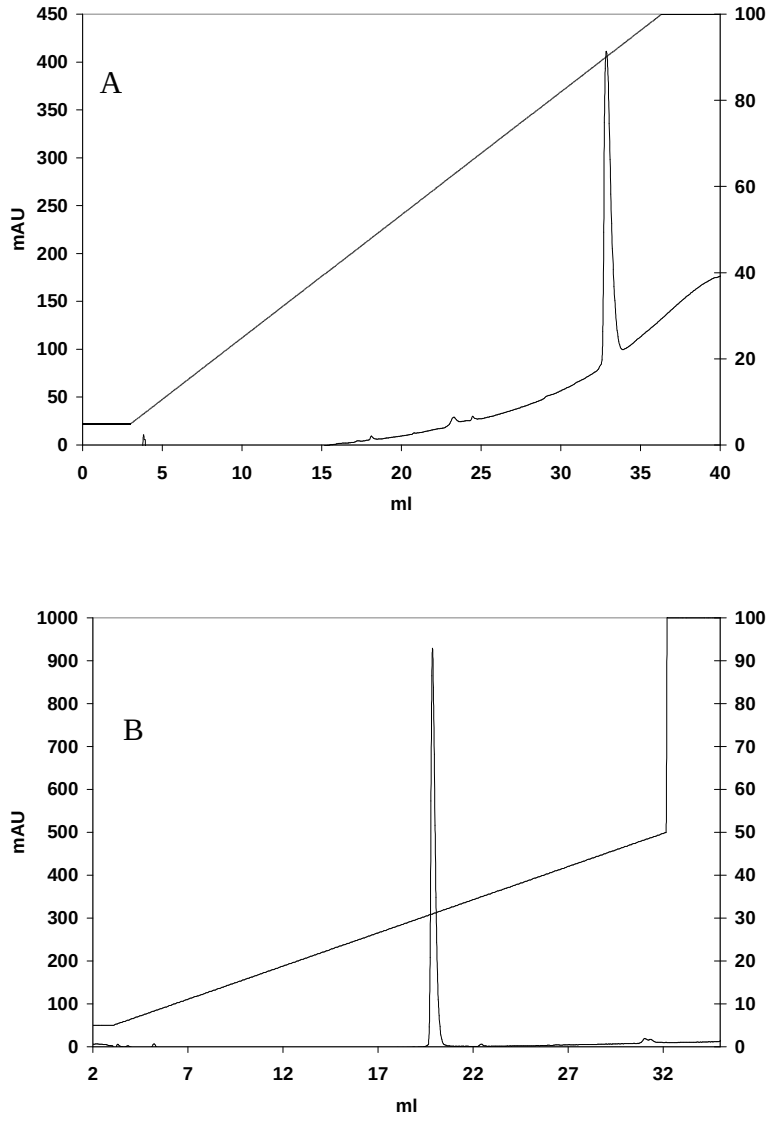

Figure 68: (A) Chromatogram of lipopeptide **67**. (B) Chromatogram of peptide **75**.

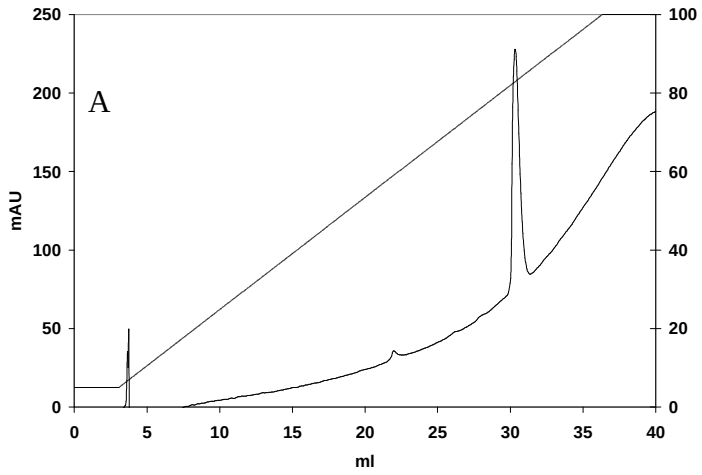

Figure 69: (A) Chromatogram of lipopeptide **68**.

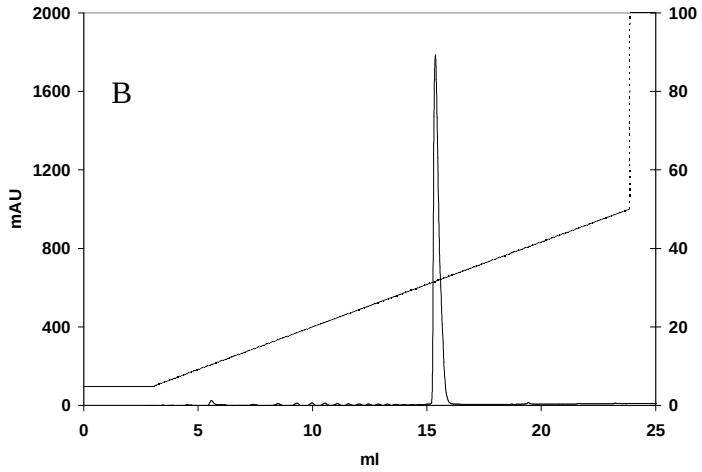

Figure 69: (B) Chromatogram of peptide **76**.

1.4.3.3 Mimetics 69 and 77

The peptide sequence GGCINEEDSEPFPRQKHKKVDNHNECG was assembled on Rink amide resin with an initial loading of 0.66 mmol/g. Single (20mins) coupling cycles were used for each amino acid, with an acetic anhydride capping step before each Fmoc deprotection, in order to cap unreacted sites and thus simplify purification steps. The peptidyl resin was then split into two batches. The first batch was treated with succinyl-PE in order to produce mimetic **69**. The coupling reaction was monitored using the Kaiser test. The second batch was treated with acetic anhydride as described above in

order to produce mimetic **77**. Both peptide mimetics were then cleaved from the solid support and side-chain deprotected using TFA containing 2.5% EDT, 2.5% water and 1% TIS.

The crude phosphatidyl-peptide was then purified by RP-HPLC to produce the intermediate product **79** with free cysteine thiol groups. This product was analysed by LC-MS: Calculated MW: 3840.38 g/mol, Measured: 1281.5 (M+3H)/3, 961.9 (M+4H)/4, 769.7 (M+5H)/5 (± 0.01%).

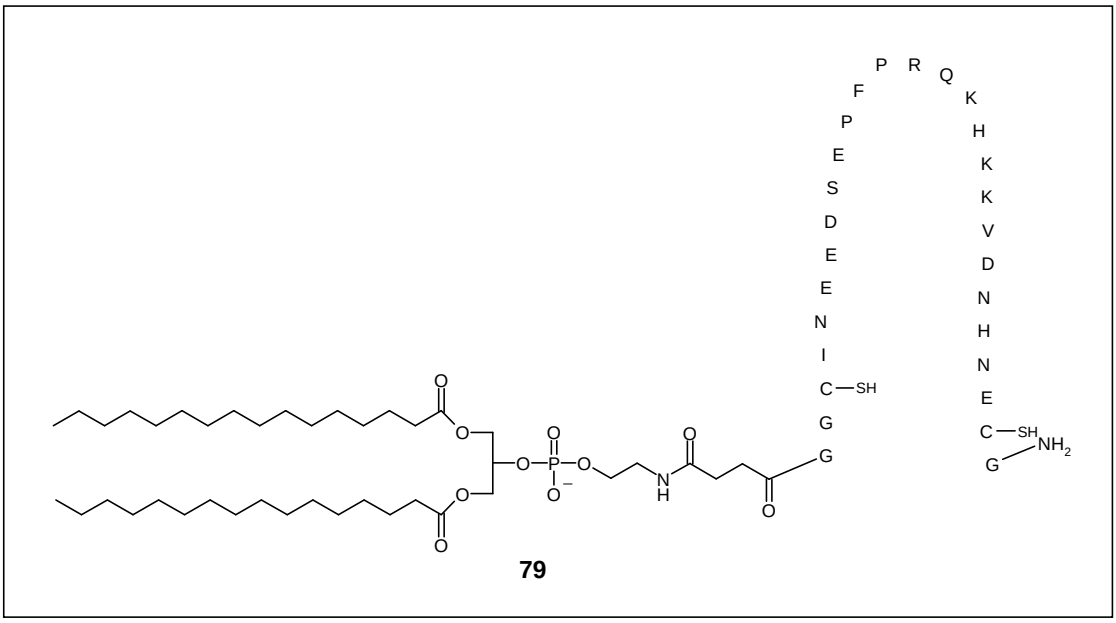

Figure 70: Structure of the intermediate product **79**.

This intermediate product was then treated with 20 eq of iodoacetamide in phosphate buffer at pH 7.5 [135], to produce mimetic **69** with almost 100% conversion after 1 hour of reaction. This reaction solution was frozen and lyophilised to stop the reaction, and then the product was redissolved in water and purified by RP-HPLC to obtain pure mimetic **69**, which was analysed by analytical HPLC and ESI-MS. The chromatogram of pure mimetic **69** is shown in **Figure 71**.

Calculated MW: 3954.48 g/mol, measured: 1319.5 (M+3H)/3, 791.9 (M+5H)/5 (± 0.01%).

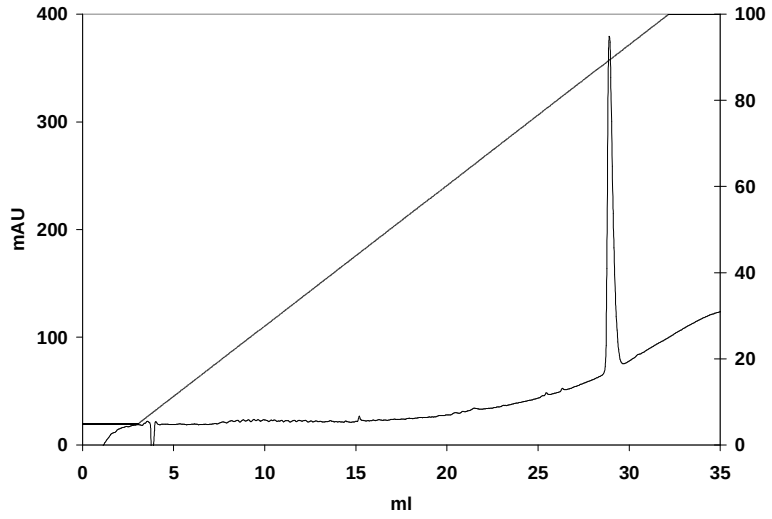

Figure 71: Chromatogram of lipopeptide **69**. For HPLC conditions see Appendix 4.

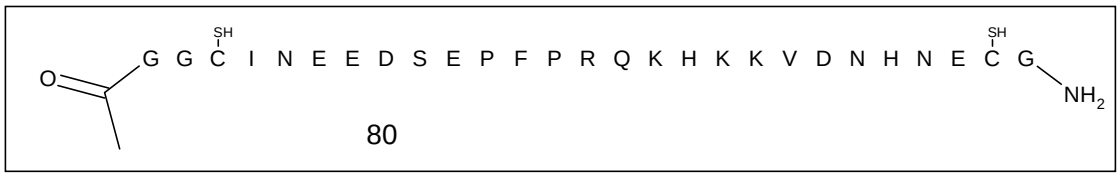

Figure 72: Structure of intermediate peptide **80**.

The crude acetylated product **80** was alkylated using iodoacetamide in phosphate buffer as described for the synthesis of mimetic **69**, to produce crude mimetic **77**, which could be purified by HPLC to obtain pure mimetic **77**, which was analysed by HPLC and ESI-MS. The chromatogram of the pure product is shown in **Figure 73**.

Calculated MW: 3221.44 g/mol, measured: 1612.2 (M+2H)/2, 1075.1 (M+3H)/3, 806.7 (M+4H)/4, 645.6 (M+5H)/5 (± 0.01%).

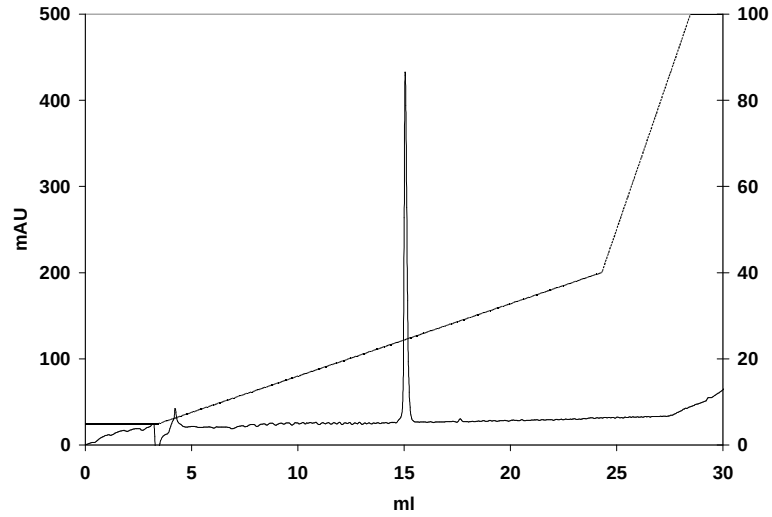

Figure 73: Chromatogram of peptide **77**. For HPLC conditions see Appendix 4.

Mimetic **69** was used for virosome formulation and immunization trials. Mimetic **77** was used for ^{1}H NMR measurements.

1.4.3.4 Mimetics 70 and 78

A new batch of the peptide sequence GGCINEEDSEPFPRQKHKKVDNHNECG was prepared on the solid support as described above, and the intermediates **79** and **80** were obtained in the same fashion. It was decided to concentrate effort on the more challenging oxidation of intermediate **79** to form mimetic **70**, and to return to the oxidation of mimetic **80** to give **78** for NMR studies after immunizations had been carried out, to evaluate whether mimetic **70** was a good vaccine candidate. Therefore, some small-scale oxidation reactions were carried out using the purified intermediate **79**, and it was found that stirring the mimetic for approximately 48 hours in a 1:1 mixture of ammonium acetate buffer (pH 8)/trifluoroethanol, in an open vessel, allowed an almost complete conversion of the starting material to a new product. This product could be purified directly from the reaction mixture, and the purified mimetic obtained was shown by Ellman test to contain no free thiol groups. The product was analysed by RP-HPLC and by ESI-MS. Chromatograms of various stages of the oxidation reaction and of the purified product are shown in **Figure 74**.

Calculated MW: 3838.29 g/mol, measured: 1920.2 (M+2H)/2, 1280.4 (M+3H)/3, 960.6 (M+4H)/4 (± 0.01%).

Mimetic **70** was used for inclusion in virosomes and immunization studies.

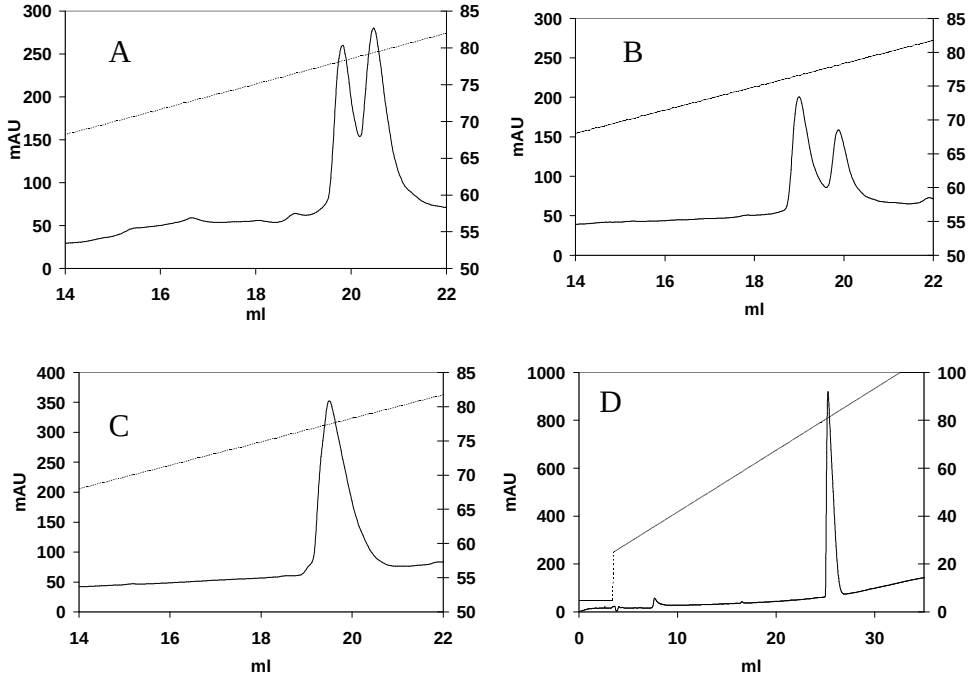

Figure 74: (A) Reaction mixture after 2 hours of oxidation. (B) Reaction mixture after 4 hours of oxidation. (C) Reaction mixture after 9 hours of reaction. (D) Purified peptide **70**. For HPLC conditions see Appendix 4.

1.4.3.5 Mimetics 71 and 72

For the synthesis of peptide **71**, the peptide sequence GGDTISTEPFPNQKHKDLQQDLNDEPLEPFPTQIHKDYKEKN was assembled on Rink amide resin with an initial loading of 0.64 mmol/g.

For the synthesis of peptide **72**, the peptide sequence GGNDEPLEPFPTQIHKDYKEKNLINEEDSEPFPRQKHKKVDN was assembled on Rink amide resin with an initial loading of 0.64mmol/g.

Single (20 mins) coupling cycles were used for each amino acid, with an acetic anhydride capping step before each Fmoc deprotection, in order to cap unreacted sites and thus simplify purification steps.

The resins were then treated with succinyl-PE to provide mimetics **71** and **72**. The peptidyl resin was then treated with TFA containing 2.5% EDT, 2.5% water and 1%

TIS, to provide the fully side-chain deprotected products which could be purified by RP-HPLC. The purified products were analysed by RP-HPLC and ESI-MS. The chromatograms of the products are shown in **Figures 75** and **76**. The masses found were as follows:

71: Calculated MW: 5666.41 g/mol, measured: 1417.2 (M+4H)/4, 1134.1 (M+5H)/5, 945.4 (M+6H)/6 (± 0.01%).

72: Calculated MW: 5735.52 g/mol, measured: 1434.3 (M+4H)/4, 1148.0 (M+5H)/5, 956.9 (M+6H)/6 (± 0.01%).

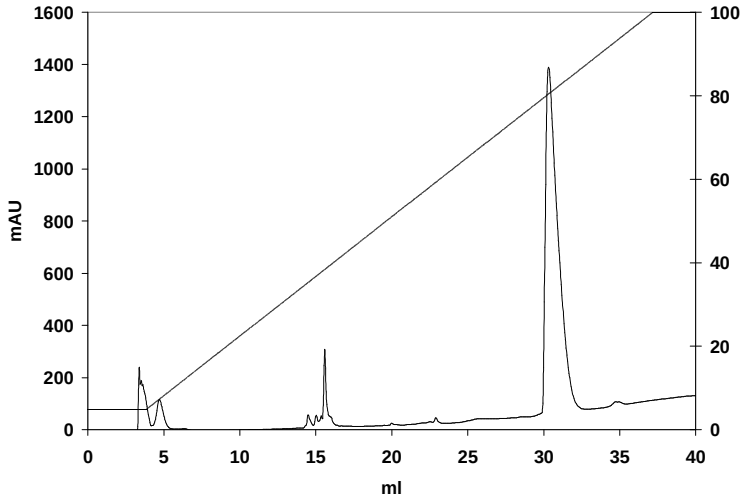

Figure 75: Chromatogram of lipopeptide **71**. For HPLC conditions see Appendix 4.

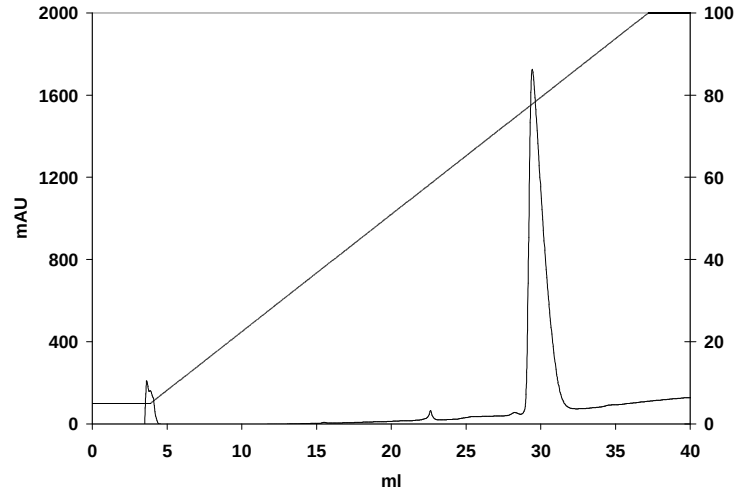

Figure 76: Chromatogram of lipopeptide **72**. For HPLC conditions see Appendix 4.

1.4.3.6 Immunization results

All of the mimetics were able to elicit a strong anti-mimetic immune response, but unfortunately, the binding of the antibodies in the sera to whole parasites in immunoflourescence assays, even after four immunizations, was very weak. The presence or absence of a disulfide bond seemed to have little influence on the immunological properties of the mimetics.

1.4.3.7 NMR results

^{1}H NMR spectra of the mimetics are presented in Appendix 2. Unfortunately, the spectra do not seem to indicate well-structured products, showing only the typical narrow range of amide NH signals seen in an unfolded protein, and not showing any NH-CH_α coupling constants indicating well-defined structure.

1.4.4 Discussion

The glutamate rich protein is expressed at all stages of the malaria parasite's life cycle, including on the surface of newly released merozoites [124]. The protein contains two repeat regions, and an N-terminal non-repeat region that is relatively well-conserved between several strains [125]. Studies revealed major B-cell epitopes in the non-repeat region which were recognised by high-titre antibodies from immune adults [126], suggesting that the non-repeat region of GLURP could provide good targets for a potential malaria vaccine. It has also been shown that high levels of anti-GLURP antibodies are associated with low levels of parasitemia in malaria endemic regions.

The aim of this project was to prepare peptide mimetics suitable for virosomal formulation based on the epitopes identified by Theisen et al. Mimetics based on each of four epitopes were designed, as were two longer peptide sequences, each spanning at least two of the epitopes proposed by Theisen et al[126].

Linear and cyclised mimetics of epitopes from the R0 non-repeat region of the glutamate-rich protein of *P. falciparum* could be prepared by solid-phase peptide synthesis. N-terminal acylated peptides could be prepared for NMR studies, and lipopeptides could be prepared via on-resin coupling of a modified phosphatidyl-ethanolamine (PE), followed by cleavage and purification of the whole mimetic. A

disulfide bridged mimetic could be prepared by introducing cysteine residues before and after the sequence of interest. The linear lipopeptide precursor could be cyclised in a clean air oxidation reaction. The PE-coupled peptides were included in virosomes prepared by Pevion Biotech and were used to elicit an immune response in mice.

Unfortunately, the sera obtained were only poorly cross-reactive with *P. falciparum* parasites in IFA. It must be concluded that the mimetics in their current form are not good candidates as potential components of a multi-stage, multi-antigen malaria vaccine. Although the work of Theisen et al. [126] showed that the peptide sequences P1 – P4 were recognised by high-titre antibodies from immune adults, there was no indication that these peptide sequences would be able to induce a meaningful immune response when taken alone. The antibodies may be able to recognise unstructured peptide sequences to a certain extent, even if the antigens required to induce the antibody response are conformational. Unfortunately, the lack of current knowledge about the three-dimensional structure of the native protein makes the design of conformational mimetics difficult. If future NMR or crystal studies were to reveal structural information about GLURP, new mimetics could be designed based on this knowledge, and constraints could be introduced in order to lock peptide structures into a conformation mimicking the protein as found in the parasite. Such mimetics may then be able to induce antibodies that would recognise the parasite and therefore play a role in protective immunity.

1.5 Conclusions

Three different proteins, MSP-1, MSP-4 and GLURP were investigated for their potential as components of a multi-antigen malaria vaccine candidate. The MSP-1 and MSP-4 mimetics both contained six cysteine residues and for both, folding in the presence of cysteine/cystine led to the formation of one main fully oxidised product.

NMR spectra of both mimetics suggested a well-structured product, and the solution structure of the MSP-1 mimetic could be determined and was shown to be very similar to the structure of the corresponding domain in the two-domain protein MSP-1_{19}. Proteolysis studies showed that the MSP-1 mimetic conformed to the EGF-like disulfide bonding pattern. The MSP-1-based lipopeptide developed for immunizations induced a good immune response and the sera obtained were cross-reactive with blood-stage *P. falciparum* parasites. This mimetic could therefore represent a good candidate for

inclusion in a multi-antigen malaria vaccine. 50 monoclonal antibodies could be derived from the mice immunized with this mimetic, and the binding of these with mutant mimetics should be investigated in the future, in order to characterise the immune response to the peptide mimetic. Based on these epitope-mapping studies, new mimetics could be developed for immunizations, perhaps eventually leading to a mimetic that could induce only inhibitory antibodies, with the exclusion of the blocking antibodies that are induced by native MSP-1_{19}.

The mimetics based on MSP-4 and GLURP unfortunately induced sera that only responded weakly to blood stage *P. falciparum* parasites in immunofluorescence assays. However, it was interesting to note that the synthetic difficulties encountered in the first attempt at synthesis of the MSP-4 mimetic could be overcome by the introduction of a pseudoproline unit during chain assembly. The oxidative folding of the linear peptide again led to one main fully oxidised product, suggesting that the method developed could serve as a good general technique for the oxidative folding of synthetic EGF-like domains. This could be of particular interest in the development of malaria vaccine candidates, since several EGF-like domains are present in merozoite surface proteins.

The development of peptide vaccines directed against other EGF-like domains, for example against human EGF or HER-2/neu, which are frequently overexpressed in cancer, is also of great interest. There is already evidence that there is a direct relationship between anti-EGF antibody titers and immune response duration with survival time in cancer patients [136]. The development of a synthetic virosome-based vaccine presenting these kinds of antigens could be envisaged, based on the methods developed in this work.

Another interesting result to emerge from this work was that the physical properties of one lipopeptide could be improved by the introduction of a series of contiguous lysine residues at the N-terminus, a technique that could be attempted with other difficult peptide products in the future.

2 Peptoid-peptide hybrids as antimicrobial agents

2.1 Antimicrobial peptides

2.1.1 Physical and structural properties

Naturally-occurring antimicrobial peptides (AMPs) have been identified in a wide variety of plant, invertebrate and vertebrate species [137-141]. They form part of the innate immune system, protecting against a broad range of microorganisms, including Gram-positive and Gram-negative bacteria, fungi and parasites. Due to their function as a first line of defence, AMPs tend to be found in those parts of organisms that most frequently come into contact with pathogens, such as skin, eyes and epithelial surfaces. Although they are found in a wide range of organisms, AMPs share several common characteristics. Most of the sequences fall into the range of ~10 to ~50 amino acid residues, although antimicrobial activity has even been reported for di- and tripeptides [142]. The largest known AMPs are made up of over 60 residues. AMPs are often charged. Cationic peptides, rich in arginine and lysine, as well as anionic peptides that are complexed with zinc, are often more active than neutral peptides or those with a low charge. AMPs can form a wide variety of secondary structures, and those with well-defined secondary structures such as antiparallel β-sheets or α-helices are often more active than those with less well-defined structures. Defined structure can be an aid to the next common characteristic of AMPs, which is amphipathicity – that is, the aligning of hydrophilic residues along one face of the molecule, and of hydrophobic residues on the opposite face. The sequence of AMPs is encoded by the genetic material of the host organism, and there can be some posttranslational modifications after transcription often including cleavage from a precursor protein, C-terminal amidation, and disulfide formation. The AMPs are therefore not to be confused with peptide antibiotics, which are mostly synthesised by special metabolic pathways and are highly modified. Over 800 antimicrobial peptides have already been discovered [143] and these can be divided into

subgroups based on their amino acid composition and structure [142]. Some subgroups are briefly described here, and examples are presented in **Table 11**.

Subgroup	Examples	Source	Sequence
α-helical, cationic	Cecropin A	insect	KWKLFKKIEKVGQNIRDGIIKAGPAVAWGQATQIAK*a*
	Magainin 2	amphibian	GIGKFLHSAKKFGKAFVGEIMNS
	LL-37	human	LLGDFFRKSKEKIGKEFKRIVQRIKDFLRNLVPRTES
	Dermaseptin	amphibian	ALWKTMLKKLGTMALHAGKAALGAAADTISQGTQ
Amino acid-enriched	Indolicidin	cow	ILPWKWPWWPWRR*a*
	Prophenin	pig	AFPPPNFPGPRFPPPNVPGPRFPPPNFPGPRFPPPNFPGPR FPPPNFPGPPFPPPIFPGPWFPPPPPFRPPPFGPPRFP
	Histatin 5	human	DSHAKRHHGYKRKFHEKHHRSHRGY
	Apidaecin	bee	GNNRPVYIPQPRPPHPRI
Disulfide-bonded	Bactenecin (1 Cys-Cys)	cow	RLCRIVVIRVCR
	Tachyplesin (2 Cys-Cys)	crab	RWCFRVCYRGICYRKCR*a*
	Protegrin 1 (2 Cys-Cys)	pig	RGGRLCYCRRRFCVCVGR*a*

Table 11: Structures of a range of naturally-occurring antimicrobial peptides. *a* indicates that the peptide is C-terminally amidated. [139]

2.1.2 Classification

A large subgroup consists of short (<40 residues) cationic peptides, that do not contain cysteine residues. Many of these peptides are unstructured in aqueous solution, but part of or even all of the molecule becomes structured as an α-helix in the presence of TFE, SDS micelles, phospholipid vesicles, liposomes or lipid A. It seems that increased α-helical content correlates with better antimicrobial activity [144]. A smaller subgroup contains peptides that also lack cysteine residues, but are enriched in certain amino acids, including proline-rich peptides, arginine-rich peptides and tryptophan-rich peptides. These peptides tend to have linear structures, although some form extended coils. The largest subgroup consists of anionic and cationic peptides that contain cysteine residues forming one or more disulfide bonds. Many of these peptides are constrained by their disulfide bonds into stable β-sheets. A fourth, smaller subgroup contains anionic

peptides that are active against Gram-positive and Gram-negative bacteria and require zinc as a co-factor for activity.

2.1.3 Selectivity and modes of action

The increasing emergence of bacterial resistance to known antibiotics has prompted intensive research into new sources of antimicrobial agents [145, 146]. One of the areas of great interest is the study of the mechanisms of action and selectivity of the antimicrobial peptides, and the development of antimicrobial peptides with clinical applicability. Obviously, if drugs are to be developed based on AMPs, they need to have a very good selectivity for microbial over eukaryotic cells. Although many AMPs, e.g. melittin [147], show poor selectivity for bacteria, several naturally-occurring AMPs have been shown to have no haemolytic activity [148, 149] at the concentration needed for antimicrobial activity, including the magainins and cecropins. It seems that the most important factor in selectivity is the difference in the composition of bacterial and eukaryotic cell membranes [139]. The outer leaflet of eukaryotic membranes is composed of zwitterionic phospholipids, whereas bacterial cell membranes contain a large proportion of negatively-charged phospholipids.

The cationic nature of most AMPs facilitates their interaction with negatively charged bacterial outer membranes. A second difference between the two types of membrane is the absence of cholesterol in bacterial cell membranes. This renders the membrane more flexible and also more susceptible to disruption and destabilization by amphiphilic AMPs. Due to the long history of the exploitation of AMPs by the innate immune system, bacterial species have had time to develop resistance mechanisms. One of the most common is the modification of the bacterial cell membrane components [150], but membrane proteases and efflux pumps are also employed by some species to deactivate or expel the peptides [151, 152]. Based on the common characteristics of AMPs, on the knowledge that in many cases, synthetic all-D-amino acid enantiomers of AMPs have comparable antimicrobial activity to their L-amino acid natural counterparts [139], and on the evidence that the presence of AMPs enhances ion permeability of lipid bilayers, it was for many years believed that all AMPs act via a membrane permeabilisation mechanism to cause leakage and eventual cell death. However, there is increasing evidence that at least some AMPs act on intracellular targets, for example by

inhibiting cell-wall synthesis [153], nucleic acid synthesis [154, 155] or protein synthesis [154, 156].

2.1.4 Design of AMP-based drug candidates

At present, understanding of the interactions between AMPs and their putative intracellular targets is not at such an advanced stage that synthetic AMP-based drug candidates can be designed to target specific bacterial mechanisms. An alternative approach is to design and synthesise peptidomimetics with consideration of the general characteristics of known AMPs, and then to conduct studies on their mechanisms of action. In any case, whether to act by membrane permeabilisation, or to act on some more specific target within the bacterial cell, AMPs and AMP-based peptidomimetics must first interact with the bacterial membrane before disrupting it or gaining access to their secondary targets via transport through the membrane. Many research groups are currently investigating the possibility of designing molecules based on AMPs, as new agents in the fight against resistant microorganisms, aiming to attain the goals of high antimicrobial activity, high selectivity, and good pharmacological properties. In the Robinson group, there has been much research into the design and synthesis of peptidomimetics based on naturally-occurring AMPs, with particular emphasis on those displaying β-hairpin like structures, and subsequent studies of their structure, antimicrobial activity, selectivity towards bacterial cells, and possible modes of action.

2.2 Peptoids

2.2.1 Peptidomimetics

Peptidomimetics are molecules designed to resemble bioactive peptides in functionality and/or overall shape, but having structural features that diverge from those of the peptide, for example in that they have different types of bonding, or conformational constraints [157]. Many different types of change can be introduced into synthetic mimetics of peptides. For example, to improve the stability of the mimetic towards proteases or to constrain the amino acid side chains into an amphipathic conformation. Many mimetics have been designed involving some kind of structural

constraint such as backbone-backbone, sidechain-backbone, or sidechain-sidechain cyclisations [158].

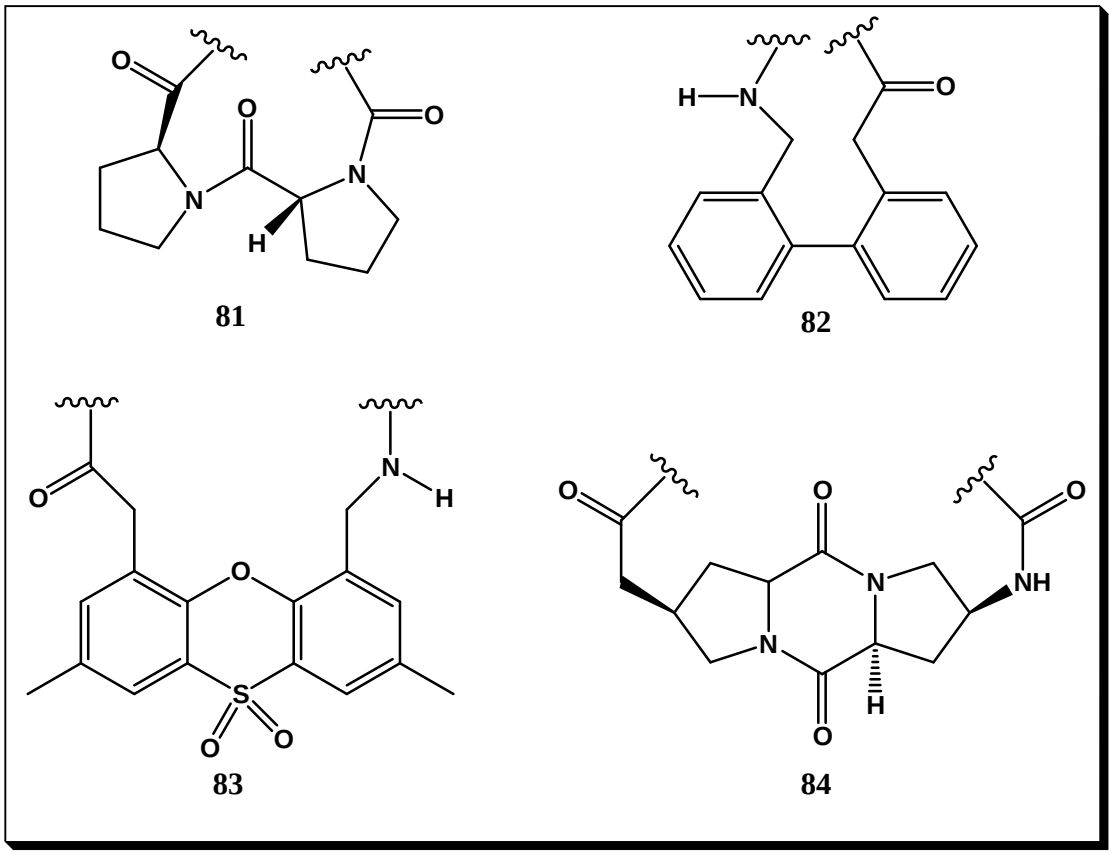

Figure 77: Templates used in the synthesis of β-sheet and β-hairpin peptide mimetics.

These constraints should help to mimic the conformation of a disulfide-bonded peptide, or should fix the mimetic into a conformation that is usually only attained by the peptide on interaction with a membrane, or perhaps increase the stability of the mimetic towards proteases. Some popular techniques for inducing a particular secondary structure include the use of β-amino acids to make β-peptides [159-161], the introduction of C^{α}-disubstituted α-amino acids into peptide sequences [162] and the use of templates to induce turn structures. Some examples of these templates are presented in **Figure 77**.

Depending on the substitution pattern of the α-and β-carbons, a 14-helix, 12-helix or 10-helix conformation can be conferred on a β-peptide. The introduction of substituted amino acids such as α-aminoisobutyric acid into a peptide sequence tends to

induce the formation of an α- or 3_{10} helix. Several organic templates have been shown to induce β-turn structures in peptide mimetics [163, 164]. Within the Robinson group, the ^{D}Pro-^{L}Pro template has been extensively exploited for its β-hairpin inducing properties [165-169].

2.2.2 Structure and synthesis of peptoids

A valuable tool available to chemists in the pursuit of antimicrobial peptide mimetics, is the diversity of structures available to them, not being restricted to the 20 naturally-occurring amino acids. One possibility is the introduction of synthetic non-natural amino acids into peptide sequences, another being the synthesis of peptoids, which are polymers of N-substituted glycines (i.e. the side-chain is 'shifted' from the α-carbon onto the amide nitrogen of the amino acid residues). The generalized structure of a peptoid is presented in **Figure 78**. Peptoid analogues of natural amino acids Xaa are usually named Nxaa [170], such that, for example a glycine substituted with -CH_3 on the N-atom is called Nala, and a glycine substituted with -CH_2COOH on the N-atom is called Nasp. Peptoid units containing side chains not occurring in natural amino acids are also assigned symbols of the form Nxxx, such as Nade – *N*-adamantylethylglycine. The most common, 'submonomer' method [171, 172] of solid-phase synthesis, illustrated in **Scheme 7,** allows the introduction of as wide a range of side chains as there are amines available for coupling, as it proceeds in two steps, the first being the introduction of an α-haloacetyl moiety and the second the substitution of the halide with a primary amine. Peptoids are additionally believed to be more stable towards proteases than their peptide analogues [173]. Although the solid phase submonomer method is synthetically the simplest route to peptoid structures, other pathways have also been successfully employed, including solid-phase synthesis based on peptoid monomers analogous to the protected amino acids used in standard Fmoc solid-phase peptide synthesis [170] and solution-phase assembly using similar Fmoc-protected monomers [174]. There have also been advances in coupling techniques in recent years, for example the use of microwave-assisted solid-phase chemistry to allow the inclusion of amine submonomer building blocks of low intrinsic reactivity [175].

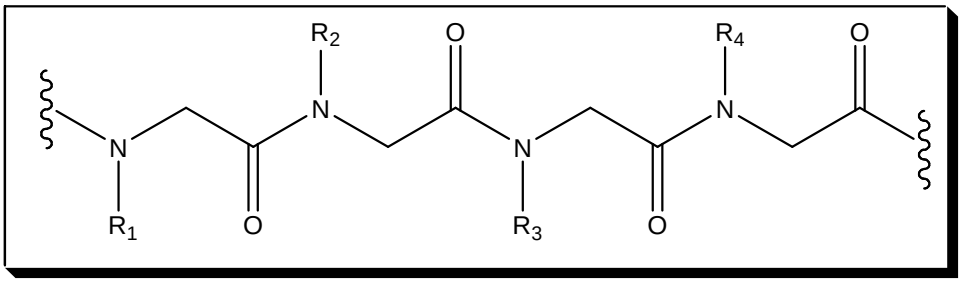

Figure 78: The generalized structure of a peptoid.

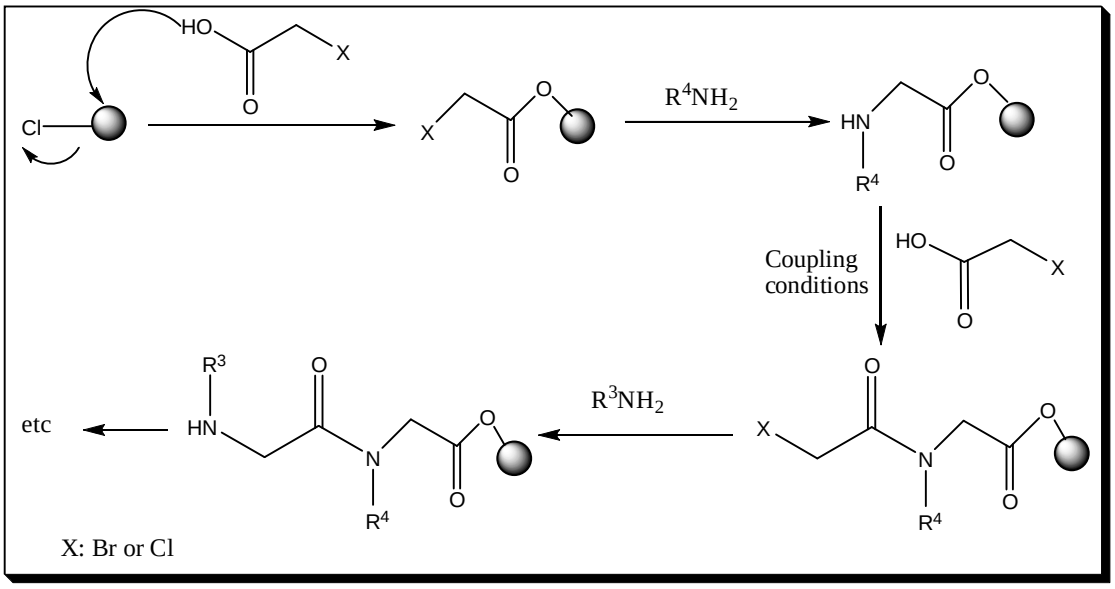

Scheme 7: The submonomer method for solid-phase synthesis of peptoids.

Some important structural features of peptoids, as compared to their peptide analogues, can be clearly observed in the sketch in **Figure 78.** Firstly, due to the presence of the side chain, the amide nitrogen atoms no longer possess a hydrogen atom which could be involved in intra- or interchain hydrogen bonding, thus precluding them from the hydrogen-bond stabilized secondary structures of natural polypeptides. Secondly, there is a loss of chirality at the α-carbon atom. Nevertheless, it has been shown that peptoid oligomers can form stable, chiral, polyproline-like helices in both organic and aqueous solvents, if they contain a high proportion of α-chiral, aromatic side chains [176]. Based on this knowledge, amphiphilic helical peptoids were designed and were found to assemble into oligomers in aqueous conditions, which could bind 1-anilinonaphthalene-8-sulfonate, suggesting that they formed a hydrophobic pocket [177].

Peptoids containing bulky chiral side-chains have also been shown to fold into an unusual 'threaded loop' structure, albeit only in the absence of hydrogen-bonding solvents [178]. Therefore, it seems that it should be possible in the future to design peptoid oligomers with defined folded structures.

2.2.3 Peptoids and peptide-peptoid hybrids with biological activity

The modular nature of peptoids makes them highly amenable to combinatorial synthetic methods. Ng et al. [179] designed a library of peptoid trimers based on structures that had shown antimicrobial activity in a screen of a wide range of combinatorial libraries. 65 pools, each containing 13 compounds were produced and screened for antimicrobial activity in a growth inhibitory assay. Peptoids containing N-terminal dehydroabietylamine (**85**) all showed growth inhibitory activity against *S. aureus* at 1μM concentration and two peptoid trimers also inhibited *E. coli* growth at the same concentration. On further investigation, the most active compounds were shown to have MICs in the micromolar range for a wide range of bacteria, including methicillin-resistant, penicillin-resistant and vancomycin-resistant strains, and showed batericidal, rather than bacteriostatic killing kinetics [180]. Unfortunately, the most active peptoids also showed significant haemolytic activity on red blood cells at higher concentrations. However, these studies, and subsequent combinatorial methods [181] have shown that it is possible to synthesize peptoid oligomers with some antimicrobial activity and selectivity for Gram-positive bacteria.

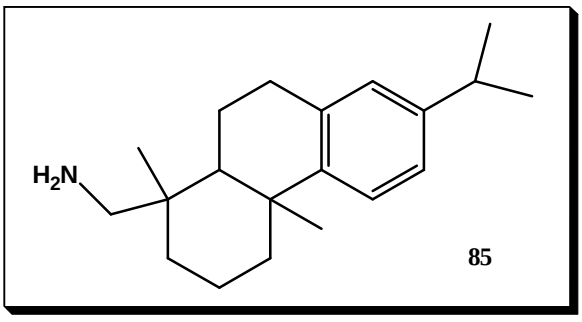

Figure 79: Structure of dehydroabietylamine.

Tripeptoids have also been discovered in a combinatorial library that can neutralize the lipopolysaccharide from Gram-negative bacteria [182], as have tripeptoids

that have some effect on multidrug resistant (MDR) tumour cells (cross-resistance of tumour cell lines to several structurally unrelated chemotherapeutic agents after exposure to a single cytotoxic drug). MDR is a major cause of treatment failure in cancer chemotherapy and is often associated with the overexpression of a transmembrane glycoprotein (P-gp) that acts as a drug efflux pump [183]. Target-oriented synthesis of peptoid oligomers to mimic known biologically active peptides, with improved properties, is also of interest, for example the magainin-2 analogues investigated by Patch et al. [184], of which some showed reasonable antimicrobial activity and low haemolysis at MIC levels.

Libraries of peptide-peptoid hybrids have also been synthesised, usually with the aim of producing molecules with a particular type of biological activity. For example, Kruijtzer et al. [185] synthesised all possible peptoid-peptide hybrids of an MC4 receptor peptide agonist. Ryge and Hansen [186] synthesised lysine-peptoid hybrids based on antimicrobially active peptoid trimers, and could produce molecules with reasonable antimicrobial activity and reasonably low haemolytic activity. Song et al. [187] incorporated peptoid residues into different positions of a model α-helical amphiphilic peptide sequence. These products showed similar or improved antimicrobial activity as compared to the pure peptide sequence, and most also showed reduced haemolytic activity. The most promising compound from this study seems to exert its antimicrobial activity by binding to intracellular targets rather than by a membrane permeabilisation mechanism.

2.2.4 Peptide-peptoid hybrids as potential antimicrobial agents

In the Robinson group, there is much interest in the design of backbone-cyclised peptides based on naturally-occurring antimicrobial peptides, as potential antimicrobial agents. In a series of compounds based on the naturally-occurring pig peptide protegrin-I, **86,** backbone cyclisation was introduced with the aim of improving stability towards proteases, and also to help to constrain the backbone conformation [165]. The natural product has a β-hairpin structure, which is stabilised by two disulfide bonds. A ^{D}Pro-^{L}Pro template was introduced into the synthetic mimetics with the aim of inducing a similar β-hairpin structure. One of the peptide mimetics that showed good antimicrobial activity, along with low haemolytic activity and a β-hairpin structure in contact with micelles was peptide **87**. It was decided to investigate the effect of introducing peptoid units into the sequence of this product, which could allow the introduction of more varied side-chain functionalities, and could help to improve proteolytic stability. Initially, the peptoid unit Nlys was to be introduced, as this would involve minimal changes in key side-chain functionalities. It was also decided to introduce the peptoid units in positions not believed to play an important role in cross-strand hydrogen bonding. The structures of the peptides on which the mimetics were based are presented in **Figure 80**. The structures of the mimetics are presented in **Figure 81**. The expected inter-strand hydrogen bonding pattern for a β-hairpin is illustrated in **Figure 82**. Based on this Figure, the changes in backbone structure caused by the introduction of peptoid units at positions 4 and 6 should have no effect on the inter-strand hydrogen bonding.

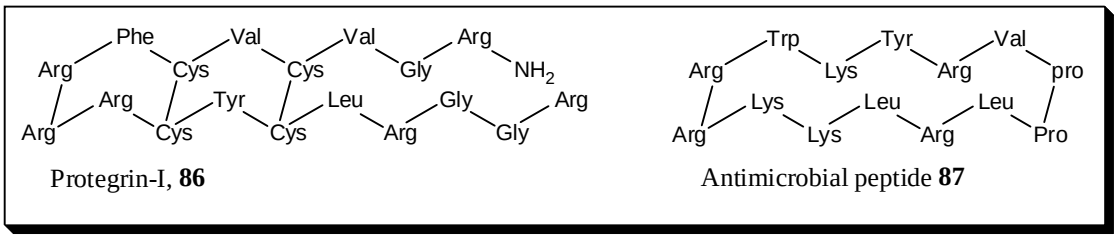

Figure 80: Structures of naturally-occurring antimicrobial peptide Protegrin-I, and synthetic peptidomimetic **87**.

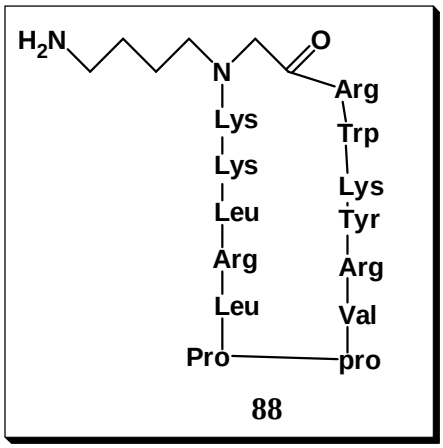

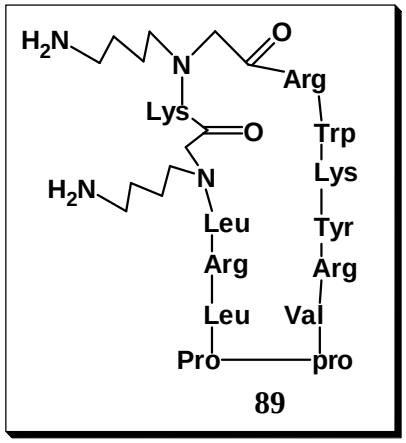

Figure 81: Structures of peptide-peptoid hybrids **88** and **89**.

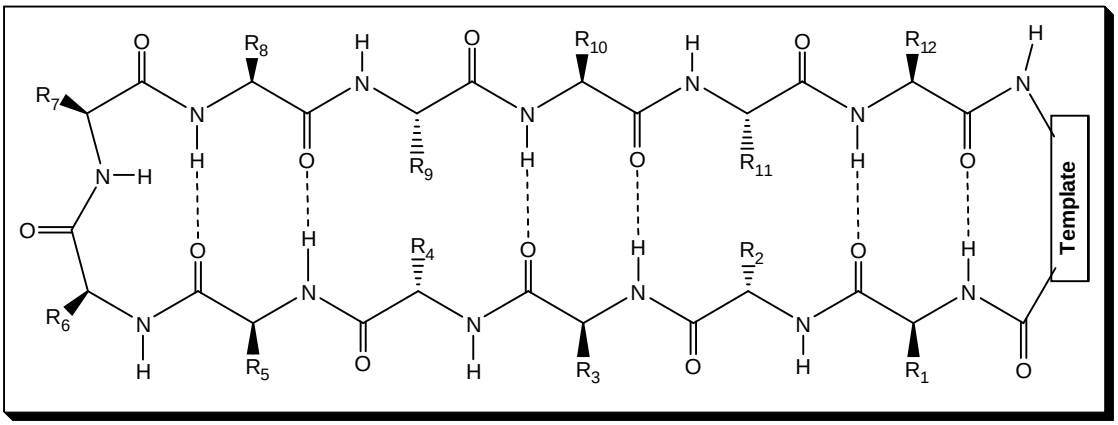

Figure 82: Cross-strand hydrogen bonding in a typical β-hairpin mimetic.

2.2.5 Peptide-peptoid hybrids containing Nlys

2.2.5.1 Synthesis via on-resin cyclisation

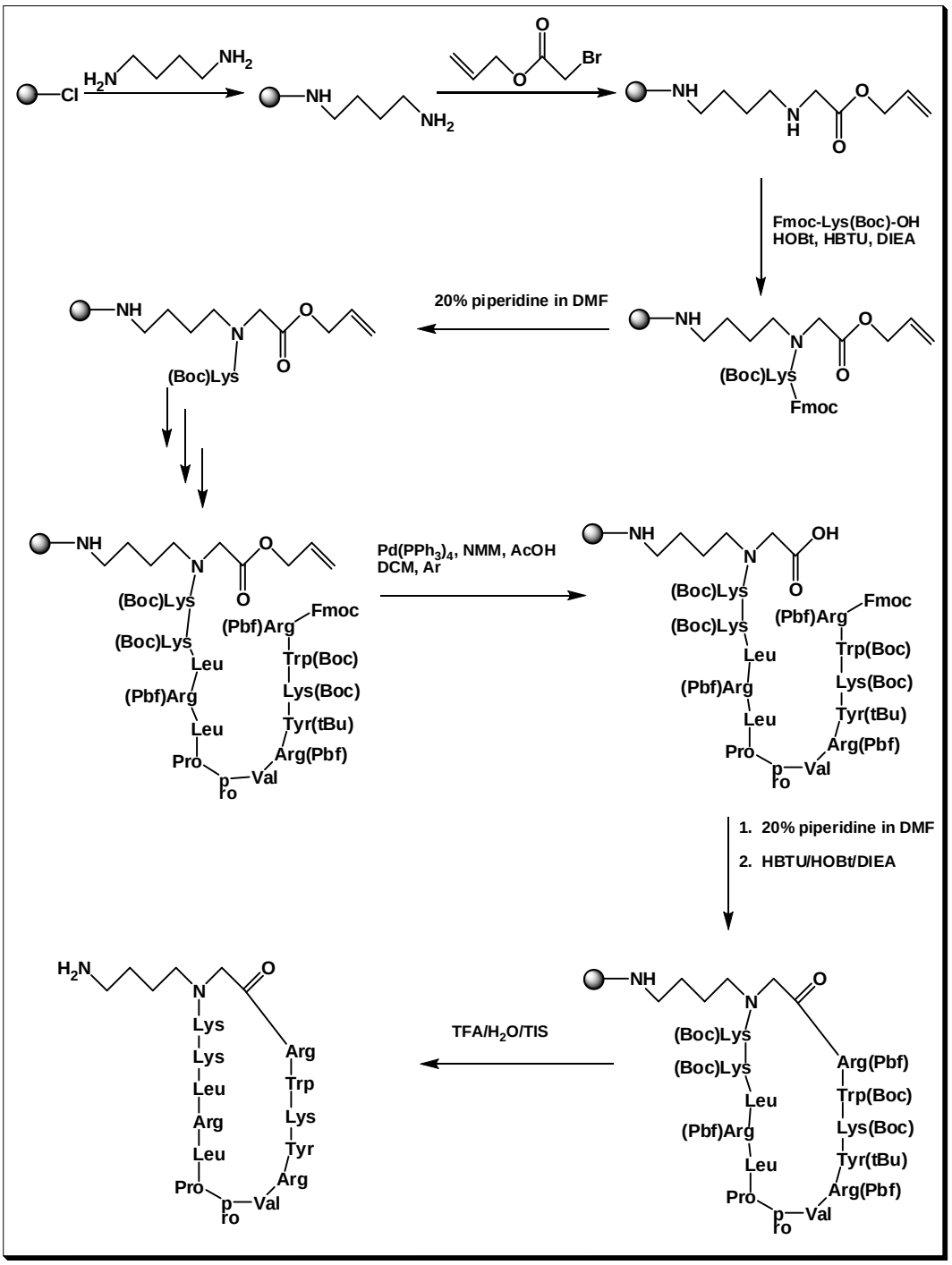

Scheme 8: Proposed synthetic strategy for the solid phase synthesis and on-resin cyclisation of a peptide-peptoid hybrid.

The initial pathway designed for the synthesis of a peptoid-peptide hybrid containing Nlys is outlined in **Scheme 8**. The intention was to couple 1,4-diaminobutane to the solid support, followed by reaction with an allyl 1-bromoacetate, in a reversal of the usual peptoid submonomer synthesis strategy. This would create an orthogonally protected C-terminus, which could be deprotected whilst still attached to the solid support, so that on-resin backbone cyclisation could be carried out on the fully side-chain protected peptide. Acidic cleavage conditions would then release the N-butylamine side chain from the resin and remove the side-chain protecting groups in one step. The coupling of the diamine to the solid support could be monitored using the Kaiser test and proceeded as expected. Allyl 1-bromoacetate **90** was prepared by azeotropic condensation of bromoacetic acid and allyl alcohol [188].

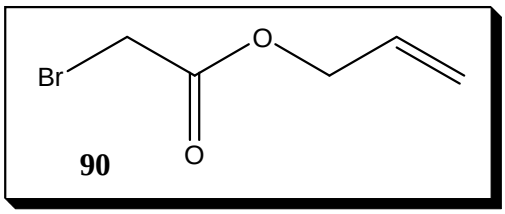

Figure 83: Structure of allyl 1-bromoacetate.

The reaction with allyl 1-bromoacetate was also monitored using the Kaiser test. A negative Kaiser test result suggested that this step had also been successful. However, the attempt to couple a further amino acid residue was unsuccessful. Therefore, it was decided to investigate the product of the first two coupling reactions by acidic cleavage from the resin and LC-MS analysis of the products. It was found that the major product was a tertiary amine, **91** as illustrated in **Figure 84**, and that the desired product **92**, was a minor constituent of the product mixture.

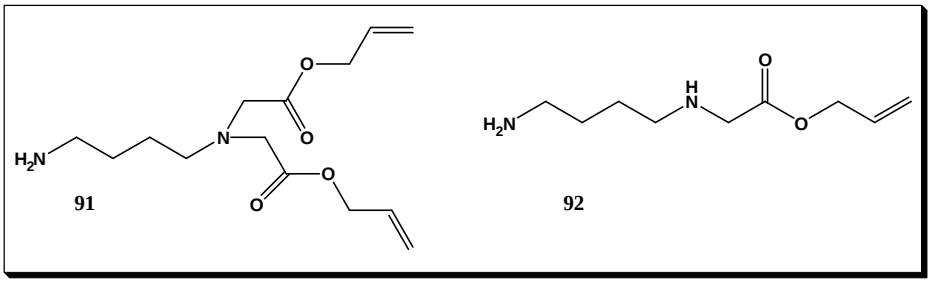

Figure 84: Products obtained from reaction of resin-bound 1,4-diaminobutane with allyl-protected bromoacetic acid.

Trial reactions were carried out where the number of equivalents of bromoacetate were varied, but in all cases, both mono- and disubstituted product was obtained. It was therefore decided to synthesise a peptoid monomer in order to introduce this peptoid unit. The advantage of solution synthesis over solid-phase synthesis in this case lies in the possibility to separate the desired product from any undesired side products, and the possibility of using a large excess of diamine. Therefore, an Fmoc-protected peptoid monomer **96** was prepared as outlined in **Scheme 9.**

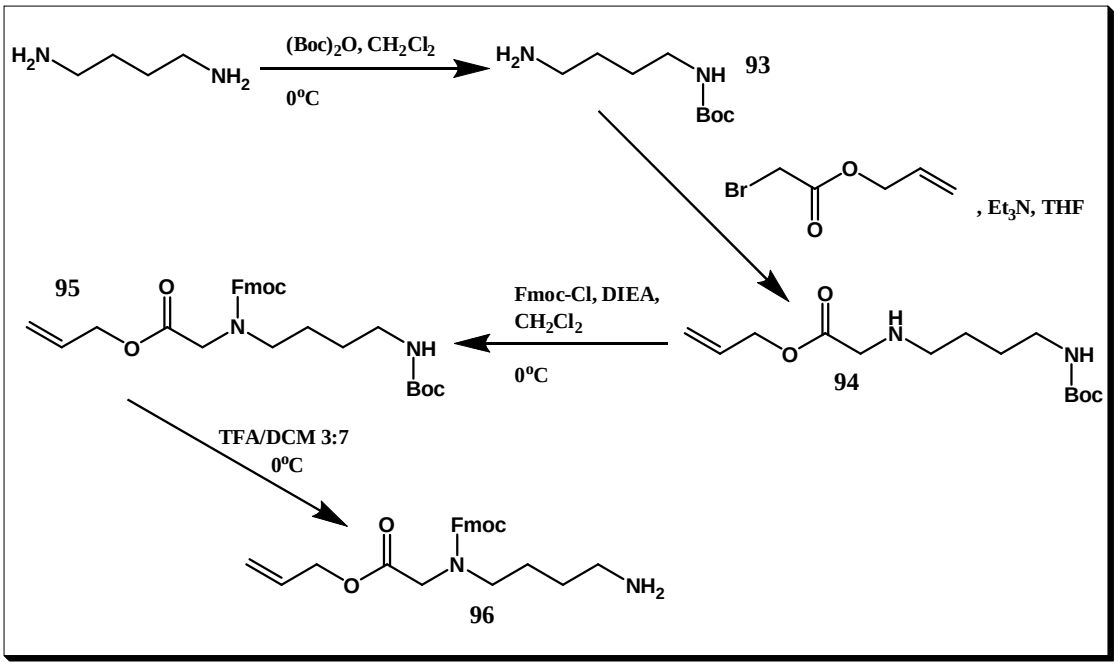

Scheme 9: Synthetic route leading to Fmoc-protected peptoid monomer **96**.

This monomer unit could be successfully coupled to the solid support through the free amine group as before. The Fmoc protecting group was removed using 20% piperidine in DMF, and Fmoc-Lys(Boc)-OH could be coupled to this unit at the less sterically hindered secondary amine position. The Fmoc protecting group of the first lysine residue was removed (to give a positive Kaiser test result), and when the coupling of the second lysine residue was attempted, a negative Kaiser test result was observed, suggesting that the coupling had been carried out successfully. However, when the Fmoc-deprotection of this lysine residue was attempted, no positive Kaiser test result could be obtained. Longer reaction times and higher concentrations of piperidine were attempted to no avail. In order to investigate the source of this problem, a portion of the

peptide-resin was treated under mild acidic conditions to cleave the product from the resin. The product obtained was then analysed by LC-ESI-MS, and found to contain mainly a product of molecular mass (M+H)/1: 357.4. This mass corresponds to the N-substituted diketopiperazine **97** (calculated mass 356.4 g/mol), which could be formed as outlined in **Scheme 10**.

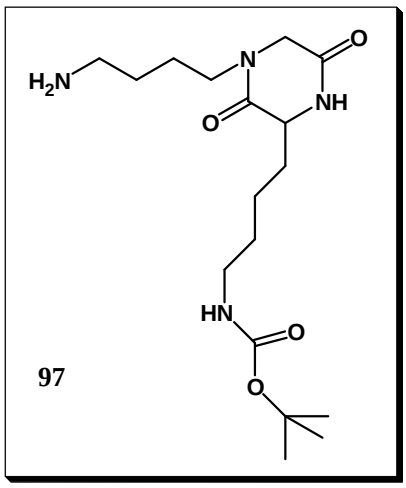

Figure 85: Structure of diketopiperazine **97.**

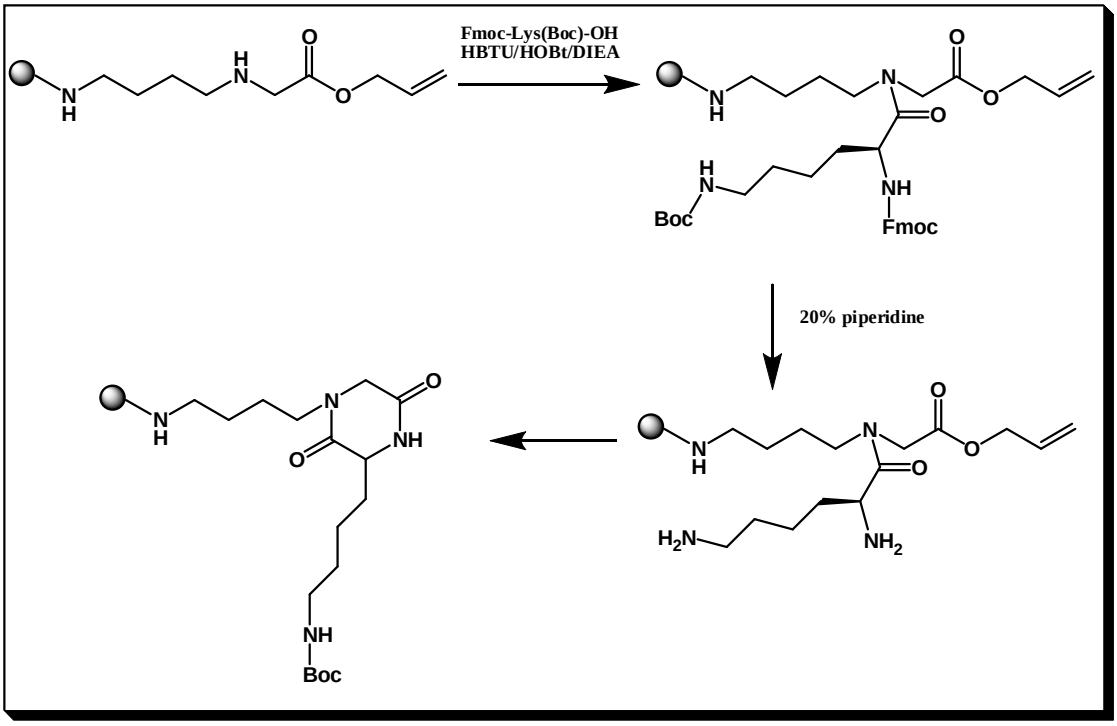

Scheme 10: Proposed pathway leading to the diketopiperazine **97**.

Our strategy to overcome this hurdle involved the separate preparation of the lysine-lysine dipeptide unit **98** illustrated in **Scheme 11**, which could then be introduced into the peptoid-peptide hybrid synthesis in the same way as a standard Fmoc-protected amino acid derivative.

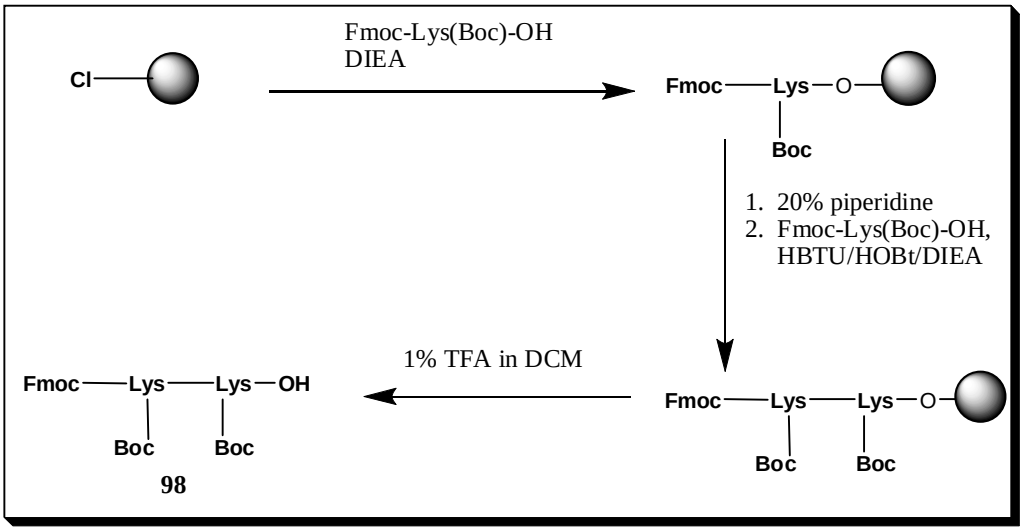

Scheme 11: Synthetic route to dipeptide unit **98**.

With these modifications, the whole of the desired peptoid-peptide chain could be assembled, to provide a product with an Fmoc-protected N-terminus, an allyl-protected C-terminus, linked to the solid support via the peptoid side chain. The allyl protecting group was removed in a palladium-catalysed reaction using N-methyl morpholine, then the Fmoc group was removed using piperidine. Finally, on-resin backbone cyclisation was carried out using HBTU and HOBt with DIEA as the base. The peptoid-peptide hybrid could then be cleaved from the solid support and side chain deprotected in one step using TFA containing 2.5% TIS and 2.5% water. The crude product was analysed by RP-HPLC. The chromatogram is shown in **Figure 86**. The four major peaks were collected and analysed by LC-MS. The largest peak was found to have the expected mass for the desired product. This product could be purified by preparative RP-HPLC to provide peptide-peptoid hybrid **88**, which was analysed by analytical RP-HPLC and ESI-MS. The chromatogram of the pure product is shown in **Figure 87**. Calculated MW: 1850.35 g/mol, measured m/z (ESI-MS): 926.5 (M+2H)/2.

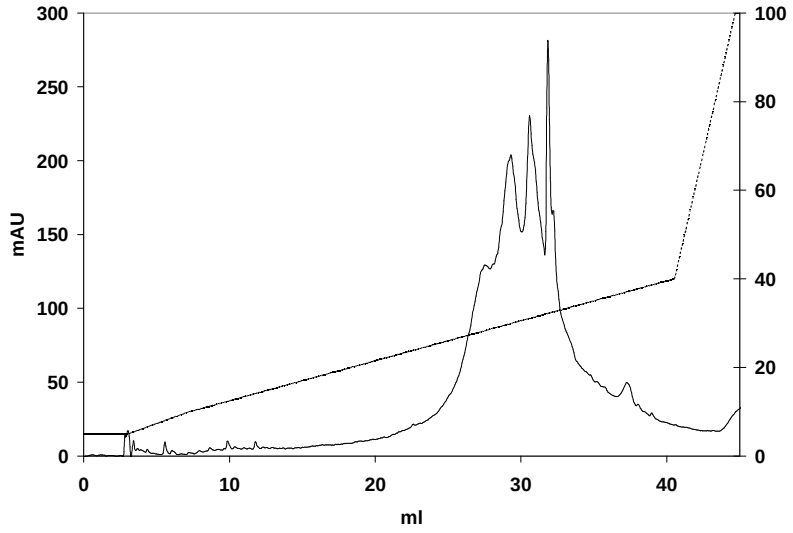

Figure 86: Chromatogram of crude peptoid-peptide hybrid **88**. For HPLC conditions see Appendix 4.

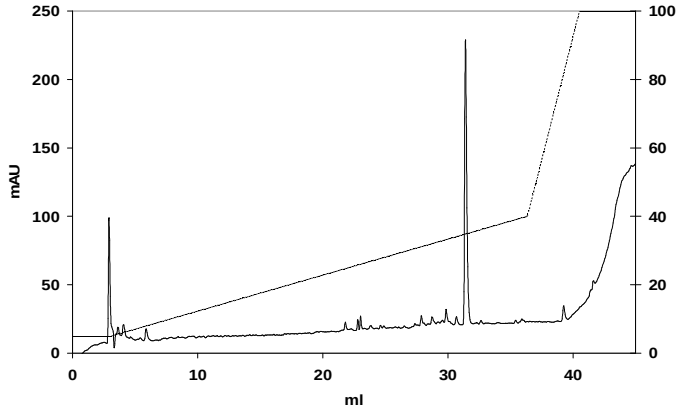

Figure 87. Chromatogram of purified peptoid-peptide hybrid **88**. For HPLC conditions see Appendix 4.

2.2.5.2 Peptide-peptoid hybrids containing Nlys via solution cyclisation

The synthesis described above demonstrated that it is possible to synthesise backbone-cyclised peptide-peptoid hybrids via an on-resin cyclisation strategy. However, the yield of the final product was rather disappointing and the necessity of using a dipeptide as one of the building blocks renders this method rather awkward for the preparation of products containing a lysine residue adjacent to the Nlys residue.

Therefore, the synthesis was also carried out using the usual submonomer method to prepare the peptoid unit, and a solution-phase cyclisation of the fully side-chain protected peptide-peptoid chain was then undertaken, after cleavage from the highly acid-labile resin. This strategy is outlined in **Scheme 12**.

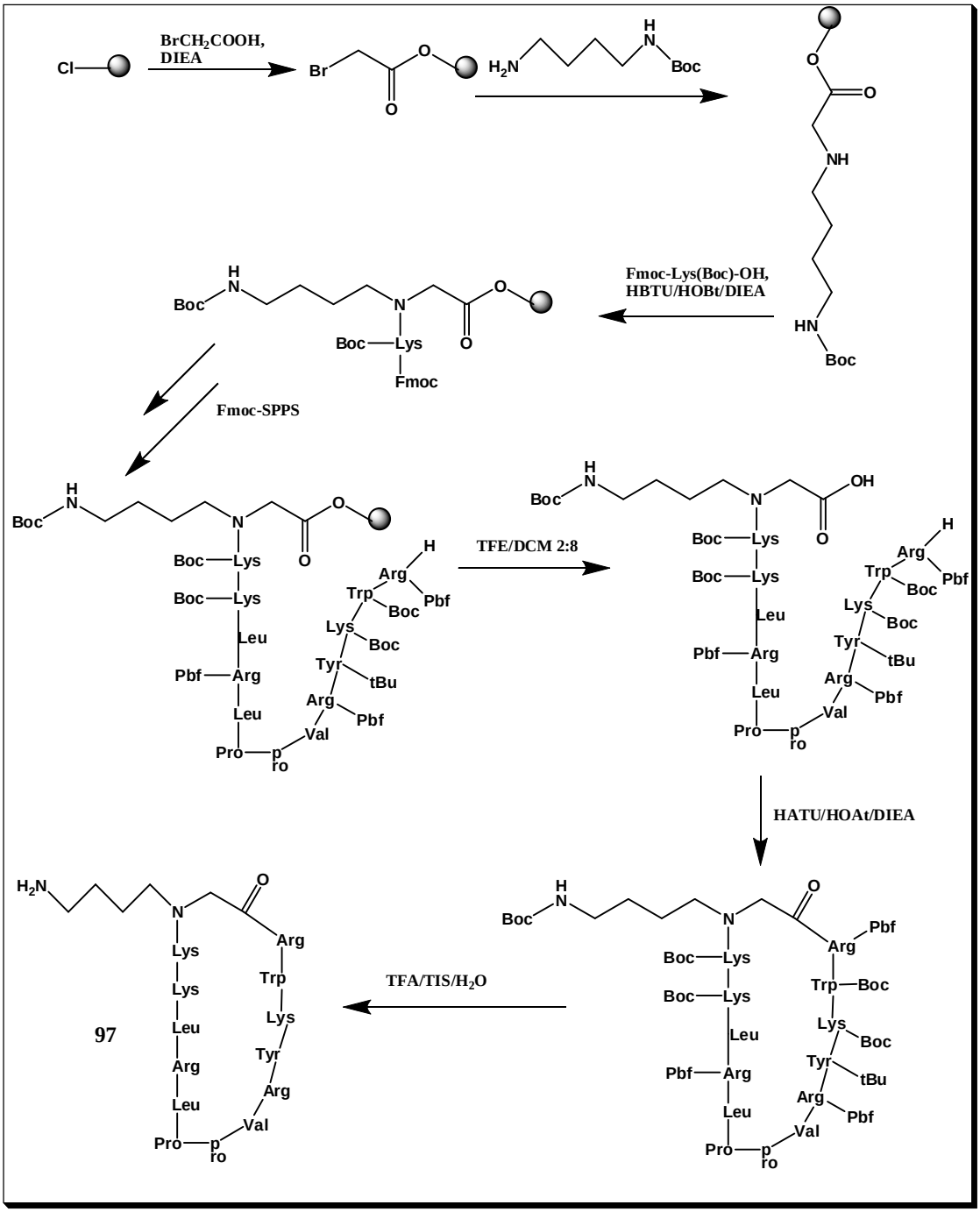

Scheme 12: Alternative synthetic route to peptoid-peptide hybrid **88**.

The attachment of bromoacetic acid to the resin was carried out as for an amino acid derivative, using DIEA as the base. Boc protected diamine **93** was prepared as described in **Scheme 9** and added in a ten fold excess to the resin to produce resin-bound, Boc-protected Nlys. Fmoc-Lys(Boc)-OH was then coupled and the level of loading was estimated by measuring the UV absorption at 290nm of two weighed samples of resin in 20% piperidine solution. The Fmoc protecting group was removed from the lysine residue using 20% piperidine, then resin was transferred to an automated peptide synthesizer and the remainder of the peptide chain was assembled by automated SPPS, with final Fmoc-deprotection to leave a free N-terminal amine group. The crude side-chain protected peptide was then cleaved from the resin using TFE/DCM (2:8) [189]. The crude product was analysed by RP-HPLC, the chromatogram is shown in **Figure 88** and the product was cyclised with HOAt and HATU. The reaction was monitored by RP-HPLC. After overnight cyclisation a new product was observed, as illustrated in **Figure 89**. This was treated with TFA to remove side-chain protecting groups. The chromatogram of the crude product showed one major peak, as illustrated in **Figure 90**. This product was purified and analysed by ESI-MS. Calculated MW: 1850.35 g/mol, measured m/z (ESI-MS): 926.5 (M+2H)/2.

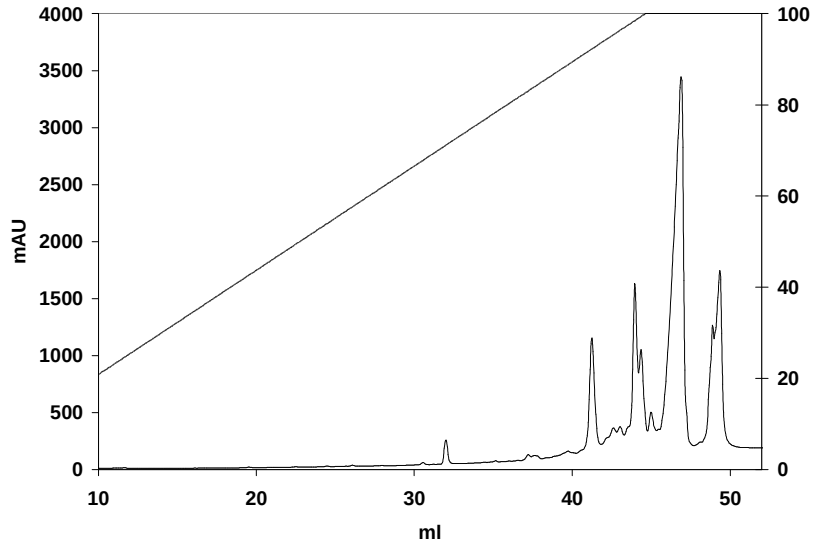

Figure 88: Chromatogram of crude linear protected peptide. For HPLC conditions see Appendix 4.

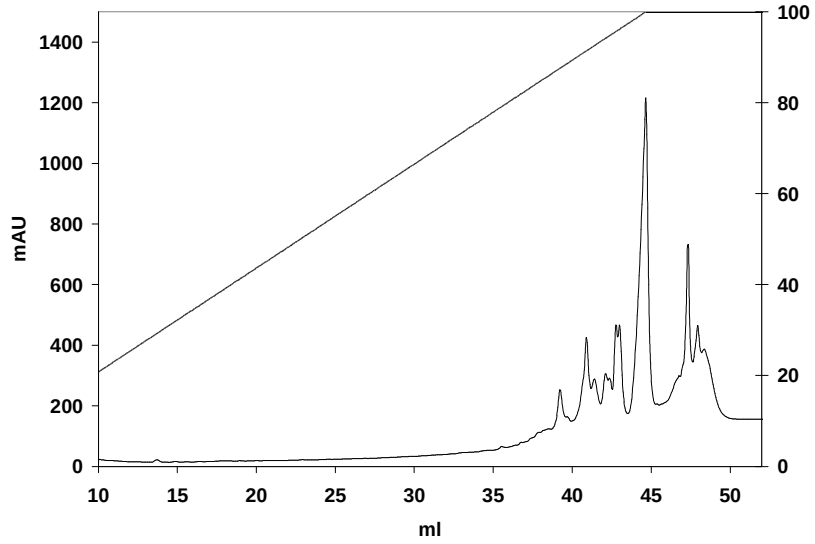

Figure 89: Chromatogram of crude cyclised protected peptide. For HPLC conditions see Appendix 4.

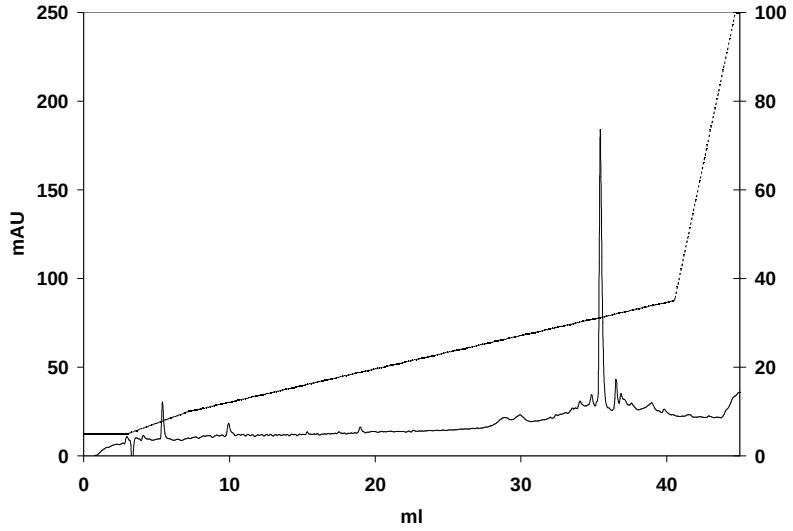

Figure 90: Chromatogram of crude cyclised peptide **88**. For HPLC conditions see Appendix 4.

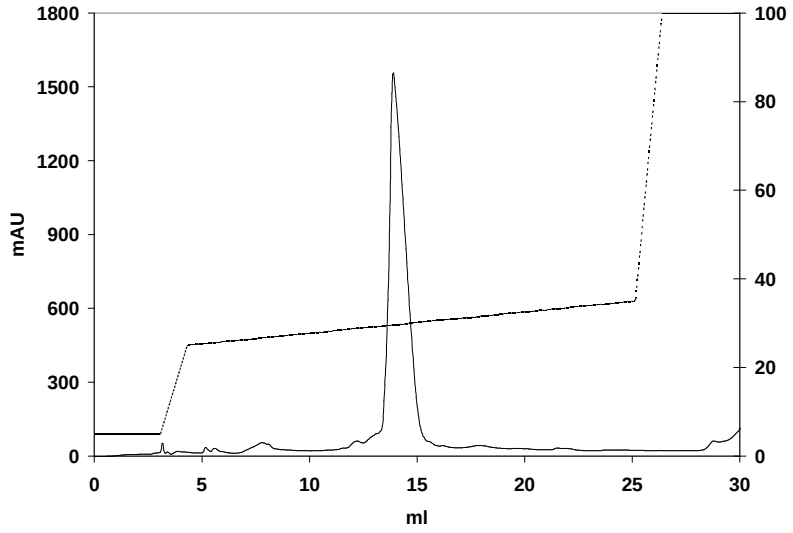

Figure 91: Chromatogram of purified cyclic peptide **88**. For HPLC conditions see Appendix 4.

2.2.5.3 Synthesis of mimetic containing two peptoid units

Based on the synthetic method outlined above, peptide-peptoid hybrid **89** was also prepared, as described in **Scheme 13**. In this case, full coupling of the leucine residue to the second peptoid unit could not be achieved using HBTU/HOBt, but the use of DIC and HOAt was found to be successful.

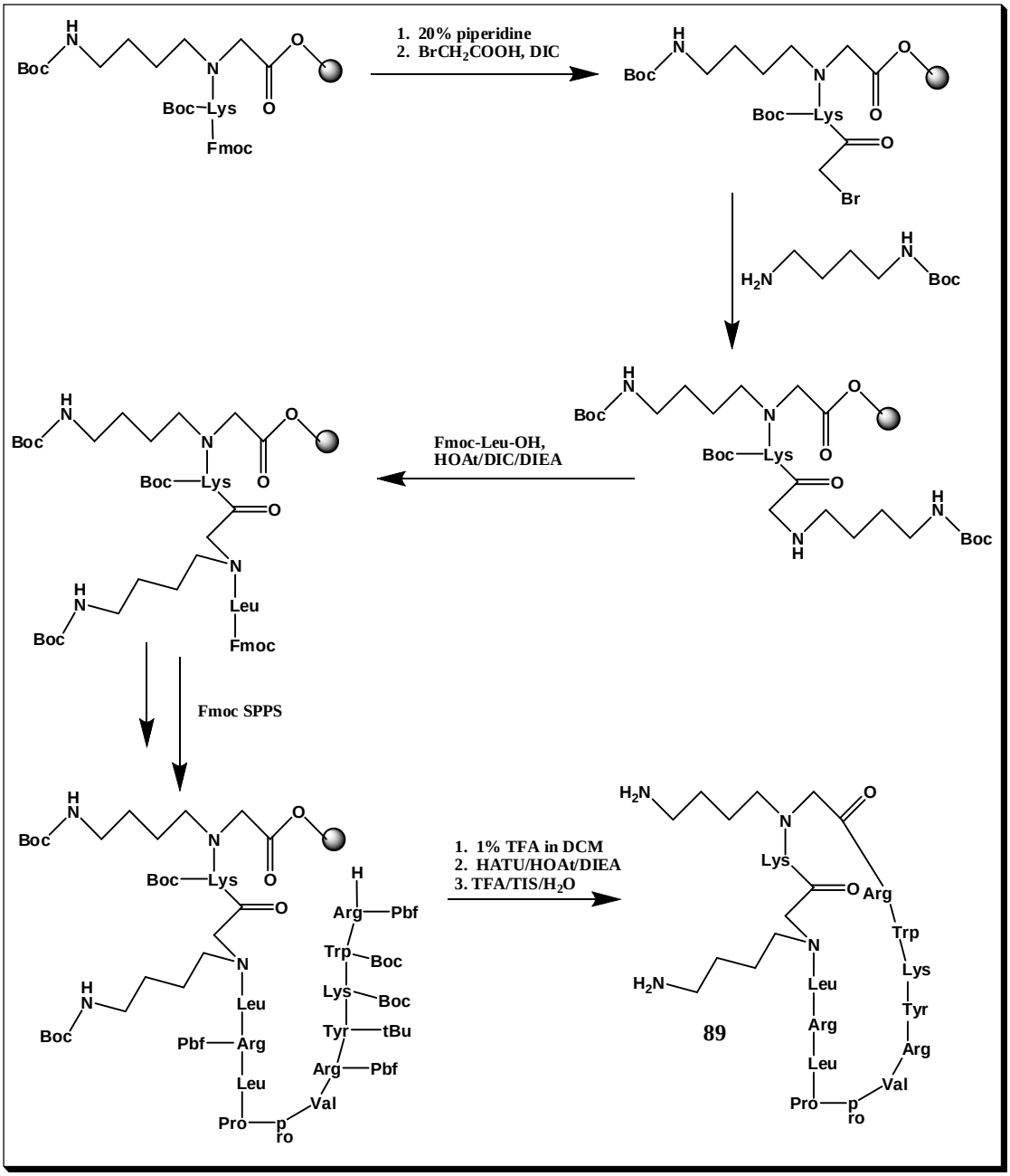

Scheme 13: Synthetic route to peptoid-peptide hybrid **89**.

Coupling of amino acids to secondary amines was monitored using the chloranil test (**Table 12**) [190]. Again, after the difficult coupling to the secondary amine, the peptide-peptoid resin was transferred to an automated peptide synthesiser and the peptide chain was assembled with final Fmoc deprotection to give a peptide-peptoid resin with free N-terminal amine. The fully side-chain protected product could be cleaved from the resin using 1% TFA in DCM [189] and backbone cyclisation was again carried out

overnight with 1.5 eq HOAt, 1.5 eq HATU and 3.5 eq DIEA. Conversion of the linear to the backbone-cyclised product was monitored by RP-HPLC. Chromatograms are shown in **Figure 92**. The side chain protecting groups of the crude cyclic product were removed using TFA containing 2.5% TIS and 2.5% water. The crude deprotected cyclic product could be purified by preparative RP-HPLC to provide the desired product **89,** which was analysed by HPLC (**Figure 93**) and ESI-MS. Calculated MW: 1850.35 g/mol., measured m/z: 926.0 (M+2H)/2

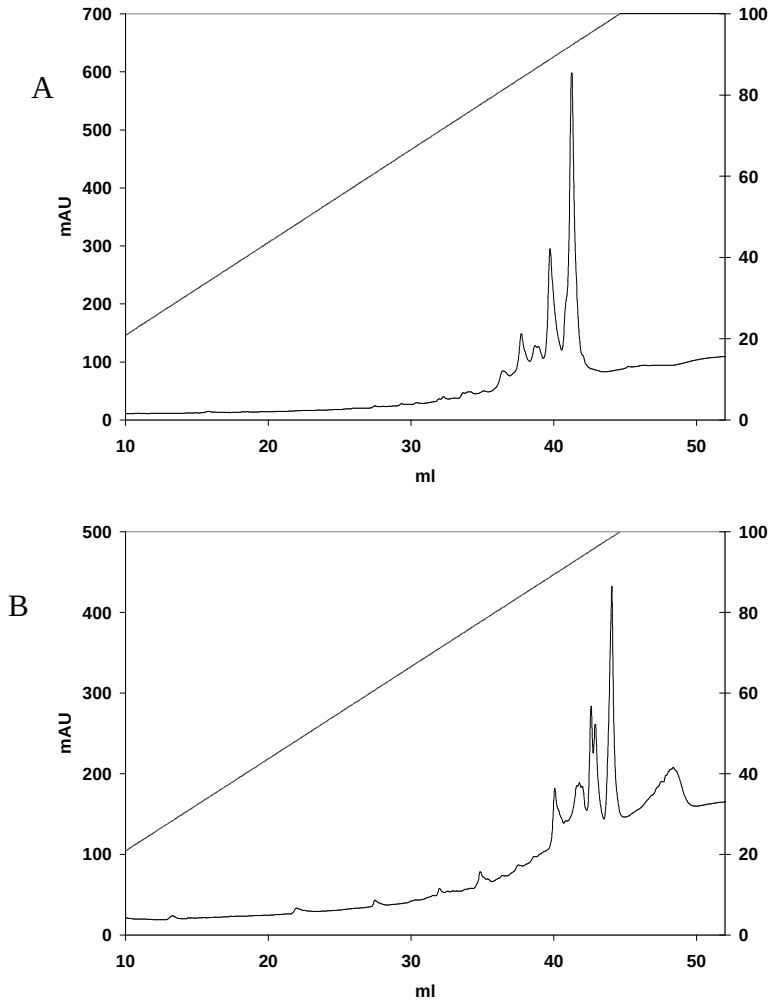

Figure 92: (A) Chromatogram of crude linear side-chain protected peptide. (B) Chromatogram of crude cyclised side-chain protected peptide. For HPLC conditions see Appendix 4.

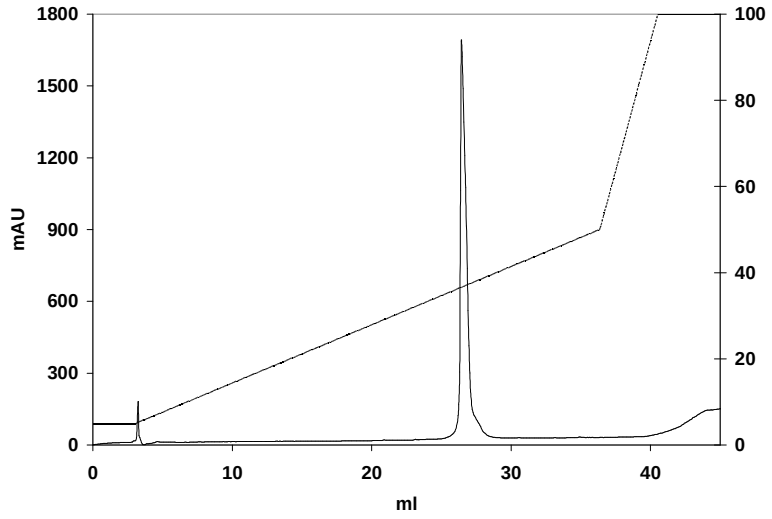

Figure 93: Chromatogram of purified peptoid-peptide hybrid **89**. For HPLC conditions see Appendix 4.

2.2.5.4 Antimicrobial activities

The antimicrobial activities of the peptide-peptoid hybrid mimetics were determined as minimum inhibitory concentrations using the NCCLS broth microdilution method [191]. The haemolytic activity of the mimetics was also measured and the values are compared here with those of the naturally-occurring antimicrobial peptide protegrin-1, **86** and the backbone-cyclised peptide mimetic on which they are based, **87**.

Test microorganism	**Peptide**			
	86	**87**	**88**	**89**
E. coli ATCC25922	4	16	8	32
P. aeruginosa ATCC27853	4	8	4	8
S. aureus ATCC29213	4	32	24	32
S. aureus ATCC25923	4	64	64	64
% haemolysis at 100μg/ml	37	1.4	0.5	1.4

Table 12: Antimicrobial activities of peptidomimetics **87, 88** and **89**.

2.2.5.5 NMR measurements

^{1}H spectra, TOCSY (100ms), DQF-COSY and ROESY (40ms, 80ms, 120ms and 250ms mixing times) of peptide-peptoid hybrids **88** and **89** were measured at pH 5 and 300K. The ^{1}H spectra showed well-defined amide proton signals, with relatively large $^{3}J_{HN\text{-}H\alpha}$ coupling constants. Such signals are often indicative of a well-defined 3D structure. The chemical shifts of the amide protons and the coupling constants are presented in **Table 13.** The ^{1}H spectra are presented in Appendix 1. From the 2D measurements, the spectra were assigned and the average solution structure of mimetic **88** was calculated by Dr Kerstin Moehle. An overlay of 15 calculated structures of the backbone of peptide-peptoid hybrid **88** is shown in **Figure 94**. A typical structure of the mimetic, illustrating side-chain orientations, is shown in **Figure 95**.

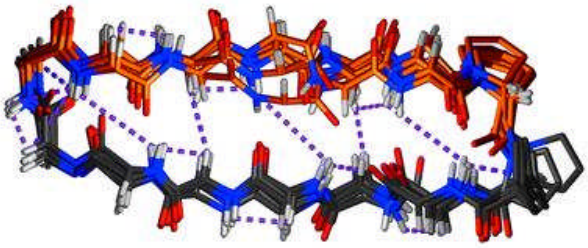

Figure 94: Overlay of 16 DYANA structures for mimetic **88**. The dotted lines indicate key NOE distance restraints.

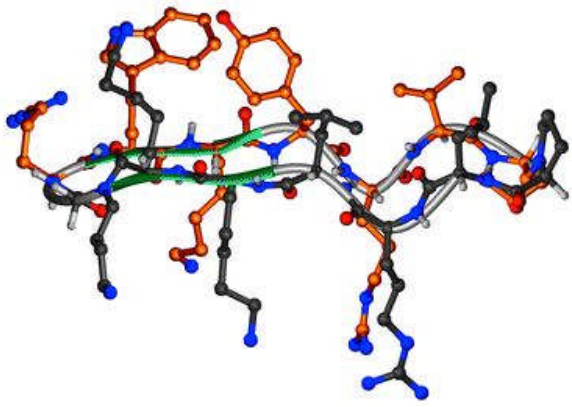

Figure 95: A typical NMR structure of mimetic **88.** The coloured ribbon traces the backbone.

The calculations describe a well-defined β–hairpin conformation in aqueous solution. This is in contrast to peptide mimetic **87**, which seems to be unstructured in aqueous solution but adopts a hairpin conformation upon contact with micelles [165]. This reflects the enhanced conformational stability of the peptide-peptoid hybrid due to the presence of the peptoid unit [192]. To complement the NMR data, H/D exchange rates and temperature coefficients for the amide protons of mimetic **88** were investigated. These data can provide a useful insight into the hydrogen bonding patterns in a compound. H/D exchange rates are measured by dissolving peptide mimetics in D_2O and repeatedly measuring ^1H spectra of the sample, recording the relative rates at which the amide proton signals disappear from the spectrum. Temperature coefficients are calculated from the measurement of ^1H spectra over a range of temperatures. Amide proton chemical shifts can be highly sensitive to temperature, and the shift of signals with changing temperature can be tracked by comparison of spectra. Protons involved in hydrogen bonding exchange more slowly with solvent deuterium and are less sensitive to temperature changes. The H/D exchange rates and temperature coefficients are presented along with the chemical shifts and coupling constants of the amide protons in **Table 13**.

Residue	Chemical shift (ppm)	^3J (α, NH) [Hz][a]	-Δδ/T [ppb/K][b]	H/D relative [c]
^{1}Leu	7.86	8.2	0.7	>
^{2}Arg	8.43	9.5	4.6	>>>
^{3}Leu	8.50	9.5	0.8	>>
^{4}Lys	8.32	8.9	5.7	>>>
^{5}Lys	8.99	8.9	5.3	>>
^{7}Arg	8.41	-	7.8	>>>
^{8}Trp	8.08	8.7	2.6	>>>
^{9}Lys	8.30	9.5	6.0	>>>
^{10}Tyr	8.69	8.0	1.6	>>
^{11}Arg	8.53	9.0	7.0	>>>
^{12}Val	8.35	9.6	0.1	>>

[a]: Measured in ^1H or COSY
[b]: Measurements made over the range 279-214K
[c]: Relative exchange rates: > slow, >> medium, >>> fast

Table 13: Chemical shifts, coupling constants, temperature coefficients and H/D exchange rates for peptoid-peptide hybrid **88**

The small temperature coefficients for the amide protons of residues ^{1}Leu, ^{3}Leu, ^{10}Tyr and ^{12}Val along with the slower H/D exchange rates for these positions suggest the presence of cross-strand H-bonding between ^{1}Leu NH and ^{12}Val CO, ^{12}Val NH and ^{1}Leu CO, ^{3}Leu NH and ^{10}Tyr CO and ^{10}Tyr NH and ^{3}Leu CO.

2.2.6 Peptide-peptoid hybrids containing triethylenetetramine

2.2.6.1 Introduction

As mentioned previously, one of the advantages of the introduction of peptoid units into peptidomimetics is the wider range of side-chain functionalities available for inclusion. That is, a peptide-peptoid sequence can be adapted for a variety of purposes by varying the peptoid side chains present. One possible target is a molecule capable of chelating a radiometal for therapeutic or diagnostic purposes. ^{99m}Tc is an ideal label for diagnostic nuclear medicine, due to its optimal half-life of 6 hours, along with its low cost and easy availability via commercial ^{99}Mo/^{99m}Tc generators. Many ^{99m}Tc-labelled receptor ligands have been prepared for receptor imaging [193] , targeting, for example, thrombosis [194], infection and inflammation [195] or tumours [196-198]. A recent publication reported the possible use of radiolabelled antifungal agents for the detection of fungal infections [199]. These studies showed that ^{99m}Tc-labelled fluconazole could distinguish *C. albicans* infections from bacterial infections and sterile inflammations, and that labelled peptides derived from human ubiquicidin and lactoferrin could distinguish fungal infections from sterile inflammation, although not from bacterial infection. The labelling of biologically-active peptides could be useful in two ways. Radiolabelled analogues of peptides with known targets and activities could be used to locate infections and other targets in radiopharmaceutical research. It could, however, also help researchers in the field of peptide-based therapeutics to better understand the possible biodistribution, excretion and metabolism of their molecules, although it must be borne in mind that the presence of the radiolabel could have some effect on these properties of the peptide.

2.2.6.2 Peptide synthesis

Our goal was to introduce a peptoid side-chain into a molecule similar to peptoid-peptide hybrid **88**, capable of chelating ^{99m}Tc. Amines have been reported to be good chelators for stable ^{99m}Tc binding [200], so the peptide-peptoid hybrid designed for this purpose was mimetic **99,** shown schematically in **Figure 96**, and the building block chosen was the triethylenediamine derivative **100**, with the intention of chelating the metal with three of the four amine groups. The synthetic route to the Boc protected building block **104** is described in **Scheme 14**.

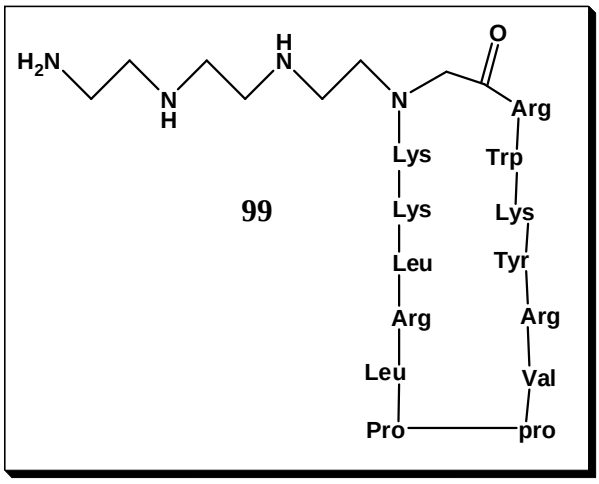

Figure 96: Structure of peptide-peptoid hybrid **99**.

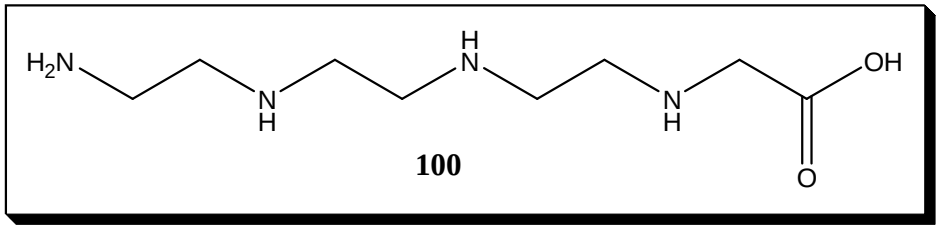

Figure 97: Structure of proposed peptoid monomer **100**.

The synthetic strategy for the preparation of the peptoid-peptide hybrid **99** is outlined in **Scheme 15**.

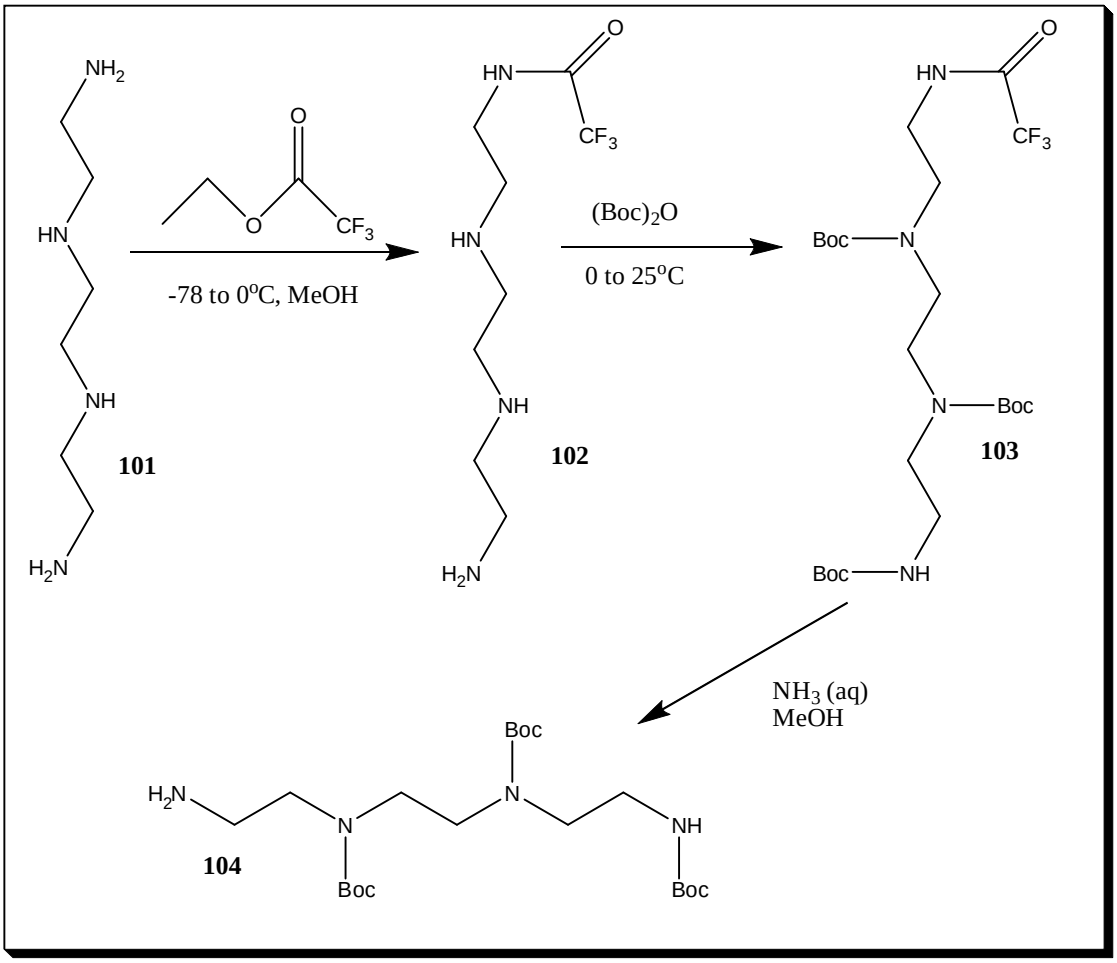

Scheme 14: Synthetic route to Boc protected building block **104**.

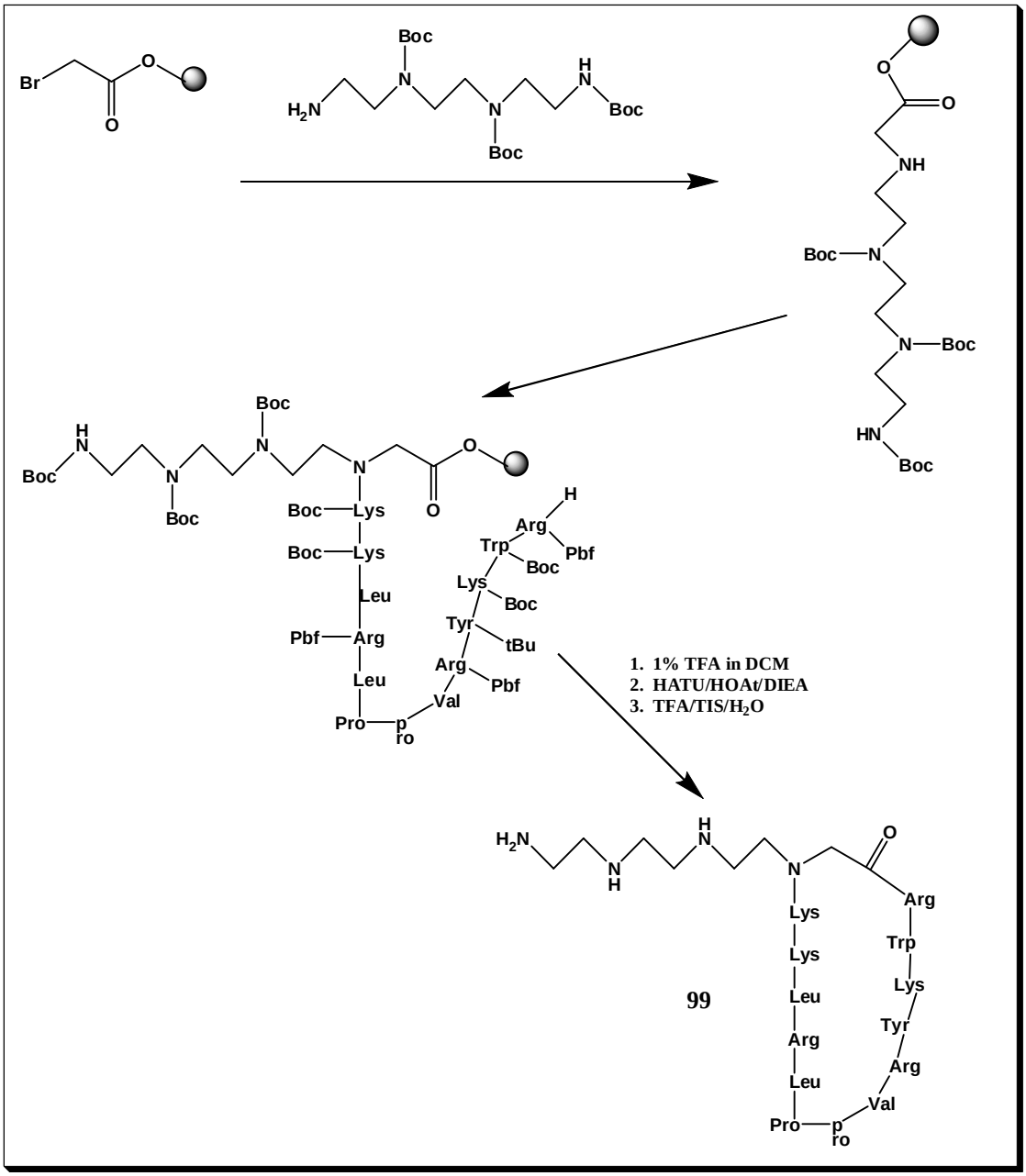

Scheme 15: Synthetic route to peptoid-peptide hybrid **99**.

The peptoid unit was prepared as before via the submonomer strategy. Subsequent coupling of Fmoc-Lys(Boc)-OH to the secondary amine was carried out using DIC and HOAt as coupling agents and monitored using the chloranil test. The peptide-peptoid resin was then transferred to an automated peptide synthesiser where the remainder of the peptide chain was assembled. After final Fmoc-deprotection, the side-chain protected peptide was cleaved from the solid support using 1% TFA in DCM, and backbone cyclisation was carried out using HOAt and HATU as coupling agents with

DIEA as the base. Finally, TFA containing TIS and water was used to remove the side-chain protection groups. The fully deprotected crude cyclic product, was purified by RP-HPLC. The chromatogram of the purified product is shown in **Figure 98**. Calculated MW: 1908.43, Measured m/z (ESI-MS): 1908.0 (± 0.01%).

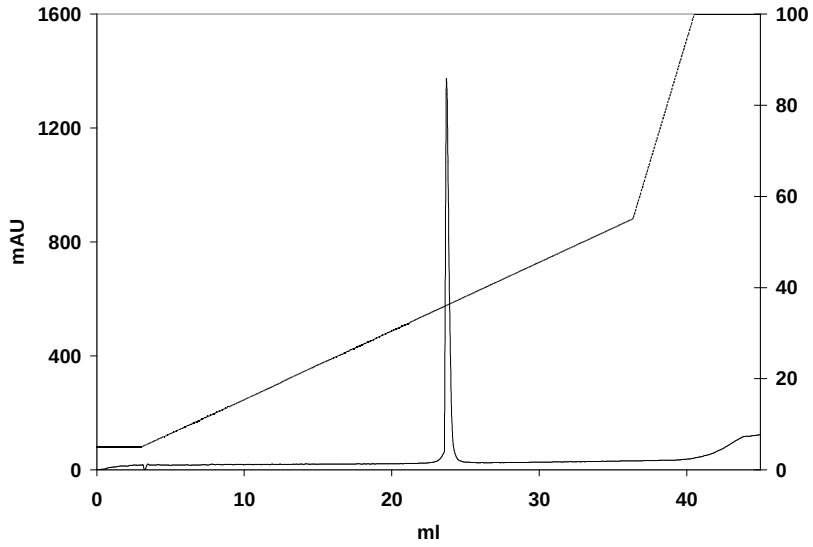

Figure 98: Chromatogram of pure peptoid-peptide hybrid **99**. For HPLC conditions see Appendix 4.

2.2.6.3 Rhenium labelling

This product could be successfully labelled with rhenium in the group of Prof. R. Alberto to provide the labelled product **105.** which Calculated MW: 2178.64, Measured m/z (ESI-MS): 1090.1 (M+2H)/2, 727.1 (M+3H)/3. (± 0.01%).

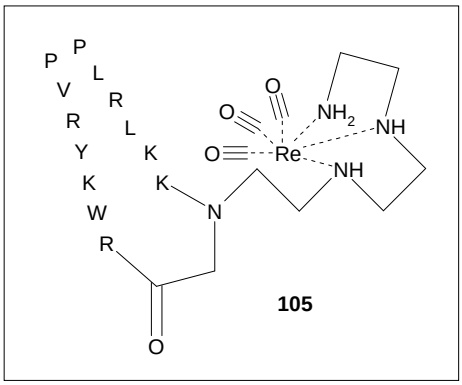

Figure 99: Structure of labelled peptoid-peptide hybrid **105**.

2.2.7 Discussion and conclusions

A backbone-cyclised peptide-peptoid hybrid **88** could be synthesised by a novel solid-phase method involving attachment of the peptoid unit **96** via its side chain to the resin, with orthogonal protection of the peptoid carboxylic acid. On-resin cyclisation could be performed to provide the desired product in reasonable yield. The problem of diketopiperazine formation **(Scheme 10)** during the synthesis could be overcome by the use of a protected dipeptide unit **(98)** as a building block. The same backbone cyclised peptide-peptoid hybrid, along with a second mimetic containing two peptoid units **(89),** was also synthesised by solid-phase assembly using the submonomer strategy for the formation of the peptoid units, followed by solution-phase cyclisation of the fully side-chain protected product, and deprotection to provide the desired backbone cyclic product. In biological assays, both of these mimetics showed antimicrobial activities **(Table 12)** comparable to, or slightly improved with respect to those of the backbone cyclic peptide **87**, on which they were based. Mimetic **88** showed a lower haemolytic activity than cyclic peptide **87**, which would be an important property for a potential candidate for clinical use as an antibiotic. Cyclic peptide **87** shows a well-defined β-hairpin structure in the presence of micelles, but is unstructured in aqueous solution [165]. However, both peptide-peptoid hybrids **88** and **89** show well-defined amide proton signals in NMR spectra measured in aqueous solution, with relatively large coupling constants, often an indication of a well-defined structure. Indeed, the solution structure of peptide-peptoid hybrid **88** could be determined and it was found to form a β-hairpin structure in aqueous solution. H/D exchange rates and temperature coefficients for the amide protons of mimetic **88** suggested that it contained at least some of the cross-strand hydrogen bonds expected for a β-hairpin structure. This work showed that in the development of peptide mimetics as potential antimicrobial agents, the inclusion of a peptoid unit at the tip of a loop could stabilise β-hairpin conformations and could be compatible with the selective targeting of bacterial cells over human erythrocytes. The inclusion of peptoid units could also help to stabilise mimetics towards enzymatic degradation, which would be an important consideration if a peptidomimetic were to be developed as a clinical antibiotic.

It was further possible to introduce a non-natural side-chain into a backbone-cyclised peptide-peptoid hybrid based on the synthetic strategy developed for the

synthesis of mimetics **88** and **89**. The peptide-peptoid hybrid **99** could be used to form a complex with $Re(CO)_3$, presumably the triamine chain chleates the metal atom. Since rhenium and technetium are believed to show similar chemical behaviour [201], these studies could form the basis for the development of a radiolabelled antimicrobial peptidomimetic for diagnostic use. A complex of this type could be used in diagnosis to distinguish between bacterial infections and non-specific inflammation, and could also be useful for research into antimicrobial peptides, to provide valuable information about their uptake, metabolism and excretion in humans. In future work, larger quantities of this kind of complex could also be prepared for crystallisation assays in order to determine the crystal structure of the mimetic.

3 Experimental part

3.1 General notes

3.1.1 Chemical synthesis

N,N'-diisopropylcarbodiimide (DIC), N,N'-dicyclohexylcarbodiimide (DCC), bromoacetic acid, methyl trifluoroacetate and 1,4,-diaminobutane were purchased from *Fluka* and used without further purification. Triethylene tetramine (technical grade, ~70%) was purchased from *Fluka* and fractionally distilled under reduced pressure. Di-tert-butyl dicarbonate ($(Boc)_2O$) was purchased from *NovaBioChem* or *Acros* organics. Dichloromethane (DCM) was distilled from $CaCl_2$ and redistilled from CaH_2. Methanol (HPLC grade) was purchased from *Biosolve Ltd*. Ethyl acetate was distilled from potassium carbonate.

Flash chromatography was carried out on silica gel 60 (230-400 mesh, 0.04-0.063 mm) from *Merck* or *Chemie Uetikon AG*. Thin layer chromatography (TLC) was performed using *Polygram SIL G/UV$_{254}$* from *Machery-Nagel* or *Silica gel 60 F$_{254}$* from *Merck*.

^{1}H NMR spectra were measured at 300 MHz on a *Bruker ARX-300* or *Bruker AV-300* spectrometer.

3.1.2 Peptide synthesis

Peptides were synthesised on an *Applied Biosystems ABI 433A* automated peptide synthesiser coupled to a *Perkin-Elmer 785A UV/VIS* detector or a *Perkin-Elmer Series 200 UV/VIS* detector using the FastMoc® method. NMP and piperidine were purchased from *Acros* and used without further distillation. DMF was purchased from *Acros* and redistilled from ninhydrin. DIEA was purchased from *Acros* and redistilled first from ninhydrin then from KOH. HOBt and HBTU were purchased from *Biosolve*. Water was purified using an *Elgastat® UHP-UF* instrument. Kaiser test kit was purchased from *Fluka*. Amino acids were purchased from *Novabiochem* or *Bachem* and Rink amide resin from *Novabiochem* or *Rapp Polymere*. 2-Chlorotrityl chloride resin (100-200 mesh) with

1.2 mmol/g loading was purchased from *Novabiochem.* The amino acids used were: Fmoc-Asn(Trt)-OH, Fmoc-Ile-OH, Fmoc-Ser(^{t}Bu)-OH, Fmoc-Gln(Trt)-OH, Fmoc-His(Trt)-OH, Fmoc-Cys(Trt)-OH, Fmoc-Val-OH, Fmoc-Lys(Boc)-OH, Fmoc-Pro-OH, Fmoc-Gly-OH, Fmoc-Phe-OH, Fmoc-Arg(Pbf)-OH, Fmoc-Leu-OH, Fmoc-Asp(^{t}Bu)-OH, Fmoc-Tyr(^{t}Bu)-OH, Fmoc-Glu(^{t}Bu)-OH and Fmoc-Thr(^{t}Bu)-OH. Capping solution for the blocking of unreacted sites contained Ac_2O (0.5 M), DIEA (0.125 M) and HOBt (0.015 M) in NMP. The monitoring of the deprotection in the ABI 433A was performed by the removal of a 6 μl aliquot of the 20% piperidine/80% NMP deprotection solution after 1.75 minutes. This sample was passed through the UV detector at 301 nm and a peak was recorded. After washing with NMP the deprotection step was repeated and a second peak recorded. If the height of the second peak was less than 4% of the first peak the deprotection was continued for another 8 minutes and then the rest of the coupling cycle was carried out. If this condition was not met, the deprotection step was carried out a third time and monitored. The deprotections were continued until the condition was met.

TFA was purchased from *Acros*, EDT and TIS from *Fluka*. Diethyl ether was redistilled from $CaCl_2$. DCM was redistilled first from $CaCl_2$ and then from CaH_2. Chloroform was purchased from *Scharlau* and THF from *Fluka*.

For purification and analysis reversed-phase high performance liquid chromatography was performed using an *Äkta purifier (Amersham Pharmacia Biotech)* system. The columns used were Vydac C4 214TP104 (10 μm, 125 Å, 4 x 100 mm, flow rate 1 ml/min), Vydac C18 218TP104(10 μm, 125 Å, 4 x 100 mm, flow rate 1 ml/min), Zorbax eclipse analytical C18, (4.6 x 250 mm, 5 μm, flow rate 1 ml/min) and Vydac C18 218TP54 (5 μm, 125 Å, 4 x 100 mm, flow rate 1 ml/min) for analytical runs. For semi-preparative runs, Vydac C18 218TP1010 (10 μm, 125 Å, 10 x 100 mm, flow rate 5 ml/min), Vydac C4 214TP104 (10 μm, 125 Å, 10 x 100 mm, flow rate 5 ml/min) and a Zorbax eclipse XDB-C18 (9.4 x 250 mm, 5 μm, 4 ml/min flow rate) were used. For large-scale preparative runs, Vydac C18 218TP1022 (10 μm, 125 Å, 22 x 100 mm, flow rate 10 ml/min), Zorbax eclipse XDB-C18 (7 μm, 21.2 x 250 mm) and Interchrom UP10WC4/25M (21.2 x 250 mm) were used. The solvents used were acetonitrile from *Biosolve* and double distilled water, each containing 0.1% TFA. UV detection was at 226 nm and 278 nm.

LC-MS analyses were carried out on an RP-HPLC system connected to a *ThermoFinnigan* Quadrupole-ESI mass spectrometer.

Mass analyses were carried out by the MS-service of the University of Zurich or the Protein Analysis Unit of the Biochemistry Institute of the University of Zurich. Electrospray measurements were performed either on a *Waters Q-tof Ultima API* instrument, a *Bruker ESQUIRE-LC* quadrupole ion trap instrument or a *Finnigan TSQ-700* instrument. Typical measurement error is 0.01%. MALDI-TOF measurements were performed either on a *Bruker Biflex III* with delayed extraction and reflection and Scout 26 ion source, or on a *Bruker Autoflex I*. Typical measurement error is 0.1%.

Amino acid analyses were carried out by the Protein Analysis Unit of the Biochemistry Institute using a *Hewlett-Packard AminoQuant II* instrument with high sensitivity fluorescence detection.

3.1.2.1 Kaiser test [134]

After normal washing of the resin, a few resin beads were place in a small test tube and washed 3 times with diethyl ether. 2 drops of 5% ninhydrin in ethanol, 3 drops of KCN in pyridine and 2 drops of 80% phenol in ethanol were added and the tube placed in an oil bath at 120^{o}C for 5 mins. Blue resin beads indicate the presence of free resin-bound amine.

3.1.2.2 Chloranil test [202]

After normal washing of the resin, a few beads were placed in a small test tube and washed 3 times with diethyl ether. 1 drop of 2% p-chloranil in DMF and 1 drop of 2% acetaldehyde in DMF were added and the beads allowed to stand at r.t. for 20 mins. Blue resin beads indicate the presence of resin-bound amines.

3.1.3 NMR analysis of peptides

1D and 2D spectra were recorded at 600MHz on a *Bruker DRX-600* or Bruker *AV-600* spectrometer, or at 700MHz on a *Bruker AV-700* spectrometer, typically at peptide concentrations of 10-20 mg/ml or with as much peptide as was available. The solvent system used was H_2O/D_2O 9:1, at pH 5, with sodium 3-trimethylsilyl (2,2,3,3,-

D_4)propionate (TSP) as an internal reference. For structural calculations, spectra were also recorded in 100% D_2O. Water suppression was performed using presaturation.

3.2 MSP-1 peptides

3.2.1 Synthesis of peptide 1

Peptide 1:

NISQHQCVKKQCPQNSGCFRHLDEREECKCLLNYKQEGDKCVENPNPT-NH_2

The linear peptide was assembled on 390 mg of Rink Amide resin (loading 0.64 mmol/g) on a 0.25 mmol scale. The standard coupling time for amino acids was 20 mins. For the following residues, an extended coupling time of 55 mins was used: Ile(2), Ser(3), Val(8), Lys(9), Lys(10), His(21), Lys(29), Cys(30), Asn(33), Lys(35), Gln(36), Lys(40), Cys(41), Asn(44), Pro(45), Asn(46), Pro(47). For some residues a long extended coupling time of 85 mins was used: Asn(1), Gln(4), His(5), Gln(6), Cys(7), Gln(11), Cys(12), Pro(13), Gln(14), Asn(15), Cys(18), Arg(20), Arg(25), Cys (28). Each coupling cycle was followed by Ac_2O capping to block unreacted sites. Following completion of peptide chain assembly, the resin was dried under vacuum over KOH for 5 hours. The peptide was cleaved from the resin and side-chain deprotected by treatment with 30 ml of a mixture of TFA/TIS/H_2O/EDT 94:1:2.5:2.5 for 3 hours. The resin was then filtered off and washed twice with 1ml TFA. The solution was concentrated under reduced pressure until a precipitate began to form. The suspension was then transferred into 2 centrifuge tubes and the product was fully precipitated by the addition of cold diethyl ether. The tubes were centrifuged at 2500 rpm for 7 minutes, then the liquid was decanted off. The peptide was washed twice with diethyl ether and centrifuged in the same way, then allowed to air-dry for 1 hour, to give approx. 1g of crude product. This product was purified by preparative RP-HPLC using a Vydac C18 218TP1022 column and a gradient of 5 to 35% acetonitrile over 25 mins. Analytical HPLC: Vydac C18 218TP54, gradient 5 to 17% acetonitrile over 4 mins then 17 to 33% over 29 mins.

Retention time: 19 mins. 72 mg of purified peptide were obtained (5% yield). Calculated MW: 5592.3 g/mol, measured m/z (ESI-Tof-MS): 5591.72 (±0.01%).

3.2.2 Oxidation trials on peptide 1

For oxidation trials 1 to 16, 4 vials were each initially prepared, each containing 2 mg of peptide, 2.5 mg of reduced glutathione and 2.6 mg of oxidised glutathione. To the first vial were added 4 ml of 0.1M Tris buffer (pH 8.4), to the second vial, 3.8 ml of the same buffer and 200 µl DMF, to the third, 3.4 ml of buffer and 600 µl DMF and to the fourth, 3 ml of buffer and 1 ml DMF. The solutions were all stirred well, then each was split into 4 separate vials, so that there were now 16 vials each containing 1 ml of solution. Varying amounts of urea were then added to the vials to give the final reaction mixtures described in **Table 1**. The solutions were stirred overnight then analysed by RP-HPLC and compared to a sample of the linear starting material (0.5 mg/ml in water). 200 µl of each solution were injected on a Vydac C18 218TP54 column with a gradient of 5 to 50% acetonitrile over 30 mins. In all cases the starting material was shown to be no longer present in the solution.

For oxidation trials 17 to 24, 8 vials were prepared containing the volumes of solvent and masses of peptide and reagents described in **Table 15**.

	peptide	$NaHCO_3$	GnHCl	Cysteine	Cystine	vol	GSH	GSSG	urea	DMF	EDTA
	(mg)	mg	M	mg	mg	ml	mg	mg	mg	%	mg
17	0.5	15	1	727	144	2	_	_	_	_	_
18	0.5	7	_	_	_	1	922	197	120	15	_
19	0.5	_	_	_	_	2	92	394	_	_	0.74
20	0.5	_	_	_	_	5	230	985	_	_	1.9
21	0.5	_	_	1817	360	5	_	_	_	_	19
22	0.5	_	_	_	_	2	615	1313	180	_	_
23	0.5	_	1	_	_	2	_	_	_	_	_
24	0.5	_	_	_	_	5	2306	9849	_	_	1.9

Table 15: Composition of oxidation trial samples.

These mixtures were also stirred overnight and then analysed by RP-HPLC in the same way as described for the previous trials. The volume injected for analysis was adjusted so that the same amount of product should be injected for each trial.

The conditions 21 were chosen as optimal and a larger-scale trial under these conditions was carried out: 5 mg of peptide **1** were dissolved in 50 ml of Tris buffer (0.1 M, pH 8.4), with 18 mg Cysteine, 3.6 mg Cystine and 186 mg EDTA. The mixture was stirred overnight and then purified by RP-HPLC using an analytical Vydac C18 218TP54 column with a gradient of 5 to 40% acetonitrile over 25 mins. The sample was frozen and lyophilised and finally submitted for ESI-Tof-MS. Calculated MW: 5586.31 g/mol, measured m/z: 5586.3 (±0.01%).

In the final trial, different concentrations of peptide were tested. 10ml of the oxidation solution were prepared (0.1 M Tris buffer, pH 8.4, 10 mM EDTA, 3 mM Cysteine, 0.3 mM Cystine). 4 vials were prepared with (a) 0.5 mg peptide, 1ml solution (0.5 mg/ml), (b) 0.5 mg peptide, 0.5 ml solution (1 mg/ml), (c) 1 mg peptide, 0.5 ml solution (2 mg/ml), (d) 2.5 mg peptide, 0.5 ml solution (5 mg/ml). The solutions were stirred overnight and then analysed by RP-HPLC. All chromatograms showed, as before, one main peak with the same retention time as the products from the previous trials, suggesting that the same product was formed and that higher peptide concentration had no detrimental effect on the oxidation process.

3.2.3 Synthesis of folded peptide 2

Peptide 2:

NISQHQCVKKQCPQNSGCFRHLDEREECKCLLNYKQEGDKCVENPNPT-NH_2

16.5 mg of peptide **1** were dissolved in 3.5 ml of an oxidation buffer made up of 0.1 M Tris buffer (pH 8.4) containing 10 mM EDTA, 3 mM Cysteine and 0.3 mM Cystine. The mixture was stirred for 48 hours and then the product was purified by semi-preparative RP-HPLC using a Vydac C18 218TP1010 column and a gradient of 5 to 30% acetonitrile over 25 mins. Analytical HPLC: Vydac C18 218TP54, 5 to 17% acetonitrile over 4 mins, then 17 to 33% over 26 mins. Retention time: 11 mins. Injections of 200 µl were made, the main peak collected each time and the collected product frozen and lyophilised to give 4 mg of pure product (24% yield). A small portion of the product was taken for ESI-MS analysis. The remainder was used in the NMR studies.

3.2.4 NMR studies on peptide 2

1D and 2D ^{1}H NMR spectra were recorded at 600 MHz at a peptide concentration of 15 mg/ml in H_2O/D_2O 9:1 and in 100% D_2O at pH 5 and 298 K. Water suppression was performed by presaturation [203]. The sequential resonance assignments were based on DQF-COSY [204] and TOCSY [205] measurements. Distance restraints were obtained from NOESY [206] spectra with mixing times of 50, 150 and 300 ms. Spectra were collected with 1024 x 256 complex data points zero-filled prior to Fourier transformation to 2048 x 1024, and transformed with a cosine-bell weighting function. Data processing was carried out with XWINNMR (Bruker) and XEASY [207].

The structure calculations were performed by restrained molecular dynamics in torsion angle space by applying the simulated annealing protocol implemented in the program CYANA [208]. Starting from 100 randomized conformations, a bundle of 20 conformations were selected with the lowest CYANA target energy function. The structures were analysed by PROCHECK-NMR [209] and have been deposited in the Protein Data Bank under the accession number 2FLG. The program MOLMOL [210] was used for structure analysis and visulisation of the molecular models.

3.2.5 Enzymatic digestions

For trypsin digestions, peptide **2** (1 mg) was digested with TPCK-treated trypsin (50 μg) in phosphate buffer (2 ml, 50 mM, pH 6.8) for 24 h at 37^{o}C. The digest was then analysed by RP-HPLC (Vydac 218TP54 column, flow rate 1 ml/min) using a gradient of 5 to 23% acetonitrile over 34 mins. The digestion products were then separated by RP-HPLC (same conditions) into the fractions identified in chapter 1.2. The fractions were analysed by LC-MS.

For thermolysin digestions, peptide **2** was digested with thermolysin (100 μg) in N-ethyl morpholine/acetate buffer (2 ml, 25 mM, pH 6.4) for 2 h at 40^{o}C. The digest was analysed by RP-HPLC (Zorbax eclipse analytical C18, 4.6 x 250 mm, 5 μm, flow rate 1 ml/min) using a gradient of 3 to 30% acetonitrile over 34 mins. The digestion products were then separated by RP-HPLC under the same conditions into the fragments identified in chapter 1.2.

For the trypsin digestion of the thermolytic fragment 11, the fraction (estimated 70 μg) was digested with TPCK-treated trypsin (3.5 μg) in phosphate buffer (200 μl, 50 mM, pH 6.8) for 24 h at 37°C. The digest was analysed by RP-HPLC (Zorbax eclipse analytical C18, 4.6 x 250 mm, 5 μm, flow rate 1 ml/min) using a gradient of 3 to 30% acetonitrile over 34 mins. The digestion products were then separated by RP-HPLC under the same conditions into the fragments identified in chapter 1.2.

Five fragments were selected for further investigation by reduction. Samples of each digestion product were treated with DTT (5 eq per cysteine residue) in ammonium carbonate buffer (0.1 M, pH 8.0) for 6 h at room temperature. To stop the reaction, 10% (v/v) acetic acid was added to each sample to give a final pH of 2-3. The samples were frozen, lyophilized and analysed by MALDI-MS.

3.2.6 Synthesis of ethyl [*N'*-(*tert*-butoxycarbonyl)hydrazino]-acetate 5

This product was prepared from **4** according to the method of Bonnet et al by F. Boato [211].

3.2.7 Synthesis of ethyl [*N'*,*N'*,*N*-Tris(*tert*-butoxycarbonyl)hydrazino] acetate 6

Ethyl [*N'*-(*tert*-butoxycarbonyl)hydrazino]-acetate **5** (10 g) was dissolved in CH_2Cl_2 (10 ml) and Et_3N (13.5 ml) at 0°C. Di-*tert*-butyl dicarbonate (21 g) and DMAP (1.75 g) were dissolved in CH_2Cl_2 (17 ml) and this solution was also cooled to 0°C. The solution of **5** was then added dropwise over 40 minutes. The mixture was stirred for 20 minutes at 0°C and then gradually allowed to reach room temperature over 2 h. The solution was diluted with CH_2Cl_2 (30 ml) and then extracted with saturated KH_2PO_4 solution (3 x 70 ml). The aqueous phase was then extracted once with CH_2Cl_2 (100 ml). The organic phases were combined, dried over Na_2SO_4, and concentrated under reduced pressure to give 15.2 g of an orange oil. Approximately half of this oil was purified by flash chromatography using silica gel (650 g) in a column of 6 cm diameter. The column was eluted with CH_2Cl_2/EtOAc 97/3 and the fastest eluting product (Rf value 0.39) was collected. The product was concentrated and dried under high vacuum to give 1.9 g of a

yellow oil (22% yield). ^{1}H NMR:($CDCl_3$, 300 MHz) 4.3-4.1 ppm, (m, 4H, C**H$_2$**COC**H$_2$**CH_3), 1.48-1.6 ppm (m, 27H), 1.3ppm (t, 3H).

3.2.8 Synthesis of [*N',N',N*-Tris(*tert*-butoxycarbonyl)hydrazino]-acetic acid (7)

Ethyl [*N',N',N*-Tris(*tert*-butoxycarbonyl)hydrazino]- acetate **6** (1.9 g) wasdissolved in ethanol (15 ml) and stirred in an ice bath. NaOH (10 ml, 1M solution) was also cooled in an ice bath and then added dropwise over 1h to the solution of **6**. The mixture was stirred at 0^{o}C for a further 30 mins. The solution was then neutralised to pH 4 using a 10% citric acid solution. At around pH 5 a precipitate began to form. The solution was diluted with water (30 ml) and then diethyl ether (50 ml) was added. The precipitate dissolved in diethyl ether and the aqueous phase was extracted twice more with diethyl ether (50 ml), then twice with CH_2Cl_2 (50 ml). The organic phases were combined and washed twice with brine, dried over Na_2SO_4 and concentrated under vacuum to leave a pale yellow oil. The oil was then cooled and a small amount of cooled diethyl ether/heptane 2/3 was added, upon which a white precipitate formed. The precipitate was filtered off and washed several times with cooled diethyl ether/heptane 2/3, then dried under vacuum to leave 1.14 g of a white powdery solid (64 % yield). ^{1}H NMR:($CDCl_3$, 300 MHz): 4.15ppm (s, 1H), 4.05ppm (s, 1H), 1.48-1.6ppm (m, 27H). ESI-MS: 413.2 (M+Na)+

3.2.9 Synthesis of peptide 8

Peptide 8:

The peptide sequence was prepared on the ABI 433A using the same method as described in section 3.2.1. Before cleavage from the resin, the hydrazinoglycine was coupled as follows.

500 mg (approx 3/10) of the resin were swelled in 2 ml DMF. **7** (75 mg, 0.19 mmol, 2.5 eq), HOAt (45 mg 0.3 mmol, 4eq), HATU (114 mg, 0.3 mmol, 4 eq) and DIEA (148 µl, 0.9 mmol, 12 eq) were dissolved in a minimal amount of DMF (~4 ml) and this solution was added to the resin. The resin suspension was agitated for 3.5 h, then the resin was filtered off and washed (3 x DMF, 5 x CH_2Cl_2).

Finally, the peptide was cleaved from the resin and deprotected using TFA/TIS/H_2O/EDT 94:1:2.5:2.5 (30 ml) for 3 h. After this time the resin was filtered off and the solution was concentrated under vacuum until a precipitate formed. The product was transferred to 2 centrifuge tubes and fully precipitated by the addition of cooled diethyl ether. The tubes were centrifuged at 2500 rpm for 7 mins at 10 ^oC, then the liquid was decanted off. The peptide was washed with diethyl ether and centrifuged twice more in the same way, and was then allowed to air-dry for 1 hour. LC-MS: 1416.7 (M+4H)/4, 1133.8 (M+5H)/5, 945.1 (M+6H)/6, 810.2 (M+7H)/7. 260 mg of peptide were obtained (46% yield).

3.2.10 Oxidative folding of peptide 8 to give peptide 9

Peptide 9:

Dry crude peptide **8** (260mg) was dissolved in 100 ml of 0.1 M Tris buffer (pH 8.4) containing EDTA (372 mg, 1 mmol). cysteine (36 mg, 0.3 mmol) and cystine (7 mg, 0.03mmol) were added and the solution was stirred overnight. RP-HPLC analysis using a Vydac C18 218TP104 column and a gradient of 5 to 35% acetonitrile over 30 mins showed that the starting material was no longer present and that one main new peak had been formed. The product was purified using semi-preparative HPLC using a Vydac C18 218TP1010 column and a gradient of 10 to 35% acetonitrile over 30 mins to collect the main peak. Analytical HPLC: Vydac C18 218TP54 , flow rate 1 ml/min, 5 to 50% acetonitrile over 29 mins.

Retention time: 12.5 mins. The fractions containing the main peak were collected together, frozen and lyophilised to give 51 mg of white powder peptide **9** (19.6% yield). Measured m/z (ESI-Tof-MS): 5658.4 (±0.01%).

3.2.11 Synthesis of PE-succ (11)

PE **(10**) (700 mg, 1mmol) was dissolved in $CHCl_3$/MeOH (100 ml, 9:1). Succinic anhydride (163 mg, 1.6mmol) was dissolved in DCM (100 ml) and added to the solution of **10**, along with Et_3N (420 µl, 3 mmol). The mixture was stirred overnight, then citrate/phosphate buffer (200 ml, 0.02 M, pH 5.5) and $CHCl_3$ (200 ml) were added, and the mixture stirred for a further 1 h. The aqueous phase was then extracted four times with $CHCl_3$ (150 ml). The organic phases were collected and dried over Na_2SO_4, then the solvents were removed under reduced pressure to give 770 mg of a white waxy product (96% yield). ^{1}H NMR: 0.8 ppm (t, 6H), 1.1-1.3 ppm (m, 48H), 1.6 ppm (m, 4H), 2.25 ppm (t, 4H), 2.5-2.65 ppm (m, 4H), 3.05 ppm (m, 4H), 3.35 ppm (m, 2H), 3.9 ppm (m, 2H), 4.2 ppm (m,4H), 4.4 ppm (m, 1H). M/z (ESI-MS): 790.7 $(M-H)^-$.

3.2.12 Synthesis of PE-succ-NHS (12)

11 (50 mg, 63 µmol) was dissolved in THF/$CHCl_3$ (approx. 2 ml, 1:1). To this solution were added DCC (11.4 mg, 55 µmol) and N-hydroxysuccinimide (7.25 mg, 63 µmol). The mixture was stirred and the reaction followed by TLC. After 6 h, the starting material had disappeared and a new product formed. The precipitated urea was filtered off. The solvents were removed by rotary evaporation and the product immediately dissolved in *tert*-butanol (10 ml) and used in the coupling reaction.

3.2.13 Synthesis of lipopeptide 13

Lipopeptide 13:

Peptide **9** (3 mg) was dissolved in water (500 µl) and the pH adjusted to 5.0-5.4 using 0.1 M NaOH. The solution of **12** in *tert*-butanol (150 µl, 1.5 eq) was added to this solution along with *tert*-butanol (350 µl). The mixture was stirred at room temperature and samples were removed at frequent intervals for LC-MS analysis. A peak appeared at high retention time with the expected mass of the desired product (calculated MW: 6432.4 g/mol, observed m/z: 1287.5 (M+5H)/5, 1073.1 (M+6H)/6, 919.7 (M+7H)/7 (±0.01%). After 1-4 h, the peak of desired mass no longer increased in size and the product was purified by RP-HPLC using an analytical Vydac C4 214TP104 column and a gradient of 10 to 100% acetonitrile over 16.5 mins. Retention time: 15 mins. The fractions containing the product peak were collected together, frozen and lyophilised. Measured m/z (ESI-Tof-MS): 6432.5 (±0.01%).

3.2.14 Immunization studies

Preparation of peptide-loaded virosomes and immunizations were carried out at Pevion Biotech. A solution of purified influenza A/Singapore virus hemagglutinin (4 mg) in phosphate-buffered saline (PBS) was centrifuged for 30 mins at 100000g and the pellet was dissolved in PBS containing 100 mM octaethyleneglycolmonodecylether (PBS-OEG). Lipopeptide **13** (4 mg), phosphatidylcholine (32 mg, Lipoid, Ludwigshafen, Germany), and phosphatidylethanolamine (6 mg) were dissolved in PBS-OEG (2.66 ml). The phospholipid and the hemagglutinin solutions were mixed and sonicated for 1 min.

This solution was then centrifuged for 1 h at 100000g, and the supernatant was filtered (0.22 mμ) under sterile conditions. Virosomes were then formed by detergent removal with SM BioBeads (Bio-Rad, Glattbrugg, Switzerland).

For immunogenicity studies, five BALB/c mice were pre-immunized intramuscularly with 2 mg of whole virus influenza antigen. Three weeks later they were immunized with peptide-loaded IRIVs at intervals of three weeks.

Analyses were carried out at the Swiss Tropical Institute. For ELISA analyses, Polysorp ™ plates (Nunc, Fisher Scientific) were coated overnight at 4°C with 100 μl of a 10μg/ml solution of **13** in PBS (pH 7.2). Wells were then blocked with 5% milk powder in PBS for 30 mins at r.t. followed by three washings with PBS containing 0.05% Tween-20. Plates were then incubated with serial dilutions of anti-**13** mouse sera in PBS containing 0.05% Tween-20 and 0.5% milk powder for 2 h at r.t. After washing, plates were incubated with alkaline phosphatase-conjugated goat anti-mouse γ heavy chain antibodies (Sigma) for 1 h at r.t. After washing again, phosphatase substrate solution was added and the plates were incubated in the dark at r.t. until the colorimetric reaction had progressed sufficiently. The optical density was measured at 405 nm on a Titertek Multiscan MCC/340 reader (Labsystems, Helsinki, Finland).

For IFA, multiwell immunofluorescence microscopy slides were pre-treated with 0.01% poly-L-lysine (Sigma) at r.t. for 30 mins and washed five times with RPMI basal salt medium (Gibco BRL). Erythrocytes from in vitro cultures of *P. falciparum* strain K1 with a parasitemia of 5-10% were washed twice in RPMI, then resuspended in RPMI and two volumes of a solution containing 4% formaldehyde and 0.1% Triton X-100. From this cell suspension, 30 μl were added to each well, incubated at r.t. for 30 mins and washed five times with PBS. Wells were then incubated for 30 mins at r.t. with blocking solution containing 1% fatty acid-free bovine serum albumin (BSA) in PBS. Immunostaining was performed by incubating the wells with 25 μl of an appropriate antibody or serum dilution in blocking solution in a humid chamber for 1 h at r.t. After five washes with blocking solution, 25 μl of 5 μg/ml cyanine dye (Cy3)-conjugated affinity-pure $F(ab')_2$ fragment goat anti-mouse γ heavy chain antibodies (Jackson Immuno Research Laboratories), diluted in blocking solution containing 0.01 mg/ml Hoechst dye no. 33256 (Sigma) were added to the wells and incubated for 1 h at r.t. Finally, wells were washed five times, mounted with mounting solution (90% v/v

glycerol containing 0.1 M Tris-Cl, pH 8.0 and 2 mg/ml o-phenylenediamine), and covered with a coverslip. Antibody binding and DNA staining were assessed by fluorescence microscopy on a Leitz Dialux 20 fluorescence microscope. For analysis of the parasite binding inhibitory activity of mimetic **13**, blood stage parasites were incubated for 30mins with serum diluted 1:1000 in the presence or absence of peptides **42, 43** or **44** at a final concentration of 50 μg/ml.

3.2.15 Synthesis of alanine-scanning library

Sequences:

15: NISQHQCV**A**KQCPQNSGCFRHLDEREECKCLLNYKQEGDKCVENPNPT
16: NISQHQCVK**A**QCPQNSGCFRHLDEREECKCLLNYKQEGDKCVENPNPT
22: NISQHQCVKKQCPQNSGC**A**RHLDEREECKCLLNYKQEGDKCVENPNPT
23: NISQHQCVKKQCPQNSGCF**A**HLDEREECKCLLNYKQEGDKCVENPNPT
24: NISQHQCVKKQCPQNSGCFR**A**LDEREECKCLLNYKQEGDKCVENPNPT
28: NISQHQCVKKQCPQNSGCFRHLDE**A**EECKCLLNYKQEGDKCVENPNPT
31: NISQHQCVKKQCPQNSGCFRHLDEREEC**A**CLLNYKQEGDKCVENPNPT
35: NISQHQCVKKQCPQNSGCFRHLDEREECKCLLN**A**KQEGDKCVENPNPT
36: NISQHQCVKKQCPQNSGCFRHLDEREECKCLLNY**A**QEGDKCVENPNPT
40: NISQHQCVKKQCPQNSGCFRHLDEREECKCLLNYKQEGD**A**CVENPNPT
41: NISQ**A**QCVKKQCPQNSGCFRHLDEREECKCLLNYKQEGDKCVENPNPT

3.2.15.1 Common sequence

Preloading of 2-chlorotrityl chloride resin with Fmoc-Thr(tBu)-OH was carried out on a 10 g scale. Fmoc-Thr(tBu)-OH (1.073 g, 2.7 mmol) was dissolved in DMF (12 ml) with DIEA (1.78 ml, 10.8 mmol). This solution was added to the pre-swelled resin which was agitated for 2 h. The resin was then washed five times with DCM/MeOH/DIEA 17:2:1, three times with DCM and three times with DMF. The level of loading was estimated using the procedure described by Chan and White [190] and found to be 0.25 mmol/g. After drying *in vacuo*, preloaded resin (4 g, 1 mmol) was taken

for the synthesis of the sequence Cys-Val-Glu-Asn-Pro-Asn-Pro-Thr. The synthesis was carried out using standard 1 mmol FastMoc chemistry. 3 mmol Fmoc amino acid, 3 mmol HBTU, 3 mmol HOBt and 6 mmol DIEA were used for each coupling reaction. A standard coupling time of 20 mins was used for each cycle. Ac_2O capping was used to block unreacted sites after each coupling cycle. After completion of the peptide assembly, the resin was split into three portions of **(A)** 25%, **(B)** 37.5% and **(C)** 37.5%. These resin portions were then treated as follows:

3.2.15.2 Synthesis of peptides 15, 16 and 41

For the synthesis of peptides **15**, **16**, and **41**, the sequence Gln-Cys-Pro-Gln-Asn-Ser-Gly-Cys-Phe-Arg-His-Leu-Asp-Glu-Arg-Glu-Glu-Cys-Lys-Cys-Leu-Leu-Asn-Tyr-Lys-Gln-Glu-Gly-Asp-Lys was appended onto the sequence described in **3.2.15.1 (A)** above. The sequence was assembled using standard 0.25 mmol FastMoc chemistry with a single coupling of 20 mins. For certain residues, an extended coupling time of 55 mins was used: His(11), Lys(19), Cys(20), Asn(23), Lys(25), Gln(26), Lys(30). For some other residues, a longer extended coupling time of 85 mins was used: Gln(1), Cys(2), Pro(3), Gln(4), Asn(5), Cys(8), Arg(10), Arg(15), Cys (18). Ac_2O capping was carried out after each coupling cycle to block the unreacted sites. After peptide chain assembly, the resin was split into three equal portions for the preparation of peptides **15**, **16** and **41**.

For peptide **41**, taking 1/3 of the resin from above, the sequence Asn-Ile-Ser-Gln-Ala-Gln-Cys-Val-Lys-Lys was appended using standard 0.1 mmol FastMoc chemistry, which uses 1mmol Fmoc-amino acid, 1 mmol HBTU, 1 mmol HOBt and 2 mmol DIEA per coupling cycle. An extended coupling time of 55 mins was used as standard. For certain residues, a longer extended coupling of 85 mins was used: Asn(1), Gln(4), Ala(5), Gln(6), Cys(7). Ac_2O capping was used after each coupling cycle to block unreacted sites.

For peptide **15**, taking 1/3 of the resin from above, the sequence Asn-Ile-Ser-Gln-His-Gln-Cys-Val-Ala-Lys was appended using standard 0.1 mmol FastMoc chemistry, which uses 1 mmol Fmoc-amino acid, 1 mmol HBTU, 1 mmol HOBt and 2 mmol DIEA per coupling cycle. An extended coupling time of 55 mins was used as standard. For certain residues, a longer extended coupling of 85 mins was used: Asn(1), Gln(4),

His(5), Gln(6), Cys(7). Ac_2O capping was used after each coupling cycle to block unreacted sites.

For peptide **16**, taking 1/3 of the resin from above, the sequence Asn-Ile-Ser-Gln-His-Gln-Cys-Val-Lys-Ala was appended using standard 0.1 mmol FastMoc chemistry, which uses 1 mmol Fmoc-amino acid, 1 mmol HBTU, 1 mmol HOBt and 2 mmol DIEA per coupling cycle. An extended coupling time of 55 mins was used as standard. For certain residues, a longer extended coupling of 85 mins was used: Asn(1), Gln(4), His(5), Gln(6), Cys(7). Ac_2O capping was used after each coupling cycle to block unreacted sites.

3.2.15.3 Synthesis of peptides 22, 23, 24 and 28

For the synthesis of peptides **22, 23, 24** and **28**, the sequence Glu-Glu-Cys-Lys-Cys-Leu-Leu-Asn-Tyr-Lys-Gln-Glu-Gly-Asp-Lys was appended onto the sequence described in **3.2.15.1 (B)** above. The sequence was assembled using standard 0.25 mmol FastMoc chemistry with a single coupling of 20 mins. For certain residues, an extended coupling time of 55 mins was used: Lys(4), Cys(5), Asn(8), Lys(10), Gln(11), Lys(15). A longer extended coupling time of 85 mins was used for Cys (3). Ac_2O capping was carried out after each coupling cycle to block the unreacted sites. After peptide chain assembly, the resin was split into four equal portions for the preparation of peptides **22, 23, 24** and **28**.

For the synthesis of peptide **28**, on ¼ of the resin from above, the sequence Asn-Ile-Ser-Gln-His-Gln-Cys-Val-Lys-Lys-Gln-Cys-Pro-Gln-Asn-Ser-Gly-Cys-Phe-Arg-His-Leu-Asp-Glu-Ala was appended. The sequence was assembled using standard 0.1 mmol FastMoc chemistry with a standard single coupling of 20 mins. For certain residues, an extended coupling of 55 mins was used: Ile(2), Ser(3), Val(8), Lys(9), Lys(10), His(21). A longer extended coupling of 85 mins was used for : Asn(1), Gln(4), His(5), Gln(6), Cys(7), Gln(11), Cys(12), Pro(13), Gln(14), Asn(15), Cys(18), Arg(20), Ala(25).

For the synthesis of peptide **24**, on ¼ of the resin from above, the sequence Asn-Ile-Ser-Gln-His-Gln-Cys-Val-Lys-Lys-Gln-Cys-Pro-Gln-Asn-Ser-Gly-Cys-Phe-Arg-Ala-Leu-Asp-Glu-Arg was appended. The sequence was assembled using standard 0.1 mmol FastMoc chemistry with a standard single coupling of 20 mins. For certain residues, an extended coupling of 55 mins was used: Ile(2), Ser(3), Val(8), Lys(9), Lys(10), Ala(21).

A longer extended coupling of 85 mins was used for : Asn(1), Gln(4), His(5), Gln(6), Cys(7), Gln(11), Cys(12), Pro(13), Gln(14), Asn(15), Cys(18), Arg(20), Arg(25).

For the synthesis of peptide **23**, on ¼ of the resin from above, the sequence Asn-Ile-Ser-Gln-His-Gln-Cys-Val-Lys-Lys-Gln-Cys-Pro-Gln-Asn-Ser-Gly-Cys-Phe-Ala-His-Leu-Asp-Glu-Arg was appended. The sequence was assembled using standard 0.1 mmol FastMoc chemistry with a standard single coupling of 20 mins. For certain residues, an extended coupling of 55 mins was used: Ile(2), Ser(3), Val(8), Lys(9), Lys(10), His(21). A longer extended coupling of 85 mins was used for : Asn(1), Gln(4), His(5), Gln(6), Cys(7), Gln(11), Cys(12), Pro(13), Gln(14), Asn(15), Cys(18), Ala(20), Arg(25).

For the synthesis of peptide **22**, on ¼ of the resin from above, the sequence Asn-Ile-Ser-Gln-His-Gln-Cys-Val-Lys-Lys-Gln-Cys-Pro-Gln-Asn-Ser-Gly-Cys-Ala-Arg-His-Leu-Asp-Glu-Arg was appended. The sequence was assembled using standard 0.1 mmol FastMoc chemistry with a standard single coupling of 20 mins. For certain residues, an extended coupling of 55 mins was used: Ile(2), Ser(3), Val(8), Lys(9), Lys(10), His(21). A longer extended coupling of 85 mins was used for : Asn(1), Gln(4), His(5), Gln(6), Cys(7), Gln(11), Cys(12), Pro(13), Gln(14), Asn(15), Cys(18), Arg(20), Arg(25).

3.2.15.4 Synthesis of peptides 31, 35, 36 and 40

For the synthesis of peptide **40**, on ¼ of the resin from **3.2.15.1 (C)** above, the sequence Asn-Ile-Ser-Gln-His-Gln-Cys-Val-Lys-Lys-Gln-Cys-Pro-Gln-Asn-Ser-Gly-Cys-Ala-Arg-His-Leu-Asp-Glu-Arg-Glu-Glu-Cys-Lys-Cys-Leu-Leu-Asn-Tyr-Lys-Gln-Glu-Gly-Asp-Ala was appended. The sequence was assembled using standard 0.1 mmol FastMoc chemistry with a standard single coupling of 20 mins. For certain residues, an extended coupling of 55 mins was used: Ile(2), Ser(3), Val(8), Lys(9), Lys(10), His(21), Lys(29), Cys(30), Asn(33), Lys(35), Gln(36), Ala(40). A longer extended coupling of 85 mins was used for : Asn(1), Gln(4), His(5), Gln(6), Cys(7), Gln(11), Cys(12), Pro(13), Gln(14), Asn(15), Cys(18), Arg(20), Arg(25), Cys (28).

For the synthesis of peptide **36,** on ¼ of the resin from above, the sequence Asn-Ile-Ser-Gln-His-Gln-Cys-Val-Lys-Lys-Gln-Cys-Pro-Gln-Asn-Ser-Gly-Cys-Ala-Arg-His-Leu-Asp-Glu-Arg-Glu-Glu-Cys-Lys-Cys-Leu-Leu-Asn-Tyr-Ala-Gln-Glu-Gly-Asp-Lys was appended. The sequence was assembled using standard 0.1 mmol FastMoc chemistry with a standard single coupling of 20 mins. For certain residues, an extended

coupling of 55 mins was used: Ile(2), Ser(3), Val(8), Lys(9), Lys(10), His(21), Lys(29), Cys(30), Asn(33), Ala(35), Gln(36), Lys(40). A longer extended coupling of 85 mins was used for : Asn(1), Gln(4), His(5), Gln(6), Cys(7), Gln(11), Cys(12), Pro(13), Gln(14), Asn(15), Cys(18), Arg(20), Arg(25), Cys (28).

For the synthesis of peptide **35,** on ¼ of the resin from above, the sequence Asn-Ile-Ser-Gln-His-Gln-Cys-Val-Lys-Lys-Gln-Cys-Pro-Gln-Asn-Ser-Gly-Cys-Phe-Arg-His-Leu-Asp-Glu-Arg-Glu-Glu-Cys-Lys-Cys-Leu-Leu-Asn-Ala-Lys-Gln-Glu-Gly-Asp-Lys was appended. The sequence was assembled using standard 0.1 mmol FastMoc chemistry with a standard single coupling of 20 mins. For certain residues, an extended coupling of 55 mins was used: Ile(2), Ser(3), Val(8), Lys(9), Lys(10), His(21), Lys(29), Cys(30), Asn(33), Lys(35), Gln(36), Lys(40). A longer extended coupling of 85 mins was used for : Asn(1), Gln(4), His(5), Gln(6), Cys(7), Gln(11), Cys(12), Pro(13), Gln(14), Asn(15), Cys(18), Arg(20), Arg(25), Cys (28).

For the synthesis of peptide **31**, on ¼ of the resin from above, the sequence Asn-Ile-Ser-Gln-His-Gln-Cys-Val-Lys-Lys-Gln-Cys-Pro-Gln-Asn-Ser-Gly-Cys-Phe-Arg-His-Leu-Asp-Glu-Arg-Glu-Glu-Cys-Ala-Cys-Leu-Leu-Asn-Tyr-Lys-Gln-Glu-Gly-Asp-Lys was appended. The sequence was assembled using standard 0.1 mmol FastMoc chemistry with a standard single coupling of 20 mins. For certain residues, an extended coupling of 55 mins was used: Ile(2), Ser(3), Val(8), Lys(9), Lys(10), His(21), Ala(29), Cys(30), Asn(33), Lys(35), Gln(36), Lys(40). A longer extended coupling of 85 mins was used for : Asn(1), Gln(4), His(5), Gln(6), Cys(7), Gln(11), Cys(12), Pro(13), Gln(14), Asn(15), Cys(18), Arg(20), Arg(25), Cys (28).

3.2.15.5 Synthesis of oxidized mimetics 45-55

These peptides are the oxidized forms of the peptides described above.

Linear peptide 15 – oxidized peptide 45

Linear peptide 16 – oxidized peptide 46

Linear peptide 22 – oxidized peptide 47

Linear peptide 23 – oxidized peptide 48

Linear peptide 24 – oxidized peptide 49

Linear peptide 28 – oxidized peptide 50

Linear peptide 31 – oxidized peptide 51

Linear peptide 35 – oxidized peptide 52

Linear peptide 36 – oxidized peptide 53

Linear peptide 40 – oxidized peptide 54

Linear peptide 41 – oxidized peptide 55

All of the mimetics were oxidized by dissolving at a concentration of 5 mg/ml in 0.1 M Tris buffer (pH 8.4) containing cysteine (3 mM), cystine (0.3 mM) and EDTA (5 mM) and stirring for 24 h. Oxidative folding was monitored by RP-HPLC using a Vydac C18 218TP54 column with a gradient of 5 to 50% acetonitrile over 30 mins. Purification was carried out by preparative RP-HPLC using a Zorbax eclipse XDB-C18 (7 μm, 21.2 x 250 mm) column (flow rate 15 ml/min, gradient 5 to 27.5% acetonitrile over 18 minutes). All of the purified oxidatively folded peptides, along with the oxidatively folded native sequence, the unfolded native sequence, and the unfolded native sequence with alkylated thiol groups, were analysed by RP-HPLC (Vydac C18 218TP54 column with a gradient of 5 to 50% acetonitrile over 30 mins), ESI-MS, NMR (^{1}H, TOCSY (80ms) and NOESY (60ms)) and by circular dichroism. Retention times, extinction coefficients and measured and calculated masses of the mimetics are summarized in **Table 16**. NMR spectra are presented in Appendix 2, CD spectra are presented in chapter 1.2.

3.2.15.6 CD measurements

Amino acid analysis of each mimetic was carried out. From these, the extinction coefficients given in **Table 16** could be calculated. This allowed an accurate calculation of peptide concentrations in stock solutions. Subsequently, samples of peptide (approximately 0.3 mg/ml, 0.05 mM) in phosphate buffer (25 mM pH 6.2), were prepared. These samples were used for CD measurements in a 0.1 mm quartz

thermostatable cuvette at 25°C, using a JASCO J-715 spectropolarimeter. A scan speed of 50 nm/min, a 1 second response time and a 1 nm spectral bandwidth were used. CD spectra are presented after subtraction of a blank containing only buffer and the optical activity is reported in units of mean residue ellipticity (deg cm^2 $dmol^{-1}$). Spectra are presented as an average of four scans and results are given for the range 185-260 nm.

peptide	Calculated mass (g/mol)	Measured m/z (MALDI-MS)	Retention time*	Extinction coefficient
43	5587.3	5585.9	14.5	2056
44	5935.7	5935.425	13.9	2338
45	5530.2	5529.838	13.8	1969
46	5530.2	5531.001	14.0	3340
47	5511.2	n.d.	n.d.	n.d.
48	5502.2	5502.351	13.3	2617
49	5521.2	5520.637	13.3	2443
50	5502.2	5502.052	13.9	2184
51	5530.2	5530.885	14.1	2605
52	5495.2	5496.490	13.6	390
53	5530.2	5530.525	15.4	2162
54	5530.2	5530.607	15.0	2157
55	5521.2	5520.631	13.9	2606

*****For HPLC conditions, see 3.2.15.5.

Table 16: Analytical data for alanine scanning mimetics

3.2.16 Synthesis of linear mimetic 42

Mimetic 42:

NlSQHQCVKKQCPQNSGCFRHLDEREECKCLLNYKQEGDKCVENPNPT

The peptide was assembled as described for peptide **1** above, but on the threonine-preloaded chlorotrityl chloride resin described in 3.2.15.1 above. One half of the cleaved crude linear product was taken for oxidation to produce mimetic **43**. The remainder was purified by semi-preparative RP-HPLC using a Zorbax eclipse XDB-C18 column (9.4 x 250 mm, 5 μm), 4 ml/min flow rate and a gradient of 5 to 33% acetonitrile over 15 minutes. 78 mg of purified peptide were obtained (yield 11%). Calculated MW: 5593.3 g/mol. Measured m/z (MALDI-Tof-MS) 5593.31 (±0.1%).

3.2.17 Synthesis of oxidised mimetic 43

Mimetic 43:

The peptide was prepared from crude peptide **42**, as described for peptide **2,** by oxidation at a concentration of 5 mg/ml in 0.1M Tris buffer (pH 8.4) containing 3mmol cysteine, 0.3 mmol cystine and 10 mmol EDTA. The oxidised peptide was purified by semi-preparative RP-HPLC using a Zorbax eclipse XDB-C18 column (9.4 x 250 mm, 5 μm), 4 ml/min flow rate and a gradient of 5 to 33% acetonitrile over 15 minutes. The mass spectrometry results and HPLC retention time are given in **Table 16**. 45 mg of purified oxidized peptide were obtained (yield 6%).

3.2.18 Synthesis of alkylated mimetic 44

Mimetic 44:

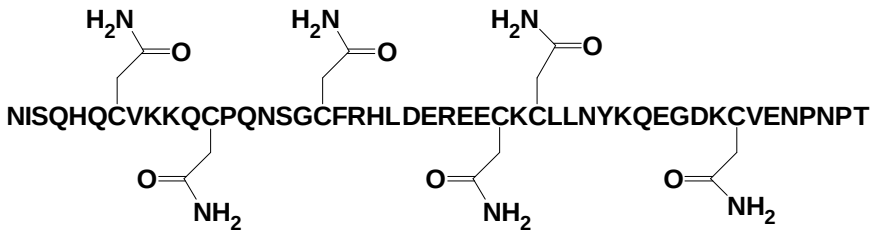

The mimetic was prepared from purified mimetic **42** (30 mg), which was dissolved in phosphate buffer (10 ml, 0.1 M, pH 7.5), with iodoacetamide (119 mg, 644 μmol, 20 eq. per thiol group). After 30 mins stirring at room temperature, only masses corresponding to the desired product could be seen in LC-MS (989.1 (M+6H)/6, 1187.0 (M+5H)/5, 1483.75 (M+4H)/4). The reaction mixture was then immediately purified by semi-preparative RP-HPLC using a Zorbax eclipse XDB-C18 column (9.4 x 250 mm, 5 μm), 4 ml/min flow rate and a gradient of 5 to 37% acetonitrile over 15 minutes. Mass spectrometry results and HPLC retention time are given in **Table 16**. 18 mg of purified product were obtained (yield 56 %).

3.3 MSP-4 peptides

3.3.1 Synthesis of peptide 56

Peptide 56:

LEDEDLCKHNNGDCGDDKLCEYVGNRRVKCKCKEGYKLEGIECVELLSLAS-NH_2

The linear peptide was assembled on Rink Amide resin (390 mg, loading 0.64 mmol/g) on a 0.25 mmol scale. For the first coupling reaction, Fmoc-Ser(tBu)-OH (0.27 mmol, 103.5 mg) were used. The standard coupling time for amino acids was 55 mins. For the following amino acids, a coupling time of 20 mins was used: Leu(49) Ala(50). For some amino acids, a long extended coupling was used: Leu(1), Glu(2), Ser(51). Double couplings were used where needed: Leu(6), Lys(8), His(9), Asn(11), Asp(13), Cys(13), Leu(19)-Val(23), Arg(26), Arg(27), Lys(29)-Glu(34), Tyr(36)-Glu(39), Cys(43)-Glu(45). Fmoc-Leu-Ser($\Psi^{Me,Me}$pro)-OH was used for Leu(47) and Ser(48). Each coupling cycle was followed by Ac_2O capping to block unreacted sites. Following completion of peptide chain assembly, the resin was dried under vacuum over KOH for 5 h. The peptide was cleaved from the resin and side-chain deprotected by treatment with a mixture of TFA/TIS/H_2O/EDT 94:1:2.5:2.5 (30 ml) for 3 h. The resin was then filtered

off and washed twice with TFA (1 ml). The solution was concentrated under reduced pressure until a precipitate began to form. The suspension was then transferred into 2 centrifuge tubes and the product was fully precipitated by the addition of cold diethyl ether. The tubes were centrifuged at 2500 rpm for 7 mins, then the liquid was decanted off. The peptide was washed twice with diethyl ether and centrifuged in the same way, then allowed to air-dry for 1 h, to give approx. 600 mg of crude product. Purification was carried out by semi-preparative RP-HPLC using a Vydac C18 218TP1010 column (10 μm, 125 A, 10 x 100 mm, flow rate 5 ml/min), and a gradient of 10 to 50% acetonitrile over 20 mins. Purification yielded 30-40 mg of linear peptide. (6% yield). Analytical HPLC: Vydac C18 218TP54, flow rate 1 ml/min, 5 to 50% acetonitrile over 29 mins, retention time 20.9 mins. Calculated MW: 5735.42 g/mol, measured ESI-Tof-MS: 5735.1±0.01% (m/z)

3.3.2 Synthesis of oxidised peptide 58

Peptide 58:

Peptide **56** was dissolved at a concentration of 5 mg/ml in an oxidation buffer made up of Tris buffer (0.1 M, pH 8.4) containing EDTA (10 mM), cysteine (3 mM) and cystine (0.3 mM). The mixture was stirred for 48 hours and then the product was purified by semi-preparative RP-HPLC using a Vydac C18 218TP1010 column and a gradient of 5 to 50% acetonitrile over 25 mins. Analytical HPLC: Vydac C18 218TP54, flow rate 1 ml/min, gradient 5 to 50% acetonitrile over 29 mins, retention time: 18.4 mins. Calculated MW: 5729.53g/mol, measured m/z (ESI-Tof MS): 5729.2 (±0.01%).

3.3.3 Synthesis of mimetic 60

Mimetic 60:

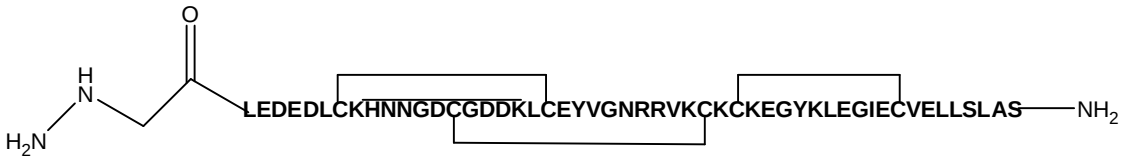

The peptide sequence was assembled as described above. Hydrazinoglycine (**7**) was coupled to the peptidyl resin as described for peptide **8**. Peptide was cleaved from the solid support and side-chain deprotected using TFA containing 1% TIS, 2.5% EDT and 2.5% water for 3 h. After this time, the solution was concentrated in vacuo until a precipitate began to form. The solution was then transferred into two centrifuge tubes and the peptide product was fully precipitated by the addition of cold diethyl ether. The tubes were centrifuged at 2500 rpm for 7 mins, then the liquid was decanted off. The peptide was washed twice with diethyl ether and centrifuged in the same way, then allowed to air-dry for 1 h, to give approx. 600 mg of crude product. This crude product was oxidised directly at a concentration of 5 mg/ml in an oxidation buffer made up of Tris buffer (0.1 M, pH 8.4) containing EDTA (10 mM), cysteine (3 mM) and cystine (0.3 mM). The mixture was stirred for 48 h and then the product was purified by semi-preparative RP-HPLC using a Vydac C18 218TP1010 column and a gradient of 5 to 50% acetonitrile over 25 mins. Typical yields of oxidised product were around 40 mg (7 % yield). Analytical HPLC: Vydac C18 218TP54, flow rate 1 ml/min, gradient 5 to 50% acetonitrile over 29 mins, retention time: 18.9 mins.Calculated MW 5801.60 g/mol, measured ESI-Tof-MS (m/z): 5801.4±0.01%.

3.3.4 Synthesis of lipopeptide 61

Lipopeptide 61:

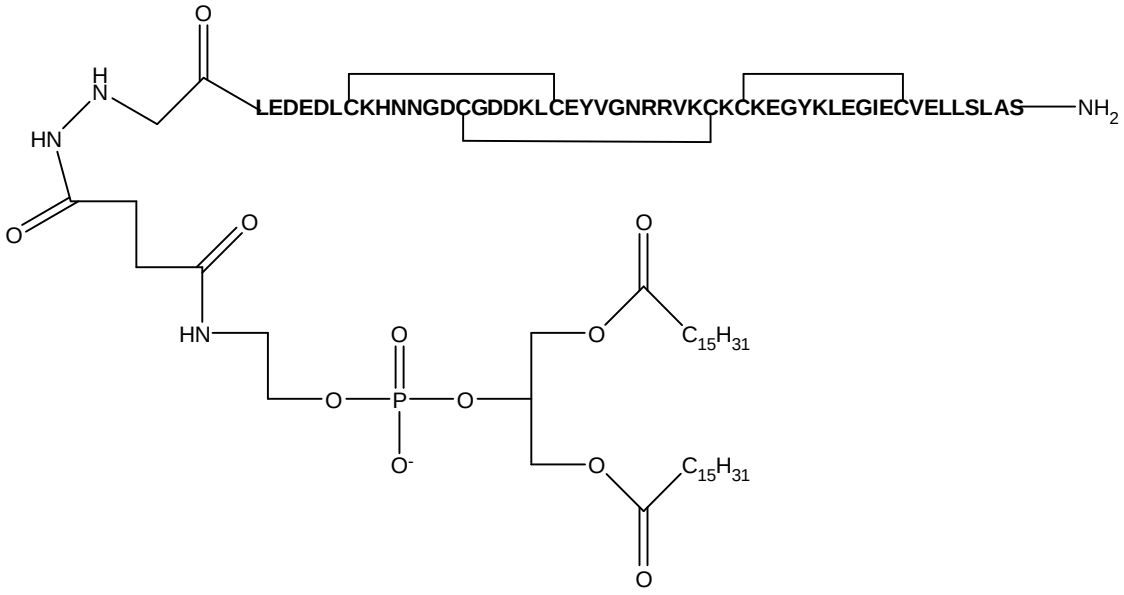

Peptide **60** (3 mg) was dissolved in water (500 μl) and the pH adjusted to 5.0-5.4 using NaOH (0.1 M). A solution of **60** (1.5 eq) in *tert*-butanol (500 μl) was added to this solution. The mixture was stirred at room temperature and samples were removed at frequent intervals for LC-MS analysis. Several peaks appeared in the chromatogram and that at highest retention time showed the expected mass of the desired product. Measured m/z: 1316 (M+5H)/5, 1097 (M+6H)/6. After 1-4 h, the peak of desired mass no longer increased in size and the solution was purified by RP-HPLC using an analytical Vydac C4 214TP104 column and a gradient of 10 to 100% acetonitrile over 45 mins. The fractions containing the product peak were collected, frozen and lyophilised. Calculated MW: 6574.45 g/mol, Measured m/z (ESI-Tof-MS): 6575.1 (± 0.01%).

3.3.5 Synthesis of oxidised peptide 63

Peptide 63:

The peptide sequence was assembled as described for peptide **56** above. The additional lysine residues were coupled using a 55 min extended single coupling cycle. Peptide was cleaved from the resin and side-chain deprotected as described above. The crude linear peptide was oxidised directly as described above. After 48 h of oxidation, the product was purified directly by semi-preparative RP-HPLC using a Vydac C18 218TP1010 column and a gradient of 5 to 50% acetonitrile over 25 mins. Around 25 mg of purified peptide were obtained (yield 1.6%). Calculated MW: 6314.30 g/mol, Measured m/z (MALDI-Tof-MS): 6314.021.

3.3.6 Synthesis of lipopeptide 64

Lipopeptide 64:

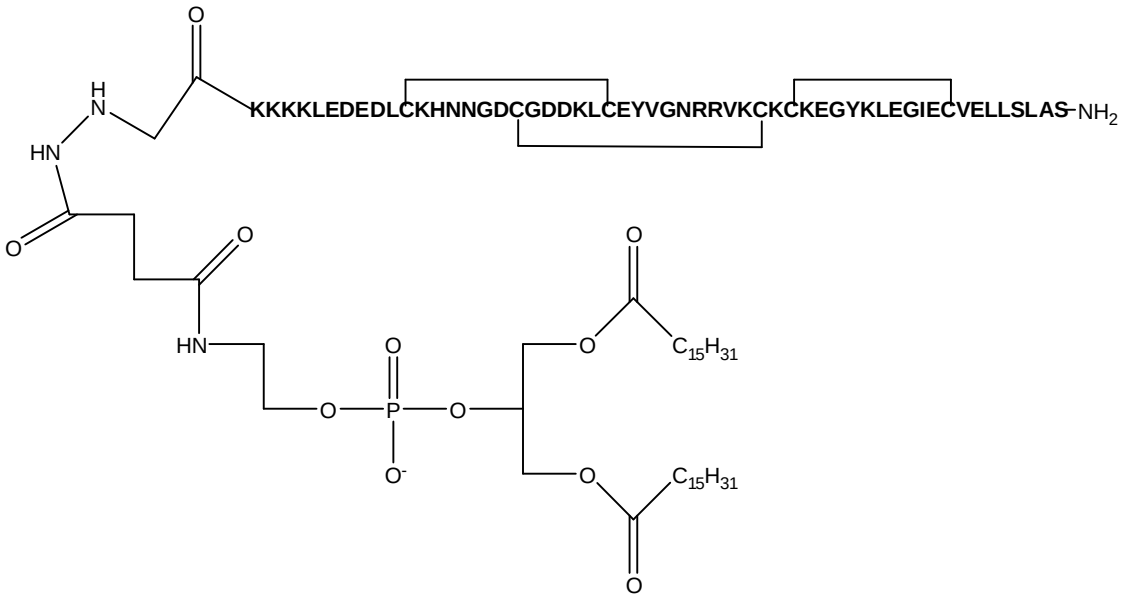

Peptide **63** (3 mg) was dissolved in water (500 μl) and the pH adjusted to 5.0-5.4 using NaOH (0.1 M). A solution of **60** (1.5 eq) in *tert*-butanol (500 μl) were added to this solution. The mixture was stirred at room temperature and samples were removed at frequent intervals for LC-MS analysis. Several peaks appeared in the chromatogram and the largest showed the expected mass of the desired product: Calculated MW: 7087.33 g/mol, Measured m/z (ESI-MS): 1418.2 (M+5H/5), 1182.0 (M+6H/6), 1012.5 (M+7H)/7). This product could be purified by RP-HPLC using an analytical Vydac C4 214TP104 column and a gradient of 10 to 100% acetonitrile over 45 mins. Measured m/z (MALDI-Tof-MS): 7088.022.

3.4 GLURP peptides

Structures of GLURP mimetics:

Peptides 65, 73

Peptides 66, 74

Peptides 67, 75

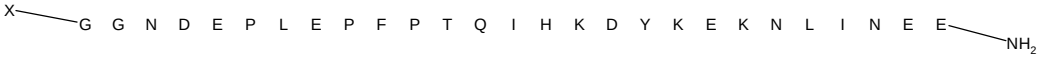

Peptides 68, 76

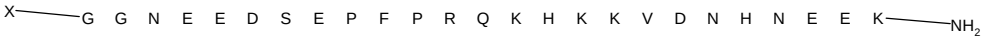

Peptides 69, 77

Peptides 70, 78

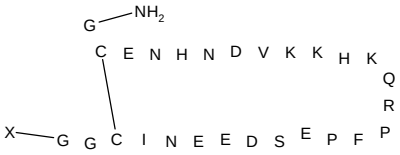

Peptide 71

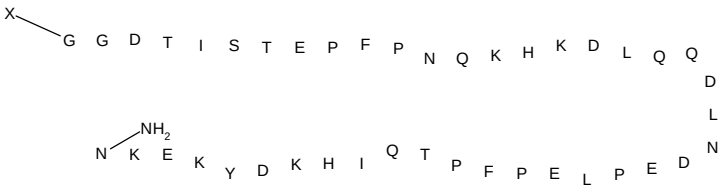

Peptide 72

For peptides 73-78, **X**= -$COCH_3$, For peptides 65-72, **X**=

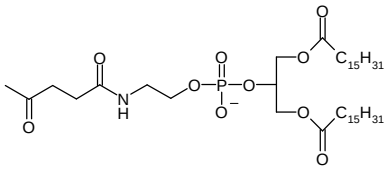

3.4.1 Synthesis of 65, 66, 67, 68, 71 and 72

Each of the six GLURP lipopeptide mimetics for immunization studies was prepared in the same way, using Rink Amide resin on the ABI 433A on a 0.25 mmol scale and a standard single coupling of 20 minutes, with Ac_2O capping after each cycle. After automated peptide synthesis, the half of the resin for PE-Succ coupling was treated with a solution of PE-Succ **(11**) as follows: **11 (**592 mg , 0.75 mmol) was dissolved in a minimal amount of DMF with HATU (286 mg, 0.75 mmol) and HOAt (116 mg, 0.75 mmol). DIEA (352 µl) was added and this solution was then added to the peptidyl-resin. The resin suspension was agitated overnight, then filtered and washed five times with DMF and five times with DCM. The resin now gave a negative result in the Kaiser test, suggesting that the PE had been fully coupled. The resin was washed five times with DMF then five times with DCM and then treated for 3 h with TFA containing 2.5% TIS and 2.5% water, and precipitated using cold diethyl ether as described previously. The peptides were then purified by preparative RP-HPLC using an Interchrom UP10WC4/25M column and a gradient of 40 to 100% acetonitrile over 35 mins.

Analytical data:

(**65)** ESI-MS (m/z): 1742.5 (M+2H)/2, 1162.3 (M+3H)/3, 871.8 (M+4H)/4. RP-HPLC. Vydac C4 214TP104 column, gradient 30 to 100% acetonitrile over 33 mins. Retention time: 21.4 mins.

(66) ESI-MS (m/z): 1762.0 (M+2H)/2, 1174.6 (M+3H)/3, 881.3 (M+4H)/4. RP-HPLC. Vydac C4 214TP104 column, gradient 30 to 100% acetonitrile over 33 mins. Retention time: 21.9 mins.

(67) ESI-MS (m/z): 1964.9 (M+2H)/2, 1310.5 (M+3H)/3, 982.8 (M+4H)/4, 786.5 (M+5H)/5. RP-HPLC. Vydac C4 214TP104 column, gradient 30 to 100% acetonitrile over 30 mins. Retention time: 22.1 mins.

(68) ESI-MS (m/z): 1241.7 (M+3H)/3, 931.4 (M+4H)/4, 745.2 (M+5H)/5, 621.2 (M+6H)/6 . RP-HPLC. Vydac C4 214TP104 column, gradient 30 to 100% acetonitrile over 33 mins. Retention time: 19.8 mins.

(71) ESI-MS (m/z): 1417.8 (M+4H)/4, 1134.1 (M+5H)/5, 945.3 (M+6H)/6, 810.6 (M+7H)/7. RP-HPLC. Vydac C4 214TP104 column, gradient 30 to 100% acetonitrile over 33 mins. Retention time: 20.34 mins.

(72) ESI-MS (m/z): 1434.6 (M+4H)/4, 1147.8 (M+5H)/5, 956.9 (M+6H)/6, 820.4 (M+7H)/7. RP-HPLC. Vydac C4 214TP104 column, gradient 30 to 100% acetonitrile over 30 mins. Retention time: 20.0 mins.

3.4.2 Synthesis of 73-76

The resin prepared as described in section 3.4.1 was treated, in each case, twice with a solution of Ac_2O/DIEA/HOBt/NMP (475 µl/225 µl/20 mg/9.3 ml), each time for 10 mins. The reaction was monitored using the Kaiser test. The resin was washed five times with NMP and five times with DCM and then cleaved and side-chain deprotected as described previously. The peptides were then purified by preparative RP-HPLC using a Vydac C18 218TP1022 column and a gradient of 5 to 45% acetonitrile over 30mins.

Analytical data:

(73**)** ESI-MS (m/z): 1376.8 (M+2H)/2, 918.0 (M+3H)/3, 688.7 (M+4H)/4, 551.3 (M+5H)/5. RP-HPLC. Vydac C18 218TP104 column, gradient 5 to 55% acetonitrile over 29 mins. Retention time: 13.4 mins.

(74) ESI-MS (m/z): 1395.8 (M+2H)/2, 930.8 (M+3H)/3, 698.6 (M+4H)/4. RP-HPLC. Vydac C18 218TP104 column, gradient 5 to 55% acetonitrile over 29 mins. Retention time: 15.1 mins.

(75) ESI-MS (m/z): 1066.2 (M+3H)/3, 800.0 (M+4H)/4. RP-HPLC. Vydac C18 218TP104 column, gradient 5 to 55% acetonitrile over 29 mins. Retention time 15.3 mins.

(76) ESI-MS (m/z): 997.6 (M+3H)/3, 748.5 (M+4H)/4, 599.0 (M+5H)/5. RP-HPLC. Vydac C18 218TP104 column, gradient 5 to 55% acetonitrile over 29 mins. Retention time: 9.4 mins.

3.4.3 Synthesis of peptides 69 and 77

The linear peptide was prepared on Rink amide resin (379 mg, loading 0.66 mmol/g) and synthesised on a 0.25 mmol scale on an ABI 433A using single coupling of 20 mins with capping for each cycle. After completion of the peptide chain assembly, with final Fmoc deprotection, a small portion of the resin was removed and found to give a positive result in the Kaiser test.

69: PE-Succ (**11**) was prepared as described above and coupled to the N-terminus of the resin-bound peptide as follows: **11** (592 mg, 0.75 mmol) was dissolved in a minimal amount of DMF with HATU (286 mg, 0.75 mmol) and HOAt (116 mg, 0.75 mmol). DIEA (352 µl) was added and this solution was then added to the peptidyl-resin. The resin suspension was agitated for 16 h, then filtered and washed five times with DMF and five times with DCM. The resin now gave a negative result in the Kaiser test, suggesting that the PE had been fully coupled.

The peptide was cleaved from the resin and deprotected using TFA containing 1% TIS, 2.5% EDT and 2.5% water, and precipitated with cold diethyl ether as described previously. The product showed two peaks in LC-MS and RP-HPLC, the second peak had the expected mass of the desired product: (m/z) 1281.7 (M+3H)/3, 961.4 (M+4H)/4, 769.7 (M+5H)/5 and was purified by preparative RP-HPLC using an Interchrom UP10WC4/25M column.

For the capping of the thiol groups, in a typical reaction, peptide **79** (6.8 mg) was dissolved in phosphate buffer (12 ml, 0.1 M, pH 7.5), along with iodoacetamide (7 mg, 20 eq.). The solution was stirred and the reaction monitored by LC-MS. After 1 h a single peak was seen in the chromatogram with the expected mass of the desired product (m/z): 1319 (M+3H)/3. The product was immediately purified by semi-preparative RP-HPLC using a Vydac C4 214TP1010 column and a gradient of 40 to 100% acetonitrile over 30mins. After purification 4.7 mg of product **69** were obtained (yield 69%).

ESI-MS (m/z): 1978.2 (M+2H)/2, 1319.5 (M+3H)/3.

77: The peptide sequence was assembled as described for peptide **69**. The N-terminal acetylation was carried out manually by treating twice with a solution of Ac_2O/DIEA/HOBt/NMP (475 µl/225 µl/20 mg/9.3 ml), each time for 10 mins.

Alkylation of the thiol groups was achieved by the same method as described for **69** above. Calculated MW: 3221.44 g/mol, Measured m/z (ESI-MS) (± 0.01%) 1612.2 (M+2H)/2, 1075.1 (M+3H)/3, 806.7 (M+4H)/4, 645.6 (M+5H)/5.

3.4.4 Synthesis of 70

The synthesis of the linear peptide was carried out in the same way as described for **69**. The formation of the disulfide bond was performed as follows: Peptide **79** (18 mg) was dissolved in ammonium acetate buffer (150 ml, 50 mM, pH 8). TFE (150 ml) was added and the mixture was stirred in an open atmosphere overnight. The reaction was monitored by analytical RP-HPLC and after 24 h the starting material had been completely converted into a product. The product was purified by semi-preparative RP-HPLC using a Vydac C4 214TP1010 column and a gradient of 40 to 100% acetonitrile over 30 mins. 4.5 mg of purified product were obtained in total. Analytical HPLC: Vydac C4 214TP104, flow rate 1 ml/min, gradient 30 to 100% acetonitrile over 29 mins, retention time 22.6 mins. Calculated MW: 3838.29 g/mol. Measured m/z: (ESI-MS): 1920.2 (M+2H)/2, 1280.4 (M+3H)/3, 960.6 (M+4H)/4.

3.4.5 Immunization studies

The immunogenicity of the lipopeptide mimetics presented on IRIVs was assayed in mice. Virosomes were prepared and immunizations carried out by Dr Rinaldo Zurbriggen and co-workers at Pevion Biotech. Analysis of the immunized mouse sera was performed by Prof. Gerd Pluschke and co-workers at the Swiss Tropical Institute.

BALB/c mice were pre-immunized intramuscularly with the commercial whole-virus influenza vaccine *Inflexal Berna* (Berna Biotech). At least three weeks later, they were immunized with mimetic-loaded IRIVs at intervals of at least two weeks, four times. Blood was collected before each immunization and after the final injection. Sera obtained from the immunizations were tested for reactivity with the mimetics by enzyme-linked immunosorbent assay (ELISA). Sera were also tested for reactivity with blood-stage parasites in immunofluorescence assays (IFA). Responses in IFA were weak, the strongest response being from the immunization with **66** and **67.**

3.5 Peptoid-peptide hybrids

3.5.1 Syntheis of bromoacetic acid allyl ester (90)

Bromoacetic acid (18.1 g, 0.13 mol) was dissolved in benzene (60 ml) containing conc. H_2SO_4. (0.12 ml). Allyl alcohol (20 ml, 0.15 mol) was added and the mixture was heated to reflux and refluxed for 6 h. A Dean-Stark trap was used to collect the water formed. The organic phase was washed three times with $NaHCO_3$ (20 ml, 1 M), then the aqueous phase was extracted three times with benzene. The organic phases were collected, dried over $MgSO_4$ and concentrated *in vacuo*. The product was purified by distillation under reduced pressure (31 mbar, 85-87^oC). Yield 16.1 g (69.3%). ^1H NMR: 4.00 ppm (s), 2H (Br**C**$\mathbf{H_2}$), 4.80 ppm (d), 2H (**C**$\mathbf{H_2}$CH=CH_2), 5.45 ppm (m), 2H (CH_2CH=**C**$\mathbf{H_2}$), 6.05 ppm (m), 1H (CH_2**C**$\mathbf{H}$=CH_2).

3.5.2 Synthesis of (4-amino-butyl)-carbamic acid *tert*-butyl ester (93)

To 1,4-diaminobutane (100 mmol, 8.8 g) in DCM (500 ml), was added $(Boc)_2O$ (20 mmol, 4.36 g) in DCM (250 ml) dropwise at 0^oC over 3-4 h. The reaction mixture was stirred at room temperature overnight. The solution was filtered and the solvent was removed by rotary evaporation. The oily residue was diluted with AcOEt (150 ml) and washed twice with 150 ml brine. The aqueous layer was then extracted three times with AcOEt (180 ml). The organic layers were dried over Na_2SO_4 and the solvent evaporated to leave a waxy white solid product in 70-80% yield. ^1H NMR: 1.45 ppm (s), 9H(-$C(CH_3)_3$), 1.55-1.7 ppm (m), 4H(-CH_2**C**$\mathbf{H_2}$**C**$\mathbf{H_2}$$CH_2$-), 2.65 ppm (t) 2H(-**C**$\mathbf{H_2}$$NH_2$), 3.15 ppm (m) 2H(-CONH**C**$\mathbf{H_2}$). Calculated MW: 188.27 g/mol. Measured m/z (ESI-MS): 189.1 (M+H).

3.5.3 Synthesis of (4-*tert*-butoxycarbonylamino-butylamino)-acetic acid allyl ester (94)

To **93** (5 g, 26.6 mmol) was dissolved in dry THF (30 ml), triethylamine (7.4 ml, 53 mmol) was added. A solution of of **90 (**4.76 g, 26.6 mmol) in dry THF (30 ml) was added dropwise over 4 h. The solution was then stirred at room temperature for 16 h.

Solvent was removed *in vacuo* and the product suspended in diethyl ether. The Et_3NHBr that precipitated was removed by filtration. The product was purified by flash chromatography (eluant: ethyl acetate). TLC: R*f* value (eluant: ethyl acetate) 0.29 (revealed using ninhydrin). Yield: 25%. ^{1}H NMR: 1.65 ppm (s), 9H (Boc), 1.75-1.95 ppm (m), 4H ($NHCH_2\mathbf{CH_2CH_2}CH_2NH$), 2.85 ppm (q), 2H ($NHCH_2CH_2CH_2\mathbf{CH_2}NH$), 3.35 ppm (q), 2H ($NH\mathbf{CH_2}CH_2CH_2CH_2NH$), 3.70 ppm (s), 2H ($NH\mathbf{CH_2}CO$), 4.85 ppm (d), 2H ($O\mathbf{CH_2}CH=CH_2$), 5.4-5.6 ppm (m), 2H ($OCH_2CH=\mathbf{CH_2}$), 6.1-6.2 ppm (m), 1H ($OCH_2\mathbf{CH}=CH_2$). Calculated MW: 286.37 g/mol. Measured m/z (ESI-MS): 287.2 (M+H).

3.5.4 Synthesis of [(4-tert-butoxycarbonylamino-butyl)-(9H-fluoren-9-ylmethoxycarbonyl)-amino]-acetic acid allyl ester (95)

To a solution of **94** (1.5 g, 5.24 mmol) in dry DCM (50 ml) at 0^{o}C was added DIEA (1.8 ml, 10.5 mmol), followed by Fmoc-Cl (1.56 g, 6 mmol). The reaction was monitored by TLC (eluant: ethyl acetate). After 2 h the solvent was removed *in vacuo*. The product was used for the next step without further purification.

3.5.5 Synthesis of [(4-amino-butyl)-(9H-fluoren-9-ylmethoxycarbonyl)-amino]-acetic acid allyl ester (96)

Crude product **95** (11 g) was dissolved in TFA/DCM 3/7 (40ml) at 0^{o}C and stirred for 20 minutes. The solution was concentrated *in vacuo*, then dissolved in cold diethyl ether. The organic phase was extracted five times with HCl (50 ml, 1M). The aqueous phases were collected and lyophilised and found to contain a small amount of the desired product. LC-MS revealed that much of the desired product was present in the organic phase which was therefore re-extracted with cold water and the product lyophilised. Trituration with cold diethyl ether/cyclohexane (9:1) yielded 3 g (yield 35%) of a yellow oil showing a single peak in LC-MS. ^{1}H NMR: 1.0-1.5 ppm (m), 4H ($NHCH_2\mathbf{CH_2CH_2}CH_2NH$), 2.85 ppm (m), 2H ($NH\mathbf{CH_2}CH_2CH_2CH_2NH$), 3.20 ppm (m), 4H ($NHCH_2CH_2CH_2\mathbf{CH_2}NH$), 3.85 ppm (d) 2H ($N\mathbf{CH_2}CO$), 4.20 ppm (m), 1H (Fmoc $\mathbf{CH}$-CH_2O), 4.40 ppm (m), 4H ($O\mathbf{CH_2}CH=CH_2$) and (Fmoc-$CH\mathbf{CH_2}O$), 5.20 ppm (m),

2H, ($OCH_2CH=\mathbf{CH_2}$), 5.80 ppm (m), 1H ($OCH_2\mathbf{CH}=CH_2$), 7.15-7.80 ppm (m), 8H (Fmoc). ESI-MS: 409.2 (M+H) (calculated mass: 408.5).

3.5.6 Synthesis of Fmoc-Lys(Boc)-Lys(Boc) dimer (98)

Dimer 96:

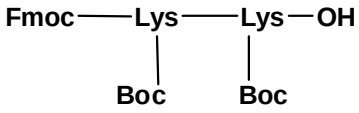

Chlorotrityl chloride resin (2.5 g, loading 1-1.2 mmol/g) was swelled in DCM (25 ml) for 60 mins. A solution containing Fmoc-Lys(Boc)-OH (1.687 g, 3.6 mmol) and DIEA (2 ml, 12 mmol) in DCM (15 ml) was then added to the resin, and the resin suspension agitated for 2 h, after which the resin was washed five times with DCM/MeOH/DIEA 17:2:1, three times with DCM, then three times with DMF. The resin was treated twice with a solution of piperidine (15 ml, 20 % in DMF) for 15 mins, then washed five times with DMF. A positive Kaiser test result showed that the Fmoc deprotection had been successful. For the coupling of the second lysine residue, a solution of Fmoc-Lys(Boc)-OH (5.622 g, 12 mmol), HBTU (4.552 g, 12 mmol) and HOBt (1.837 g, 12 mmol) in DMF (20 ml) with DIEA (6 ml) was added to the resin. The resin suspension was agitated for 1.5 h, after which time it was washed five times with DMF. A negative Kaiser test result showed that coupling was complete. The resin was washed five times with DCM, then treated five times for one minute with a solution of TFA (1% in DCM). The resin was washed five times with DCM and the organic phases were collected. Solvent was removed *in vacuo*, and the product was triturated with cold water to provide 1.2 g of a white solid (yield 68%).

3.5.7 Peptide-peptoid hybrid mimetic 88

Mimetic 88:

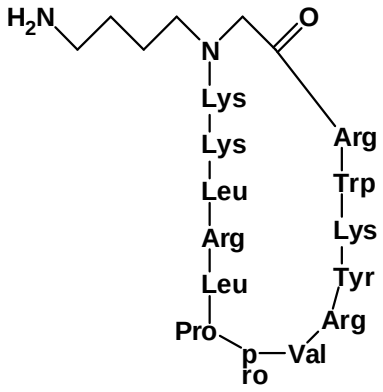

(A) Via on-resin cyclisation:

2-chlorotrityl chloride resin (1 g, loading 1-1.2 mmol/g) was swelled in DCM for 1 h. The oily product **96** (2.99 g, 7.3 mmol) from 3.5.5 above was dissolved in dry DCM (50 ml). This solution (10.5 ml, 0.63 g of product, 1.53 mmol) were added to the resin with DIEA (0.6 ml, 3.6 mmol). The resin suspension was agitated for 40 mins, then washed five times with DCM, once with MeOH for 15 minutes, and again with DCM. Level of loading was estimated according to Chan and White [190] and found to be 1 mmol/g.

The pre-loaded resin (250 mg) was swelled in DCM for 30 mins, then the resin washed five times with DMF. The resin was treated twice with a solution of piperidine (20% in DMF, 5 ml), then the resin was washed five times with DMF.

The Fmoc-Lys(Boc)-Lys(Boc) dimer **98** (697 mg, 1 mmol) from 3.5.6 above, HOBt (153 mg, 1 mmol) and HBTU (379 mg, 1 mmol) in DMF (5 ml) with DIEA (650 μl, 3.7 mmol) were added to the resin, then the resin suspension was agitated for 1.5 h. The resin was washed five times with DMF and three times with DCM. A negative Kaiser test result showed that the coupling was complete. The assembly of the peptide sequence was then continued manually, using protected amino acid (1 mmol), HBTU (1 mmol), HOBt (1 mmol) and DIEA (3 mmol) in DMF for each coupling step, and two 15 minute Fmoc deprotection cycles with piperidine (20 % in DMF, 5 ml) each time. Each coupling step lasted 1.5 hs and was monitored using the Kaiser test.

For the deprotection of the allyl group, the peptidyl resin was swelled for 30 minutes in dry DCM. Under argon, $Pd(PPh_3)_4$ (289 mg, 0.25 mmol) was dissolved in dry DCM (4 ml). To this solution, acetic acid (0.25 ml) and NMM (0.125 ml) were added. This solution was added to the resin, and the peptidyl resin was agitated for 1.5 h with exclusion of light. The resin was then washed three times with DCM, three times with DMF, three times with DCM, once with 0.5% DIEA in DMF, three times with 0.5% diethyldithiocarbamate in DMF, three times with DMF and finally three times with DCM.

For the cyclisation, peptidyl resin (80 mg) was swelled overnight in DMF. HOBt (184 mg, 1.2 mmol), HBTU (455 mg, 1.2 mmol) and DIEA (356 µl, 2 mmol) were dissolved in DMF (2.5 ml) and added to the resin. The resin suspension was agitated for 5 h. The resin was then washed three times with DMF, twice with DCM, three times with DMF, twice with MeOH, twice with DMF and twice with diethyl ether. The peptide was then cleaved from the resin and side-chain deprotected using TFA/TIS/H_2O (95:2.5:2.5) for 3 h. The resin was washed twice with TFA and the washings collected. TFA was then removed *in vacuo*, and the oily product obtained was washed five times with cold diethyl ether. It was then dissolved in water and lyophilised to provide a white powder. The product was purified by RP-HPLC using a Vydac C18 218TP1022 column (10 µm, 125 Å, 22 x 100 mm, flow rate 10 ml/min) and a gradient of 24 to 34% acetonitriles over 11 minutes. The purified product was analysed by RP-HPLC (Vydac C18 218TP54 (5 µm, 125 Å, 4 x 100 mm, flow rate 1 ml/min), gradient 5 to 40% acetonitrile over 33 minutes, retention time 28.4 mins) HPLC-MS and ESI-MS, which showed it to have the expected mass for the desired product. Calculated MW: 1850.35 g/mol, Measured m/z (ESI-MS): 926.5 (M+2H)/2.

(B) Via solution cyclisation:

2-chlorotrityl chloride resin (1 g, loading 1-1.2 mmol/g) was swelled for 20 mins in DCM. The resin was then washed twice with DCM. Bromoacetic acid (4.8 mmol, 0.67 g, 4 eq) was dissolved in a minimal amount of DCM and DIEA (9.6 mmol, 1.64 ml, 8 eq) was added with stirring. The resin suspension was agitated gently for 1 h and the resin was then washed 6 times with DCM. (4-amino-butyl)-Carbamic acid tert-butyl ester (12 mmol, 2.6 g, 10 eq) dissolved in a minimal amount of DMF was added to the

resin and the resin suspension gently agitated overnight. After this time the resin was washed 5 times with DMF and 5 times with DCM. The peptoid-resin was then transferred to the synthesis vessel of an Applied Biosystems ABI 433A synthesiser and the remainder of the peptide chain was built up using FastMoc® chemistry, with single coupling cycles of 20 minutes. An extended coupling of 55 mins was used for Lys, Pro and ^{D}Pro residues. A long extended coupling of 85 mins was used for Arg residues.

To cleave the mimetic from the solid phase, resin was washed twice with DCM and then treated three times with a solution of 1% TFA in DCM (10 ml) for 1 minute, then 7 times for two minutes. Finally, the resin was washed twice with DCM and twice with MeOH. The solutions were collected in a flask containing pyridine (0.5 ml) Solvents were removed by rotary evaporation until around 4 ml of solution remained. Cold water (100 ml) was added to this solution in order to precipitate the linear protected peptide. The slightly off-white product was filtered off using a Buchner funnel and washed three times with water, twice with aqueous $NaHCO_3$ (5%), three times with water, twice with aqueous $NaHSO_4$ (0.05 M) and finally five times with water. The product was then dried *in vacuo* over KOH for 3 hours. 420 mg of dry product were obtained.

Cyclisation: The linear protected peptide (200 mg) was dissolved in DMF (80 ml). An RP-HPLC (C4) chromatogram of this solution was recorded. HOAt (16 mg, 1.5 eq), HATU (38 mg, 1.5 eq). and DIEA (12 μl, 3.5 eq) were added to the solution, which was then stirred overnight. RP-HPLC using the same column and gradient showed that after this time the linear product had been consumed and a new peak had appeared. This observation was consistent with the formation of a cyclic product. The DMF was then removed under reduced pressure to leave a sticky pale yellow product.

For side-chain deprotection, a mixture of TFA/TIS/H_2O (95:2.5:2.5) (20 ml) was added to the cyclic product and the solution was stirred under nitrogen for 3 h. During this time the solution changed from pale yellow to a deep red. The stirring was then stopped and TFA was removed from the solution by rotary evaporation until around 3ml remained. This solution was split into two centrifuge tubes. Cold diethyl ether was then added to the tubes to precipitate the side-chain deprotected cyclic product. The tubes were centrifuged for 8 mins at 2200 rpm. The solution was decanted off and the white product was washed and centrifuged twice with diethyl ether in the same way. Finally

the product was allowed to air-dry for 1 h and was then weighed. Mass of crude cyclic product obtained:100 mg.

The product was dissolved in water (10 mg/ml) and purified by RP-HPLC using a Vydac C18 218TP1022 column (10 μm, 125 Å, 22 x 100 mm, flow rate 10 ml/min) and a gradient of 24 to 34 % acetonitrile over 11 minutes. One main peak was seen in the chromatogram and when this peak was collected and concentrated, HPLC-MS and ESI-MS showed it to have the expected mass for the desired product. M/z (M+H): 1850, (M+2H)/2: 925, (M+3H)/3: 617, (M+4H)/4: 463. The purified product was analysed by RP-HPLC (Vydac C18 218TP54 (5 μm, 125 Å, 4 x 100 mm, flow rate 1 ml/min), gradient 22 to 34% acetonitrile in 19 minutes, Retention time 16.9 mins). The cyclization, deprotection and purification steps were repeated for the remaining material. Total purified product obtained: 14 mg.

3.5.8 Peptoid-peptide hybrid mimetic 89

Mimetic 98:

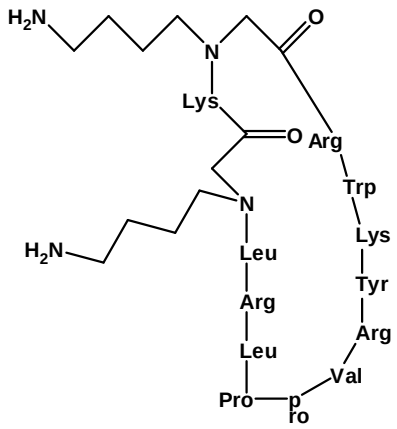

The loading of the resin with bromoacetic acid and displacement of the bromo group were carried out in the same way as described for mimetic **88**, but on a 2 g rather than a 1 g scale.

Fmoc-Lys(Boc)-OH, (3.75 g, 4 eq), HOBt (1.22 g 4 eq) and HBTU (3.03 g, 4 eq) were dissolved in a minimal amount of DMF. DIEA (4.1 ml, 12 eq) were added with stirring, then this solution was added to the resin. The resin suspension was agitated

overnight. After this time the resin was filtered and washed 5 times with DMF and 5 times with DCM. The resin was then treated twice with a solution of piperidine (15 ml, 20% in DMF) for 15 mins. The resin was washed 5 times with DMF and 5 times with DCM. A positive Kaiser test showed that the deprotection had occurred.

To bromoacetic acid (2.78 g, 10 eq) dissolved in a minimal amount of DMF was added DIC (3.1 ml, 10 eq) dropwise. The solution was stirred for 5 mins then added to the resin. The resin suspension was agitated for 2 h, then washed 5 times with DMF and 5 times with DCM. A negative Kaiser test showed that coupling was complete.

(4-amino-butyl)-Carbamic acid tert-butyl ester (3.77 g, 10 eq) were then dissolved in a minimal amount of DMF and added to the resin. The resin suspension was agitated overnight. After this time the resin was washed 5 times with DMF and 5 times with DCM.

For the leucine coupling, to a solution of Fmoc-Leu-OH (7 g, 10 eq) and HOAt (3.1 g, 10 eq) dissolved in a minimal amount of DMF was added DIC (3.1 ml, 10 eq) dropwise and the solution was stirred for 20 mins. The solution was then added to the resin and the resin suspension agitated for 4 hours. The resin was finally washed 5 times with DMF and 5 times with DCM.

The resin was then transferred to the synthesis vessel of an ABI 433A and the peptide chain was built up using FastMoc® chemistry. Single couplings of 20 mins without capping were used. An extended coupling of 55 mins was used for Lys, Pro and DPro residues. A long extended coupling of 85 mins was used for Arg residues.

Cleavage, cyclisation, deprotection. These three steps were carried out in the same way as for mimetic **88**. The purified product was analysed by RP-HPLC (Vydac C18 218TP54 (5 μm, 125 Å, 4 x 100 mm, flow rate 1 ml/min), gradient 5 to 40% acetonitrile over 33 minutes, retention time 27.5 minutes). Mass of linear protected product obtained: 470 mg. Mass of crude deprotected cyclic product: 303 mg. Mass of purified product: 15 mg. Measured m/z (ESI-MS): (M+H): 1851, (M+2H)/2: 926, (M+3H)/3: 618.

3.5.9 NMR Studies on peptides 88 and 89

1D and 2D ^{1}H NMR spectra were recorded at 600 MHz at a peptide concentration of 20 mg/ml in H_2O/D_2O 9:1 and in D_2O at pH 5 and 298 K. Water suppression was performed by presaturation [203]. The sequential resonance assignments were based on DQF-COSY [204] and TOCSY [205] measurements. Distance restraints were obtained from ROESY [212] [213] spectra with mixing times of 40, 80, 120 and 250 ms. Spectra were collected with 1024 x 256 complex data points zero-filled prior to Fourier transformation to 2048 x 1024, and transformed with a cosine-bell weighting function. Data processing was carried out with XWINNMR (Bruker) and XEASY [207].

The structure calculations were performed by restrained molecular dynamics in torsion angle space by applying the simulated annealing protocol implemented in the program DYANA [96].

3.5.10 Antimicrobial activity assays

Lyophilized peptides were weighed and dissolved in 0.01% acetic acid. The antimicrobial activities of the peptides were determined by the standard NCCLS broth microdilution method[191] in sterile 96-well plates (Nunclon polystyrene microtiter plates). Innocula of the bacteria were diluted into Mueller-Hinton (MH) broth to give approximately 10^6 colony forming units (CFU) per ml. Aliquots (50 µl) of the innocula were added to MH broth (50 µl) containing the peptide in serial two-fold dilutions. Antimicrobial activities are expressed as the minimal inhibitory concentration in µg/ml, the minimal concentration at which 100% inhibition of growth was observed after 18-20 h incubation at 37^{o}C. Determinations were performed in triplicate. Microorganisms tested were *Escherichia coli* (ATCC 25922), *Pseudomonas aeruginosa* (ATCC 27853) and *Staphylococcus aureus* (ATCC 29213 and ATCC 25923).

3.5.11 Haemolytic activity measurements

Fresh human red blood cells were washed three times with phosphate-buffered saline (PBS), and then incubated with peptide at a concentration of 100 μg/ml for 1 h at 37°C. The final erythrocyte concentration was approximately 0.9 x 10^9 per ml. The values at 0% and 100% lysis were determined by incubation of cells with PBS or 0.1% Triton X-100 in water, respectively. The samples were centrifuged, the supernatant diluted twentyfold in PBS, and the optical density was measured at 540 nm.

3.5.12 *N*-{2-[2-(2-amino-ethylamino)-ethylamino]-ethyl}-2,2,2-trifluoroacetamide (102)

To triethylene tetramine (7.3 g, 50 mmol) was dissolved in MeOH (700 ml) and cooled to ~ 83°C was added ethyl trifluoroacetate (5.96 ml, 50 mmol) dropwise over 1 h. The solution was then stirred for a further 30 mins under nitrogen.

3.5.13 {2-[tert -butoxycarbonyl-(2-{tert -butoxycarbonyl-[2-(2,2,2-trifluoro-acetylamino)-ethyl]-amino}-ethyl)-amino]-ethyl}-carbamic acid tert -butyl ester (103)

The flask containing the product from 3.5.12 was transferred to an ice bath. $(Boc)_2O$ (42.3 g, 200 mmol) was dissolved in MeOH 100 ml. This solution was added dropwise to the flask over 20 mins. The ice bath was then removed and the mixture stirred at r.t. overnight.

3.5.14 {2-[(2-amino-ethyl)-*tert* -butoxycarbonyl-amino]-ethyl}-(2-*tert* -butoxy carbonylamino-ethyl)-carbamic acid *tert* -butyl (104)

The solution from 3.5.13 was treated with aqueous ammonia until it reached pH>11. The solution was then stirred at room temperature overnight. The solvents were removed by rotary evaporation to yield 12.8 g of a sticky pale orange solid. This product was purified by flash chromatography in 3 batches of 4-5 g using a 7 cm diameter column with DCM/MeOH/NH_4OH (95:5:1) as eluant. The fractions containing the desired

product (from comparison by TLC to a known sample) together gave 6.3 g of an oily yellow product.

^{1}H NMR (in MeOD): 1.25-1.45ppm (m), 29H; 3.1-3.3ppm (m), 12H.

Measured m/z (ESI-MS): (M+H): 447.3, (M+Na): 469.2

3.5.15 Peptide-peptoid hybrid mimetic 99

Mimetic 99:

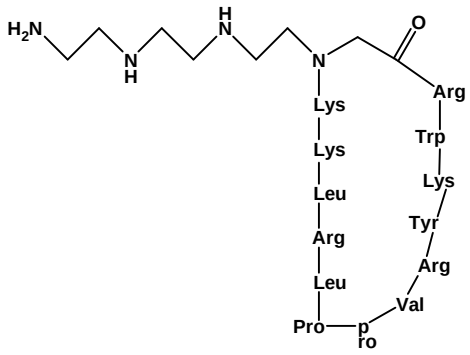

2-chlorotrityl resin (500 mg) was swelled in DCM for 30 mins, then the resin was washed 3 times with DCM. A solution of bromoacetic acid (500 mg, 5 eq) and DIEA (3 ml, 12 eq) in DCM (5 ml) was added to the resin and the resin suspension was agitated for 1 h. The resin was then washed 5 times with DCM.

The tri-Boc protected tetramine **104** (1.5 g, 5 eq) was dissolved in DCM (4 ml) and added to the resin and the suspension was agitated overnight. The resin was then washed 5 times with DCM.

To check that the correct product was present on the resin, a small portion (~40 mg) of the resin was transferred to a Pasteur pipette plugged with cotton wool. The resin was treated with 1% TFA in DCM 8 times to cleave the protected peptoid unit from the resin. The solvents were evaporated off to leave a film of product on the inside of the r.b. flask. This film was washed with ether. The washing was repeated twice, then the product was dissolved in MeOH (0.5 ml). A main peak with the expected mass of the desired product m/z: [(M+H): 505] was observed in ESI-MS..

To a solution of Fmoc-Lys(Boc)-OH (1.64 g, 5 eq) and HOAt (0.54 g, 5 eq) dissolved in a minimal amount of DMF, DIC (0.54 g, 5 eq) was added dropwise. The resin suspension was agitated for 20 mins. A little more DMF was added to dissolve the ppt which had formed, then the solution was added to the resin and the resin suspension agitated for 4 h. The solution was drained off from the resin and the resin washed 5 times with DMF.

The resin was then transferred to the synthesis vessel of the ABI 433A and the remainder of the peptide chain was built up using FastMoc ® chemistry. Single coupling

cycles of 20 mins were used. An extended coupling of 55 mins was used for Lys, Pro and DPro residues. A long extended coupling of 85 mins was used for Arg residues.

Cleavage of the fully protected linear peptide from the resin was carried out in the same way as for mimetic **88.** 700 mg of dry product obtained.

For the cyclisation, the product (350 mg) was dissolved in DMF (140 ml). This solution was analysed by RP-HPLC. HATU (57 mg, 1.5 eq), HOAt (23mg, 1.5eq) and DIEA (60 µl, 3.5 eq) were added to this solution and the mixture was stirred overnight. RP-HPLC analysis showed that the starting material had disappeared after this time and that a new product had been formed with a longer retention time. The DMF was removed under reduced pressure.

The sticky colourless product was dissolved in TFA/TIS/H_2O 95:2.5:2.5 (30 ml) and stirred under nitrogen for 3 h. Approx. 4/5 of the TFA was removed by rotary evaporation and the remaining solution was split between two centrifuge tubes. The product was precipitated and washed as previously described. 160 mg of crude product obtained.

Purification was carried out by preparative RP-HPLC using a C18 Xterra column. 25 mg of pure product were obtained.

Analytical RP-HPLC: The purified product was analysed by RP-HPLC (Vydac C18 218TP54 (5 µm, 125 Å, 4 x 100 mm, flow rate 1 ml/min), gradient 5 to 55% acetonitrile over 33 minutes, retention time 23.5 mins)

Measured m/z ESI-MS: (M+H): 1908, (M+2H)/2: 955.2, (M+3H)/3: 637.1, (M+4H)/4: 478, (M+5H)/5: 382.5

Appendix 1: Abbreviations

Acm	……Acetamidomethyl
aq.	……..……..Aqueous
Boc	……..……*Tert*-butyloxycarbonyl
$(Boc)_2O$	……..di- *tert*-butyl dicarbonate
CS	……Circumsporozoite
DCC	……...Dicyclohexylcarbodiimide
DCM	……..…….Dichloromethane
DNA	……..……Deoxyribonucleic acid
DIC	……...…….Diisoproplcarbodiimide
DIEA	……...……..Diisopropylethylamine
DMF	……...……..Dimethylformamide
DQF-COSY	……Double quantum filtered correlated spectroscopy
EDT	……Ethanedithiol
EGF	……..……Epidermal growth factor
ELISA	……Enzyme-linked immunosorbant assay
eq.	……..……..……Equivalents
ESI-MS	……Electrospray ionisation mass spectrometry
Fmoc	……..……(9*H*-fluoren-9-yl)methyloxycarbonyl
GLURP	……Glutamate-rich protein
HATU	……...…O-(7-azabenzotriazol-1-yl)-*N*,*N*,*N’*,*N’*, tetramethyluronium
	……..……hexafluorophoshate
HBTU	……..…….O-(benzotriazol-1-yl)-*N*,*N*,*N’*,*N’*, tetramethyluronium
	……..……hexafluorophoshate
HOAt	……..……1-hydroxy-7-azabenzotriazol
HOBt	……1-hydroxybenzotriazol
HPLC	……..……..High pressure/performance liquid chromatography
IFA	……Immunofluorescence assay
IRIV	……..Immunopotentiating reconstituted influenza virosome
MALDI	……Matrix desorption laser-assisted ionisation
MSP	……Merozoite surface protein

NHS	N-hydroxysuccinimide
NMP	*N*-methylpyrrolidine
NMR	Nuclear magnetic resonance
NOESY	Nuclear Overhauser effect spectroscopy
Pbf	Pentamethyldihydrobenzofuran-5-sulfonyl
PBS	Phosphate-buffered saline
PE	1,3-dipalmitoylphosphatidylethanolamine
r.b.	Round-bottomed
ROESY	Rotating frame nuclear Overhauser effect spectroscopy
RP-HPLC	Reversed-phase HPLC
Rpm	Revolutions per minute
r.t.	Room temperature
TFA	Trifluoroacetic acid
TFE	Trifluoroethanol
TIS	Triisopropylsilane
TLC	Thin layer chromatography
TMS	Tetramethylsilane
TOCSY	Totally correlated spectroscopy
Trt	Trityl
TSP	3-trimethylsilylpropionic acid-d_4 soldium salt

Appendix 2: NMR data

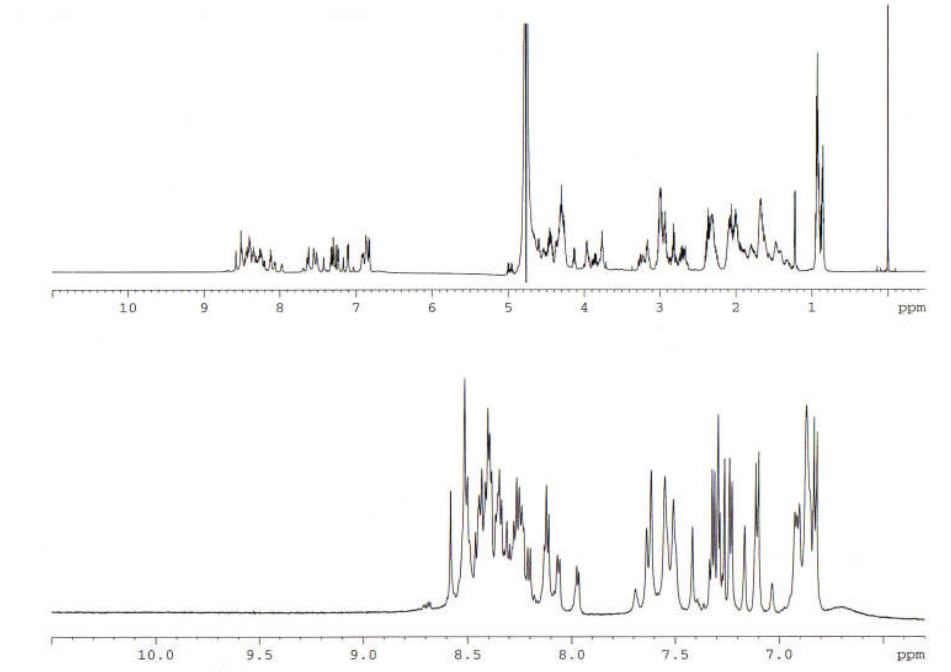

Figure 97: *Top*: ^{1}H-NMR spectrum (600MHz) of peptide **1** in H_2O/D_2O (9:1), pH 5, 300K. *Bottom*: expansion of the amide NH region.

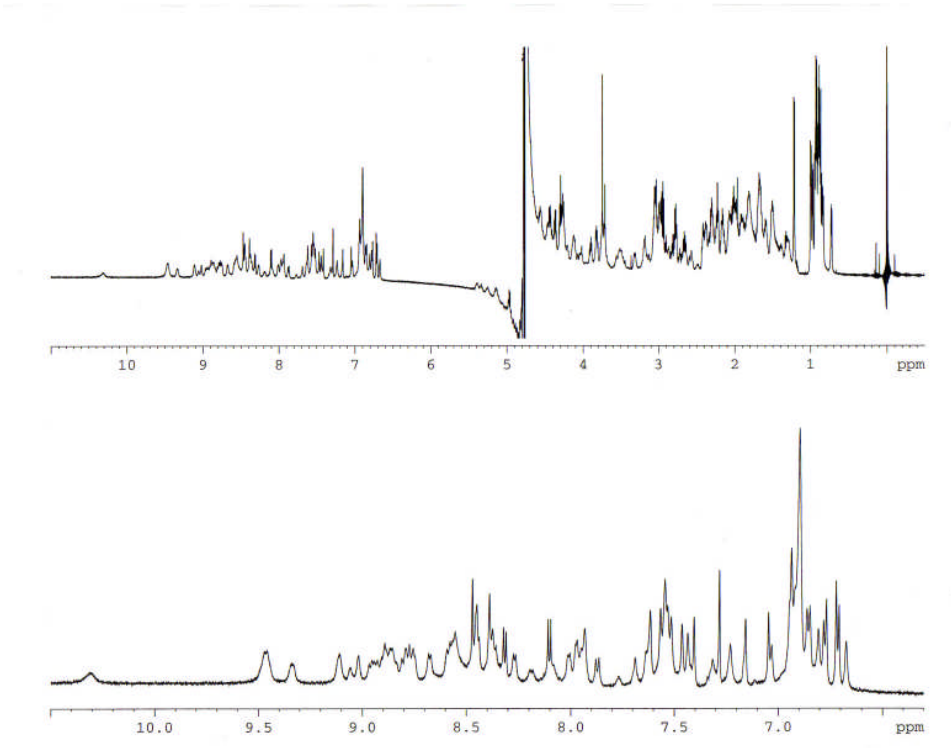

Figure 98: *Top*: ^{1}H-NMR spectrum (600MHz) of peptide **2** in H_2O/D_2O (9:1), pH 5, 300K. *Bottom*: expansion of the amide NH region.

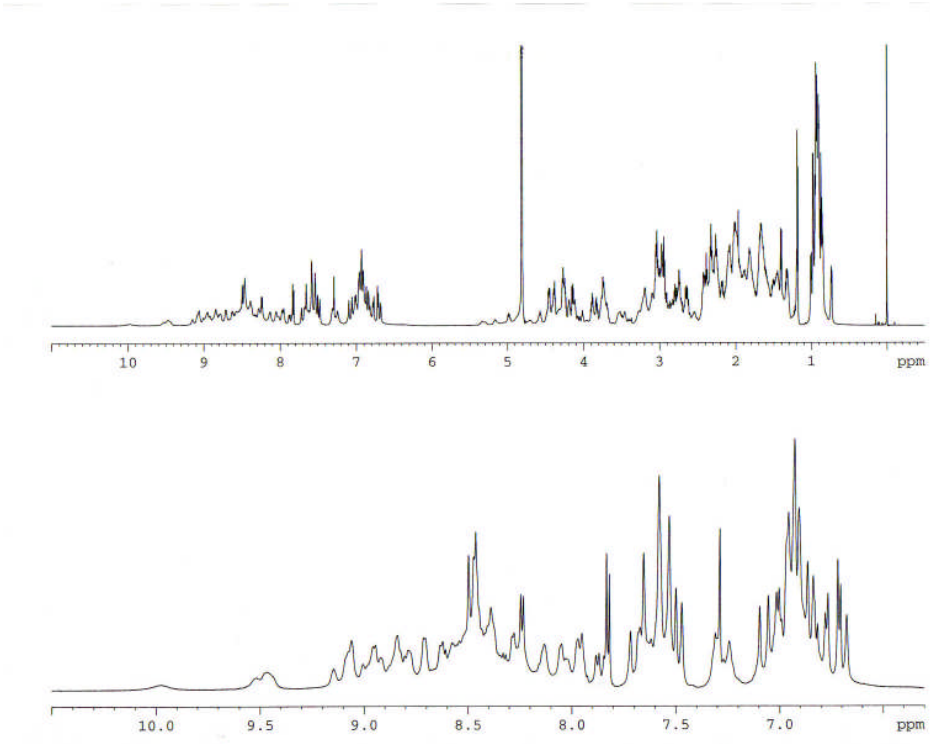

Figure 99: *Top*: ^{1}H-NMR spectrum (600MHz) of peptide **45** in H_2O/D_2O (9:1), pH 5, 300K. *Bottom*: expansion of the amide NH region.

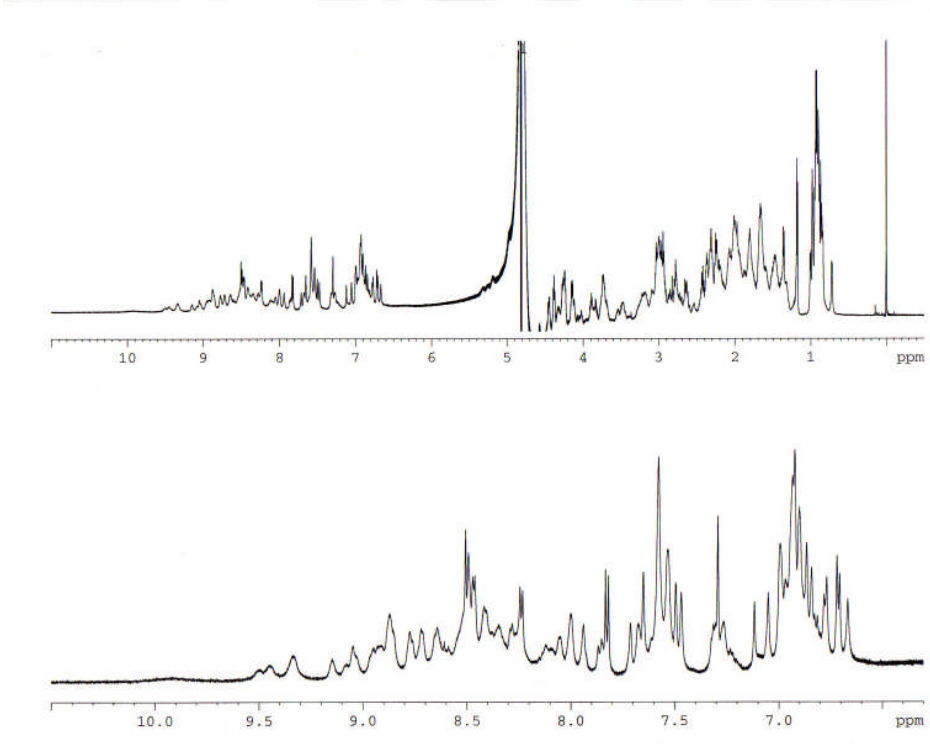

Figure 100: *Top*: ^{1}H-NMR spectrum (600MHz) of peptide **46** in H_2O/D_2O (9:1), pH 5, 300K. *Bottom*: expansion of the amide NH region.

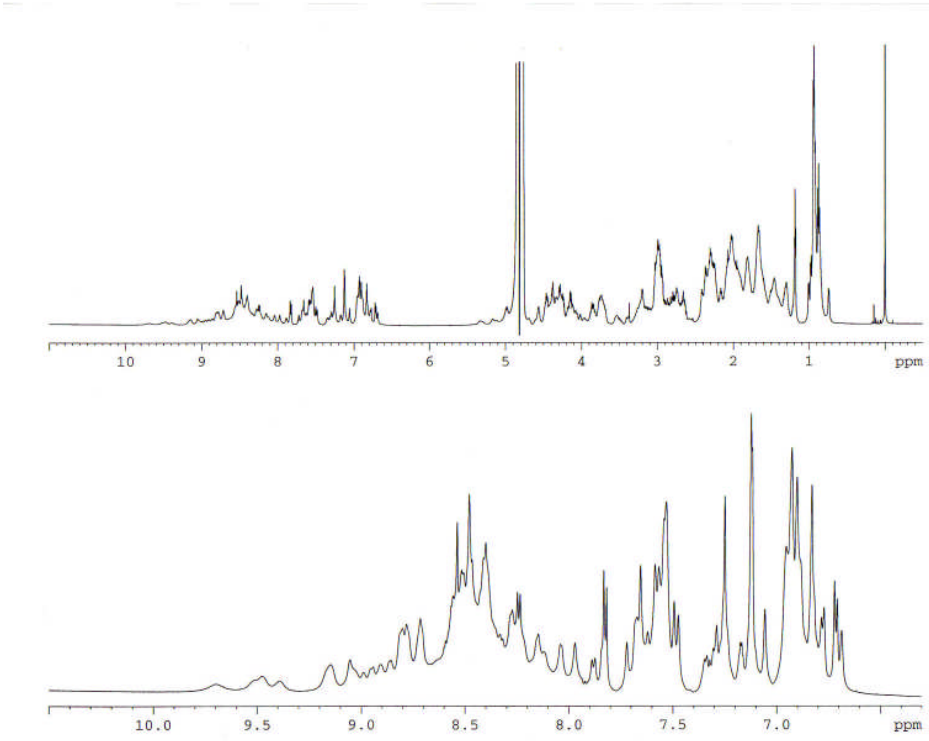

Figure 101: *Top*: ^{1}H-NMR spectrum (600MHz) of peptide **48** in H_2O/D_2O (9:1), pH 5, 300K. *Bottom*: expansion of the amide NH region.

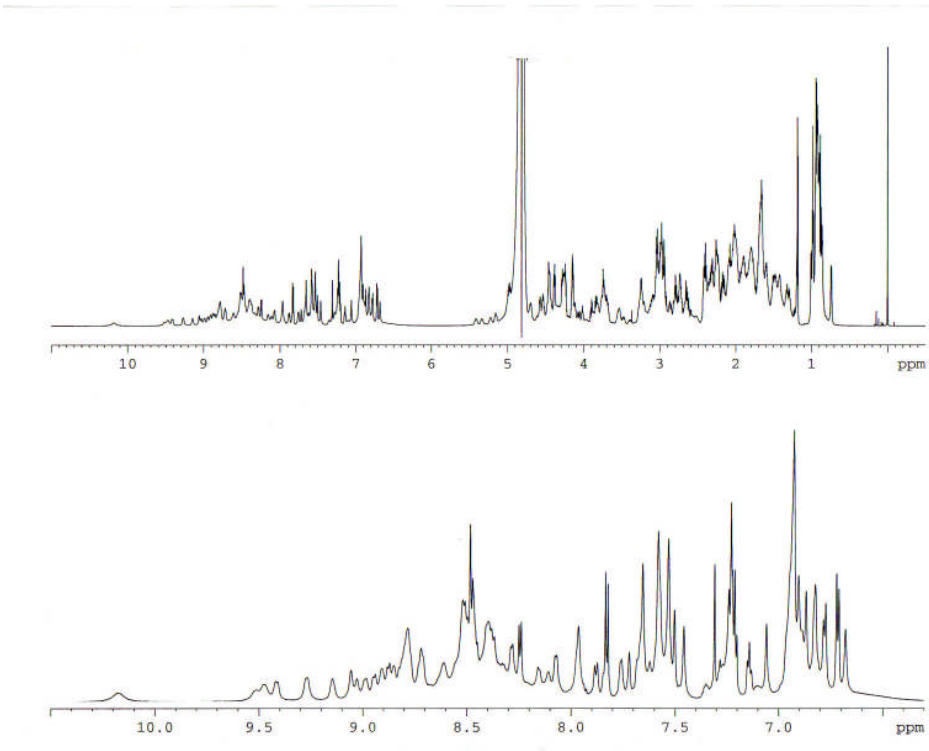

Figure 102: *Top*: ^{1}H-NMR spectrum (700MHz) of peptide **49** in H_2O/D_2O (9:1), pH 5, 300K. *Bottom*: expansion of the amide NH region.

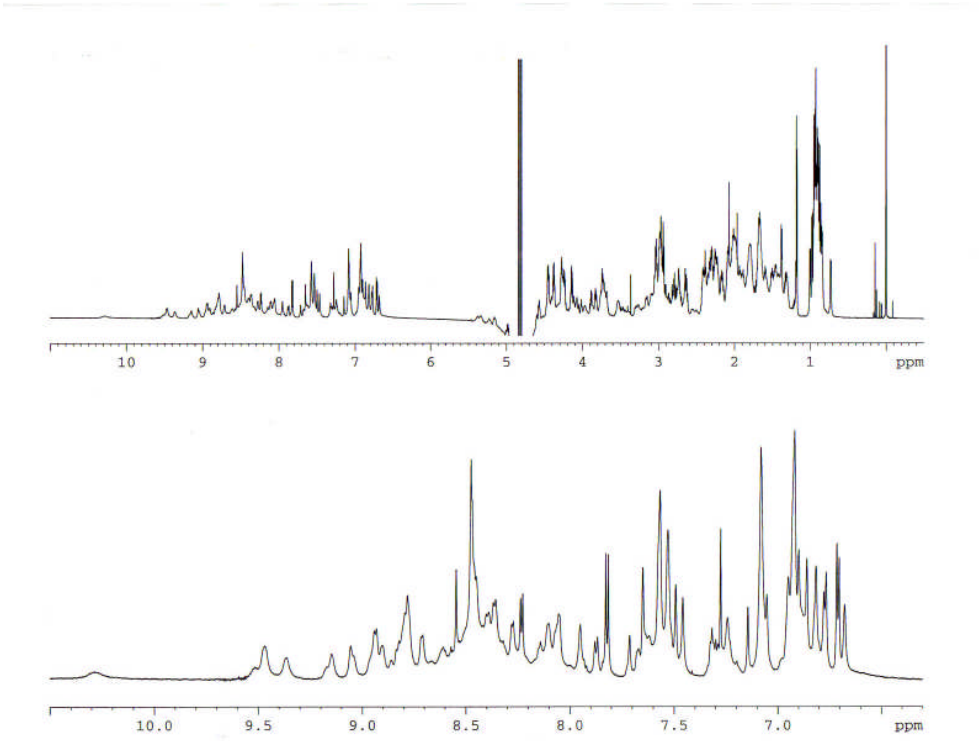

Figure 103: *Top*: ^{1}H-NMR spectrum (700MHz) of peptide **50** in H_2O/D_2O (9:1), pH 5, 300K. *Bottom*: expansion of the amide NH region.

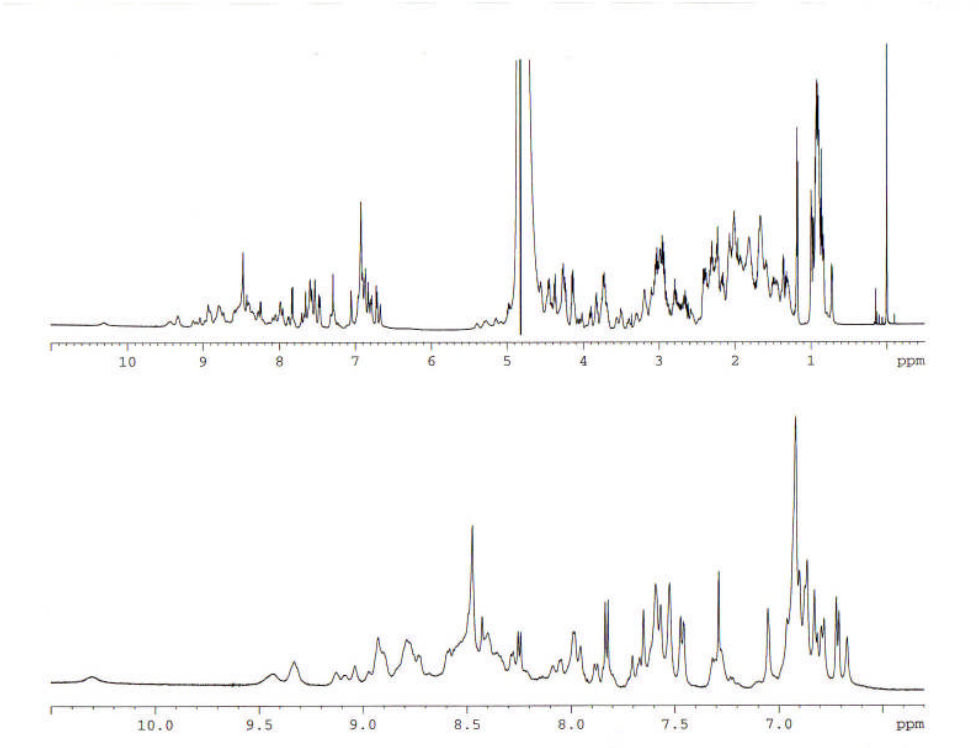

Figure 104: *Top*: ^{1}H-NMR spectrum (600MHz) of peptide **51** in H_2O/D_2O (9:1), pH 5, 300K. *Bottom*: expansion of the amide NH region.

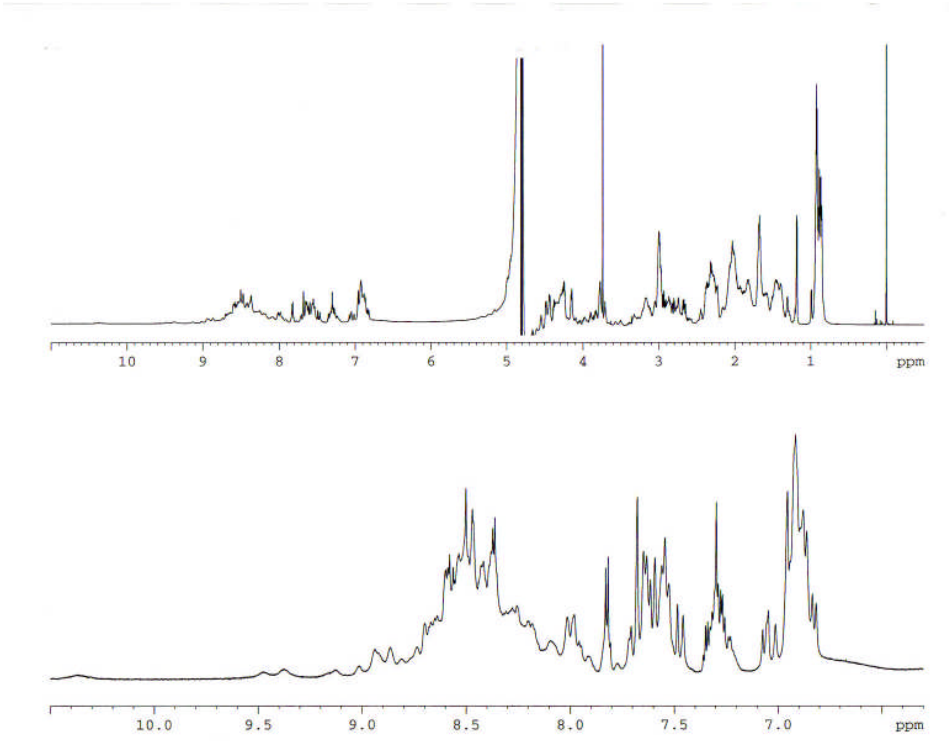

Figure 105: *Top*: ^{1}H-NMR spectrum (700MHz) of peptide **52** in H_2O/D_2O (9:1), pH 5, 300K. *Bottom*: expansion of the amide NH region.

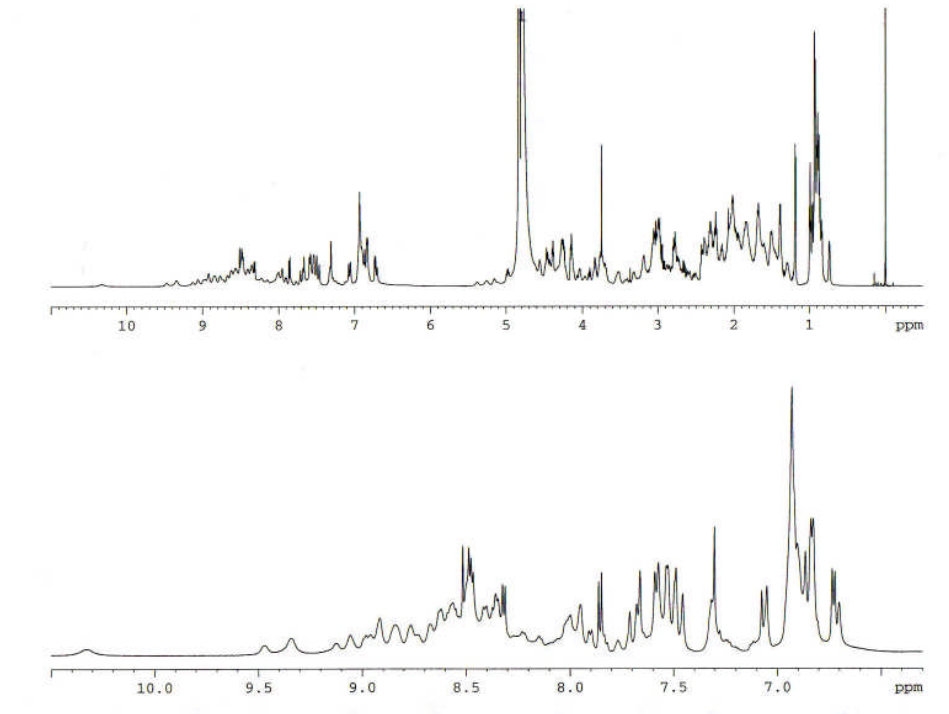

Figure 106: *Top*: ^{1}H-NMR spectrum (600MHz) of peptide **53** in H_2O/D_2O (9:1), pH 5, 300K. *Bottom*: expansion of the amide NH region.

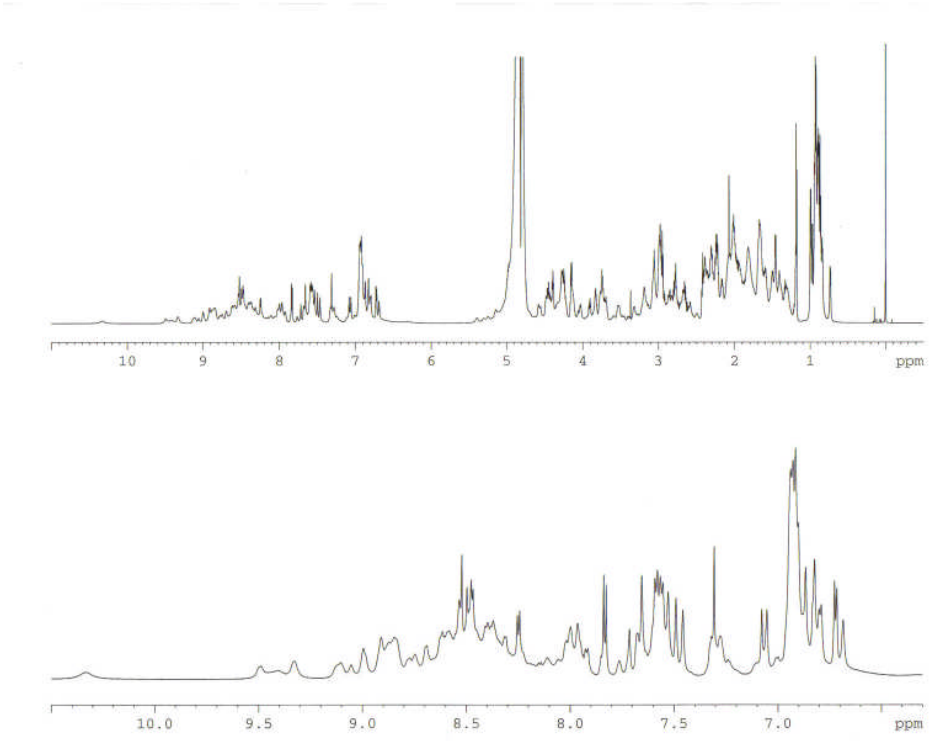

Figure 107: *Top*: ^{1}H-NMR spectrum (700MHz) of peptide **54** in H_2O/D_2O (9:1), pH 5, 300K. *Bottom*: expansion of the amide NH region.

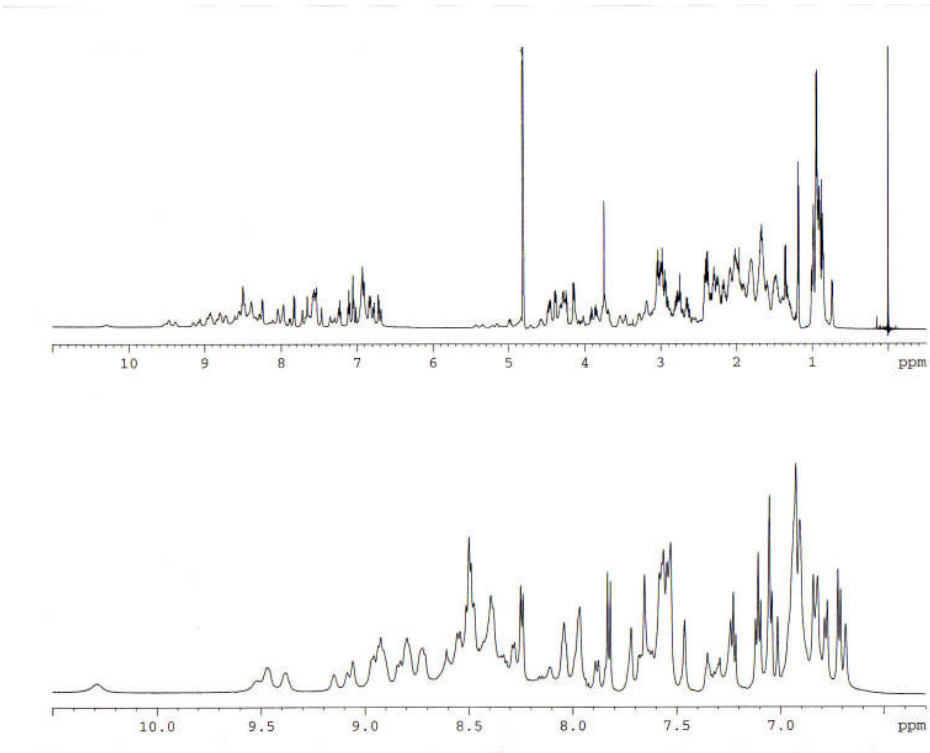

Figure 108: *Top*: ^{1}H-NMR spectrum (600MHz) of peptide **55** in H_2O/D_2O (9:1), pH 5, 300K. *Bottom*: expansion of the amide NH region.

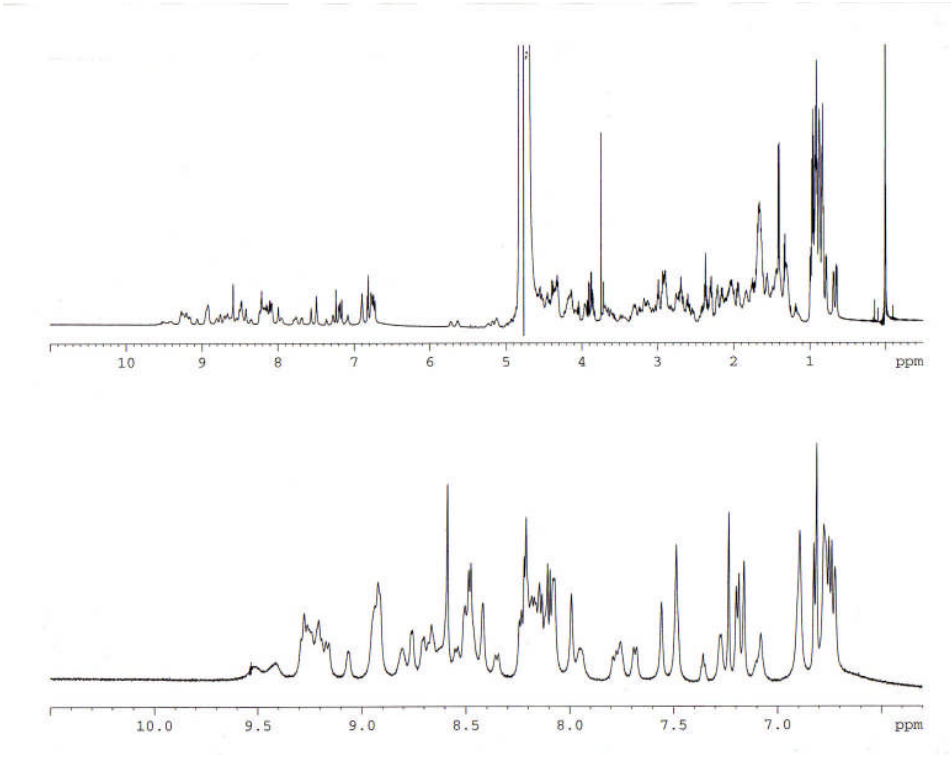

Figure 109: *Top*: ^{1}H-NMR spectrum (600MHz) of peptide **58** in H_2O/D_2O (9:1), pH 5, 300K. *Bottom*: expansion of the amide NH region.

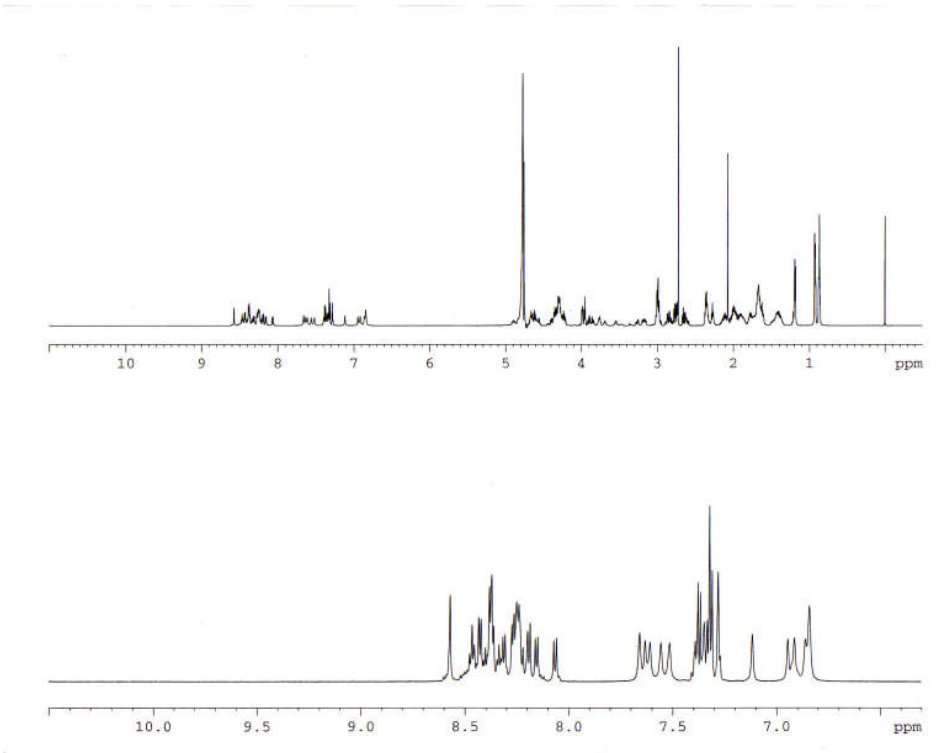

Figure 110: *Top*: ^{1}H-NMR spectrum (600MHz) of peptide **73** in H_2O/D_2O (9:1), pH 5, 300K. *Bottom*: expansion of the amide NH region.

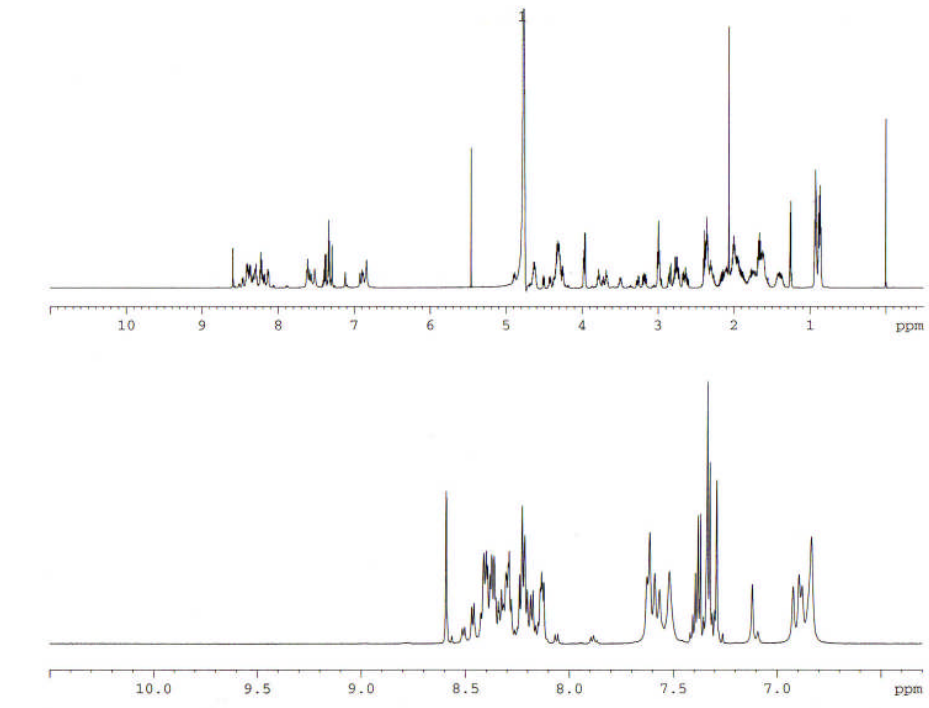

Figure 111: *Top*: ^{1}H-NMR spectrum (600MHz) of peptide **74** in H_2O/D_2O (9:1), pH 5, 300K. *Bottom*: expansion of the amide NH region.

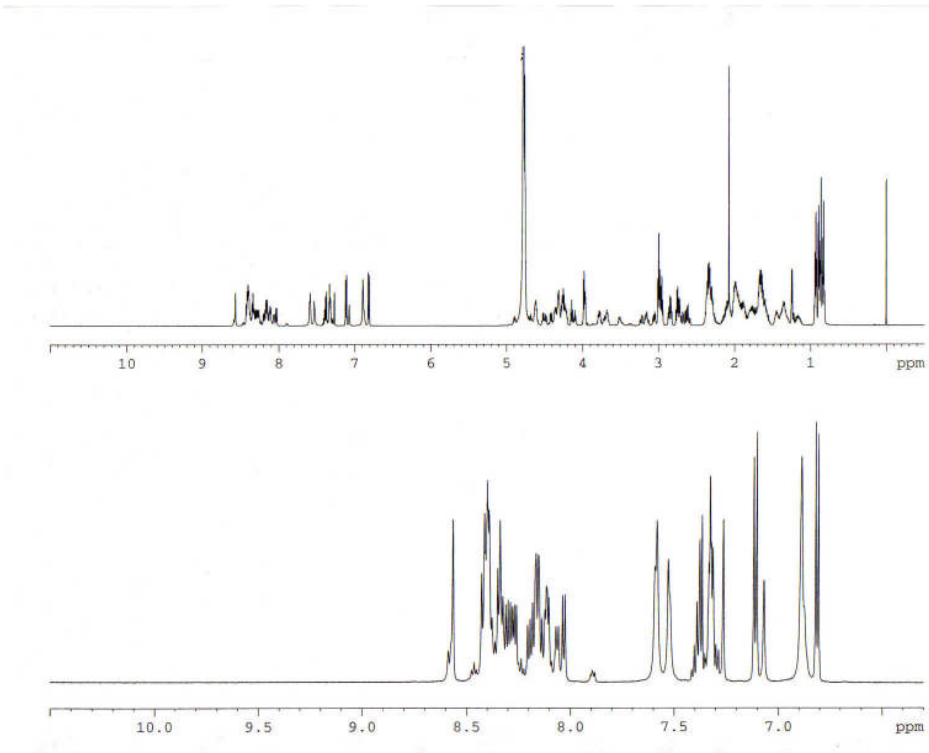

Figure 112: *Top*: ^{1}H-NMR spectrum (600MHz) of peptide **75** in H_2O/D_2O (9:1), pH 5, 300K. *Bottom*: expansion of the amide NH region.

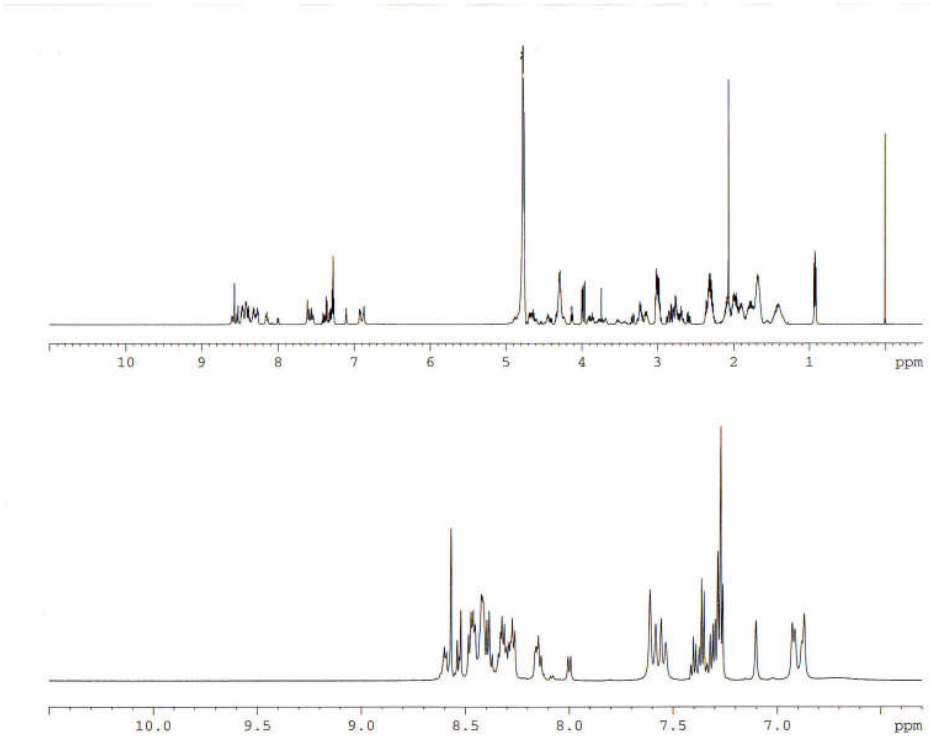

Figure 113: *Top*: ^{1}H-NMR spectrum (600MHz) of peptide **76** in H_2O/D_2O (9:1), pH 5, 300K. *Bottom*: expansion of the amide NH region.

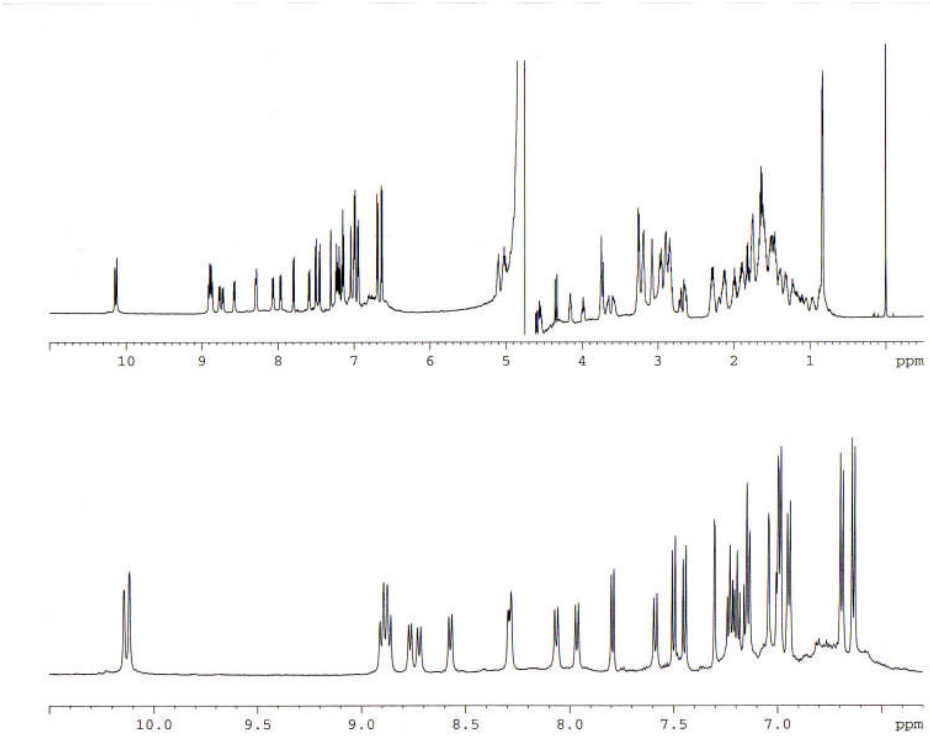

Figure 114: *Top*: ^{1}H-NMR spectrum (600MHz) of peptide **97** in H_2O/D_2O (9:1), pH 5, 300K. *Bottom*: expansion of the amide NH region.

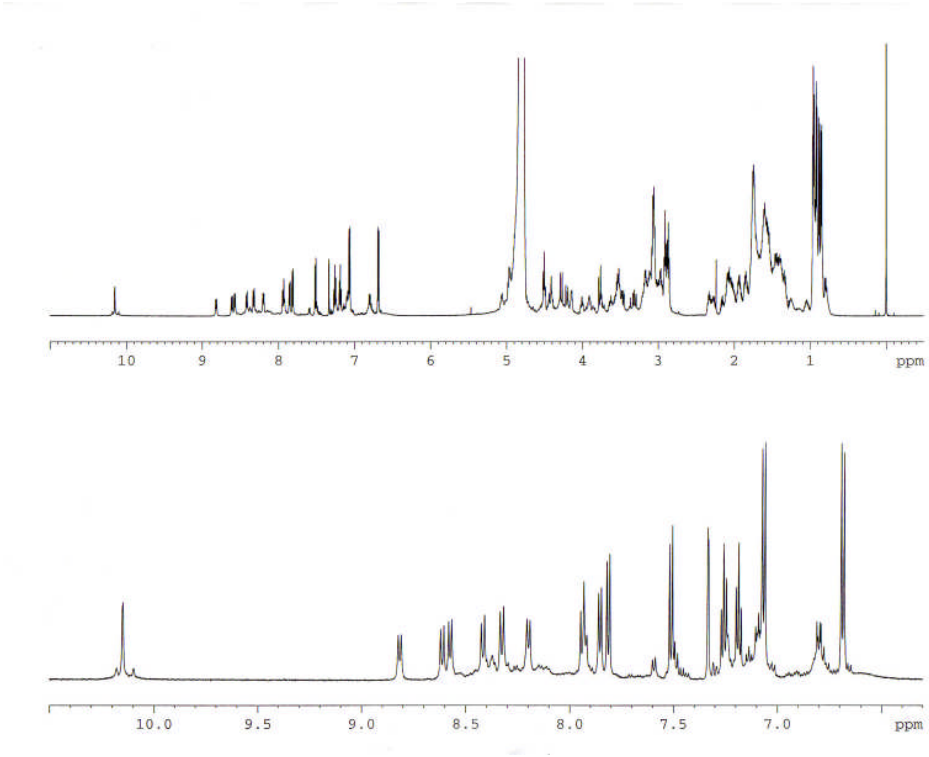

Figure 115: *Top*: ^{1}H-NMR spectrum (600MHz) of peptide **98** in H_2O/D_2O (9:1), pH 5, 300K. *Bottom*: expansion of the amide NH region.

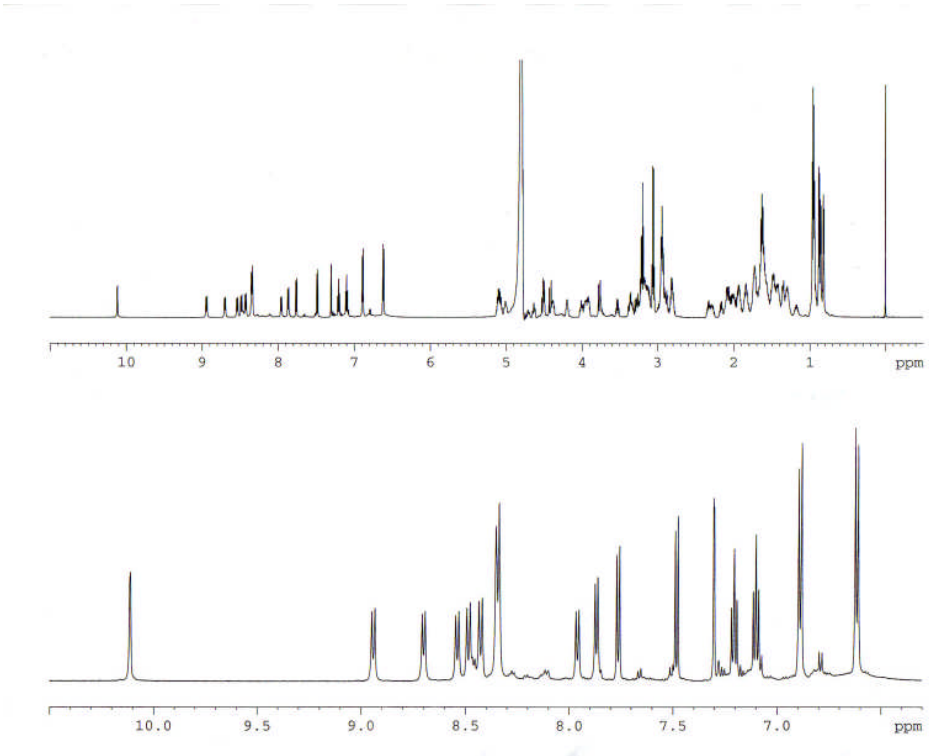

Figure 116: *Top*: ^{1}H-NMR spectrum (600MHz) of peptide **104** in H_2O/D_2O (9:1), pH 5, 300K. *Bottom*: expansion of the amide NH region.

Residue	NH	CH_α	CH_β	Others
Asn[1]		4.388	2.962, 2.962	$NH_2\delta$ 7.705, 7.045
Ile[2]	8.615	4.265	1.876	$CH_3\delta$ 0.922
Ser[3]	8.461	4.435	3.815, 3.898	-
Gln[4]	8.468	4.215	1.848, 1.941	$CH_2\gamma$ 2.234, 2.234; $NH_2\varepsilon$ 7.482, 6.860
His[5]	8.363	4.854	2.999, 2.999	CHδ 7.306; CHε 8.522
Gln[6]	7.975	4.419	2.004, 2.067	$CH_2\gamma$ 2.385, 2.385; $NH_2\varepsilon$ 7.580, 6.913
Cys[7]	8.907	4.271	3.126, 3.317	-
Val[8]	10.307	4.274	2.153	$CH_3\gamma$ 0.879, 0.879
Lys[9]	9.332	4.463	1.819, 1.819	$CH_2\gamma$ 1.397, 1.437; $CH_2\delta$ 1.680, 1.680; $CH_2\varepsilon$ 2.988, 2.988
Lys[10]	8.554	4.125	1.822, 1.822	$CH_2\gamma$ 1.295, 1.295; $CH_2\delta$ 1.598, 1.680; $CH_2\varepsilon$ 3.056, 3.056
Gln[11]	8.396	4.469	1.908, 2.059	$CH_2\gamma$ 2.301, 2.301; $NH_2\varepsilon$ 7.449, 6.819
Cys[12]	8.561	5.150	2.374, 3.462	-
Pro[13]		4.564	2.033, 2.408	$CH_2\gamma$ 1.790, 2.068; $CH_2\delta$ 3.516, 3.822
Gln[14]	8.467	4.020	1.939, 1.989	$CH_2\gamma$ 2.417, 2.417; $NH_2\varepsilon$ 7.241, 6.936
Asn[15]	8.886	3.889	1.493, 2.646	$NH_2\delta$ 7.243, 6.934
Ser[16]	7.629	4.967	3.515, 3.754	-
Gly[17]	8.778	3.697, 4.524		-
Cys[18]	8.569	5.255	2.965, 3.032	-
Phe[19]	9.471	-	2.907, 2.907	CHδ 6.913, 6.913; CHε 6.944, 6.944
Arg[20]	8.221	4.903	1.283, 1.469	$CH_2\gamma$ 1.482, 1.585; $CH_2\delta$ 3.065, 3.318; NHε 7.318
His[21]	9.127	-	3.506, 3.506	CHδ 7.078; CHε 8.483
Leu[22]	8.889	4.141	1.679, 1.825	CHγ 1.743; $CH_3\delta$ 0.890, 0.989
Asp[23]	7.950	4.551	2.592, 3.060	-
Glu[24]	8.017	3.829	2.181, 2.494	$CH_2\gamma$ 2.256, 2.280

Table 17: Chemical shifts (600MHz) for **2** at 298K in H_2O/D_2O (9:1), pH 5

Arg[25]	7.994	4.248	1.744, 1.848	$CH_2\gamma$ 1.514, 1.600; $CH_2\delta$ 3.179, 3.179; NHε 7.762
Glu[26]	8.615	5.107	1.908, 1.908	$CH_2\gamma$ 2.107, 2.586
Glu[27]	8.920	4.720	1.994, 2.142	$CH_2\gamma$ 2.269, 2.269
Cys[28]	8.976	5.396	2.813, 3.042	-
Lys[29]	8.858	-	1.680, 1.773	$CH_2\gamma$ 1.393, 1.393; $CH_2\delta$ 1.499, 1.499; $CH_2\varepsilon$ 2.774, 2.774
Cys[30]	9.078	-	2.661, 3.047	-
Leu[31]	8.091	4.257	1.492, 1.671	$CH\gamma$ 1.234; $CH_3\delta$ 0.723, 0.832
Leu[32]	7.945	4.112	1.597, 1.652	$CH\gamma$ 1.652; $CH_3\delta$ 0.956, 0.956
Asn[33]	8.699	4.386	2.862, 3.074	$NH_2\delta$ 7.530, 6.916
Tyr[34]	8.386	4.867	2.556, 3.207	CHδ 6.774, 6.774; CHε 6.720, 6.720
Lys[35]	9.489	-	1.770, 1.770	$CH_2\gamma$ 1.327, 1,327; $CH_2\delta$ 1.607, 1.654; $CH_2\varepsilon$ 2.947, 2.947
Gln[36]	8.771	4.725	2.077, 2.077	$CH_2\gamma$ 2.328, 2.388; $NH_2\varepsilon$ 7.540, 6.678
Glu[37]	8.921	4.579	1.802, 1.994	$CH_2\gamma$ 2.181, 2.181
Gly[38]	9.133	3.712, 4.060		-
Asp[39]	8.792	4.694	2.779, 2.779	-
Lys[40]	7.869	4.696	1.844, 1.885	$CH_2\gamma$ 1.504, 1.504; $CH_2\delta$ 1.693, 1.693; $CH_2\varepsilon$ 3.033, 3.033
Cys[41]	8.825	5.336	2.649, 2.881	-
Val[42]	9.462	4.722	2.213	$CH_3\gamma$ 0.918, 0.997
Glu[43]	9.033	3.548	1.804, 1.804	$CH_2\gamma$ 2.071, 2.169
Asn[44]	8.285	4.865	2.351, 2.706	$NH_2\delta$ 7.561, 6.876
Pro[45]		4.364	1.906, 2.223	$CH_2\gamma$ 1.963, 1.963; $CH_2\delta$ 3.721, 3.721
Asn[46]	8.329	4.970	2.663, 2.798	$NH_2\delta$ 7.630, 6.907
Pro[47]		4.438	1.997, 2.276	$CH_2\gamma$ 2.017, 2.017; $CH_2\delta$ 3.747, 3.747
Thr-NH_2[48]	8.123	4.306	4.272	$CH_3\gamma$ 1.229 NH_2 7.423, 7.172

Table 17 (continued): Chemical shifts (600MHz) for **2** at 298K in H_2O/D_2O (9:1), pH 5

Residue	**NH**	**CH_α**	**CH_β**	**Others**
Leu[1]	7.86	4.39	1.47, 1.84	CHγ 1.60; CH_3δ 0.87, 0.96
Arg[2]	8.43	4.70	1.72, 1.72	CH_2γ 1.47, 1.61; CH_2δ 3.14, 3.14; NHε 7.13
Leu[3]	8.50	4.63	0.90, 1.34	CHγ 1.34; CH_2δ 0.82, 0.85
Lys[4]	8.32	5.12	1.64, 1.82	CH_2γ 1.31, 1.31; CH_2δ 1.64, 1.64; CH_2ε 2.95, 2.95
Lys[5]	8.99	5.05	1.91, 2.02	CH_2γ 1.42, 1.51; CH_2δ 1.64, 1.64; CH_2ε 2.84, 2.84
Nlys[6]	-	3.75, 4.35	-	CH_2Nβ 3.58, 3.70; CH_2Nγ 1.75, 1.78; CH_2Nε 3.09, 3.09
Arg[7]	8.41	4.20	1.44, 1.60	CH_2γ 1.03, 1.23; CH_2δ 2.97, 2.97; NHε 6.95
Trp[8]	8.08	4.85	3.28, 3.39	$H\delta^1$ 7.30; $H\varepsilon^3$ 7.75; $H\zeta^3$ 7.08, $H\eta^2$ 7.19; $H\zeta^2$ 7.47; $NH\varepsilon^1$ 10.10
Lys[9]	8.30	5.04	1.63, 1.73	CH_2γ 1.30, 1.43; CH_2δ 1.63, 1.63; CH_2ε 2.93, 2.93
Tyr[10]	8.69	4.78	2.82, 2.82	Hδ 6.84, 6.84; Hε 6.59, 6.59
Arg[11]	8.53	5.12	1.72, 1.85	CH_2γ 1.50, 1.64; CH_2δ 3.16, 3.16; NHε 7.13
Val[12]	8.35	4.51	2.00	CH_3γ 0.95 0.95
^{D}Pro[13]	-		1.93, 2.32	CH_2γ 2.05, 2.16; CH_2δ 3.53, 3.91;
Pro[14]	-	4.50		CH_2γ 1.94, 2.09; CH_2δ 3.75, 4.01

Table 18: Chemical shifts for peptide **97** at 300K in H_2O/D_2O (9:1), pH 5.

Appendix 3: Amino acid analysis

Peptide 2:

Amino acid	Residues (theoretical)	Residues (measured)	Error (%)
Asp	7	7.9	12.30
Glu	10	8.3	16.69
Ser	2	1.7	15.33
His	2	1.6	
Gly	2	2.1	5.33
Thr	1	1.1	7.44
Ala	0	0.1	
Arg	2	1.9	6.69
Tyr	1	1.2	
Val	2	2.0	1.90
Met	0	0.1	
Phe	1	0.9	7.60
Ile	1	0.8	16.60
Leu	3	3.1	2.09
Lys	5	4.9	2.33
Pro	3	3.9	

Peptide 42:

Amino acid	Residues (theoretical)	Residues (measured)	Error (%)
Asp	7	7.8	11.55
Glu	10	10.5	5.2
Ser	2	1.6	19.9
His	2	1.7	
Gly	2	2.2	
Thr	1	1.0	3.22
Ala	0		
Arg	2	1.8	8.08
Tyr	1	1.2	
Val	2	1.9	5.32
Met	0	0.2	
Phe	1	0.9	8.97
Ile	1	1.1	6.06
Leu	3	3.2	5.03
Lys	5	4.7	5.87
Pro	3	3.2	5.99

Peptide 73

Amino acid	Residues (theoretical)	Residues (measured)	Error (%)
Asp	5	5.5	10.82
Glu	4	4.4	10.90
Ser	1	0.9	12.08
His	1	0.9	6.58
Gly	2	2.0	0.04
Thr	2	1.8	10.61
Ala	0	0.0	
Arg	0		
Tyr	0		
Val	0	0.0	
Met	0	0.1	
Phe	1	1.0	0.66
Ile	1	1.0	1.95
Leu	2	2.0	1.62
Lys	3	2.8	5.08
Pro	2	2.1	3.13

Peptide 74

Amino acid	Residues (theoretical)	Residues (measured)	Error (%)
Asp	5	5.3	6.21
Glu	6	6.6	9.88
Ser	0	0.0	
His	1	0.8	16.50
Gly	2	1.9	4.13
Thr	1	0.9	10.36
Ala	0	0.0	
Arg	0		
Tyr	0		
Val	0	0.0	
Met	0	0.1	
Phe	1	1.0	0.73
Ile	0	0.0	
Leu	3	3.0	0.42
Lys	2	1.8	8.71
Pro	3	3.1	4.13

Peptide 75

Amino acid	Residues (theoretical)	Residues (measured)	Error (%)
Asp	5	5.6	11.60
Glu	6	6.6	10.65
Ser	0	0.1	
His	1	0.7	
Gly	2	2.1	3.53
Thr	1	0.9	9.51
Ala	0	0.1	
Arg	0		
Tyr	1	0.9	14.89
Val	0	0.0	
Met	0	0.2	
Phe	1	1.0	1.65
Ile	2	1.9	3.13
Leu	2	2.1	3.93
Lys	3	2.9	4.05
Pro	3	3.1	3.75

Peptide 76

Amino acid	Residues (theoretical)	Residues (measured)	Error (%)
Asp	5	6.6	32.50
Glu	6	6.3	4.51
Ser	1	0.9	8.58
His	2	1.9	
Gly	2	2.0	0.63
Thr	0		
Ala	0	0.0	
Arg	1	0.9	9.01
Tyr	0		
Val	1	1.0	3.93
Met	0	0.1	
Phe	1	1.1	6.94
Ile	0	0.0	
Leu	0	0.0	
Lys	4	4.0	0.27
Pro	2	2.2	9.79

Peptide 77

Amino acid	Residues (theoretical)	Residues (measured)	Error (%)
Asp	5	6.3	26.93
Glu	5	5.1	2.24
Ser	1	0.8	16.83
His	2	1.9	6.72
Gly	3	2.8	5.12
Thr	0		
Ala	0	0.0	
Arg	1	0.9	12.63
Tyr	0	0.0	
Val	1	1.1	5.16
Met	0		
Phe	1	0.9	5.19
Ile	1	1.0	3.47
Leu	0	0.0	
Lys	3	3.3	11.19
Pro	2	2.3	14.54

Peptide 97

Amino acid	Residues (theoretical)	Residues (measured)	Error (%)
Asp	0	0.0	
Glu	0	0.1	
Ser	0	0.0	
His	0		
Gly	0	0.1	
Thr	0		
Ala	0	0.0	
Arg	3	2.8	6.97
Tyr	1	1.0	2.72
Val	1	0.9	5.57
Met	0	0.0	
Phe	0	0.0	
Ile	0	0.0	
Leu	2	2.1	5.23
Lys	3	3.0	0.09
Pro	2	2.2	10.12

Peptide 98

Amino acid	Residues (theoretical)	Residues (measured)	Error (%)
Asp	0	0.0	
Glu	0	0.1	
Ser	0	0.0	
His	0		
Gly	0	0.1	
Thr	0		
Ala	0	0.0	
Arg	3	2.8	5.74
Tyr	1	1.0	3.39
Val	1	1.0	3.83
Met	0	0.1	
Phe	0		
Ile	0	0.0	
Leu	2	2.2	8.96
Lys	2	1.8	9.25
Pro	2	2.3	13.25

Peptide 104

Amino acid	Residues (theoretical)	Residues (measured)	Error (%)
Asp	0	0.4	
Glu	0	0.4	
Ser	0	0.2	
His	0		
Gly	0	0.5	
Thr	0		
Ala	0	0.2	
Arg	3	2.8	7.20
Tyr	1	1.1	5.40
Val	1	1.0	2.16
Met	0	0.3	
Phe	0		
Ile	0		
Leu	2	2.2	8.38
Lys	3	2.9	4.41
Pro	2	2.9	

Appendix 4: HPLC conditions

Figure 16 (A): Vydac C18 218TP54, flow rate 1 ml/min, 5 to 100% acetonitrile over 29 mins. **(B):** Vydac C18 218TP54, 5 to 17% acetonitrile over 4 mins, then 17 to 33% over 29 mins.

Figure 18: Vydac C18 218TP54 , flow rate 1 ml/min, 5 to 50% acetonitrile over 29 mins.

Figure 19: Vydac C18 218TP54 , flow rate 1 ml/min, 5 to 50% acetonitrile over 29 mins.

Figure 20: Vydac C18 218TP54, flow rate 1 ml/min, 5 to 17% acetonitrile over 4 mins, then 17 to 33% over 26 mins.

Figure 22: Vydac 218TP54 column, flow rate 1 ml/min, 5 to 23% acetonitrile over 34 mins.

Figure 23: Zorbax eclipse analytical C18, (4.6 x 250 mm, 5 μm, flow rate 1 ml/min), 3 to 30% acetonitrile over 34 mins.

Figure 27: Vydac C4 214TP104 (10 μm, 125 Å, 4 x 100 mm, flow rate 1 ml/min), 40-100% acetonitrile over 29 mins.

Figure 31: Vydac C18 218TP54, flow rate 1 ml/min, 5 to 17% acetonitrile over 4 mins, then 17 to 33% over 26 mins.

Figure 32: Vydac C18 218TP54, flow rate 1 ml/min, 5 to 17% acetonitrile over 4 mins, then 17 to 33% over 26 mins.

Figure 33: Vydac C18 218TP54 , flow rate 1 ml/min, 5 to 50% acetonitrile over 29 mins.

Figure 35: Vydac C4 214TP104 (10 μm, 125 Å, 4 x 100 mm, flow rate 1 ml/min), 10-100% acetonitrile over 16.5 mins.

Figure 37: Vydac C18 218TP54 , flow rate 1 ml/min, 5 to 100% acetonitrile over 34 mins.

Figure 38: Vydac C18 218TP54 , flow rate 1 ml/min, 5 to 50% acetonitrile over 29 mins.

Figure 39: Vydac C18 218TP54 , flow rate 1 ml/min, 5 to 50% acetonitrile over 29 mins.

Figure 40 (A): Vydac C18 218TP54 , flow rate 1 ml/min, 5 to 50% acetonitrile over 29 mins. **(B):** Zorbax eclipse XDB-C18 (7 μm, 21.2 x 250 mm), flow rate 15 ml/min, 5 to 27.5% acetonitrile over 18 minutes. **(C):** Vydac C18 218TP54 , flow rate 1 ml/min, 5 to 50% acetonitrile over 29 mins.

Figure 48: Vydac C18 218TP54 , flow rate 1 ml/min, 5 to 50% acetonitrile over 29 mins.

Figure 49: Vydac C18 218TP54 , flow rate 1 ml/min, 5 to 50% acetonitrile over 29 mins.

Figure 50: Vydac C18 218TP54 , flow rate 1 ml/min, 5 to 50% acetonitrile over 29 mins.

Figure 51: Vydac C18 218TP54 , flow rate 1 ml/min, 5 to 50% acetonitrile over 29 mins.

Figure 55: Vydac C18 218TP54 , flow rate 1 ml/min, 5 to 50% acetonitrile over 29 mins.

Figure 56: Vydac C4 214TP104 (10 μm, 125 Å, 4 x 100 mm, flow rate 1 ml/min), 10-100% acetonitrile over 16.5 mins.

Figure 59: Vydac C18 218TP54 , flow rate 1 ml/min, 5 to 60% acetonitrile over 39 mins.

Figure 61: Vydac C4 214TP104 (10 μm, 125 Å, 4 x 100 mm, flow rate 1 ml/min), 10-100% acetonitrile over 16.5 mins.

Figures 66-69 (A): Vydac C4 214TP104, 30 to 100% acetonitrile over 33 mins. **(B):** Vydac C18 218TP104 column, gradient 5 to 55% acetonitrile over 29 mins.

Figure 71: Vydac C4 214TP104, 30 to 100% acetonitrile over 33 mins.

Figure 73: Vydac C18 218TP104 column, gradient 5 to 40% acetonitrile over 21 mins.

Figure 74 (A), (B), (C): Vydac C4 214TP104, 50 to 100% acetonitrile over 29 mins. **(D):** Vydac C4 214TP104, 30 to 100% acetonitrile over 33 mins.

Figures 75 and 76: Vydac C4 214TP104, 30 to 100% acetonitrile over 33 mins.

Figure 86: Vydac C18 218TP54 column, gradient 5 to 40% acetonitrile over 39 mins.

Figure 87: Vydac C18 218TP54 column, gradient 5 to 40% acetonitrile over 33 mins.

Figures 88 and 89: Vydac C4 214TP104, 5 to 100% acetonitrile over 41 mins.

Figure 90: Vydac C18 218TP54 column, gradient 5 to 37% acetonitrile over 39 mins.

Figure 91: Vydac C18 218TP54 column, gradient 5 to 27% acetonitrile over 1 minute, then 27 to 33% over 19 mins.

Figure 92: Vydac C4 214TP104, 5 to 100% acetonitrile over 41 mins.

Figure 93: Vydac C18 218TP54 column, gradient 5 to 50% acetonitrile over 33 mins.

Figure 98: Vydac C18 218TP54 column, gradient 5 to 55% acetonitrile over 33 mins.

References

[1] W. H. O. Roll Back Malaria, UNICEF, *World Malaria Report 2005*, World Health Organization and UNICEF, Geneva, **2005**.
[2] M. M. Mota, G. Pradel, J. P. Vanderberg, J. C. Hafalla, U. Frevert, R. S. Nussenzweig, V. Nussenzweig, A. Rodriguez, *Science* **2001**, *291*, 141.
[3] M. M. Mota, J. C. R. Hafalla, A. Rodriguez, *Nat Med* **2002**, *8*, 1318.
[4] Encarta, *Life Cycle of the Malaria Parasite*, Microsoft Corporation.
[5] J. D. Lines, *Med. Vet. Entomol* **1987**, *1*, 37.
[6] P. Olliaro, *Pharmacol Therapeut* **2001**, *89*, 207.
[7] J. E. Hyde, *Trends Parasitol* **2005**, *21*, 494.
[8] W. H. O. Roll Back Malaria, UNICEF, *Facts on ACTs*, **2005**.
[9] Q. C-ORGo, *Kuo Xue Tung Bao* **1977**, *22*, 142.
[10] U. Eckstein-Ludwig, R. J. Webb, I. D. Van Goethem, J. M. East, A. G. Lee, M. Kimura, P. M. O'Neill, P. G. Bray, S. A. Ward, S. Krishna, *Nature* **2003**, *424*, 957.
[11] T. T. Hien, N. J. White, *Lancet* **1993**, *341*, 603.
[12] F. Nosten, M. van Vugt, R. Price, C. Luxemburger, K. L. Thway, A. Brockman, R. McGready, F. ter Kuile, S. Looareesuwan, N. J. White, *Lancet* **2000**, *356*, 297.
[13] J. L. Vennerstrom, S. Arbe-Barnes, R. Brun, S. A. Charman, F. C. Q. Chiu, J. Chollet, Y. Dong, A. Dorn, D. Hunziker, H. Matile, K. McIntosh, M. Padmanilayam, J. Santo Tomas, C. Scheurer, B. Scorneaux, Y. Tang, H. Urwyler, S. Wittlin, W. N. Charman, *Nature* **2004**, *430*, 900.
[14] R. Jambou, E. Legrand, M. Niang, N. Khim, P. Lim, B. Volney, M. T. Ekala, C. Bouchier, P. Esterre, T. Fandeur, O. Mercereau-Puijalon, *Lancet* **2005**, *366*, 1960.
[15] R. S. Nussenzweig, J. Vanderberg, H. Most, C. Orton, *Nature* **1967**, *216*, 160.
[16] K. H. Rieckmann, P. E. Carson, R. L. Beaudoin, J. S. Cassells, K. W. Sell, *Trans R Soc Trop Med Hyg* **1974**, *68*, 258.
[17] K. H. Rieckmann, R. L. Beaudoin, J. S. Cassells, K. W. Sell, *Bull World Health Organ* **1979**, *57 Suppl 1*, 261.
[18] D. F. Clyde, H. Most, V. C. McCarthy, J. P. Vanderberg, *Am J Med Sci* **1973**, *266*, 169.
[19] D. F. Clyde, V. C. McCarthy, R. M. Miller, R. B. Hornick, *Am J Med Sci* **1973**, *266*, 398.
[20] I. A. McGregor, *Bull World Health Organ* **1974**, *50*, 259.
[21] WHO, *immunization against diseases of public health importance*, **2005**.
[22] S. L. Hoffman, L. M. Goh, T. C. Luke, I. Schneider, T. P. Le, D. L. Doolan, J. Sacci, P. de la Vega, M. Dowler, C. Paul, D. M. Gordon, J. A. Stoute, L. W. Church, M. Sedegah, D. G. Heppner, W. R. Ballou, T. L. Richie, *J Infect Dis* **2002**, *185*, 1155.
[23] V. S. Moorthy, M. F. Good, A. V. Hill, *Lancet* **2004**, *363*, 150.
[24] E. H. Nardin, R. S. Nussenzweig, *Annu Rev Immunol* **1993**, *11*, 687.
[25] R. S. Nussenzweig, V. Nussenzweig, *Adv Immunol* **1989**, *45*, 283.
[26] S. H. I. Kappe, C. A. Buscaglia, V. Nussenzwieg, *Annu Rev Dev Cell Biol* **2004**, *20*, 29.

[27] T. F. McCutchan, J. C. Kissinger, M. G. Touray, M. J. Rogers, J. Li, M. Sullivan, E. M. Braga, A. U. Krettli, L. H. Miller, *Proc Natl Acad Sci U S A* **1996**, *93*, 11889.
[28] A. Saul, R. S. Nussenzweig, V. Nussenzweig, in *Novel Vaccination Strategies* (Ed.: S. H. E. Kaufmann), Wiley-VCH, Weinheim, **2004**.
[29] P. L. Alonso, J. Sacarlal, J. J. Aponte, A. Leach, E. Macete, P. Aide, B. Sigauque, J. Milman, I. Mandomando, Q. Bassat, C. Guinovart, M. Espasa, S. Corachan, M. Lievens, M. M. Navia, M. C. Dubois, C. Menendez, F. Dubovsky, J. Cohen, R. Thompson, W. R. Ballou, *Lancet* **2005**, *366*, 2012.
[30] A. A. Sultan, V. Thathy, U. Frevert, K. J. Robson, A. Crisanti, V. Nussenzweig, R. S. Nussenzweig, R. Menard, *Cell* **1997**, *90*, 511.
[31] S. Gantt, C. Persson, K. Rose, A. J. Birkett, R. Abagyan, V. Nussenzweig, *Infect Immun* **2000**, *68*, 3667.
[32] L. Renia, M. M. Rodrigues, V. Nussenzweig, *Immunology* **1994**, *82*, 164.
[33] M. Tsuji, C. C. Bergmann, Y. Takita-Sonoda, K. Murata, E. G. Rodrigues, R. S. Nussenzweig, F. Zavala, *J Virol* **1998**, *72*, 6907.
[34] P. Daubersies, A. W. Thomas, P. Millet, K. Brahimi, J. A. Langermans, B. Ollomo, L. BenMohamed, B. Slierendregt, W. Eling, A. Van Belkum, G. Dubreuil, J. F. Meis, C. Guerin-Marchand, S. Cayphas, J. Cohen, H. Gras-Masse, P. Druilhe, *Nat Med* **2000**, *6*, 1258.
[35] S. J. McConkey, W. H. Reece, V. S. Moorthy, D. Webster, S. Dunachie, G. Butcher, J. M. Vuola, T. J. Blanchard, P. Gothard, K. Watkins, C. M. Hannan, S. Everaere, K. Brown, K. E. Kester, J. Cummings, J. Williams, D. G. Heppner, A. Pathan, K. Flanagan, N. Arulanantham, M. T. Roberts, M. Roy, G. L. Smith, J. Schneider, T. Peto, R. E. Sinden, S. C. Gilbert, A. V. Hill, *Nat Med* **2003**, *9*, 729.
[36] M. Arevalo-Herrera, Y. Solarte, M. F. Yasnot, A. Castellanos, A. Rincon, A. Saul, J. Mu, C. Long, L. Miller, S. Herrera, *Am J Trop Med Hyg* **2005**, *73*, 32.
[37] T. Arakawa, A. Komesu, H. Otsuki, J. Sattabongkot, R. Udomsangpetch, Y. Matsumoto, N. Tsuji, Y. Wu, M. Torii, T. Tsuboi, *Infect Immun* **2005**, *73*, 7375.
[38] N. Hilf, M. Radsak, H. Schild, in *Novel Vaccination Strategies* (Ed.: S. H. E. Kaufmann), Wiley-VCH, Weinheim, **2004**.
[39] K. Heeg, S. Zimmermann, A. Dalpke, in *Novel Vaccination Strategies* (Ed.: S. H. E. Kaufmann), Wiley-VCH, Weinheim, **2004**.
[40] I. Desombere, M. Van der Wielen, P. Van Damme, M. Stoffel, N. De Clercq, C. Goilav, G. Leroux-Roels, *Vaccine* **2002**, *20*, 2597.
[41] F. Belli, A. Testori, L. Rivoltini, M. Maio, G. Andreola, M. R. Sertoli, G. Gallino, A. Piris, A. Cattelan, I. Lazzari, M. Carrabba, G. Scita, C. Santantonio, L. Pilla, G. Tragni, C. Lombardo, F. Arienti, A. Marchiano, P. Queirolo, F. Bertolini, A. Cova, E. Lamaj, L. Ascani, R. Camerini, M. Corsi, N. Cascinelli, J. J. Lewis, P. Srivastava, G. Parmiani, *J Clin Oncol* **2002**, *20*, 4169.
[42] D. T. O'Hagan, M. Singh, in *Novel Vaccination Strategies* (Ed.: S. H. E. Kaufmann), Wiley-VCH, Weinheim, **2004**.
[43] R. Zurbriggen, *Vaccine* **2003**, *21*, 921.
[44] M. Tsurodome, R. Gluck, R. Graf, R. Falchetto, U. Schaller, J. Brunner, *J Biol Chem* **1992**, *267*, 20225.
[45] R. Zurbriggen, I. Novak-Hofer, A. Seelig, R. Gluck, *Progr Lipid Res* **2000**, *39*, 3.
[46] B. Pfeiffer, E. Peduzzi, K. Moehle, R. Zurbriggen, G. Pluschke, J. A. Robinson, *Angew Chem Int Ed* **2003**, *42*, 2368.

[47] R. Moreno, L. Jiang, K. Moehle, R. Zurbriggen, R. Gluck, J. A. Robinson, G. Pluschke, *ChemBioChem* **2001**, *2*, 838.
[48] C. R. Savage, Jr, T. Inagami, S. Cohen, *J Biol Chem* **1972**, *247*, 7612.
[49] I. D. Campbell, P. Bork, *Curr Opin Struct Biol* **1993**, *3*, 385.
[50] C. R. Savage, Jr, J. H. Hash, S. Cohen, *J Biol Chem* **1973**, *248*, 7669.
[51] W. D. Morgan, B. Birdsall, T. A. Frenkiel, M. G. Gradwell, P. A. Burghaus, S. E. Syed, C. Uthaipibull, A. A. Holder, J. Feeney, *J Mol Biol* **1999**, *289*, 113.
[52] J. Wu, Y. Yang, J. T. Watson, *Protein Sci* **1998**, *7*, 1017.
[53] J. Y. Chang, L. Li, P. H. Lai, *J Biol Chem* **2001**, *276*, 4845.
[54] J. Y. Chang, P. Schindler, U. Ramseier, P. H. Lai, *J Biol Chem* **1995**, *270*, 9207.
[55] J. Y. Chang, L. Li, A. Bulychev, *J Biol Chem* **2000**, *275*, 8287.
[56] D. Gaur, D. C. Mayer, L. H. Miller, *Int J Parasitol* **2004**, *34*, 1413.
[57] J. S. McBride, H. G. Heidrich, *Mol Biochem Parasitol* **1987**, *23*, 71.
[58] A. A. Holder, J. S. Sandhu, Y. Hillman, L. S. Davey, S. C. Nicholls, H. Cooper, M. J. Lockyer, *Parasitology* **1987**, *94 (Pt 2)*, 199.
[59] M. J. Blackman, H. G. Heidrich, S. Donachie, J. S. McBride, A. A. Holder, *J Exp Med* **1990**, *172*, 379.
[60] M. J. Blackman, H. Whittle, A. A. Holder, *Mol Biochem Parasitol* **1991**, *49*, 35.
[61] M. J. Blackman, E. D. Dennis, E. M. Hirst, C. H. Kocken, T. J. Scott-Finnigan, A. W. Thomas, *Exp Parasitol* **1996**, *83*, 229.
[62] M. J. Blackman, I. T. Ling, S. C. Nicholls, A. A. Holder, *Mol Biochem Parasitol* **1991**, *49*, 29.
[63] V. Chitarra, I. Holm, G. A. Bentley, S. Petres, S. Longacre, *Mol Cell* **1999**, *3*, 457.
[64] J. A. Chappel, A. A. Holder, *Mol Biochem Parasitol* **1993**, *60*, 303.
[65] D. Zhang, W. Pan, *Infect Immun* **2005**, *73*, 6530.
[66] I. T. Ling, S. A. Ogun, A. A. Holder, *Parasite Immunol* **1994**, *16*, 63.
[67] S. Kumar, A. Yadava, D. B. Keister, J. H. Tian, M. Ohl, K. A. Perdue-Greenfield, L. H. Miller, D. C. Kaslow, *Mol Med* **1995**, *1*, 325.
[68] T. M. Daly, C. A. Long, *Infect Immun* **1993**, *61*, 2462.
[69] S. Singh, M. C. Kennedy, C. A. Long, A. J. Saul, L. H. Miller, A. W. Stowers, *Infect Immun* **2003**, *71*, 6766.
[70] S. Kumar, W. Collins, A. Egan, A. Yadava, O. Garraud, M. J. Blackman, J. A. Guevara Patino, C. Diggs, D. C. Kaslow, *Infect Immun* **2000**, *68*, 2215.
[71] P. H. Corran, R. A. O'Donnell, J. Todd, C. Uthaipibull, A. A. Holder, B. S. Crabb, E. M. Riley, *Infect Immun* **2004**, *72*, 6185.
[72] A. F. Egan, P. Burghaus, P. Druilhe, A. A. Holder, E. M. Riley, *Parasite Immunol* **1999**, *21*, 133.
[73] M. J. Blackman, T. J. Scott-Finnigan, S. Shai, A. A. Holder, *J Exp Med* **1994**, *180*, 389.
[74] J. A. Guevara Patino, A. A. Holder, J. S. McBride, M. J. Blackman, *J Exp Med* **1997**, *186*, 1689.
[75] W. D. Morgan, T. A. Frenkiel, M. J. Lock, M. Grainger, A. A. Holder, *Biochemistry* **2005**, *44*, 518.
[76] C. Uthaipibull, B. Aufiero, S. E. Syed, B. Hansen, J. A. Guevara Patino, E. Angov, I. T. Ling, K. Fegeding, W. D. Morgan, C. Ockenhouse, B. Birdsall, J. Feeney, J. A. Lyon, A. A. Holder, *J Mol Biol* **2001**, *307*, 1381.
[77] J. A. G. Patino, A. A. Holder, J. S. McBride, M. J. Blackman, *J Exp Med* **1997**, *186*, 1689.

[78] M. Hensmann, C. Li, C. Moss, V. Lindo, F. Greer, C. Watts, S. A. Ogun, A. A. Holder, J. Langhorne, *Eur J Immunol* **2004**, *34*, 639.
[79] U. Kienzl, PhD thesis, University of Zurich (Zurich), **2003**.
[80] *Unpublished results*, Robinson Group, Zurich.
[81] J. C. Spetzler, C. Rao, J. P. Tam, *Int J Pept Protein Res* **1994**, *43*, 351.
[82] F. Vella, J. F. Hernandez, A. Molla, M. R. Block, G. J. Arlaud, *J Pept Res* **1999**, *54*, 415.
[83] S. J. Freedman, D. G. Sanford, W. W. Bachovchin, B. C. Furie, J. D. Baleja, B. Furie, *Biochemistry* **1996**, *35*, 13733.
[84] E. Kluver, A. Schulz, W. G. Forssmann, K. Adermann, *J Pept Res* **2002**, *59*, 241.
[85] S. Y. Shin, T. Takenouchi, T. Yokoyama, T. Ohtaki, E. Munekata, *Int J Pept Protein Res* **1994**, *44*, 485.
[86] J. F. Hernandez, B. Bersch, Y. Petillot, J. Gagnon, G. J. Arlaud, *J Pept Res* **1997**, *49*, 221.
[87] T. Takenouchi, M. Kadosaka, S. Y. Shin, E. Munekata, *Int J Pept Protein Res* **1995**, *46*, 391.
[88] Z. Wu, R. Powell, W. Lu, *J Am Chem Soc* **2003**, *125*, 2402.
[89] T. M. Hackeng, J. A. Fernandez, P. E. Dawson, S. B. Kent, J. H. Griffin, *Proc Natl Acad Sci U S A* **2000**, *97*, 14074.
[90] S. Y. Shin, T. Yokoyama, T. Takenouchi, E. Munekata, *J Pept Sci* **2003**, *9*, 244.
[91] Y. Stenberg, K. Julenius, I. Dahlqvist, T. Drakenberg, J. Stenflo, *Eur J Biochem* **1997**, *248*, 163.
[92] N. D. Kurniawan, J. M. O'Leary, A. M. Thamlitz, R. Sofair, J. M. Werner, J. Stenflo, A. K. Downing, *Biochemistry* **2004**, *43*, 9352.
[93] J. S. Whoriskey, S. K. Pekar, G. S. Elliott, S. Hara, N. Liu, D. M. Lenz, T. Zamborelli, J. P. Mayer, J. E. Tarpley, D. L. Lacey, B. Ratzkin, S. K. Yoshinaga, *Growth Factors* **1998**, *15*, 307.
[94] A. Muranyi, B. E. Finn, G. P. Gippert, S. Forsen, J. Stenflo, T. Drakenberg, *Biochemistry* **1998**, *37*, 10605.
[95] M. Lohmeyer, P. M. Harrison, S. Kannan, M. DeSantis, N. J. O'Reilly, M. J. Sternberg, D. S. Salomon, W. J. Gullick, *Biochemistry* **1997**, *36*, 3837.
[96] P. Guntert, C. Mumenthaler, K. Wuthrich, *J Mol Biol* **1997**, *273*, 283.
[97] E. G. Hutchinson, J. M. Thornton, *Protein Sci* **1994**, *3*, 2207.
[98] A. V. Efimov, *Protein Eng* **1991**, *4*, 245.
[99] B. L. Sibanda, T. L. Blundell, J. M. Thornton, *J Mol Biol* **1989**, *206*, 759.
[100] D. Bonnet, N. Ollivier, H. Gras-Masse, O. Melnyk, *J Org Chem* **2001**, *66*, 443.
[101] D. Bonnet, C. Grandjean, P. Rousselot-Pailley, P. Joly, L. Bourel-Bonnet, V. Santraine, H. Gras-Masse, O. Melnyk, *J Org Chem* **2003**, *68*, 7033.
[102] L. Schmitt, C. Dietrich, R. Tampe, *J Am Chem Soc* **1994**, *116*, 8485.
[103] B. Pfeiffer, *Angew Chem Int Ed* **2003**, *42*, 2368.
[104] F. Poeltl-Frank, *Clin Exp Immunol* **1999**, *117*, 496.
[105] D. Alewood, K. Nielsen, P. F. Alewood, D. J. Craik, P. Andrews, M. Nerrie, S. White, T. Domagala, F. Walker, J. Rothacker, A. W. Burgess, E. C. Nice, *Growth Factors* **2005**, *23*, 97.
[106] F. Zanuttin, C. Guarnaccia, A. Pintar, S. Pongor, *Eur J Biochem* **2004**, *271*, 4229.
[107] W. R. Ballou, M. Arevalo-Herrera, D. Carucci, T. L. Richie, G. Corradin, C. Diggs, P. Druilhe, B. K. Giersing, A. Saul, D. G. Heppner, K. E. Kester, D. E.

Lanar, J. Lyon, A. V. Hill, W. Pan, J. D. Cohen, *Am J Trop Med Hyg* **2004**, *71*, 239.
[108] D. C. Kaslow, I. A. Quakyi, C. Syin, M. G. Raum, D. B. Keister, J. E. Coligan, T. F. McCutchan, L. H. Miller, *Nature* **1988**, *333*, 74.
[109] C. G. Black, T. Wu, L. Wang, A. R. Hibbs, R. L. Coppel, *Mol Biochem Parasitol* **2001**, *114*, 217.
[110] D. R. Drew, R. A. O'Donnell, B. J. Smith, B. S. Crabb, *J Biol Chem* **2004**, *279*, 20147.
[111] C. G. Black, T. Wu, L. Wang, A. E. Topolska, R. L. Coppel, *Mol Biochem Parasitol* **2005**, *144*, 27.
[112] V. M. Marshall, A. Silva, M. Foley, S. Cranmer, L. Wang, D. J. McColl, D. J. Kemp, R. L. Coppel, *Infect Immun* **1997**, *65*, 4460.
[113] L. Wang, C. G. Black, V. M. Marshall, R. L. Coppel, *Infect Immun* **1999**, *67*, 2193.
[114] L. Wang, L. Kedzierski, S. L. Wesselingh, R. L. Coppel, *Infect Immun* **2003**, *71*, 2356.
[115] L. Kedzierski, C. G. Black, M. W. Goschnick, A. W. Stowers, R. L. Coppel, *Infect Immun* **2002**, *70*, 6606.
[116] L. Wang, M. W. Goschnick, R. L. Coppel, *Infect Immun* **2004**, *72*, 6172.
[117] M. W. Goschnick, C. G. Black, L. Kedzierski, A. A. Holder, R. L. Coppel, *Infect Immun* **2004**, *72*, 5840.
[118] H. E. Polson, D. J. Conway, T. Fandeur, O. Mercereau-Puijalon, S. Longacre, *Mol Biochem Parasitol* **2005**, *142*, 110.
[119] J. P. Tam, Y.-A. Lu, *J Am Chem Soc* **1995**, *117*, 12058.
[120] I. M. K. Kumar, V. N. R. Pillai, B. Mathew, *J Pept Sci* **2002**, *8*, 183.
[121] G. A. Cremer, H. Tariq, A. F. Delmas, *J Pept Sci* **2006**.
[122] T. Woehr, F. Wahl, A. Nefzi, B. Rohwedder, T. Sato, X. Sun, M. Mutter, *J Am Chem Soc* **1996**, *118*, 9218.
[123] T. Johnson, M. Quibell, D. Owen, R. C. Sheppard, *J Chem Soc, Chem Comm* **1993**, 369.
[124] M. B. Borre, M. Dziegel, B. Hoegh, E. Petersen, K. Rieneck, E. Riley, J. F. Meis, M. Aikawa, K. Nakamura, M. Harada, A. Wind, P. H. Jakobsen, J. Cowland, J. Soeren, N. H. Axelsen, J. Vuust, *Mol Biochem Parasitol* **1991**, *49*, 119.
[125] K. de Stricker, J. Vuust, S. Jepsen, C. Oeuvray, M. Theisen, *Mol Biochem Parasitol* **2000**, *111*, 123.
[126] M. Theisen, S. Soe, S. G. Jessing, L. M. Okkels, S. Danielsen, C. Oeuvray, P. Druilhe, S. Jepsen, *Vaccine* **2001**, *19*, 204.
[127] B. Hoegh, E. Petersen, M. Dziegel, K. David, A. Hanson, M. B. Borre, A. Holm, J. Vuust, S. Jepsen, *Am J Trop Med Hyg* **1992**, *46*, 307.
[128] C. Boudin, B. Chumpitazi, M. Dziegel, F. Peyron, S. Picot, B. Hoegh, P. Ambroise-Thomas, *J Clin Microbiol* **1993**, *31*, 636.
[129] M. Dziegel, P. Rowe, S. Bennet, S. J. Allen, O. Olerup, A. Gottschau, M. B. Borre, E. M. Riley, *Infect Immun* **1993**, *61*, 103.
[130] D. Dodoo, M. Theisen, J. A. Kurtzhals, B. D. Akanmori, K. A. Koram, S. Jepsen, F. K. Nkrumah, T. G. Theander, L. Hviid, *J Infect Dis* **2000**, *181*, 1202.
[131] C. Oeuvray, M. Theisen, C. Rogier, J. F. Trape, S. Jepsen, P. Druilhe, *Infect Immun* **2000**, *68*, 2617.

[132] M. Theisen, S. Soe, C. Oeuvray, A. W. Thomas, J. Vuust, S. Danielsen, S. Jepsen, P. Druilhe, *Infect Immun* **1998**, *66*, 11.
[133] L. J. M. Carvalho, F. A. Alves, C. Bianco Jr. , S. G. Oliveira, G. M. Zanini, S. Soe, P. Druilhe, M. Theisen, J. A. P. C. Muniz, C. T. Daniel-Ribeiro, *Clin Diagn Lab Immunol* **2005**, *12*, 242.
[134] E. Kaiser, R. L. Colescott, C. D. Bossinger, P. I. Cook, *Anal Biochem* **1970**, *34*, 595.
[135] M. S. Mueller, A. Renard, F. Boato, D. Vogel, M. Naegeli, R. Zurbriggen, J. A. Robinson, G. Pluschke, *Infect Immun* **2003**, *71*, 4749.
[136] G. Gonzalez, T. Crombet, F. Torres, M. Catala, L. Alfonso, M. Osorio, E. Neninger, B. Garcia, A. Mulet, R. Perez, R. Lage, *Ann Oncol* **2003**, *14*, 461.
[137] T. Ganz, *Nat Rev Immunol* **2003**, *3*, 710.
[138] R. I. Lehrer, *Nat Rev Microbiol* **2004**, *2*, 727.
[139] M. Zasloff, *Nature* **2002**, *415*, 389.
[140] K. A. Brogden, M. Ackermann, P. B. McCray, Jr., B. F. Tack, *Int J Antimicrob Agents* **2003**, *22*, 465.
[141] O. Toke, *Biopolymers* **2005**, *80*, 717.
[142] K. A. Brogden, *Nat Rev Microbiol* **2005**, *3*, 238.
[143] A. Tossi, *Antimicrobial sequences database, AMSDb*, University of Trieste.
[144] C. B. Park, K. S. Yi, K. Matsuzaki, M. S. Kim, S. C. Kim, *Proc Natl Acad Sci U S A* **2000**, *97*, 8245.
[145] M. L. Cohen, *Nature* **2000**, *406*, 762.
[146] C. Walsh, *Nature* **2000**, *406*, 775.
[147] C. Hetru, L. Letellier, Z. Oren, J. A. Hoffmann, Y. Shai, *Biochem J* **2000**, *345*, 653.
[148] R. Bessale, A. Kapitkovski, A. Gorea, I. Shalit, M. Fridkin, *FEBS Lett* **1990**, *274*, 151.
[149] D. Wade, A. Boman, B. Wahlin, C. M. Drain, D. Andreu, H. G. Boman, R. B. Merrifield, *Proc Natl Acad Sci U S A* **1990**, *87*, 4761.
[150] A. Peschel, *Trends Microbiol* **2002**, *10*, 179.
[151] T. Guina, E. C. Yi, H. Wang, M. Hackett, S. I. Miller, *J Bacteriol* **2000**, *182*, 4077.
[152] W. M. Shafer, X. Qu, A. J. Waring, R. I. Lehrer, *Proc Natl Acad Sci U S A* **1998**, *95*, 1829.
[153] H. Brotz, G. Bierbaum, K. Leopold, P. E. Reynolds, H. G. Sahl, *Antimicrob Agents Chemother* **1998**, *42*, 154.
[154] H. G. Boman, B. Agerberth, A. Boman, *Infect Immun* **1993**, *61*, 2978.
[155] C. Subbalakshmi, N. Sitaram, *FEMS Microbiol Lett* **1998**, *160*, 91.
[156] A. Patrzykat, C. L. Friedrich, L. Zhang, V. Mendoza, R. E. Hancock, *Antimicrob Agents Chemother* **2002**, *46*, 605.
[157] J. H. Jones, *J Pept Sci* **2006**, *12*, 79.
[158] J. S. Davies, *J Pept Sci* **2003**, *9*, 471.
[159] R. P. Cheng, S. H. Gellman, W. F. DeGrado, *Chem Rev* **2001**, *101*, 3219.
[160] T. L. Raguse, E. A. Porter, B. Weisblum, S. H. Gellman, *J Am Chem Soc* **2002**, *124*, 12774.
[161] D. Liu, W. F. DeGrado, *J Am Chem Soc* **2001**, *123*, 7553.
[162] S. R. Haynes, S. D. Hagins, M. M. Juban, P. H. Elzer, R. P. Hammer, *J Pept Res* **2005**, *66*, 333.

[163] G. Muller, G. Hessler, H. Y. Decornez, *Angew Chem Int Ed Engl* **2000**, *39*, 894.
[164] V. Brandmeier, W. H. B. Sauer, M. Feigel, *Helv Chim Acta* **1994**, *77*, 70.
[165] S. C. Shankaramma, Z. Athanassiou, O. Zerbe, K. Moehle, C. Mouton, F. Bernadini, J. W. Vrijbloed, D. Obrecht, J. A. Robinson, *ChemBioChem* **2002**, *3*, 1126.
[166] M. Favre, K. Moehle, L. Jiang, B. Pfeiffer, J. A. Robinson, *J Am Chem Soc* **1999**, *121*, 2679.
[167] A. Descours, K. Moehle, A. Renard, J. A. Robinson, *ChemBioChem* **2002**, *3*, 318.
[168] Z. Athanassiou, R. L. A. Dias, K. Moehle, N. Dobson, G. Varani, J. A. Robinson, *J Am Chem Soc* **2004**, *126*, 6906.
[169] J. A. Robinson, S. C. Shankaramma, P. Jetter, U. Kienzl, R. A. Schwendener, J. W. Vrijbloed, D. Obrecht, *Bioorg Med Chem* **2005**, *13*, 2055.
[170] R. J. Simon, R. S. Kania, R. N. Zuckermann, V. D. Huebner, D. A. Jewell, S. Banville, S. Ng, L. Wang, S. Rosenberg, C. K. Marlowe, et al., *Proc Natl Acad Sci U S A* **1992**, *89*, 9367.
[171] R. N. Zuckermann, J. M. Kerr, S. B. H. Kent, W. H. Moos, *J Am Chem Soc* **1992**, *114*, 10646.
[172] G. M. Figliozzi, R. Goldsmith, S. Ng, S. C. Banville, R. N. Zuckermann, *Meth Enzymol* **1996**, *267*, 437.
[173] S. M. Miller, R. J. Simon, S. Ng, R. N. Zuckermann, J. M. Kerr, W. H. Moos, *Bioorg Med Chem Lett* **1994**, *4*, 2657.
[174] J. A. W. Kruijtzer, R. M. J. Liskamp, *Tetrahedron Lett* **1995**, *36*, 6969.
[175] B. C. Gorske, S. A. Jewell, E. J. Guerard, H. E. Blackwell, *Org Lett* **2005**, *7*, 1521.
[176] C. W. Wu, T. J. Sanborn, K. Huang, R. N. Zuckermann, A. E. Barron, *J Am Chem Soc* **2001**, *123*, 6778.
[177] T. S. Burkoth, E. Beausoleil, S. Kaur, D. Tang, F. E. Cohen, R. N. Zuckermann, *Chem Biol* **2002**, *9*, 647.
[178] K. Huang, C. W. Wu, T. J. Sanborn, J. A. Patch, K. Kirshenbaum, R. N. Zuckermann, A. E. Barron, I. Radhakrishnan, *J Am Chem Soc* **2006**, *128*, 1733.
[179] S. Ng, B. Goodson, A. Ehrhardt, W. H. Moos, M. Siani, J. Winter, *Bioorg Med Chem* **1999**, *7*, 1781.
[180] B. Goodson, A. Ehrhardt, S. Ng, J. Nuss, K. Johnson, M. Giedlin, R. Yamamoto, W. H. Moos, A. Krebber, M. Ladner, M. B. Giacona, C. Vitt, J. Winter, *Antimicrob Agents Chemother* **1999**, *43*, 1429.
[181] M. Humet, T. Carbonell, I. Masip, F. Sanchez-Baeza, P. Mora, E. Canton, M. Gobernado, C. Abad, E. Perez-Paya, A. Messeguer, *J Comb Chem* **2003**, *5*, 597.
[182] P. Mora, I. Masip, N. Cortes, R. Marquina, R. Merino, J. Merino, T. Carbonell, I. Mingarro, A. Messeguer, E. Perez-Paya, *J Med Chem* **2005**, *48*, 1265.
[183] I. Masip, N. Cortes, M. J. Abad, M. Guardiola, E. Perez-Paya, J. Ferragut, A. Ferrer-Montiel, A. Messeguer, *Bioorg Med Chem* **2005**, *13*, 1923.
[184] J. A. Patch, A. E. Barron, *J Am Chem Soc* **2003**, *125*, 12092.
[185] J. A. Kruijtzer, W. A. Nijenhuis, N. Wanders, W. H. Gispen, R. M. Liskamp, R. A. Adan, *J Med Chem* **2005**, *48*, 4224.
[186] T. S. Ryge, P. R. Hansen, *J Pept Sci* **2005**, *11*, 727.
[187] Y. M. Song, Y. Park, S. S. Lim, S. T. Yang, E. R. Woo, I. S. Park, J. S. Lee, J. I. Kim, K. S. Hahm, Y. Kim, S. Y. Shin, *Biochemistry* **2005**, *44*, 12094.

[188] K. Kimura, Y. Tsujimura, M. Yokoyama, T. Maeda, *Bull Chem Soc Jpn* **1998**, *71*, 657.
[189] K. Balos, D. Gatos, in *Fmoc Solid Phase Peptide Synthesis* (Eds.: W. C. Chan, P. D. White), Oxford University Press, New York, **2000**.
[190] W. C. Chan, P. D. White, in *Fmoc Solid Phase Peptide Synthesis* (Eds.: W. C. Chan, P. D. White), Oxford University Press, New York, **2000**.
[191] NCCLS, *Approved standard M7-A3*, 3rd ed., Villanova. Pa., **1993**.
[192] M. Rainaldi, V. Moretto, M. Crisma, E. Peggioni, S. Mammi, C. Toniolo, G. Cavicchioni, *J Pept Sci*
2002, *8*, 241.
[193] S. Liu, D. S. Edwards, *Chem Rev* **1999**, *99*, 2235.
[194] S. Ben-Haim, D. Kahn, G. J. Weiner, M. T. Madsen, A. D. Waxman, C. M. Williams, D. L. Clarke-Pearson, R. E. Coleman, R. T. Maguire, *Nucl Med Biol* **1994**, *21*, 131.
[195] B. R. Moyer, S. Vallabhajosula, J. Lister-James, L. R. Bush, J. E. Cyr, D. A. Snow, D. Bastidas, H. Lipszyc, R. T. Dean, *J Nucl Med* **1996**, *37*, 673.
[196] J. C. Reubi, *J Nucl Med* **1995**, *36*, 1825.
[197] B. Wangberg, O. Nilsson, E. Theodorsson, A. Dahlstrom, H. Ahlman, *Br J Cancer* **1991**, *64*, 23.
[198] S. W. Lamberts, *Endocr Rev* **1988**, *9*, 417.
[199] A. Lupetti, M. M. Welling, E. K. Pauwels, P. H. Nibbering, *Curr Drug Targets* **2005**, *6*, 945.
[200] P. Haefliger, S. Mundwiler, K. Ortner, B. Spingler, R. Alberto, G. Andocs, L. Balogh, K. Bodo, *Synthesis and Reactivity in Inorganic, Metal-Organic and Nano-Metal Chemistry* **2005**, *35*, 27.
[201] R. Garcia, A. Paulo, A. Domingos, I. Santos, K. Ortner, R. Alberto, *J Am Chem Soc* **2000**, *122*, 11240.
[202] T. Vojkovsky, *Pept Res* **1995**, *8*, 236.
[203] M. Gueron, P. Plateau, M. Decorps, *Progr Nucl Reson Spectros* **1991**, *23*, 135.
[204] U. Piantini, O. W. Soerensen, R. R. Ernst, *J Am Chem Soc* **1982**, *53*, 6800.
[205] L. Braunschweiler, R. R. Ernst, *J Mag Res* **1983**, *53*, 521.
[206] J. Jeener, B. H. Meier, P. Bachmann, R. R. Ernst, *J Chem Phys* **1979**, *71*, 4646.
[207] C. Bartels, T. Xia, M. Billeter, P. Guntert, K. Wuthrich, *J Biomol. NMR* **1995**, *6*, 1.
[208] P. Guntert, *Methods Mol Biol* **2004**, *278*, 353.
[209] R. A. Laskowski, J. A. Rullmannn, M. W. MacArthur, R. Kaptein, J. M. Thornton, *J Biomol NMR* **1996**, *8*, 477.
[210] R. Koradi, M. Billeter, K. Wuthrich, *J Mol Graph* **1996**, *14*, 51.
[211] F. Boato, *PhD Thesis: Protein Epitope Mimetics in Synthetic Vaccine Design*, University of Zurich, Zurich, **2006**.
[212] A. Bax, M. F. Summers, *J Am Chem Soc* **1986**, *108*, 2093.
[213] A. A. Bothnerby, R. L. Stephens, J. M. Lee, C. D. Warren, R. W. Jeanloz, *J Am Chem Soc* **1984**, *106*, 811.

Summary

This work deals with the development of new synthetic peptide-based molecules designed either to play a role in preventing disease as components of a malaria vaccine, or to treat infections as antimicrobial peptidomimetics.

As parasites develop resistance to traditional antimalarial drugs and mosquitoes develop resistance to known insecticides, the need for an effective vaccine to control malaria becomes greater than ever. In this project, mimetics of malaria vaccine candidate proteins MSP-1, MSP-4 and GLURP were synthesised and tested in animal models, exploiting the virosome technology for the presentation of the mimetics to the immune system. Multiple copies of the mimetics were inserted into the lipid bilayer of immunostimulating reconstituted influenza virosomes by virtue of a phospholipid tail coupled to the N-terminus of the mimetic.

Merozoite surface protein 1 (MSP-1) is the major surface protein on the erythrocyte-invasive form of *Plasmodium* parasites. The protein undergoes proteolytic processing after merozoite release into the plasma, leading to a 42-kDa membrane-bound fragment ($MSP\text{-}1_{42}$), which is further processed around the time of erythrocyte invasion to leave a 19 kDa C-terminal fragment ($MSP\text{-}1_{19}$) which is carried into the invaded erythrocyte. Antibodies that bind to $MSP\text{-}1_{19}$ can inhibit both the second processing step and erythrocyte invasion. $MSP\text{-}1_{19}$ consists of two epidermal growth factor (EGF)-like domains.

In this project, a synthetic peptide mimetic of the first EGF-like domain of MSP-1 was synthesised and suitable conditions were found for oxidative folding of the linear peptide to give one major, fully oxidised product. NMR studies proved that the structure of the synthetic peptide was closely related to that of the corresponding domain in the two-domain protein $MSP\text{-}1_{19}$. Enzymatic digestion studies revealed that the disulfide bonding pattern of the synthetic peptide corresponded to the known pattern for the two-domain protein. Thus, the mimetic should represent a good mimetic of the first EGF-like domain of MSP-1.

A modified peptide mimetic containing an N-terminal hydrazinoglycine could be oxidatively folded in the same way and was chemoselectively coupled to a phospholipid moiety to provide a suitable mimetic for insertion into virosomes. Immunizations with virosomes loaded with this mimetic induced sera which were able to recognise blood-

stage parasites. These promising results suggest that this mimetic could form a component of a multi-antigen synthetic peptide malaria vaccine.

Merozoite surface protein 4 (MSP-4) is another membrane-bound merozoite surface protein containing an EGF-like domain. Based on the successful synthesis of the MSP-1 mimetic, a peptide mimetic of the EGF-like domain of MSP-4 was prepared and oxidised under analogous conditions. Initial synthetic problems in the peptide chain assembly were overcome by the introduction of a pseudoproline residue, intended to disrupt interchain aggregation, which is believed to be the main cause of low coupling yields. On reaction of the hydrazinoglycine-coupled folded peptide with phospholipid, a sticky product was formed that was difficult to handle. Immunological studies with this product failed to produce sera that were cross-reactive with the parasite, probably due to the physical properties of the mimetic. Therefore, a related phospholipid-bound folded peptide product with improved physical characteristics was prepared by the inclusion of a series of extra lysine residues at the N-terminal of the peptide sequence. Immunological testing of this product has not yet been carried out. Despite the problems encountered, the work proved the possibility of the synthesis of another EGF-like domain of interest here. There are also several other EGF-like domains present in *Plasmodium falciparum* proteins that could be investigated by similar methods in the future.

The third *Plasmodium* protein to be investigated was the glutamate rich protein (GLURP). This protein is expressed at all stages of the parasite life cycle, and can be found on the surface of erythrocytes. A series of peptide mimetics directly coupled to phospholipid tails were prepared in this project, based on epitopes identified by other groups, found in the well-conserved non-repeat region of the protein. NMR spectra of non-phospholipid-coupled analogues of these mimetics were also measured. Unfortunately the spectra suggested that the peptides were not well-structured, and the mimetics failed to induce immune responses that cross-reacted with the parasites. Therefore, these mimetics in their current form do not represent good candidates for a malaria vaccine.

In the second part of this work, the synthesis of some macrocyclic peptoid-peptide hybrid mimetics is presented. One or two peptoid units were included in the sequence of a backbone cyclic peptide with known antimicrobial activity. Studies showed that the inclusion of a peptoid unit did not have a detrimental effect of antimicrobial activity, and

in one case seemed to reduce the haemolytic activity of the peptide. The inclusion of peptoid units could help to improve the stability of antimicrobial peptidomimetics towards proteolysis. A different peptoid monomer unit was introduced into the same sequence to lead to a peptide which could bind to $Re(CO)_3$. Rhenium is believed to behave chemically in a similar way to ^{99}Technetium. Therefore, this work suggests it would be possible to build a ^{99}Technetium-labelled antimicrobial peptidomimetic, which could be useful for imaging studies of the uptake, processing, and excretion of antimicrobial peptidomimetics in humans.

Zusammenfassung

Diese Arbeit befasst sich mit der Entwicklung neuer synthetischer, peptidbasierter Moleküle, die entworfen wurden um entweder eine Rolle bei der Krankheitsprävention als Bestandteile eines Malaria-Impfstoffes oder zur Behandlung von Infektionskrankheiten in der Form antimkrobieller Peptidmimetika zu spielen.

Da einerseits Parasiten Resistenz gegen traditionelle Antimalariawirkstoffe, sowie andererseits die Anophelesmücke Resistenz gegen gebräuchliche Insektizide entwickeln, wird der Bedarf für einen effektiven Malariaimpfstoff grösser denn je. Bei diesem Projekt wurden Mimetika der Malariaimpfstoffanwärter-Proteine MSP-1, MSP-4 und GLURP synthetisiert und in Tiermodellen unter Verwendung der Virosom Technologie, welche der Präsentation der Mimetika für das Immunsystem dient, getestet. Unter Zuhilfenahme eines Phospholipidschwanzes, welcher über die N-Termina der Mimetikas gekoppelt ist, wurden vielfache Kopien derselben in die Lipid-Doppelschicht der immunostimulierenden rekonstituierten Influenza Virosome insertiert.

Merozoiten Oberflächenprotein 1 (MSP-1) ist das hauptsächlich vorkommende Oberflächenprotein der Erythrozyten-invasiven Form des *Plasmodium* Parasiten. Dieses Protein unterliegt nach seiner Freisetzung ins Plasma einer proteolytischer Veränderung, welche zu einem 42 kDa membrangebunden Fragment ($MSP\text{-}1_{42}$) führt. Dieses Fragment wird zum Zeitpunkt des Erythrozytenbefalls weiter zu einem 19 kDa ($MSP\text{-}1_{19}$) Fragment prozessiert, welches in den befallenen Erythrozyten übertragen wird. Antikörper die an $MSP\text{-}1_{19}$ binden, können sowohl den zweiten Prozessierungsschritt als auch den Befall des Erythrozyten verhindern. $MSP\text{-}1_{19}$ besteht aus zwei epidermalen Wachstumsfaktor-ähnlichen (EGF-ähnlichen) Domänen.

In diesem Projekt wurden ein synthetisches Peptidmimetikum der ersten EGF-ähnlichen Domäne des MSP-1 synthetisiert und passende Bedingungen für die oxidative Faltung des linearen Peptides, die zu einem vollständig oxidierten Hauptprodukt führten, gefunden. NMR Untersuchungen zeigten, dass die Struktur des synthetischen Peptids eng mit der Struktur der entsprechenden Domäne des aus zwei Domänen bestehenden $MSP\text{-}1_{19}$ Proteins verwandt ist. Enzymatische Verdauexperimente ergaben, dass das Dissulfidbrücken-Bindungsmuster des synthetischen Peptids dem bekannten Muster des

die beiden Domänen umfassenden Proteins entsprach. Folglich sollte diese Verbindung ein gutes Mimetikum der ersten EGF-ähnlichen Domäne des MSP-1 darstellen.

Ein modifiziertes Mimetikum welches ein N-terminales Hydrazinoglycin enthält, konnte auf die gleiche Weise oxidativ gefaltet werden und wurde chemoselektiv an eine Phospholipideinheit gekuppelt, um ein geeignetes Mimetikum für die Einführung in Virosomen zu erhalten. Immunisierungen mit Virosomen welche mit diesem Mimetikum beladen waren, induzierten Sera die in der Lage waren Parasiten in der Blut-Phase zu erkennen. Diese vielversprechenden Ergebnisse deuten darauf hin, dass dieses Mimetikum Bestandteil eines synthetischen Multi-Antigen Peptid Malaria Impfstoffes bilden könnte.

Merozoitenoberflächenprotein 4 (MSP-4) ist ein weiteres membran-gebundenes Merozoitenoberflächenprotein, welches eine EGF-ähnliche Domäne enthält. Basierend auf der erfolgreichen Synthese des MSP-1 Mimetikums wurde ein Peptidmimetikum der EGF-ähnlichen Domäne von MSP-4 hergestellt und unter analogen Bedingungen oxidiert. Anfängliche Probleme beim Aufbau des Peptidgerüstes wurden durch Einführung eines Pseudoprolinrestes, welcher eine Aggregation der Peptidketten während der Festphasensynthese verhindern sollte - was mutmasslich die Hauptursache niedriger Kopplungsausbeuten war - überwunden. Bei der Reaktion des an Hydrazinoglycin gekuppelten, gefalteten Peptides mit dem Phospholipid wurde ein hochviskoses, schwer handhabbares Produkt gebildet. Immunologische Studien mit diesem Produkt ergaben keine Sera die Kreuzreaktivität mit dem Parasiten aufwiesen, was wahrscheinlich durch die physikalischen Eigenschaften des Peptides bedingt war. Aus diesem Grund wurde durch Einbau einer Reihe von zusätzlichen Lysin Resten am N-Terminus der Peptidsequenz, ein verwandtes phospholipidgebundenes gefaltetes Peptidprodukt mit verbesserten physikalischen Eigenschaften hergestellt. Immunologische Untersuchungen mit diesem Produkt wurden noch nicht durchgeführt. Trotz der aufgetretenen Schwierigkeiten bestätigte diese Arbeit die Möglichkeit der Synthese einer anderen EGF-ähnlichen Domänen von Interesse. Darüberhinaus existieren mehrere weitere EGF-ähnliche Domänen in Proteinen aus *Plasmodium falciparum* die mit vergleichbarer Methodik in Zukunft untersucht werden könnten.

Das dritte *Plasmodium* Protein welches untersucht werden sollte war das glutamatreiche Protein (GLURP). Die Expression dieses Proteins, welches an der Oberfläche von Erythrozyten gefunden werden kann, findet während allen Phasen des parasitären Lebenszyklusses statt. Bei diesem Projekt wurden eine Reihe von direkt an Phospholipidschwänze gebundenen Peptidmimetika hergestellt, die auf von anderen Arbeitsgruppen in der hochkonservierten nicht repetetiven Region des Proteins identifizierten Epitopen basieren. Die NMR Spektren der nicht an Phospholipid gekuppelten Analoga dieser Mimetika wurden ebenfalls aufgenommen. Unglücklicherweise deuteten diese Spektren darauf hin, dass die Peptide in Lösung nicht wohlstrukturiert sind; ebenfalls misslang die Induktion einer Immunantwort welche Kreuzreaktivität mit den Parasiten aufweist. Aus diesem Grund stellen diese Mimetika in ihrer jetzigen Form keine guten Kandidaten für einen Malariaimpfstoff dar.

Im zweiten Teil dieser Arbeit wird die Synthese einiger makrozyklischer Peptoid-Peptid Hybridmimetika beschrieben. Eine, beziehungsweise zwei Peptoideinheiten wurden hierbei in die Sequenz eines Rückgrat-zyklisierten Peptids mit bekannter antimikrobieller Aktivität eingefügt. Untersuchungen zeigten, dass die Einführung der Peptoideinheiten keinen nachteiligen Einfluss auf die antimikrobielle Aktivität hatten, und in einem Fall sogar die hämolytische Aktivität des Peptides reduzierten. Der Einbau von Peptoideinheiten könnte somit helfen die proteolytische Stabilität antimikrobieller Peptidmimetika zu verbessern. Eine unterschiedliche Peptoideinheit wurde in dieselbe Sequenz eingefuehrt und ergab ein Peptid, an welches $Re(CO)_3$ gebunden werden konnte. Da davon ausgegangen wird, dass sich Rhenium chemisch ähnlich zu ^{99}Technetium verhält, deutetet diese Arbeit darauf hin, dass es möglich sein sollte ^{99}Technetium markierte antimikrobielle Peptidmimetika aufzubauen, welche von Nutzen bei der Untersuchung der Aufnahme, der Prozessierung, und der Ausscheidung von antimikrobiellen Peptiden beim Menschen, sein könnten.

Acknowledgements

I would like to thank my supervisor, *Prof. John A. Robinson* for giving me the opportunity to work on the interesting topics presented in this thesis, and for his guidance, advice and encouragement throughout my time here.

Many thanks also to all the people who helped in the completion of this work, particularly:

Prof. Gerd Pluschke and co-workers from the Swiss Tropical Institute, and *Dr Rinaldo Zurbriggen* and co-workers from Pevion Biotech for the immunological part of this work and for their commitment to the malaria vaccine project.

Dr Annabelle Freund-Renard for her contribution to the enzymatic digestion studies, her advice and encouragement, and for sharing her knowledge and experience so generously.

Dr Kerstin Moehle for NMR analysis and structure calculations.

The *NMR and MS service teams* of the OCI and the Protein Analysis Unit of the Biochemistry Institute. Special thanks to *Nadja Bross* and *Simon Jurt* for the pleasant atmosphere in the NMR service.

Annelies Meier for the antimicrobial activity measurements.

I would like to thank all members of the *Robinson group*, past and present, for the great atmosphere in the lab, and for the support, advice, encouragement, friendship (and coffee breaks) that helped me so much in many ways throughout my PhD.

I thank my family for their encouragement and understanding throughout my studies, without which I would never have had the strength to achieve this work.

Thanks to Peter for always being there for me.

Curriculum Vitae

Name Sonya Marie James

Born 9 April 1979, Bradford, West Yorkshire, UK

Education

2001-2006 *Organic Chemistry Institute, University of Zurich, Switzerland.*
Working for PhD in group of Prof. J. Robinson on Protein Epitope Mimetics as Potential Malaria Vaccine Candidates and Antimicrobial Agents.

2003-2005 Assistant in NMR Service

2004-2006 Assistant in the chemistry practical class for medicine students

1997 - 2001 *University of Sheffield, Sheffield, UK.*
Master of Chemistry (Chemistry with Study In Europe): 1st class Honours

1999-2000 Erasmus year spent studying at the Institut de Chimie, Université de Neuchâtel, Switzerland.

1992-1997 *Bingley Grammar School, Bingley, West Yorkshire, UK.*
1997 GCE Advanced level: Chemistry (A), Mathematics (A), French (A), General Studies (A).